HIO STATE
NIVERSITY
JUN 9 1961
LI...

CHEMISTRY HALL LIBRARY

BULLETIN
OF THE
CHEMICAL SOCIETY OF JAPAN

Vol. 34 No. 3 March 1961

CONTENTS

General and Physical

Über die Kupfer-salze der ω-Aminosäuren. III. Über die Kristallstruktur von Kupfersalz des β-Alanins . . . . . K. TOMITA 297

Interaction Polarization of the Hydrogen Bonded Complexes. II. . K. KIMURA and R. FUJISHIRO 304

Colloid Chemical Studies on Starching Materials. III. Dynamic Viscosity and Dynamic Rigidity of Starch Solutions . . . . . M. NAKAGAKI and K. MURAGISHI 316

Dielectric Investigation on Coals. V. Microwave Dielectric Constant . . . . . K. CHITOKU and K. HIGASI 320

The Thermal Decomposition of Dimethyl Ether in the Presence of Hydrogen Sulfide . . . . . N. IMAI and O. TOYAMA 328

Microwave Spectrum and Molecular Structure of Monochloroacetonitrile, CH_2ClCN . . . . . K. WADA, Y. KIKUCHI, C. MATSUMURA, E. HIROTA and Y. MORINO 337

Microwave Spectrum of Propargyl Halides. I. Molecular Structure, Dipole Moment, and Quadrupole Coupling Constant of Propargyl Chloride . . . . . E. HIROTA and Y. MORINO 341

Microwave Spectrum of Propargyl Halides. II. Molecular Structure and Second-Order Quadrupole Effect of Propargyl Bromide . . . . . Y. KIKUCHI, E. HIROTA and Y. MORINO 348

Nuclear Magnetic Resonance Study of Hydrogen Bond in Salicylaldehyde . . . . I. YAMAGUCHI 353

Normal Coordinate Treatment and Assignment of Infrared Absorption Bands of Polyvinyl Chloride . . . . . T. SHIMANOUCHI and M. TASUMI 359

Molecular Structure of Epibromohydrin and Glycidol by Electron Diffraction . . M. IGARASHI 365

An Electron Diffraction Investigation of the Molecular Structure of Ethylenimine. . M. IGARASHI 369

Stereoregular Polymers. VII. Infrared Spectra of Isotactic Polystyrene, Isotactic Poly-α, β, β-trideuterostyrene and Isotactic Poly-*p*-deuterostyrene. . . . . H. TADOKORO, Y. NISHIYAMA, S. NOZAKURA and S. MURAHASHI 381

An X-ray Study on the Phase Transition of Aniline Hydrobromide, $C_6H_5NH_3Br$ . . I. TAGUCHI 392

The Effect of Alcohols on the Solubilization of Oleic Acid in the Aqueous Solution of Sodium Dodecyl Sulfate . . . . . R. MATUURA, K. FURUDATE, H. TSUTSUMI and S. MIIDA 395

On the Differences in Monolayer Properties of Poly-γ-benzyl-L-glutamate and Poly-β-benzyl-L-aspartate . . . . . S. IKEDA and T. ISEMURA 416

Monolayer Studies on Polyanhydro-L-glutamic and Polyanhydro-L-aspartic Acids. . . . . S. IKEDA and T. ISEMURA 422

On the Orientational Order-Disorder Transition in Crystalline Aniline Hydrobromide. . H. SUGA 426

Optical Properties of Colored Colloidal Systems. II. Apparent Refractive Index and Extinction Coefficient of the System of Small Spherical Particles . . . . . M. NAKAGAKI and T. FUJII 433

A Diffusion Mechanism for Liesegang Rings. I. Spacing Law. . . . . P. B. MATHUR 437

Structural Analysis of Liesegang Ring Systems . . . . . P. B. MATHUR 440

"Frontier Electron Density" in Saturated Hydrocarbons. . K. FUKUI, H. KATO and T. YONEZAWA 442

Analytical and Inorganic

Polarographic Behavior of Vanadium and Iron in Thiocyanate . . . . . G. S. DESHMUKH and J. P. SRIVASTAVA 325

Distribution of Neptunium between Di-(2-ethyl hexyl)-phosphoric Acid and Mineral Acids . . . . . E. NAKAMURA 402

Studies on Extraction of Polonium(IV) by Hexone from Acid Solution . . . . . N. MATSUURA, A. OUCHI and M. KOJIMA 411

Studies on the Catalytic Double Wave of Cystine by Oscillographic Polarography . . . . . M. SHINAGAWA, H. IMAI and H. NEZU 445

(Continued on inside cover)

Published by the Chemical Society of Japan

THE CHEMICAL SOCIETY OF JAPAN
(NIPPON KAGAKUKAI)

Founded in 1948

Successor to the former Chemical Society of Japan founded in 1878 and to the Society of Chemical Industry, Japan founded in 1898.

OFFICERS

Shoichiro NAGAI, *President*, Nihon University, Tokyo
Eiichi IWASE, *Vice-President*, Institute of Physical and Chemical Research, Tokyo
Wasaburo KIMURA, *Vice-President*, Nagoya University
Sojiro OKA, *Vice-President*, The University of Tokyo
Ichiro SAKURADA, *Vice-President*, Kyoto University
Hiroshi SOBUE, *Vice-President*, The University of Tokyo

BULLETIN OF THE CHEMICAL SOCIETY OF JAPAN

Editor: Yoshiyuki URUSHIBARA, The University of Tokyo, Tokyo
Assistant Editor: Saburo NAGAKURA, The University of Tokyo, Tokyo
Editorial Board:

Toshio ANDO	Ichiro MIYAGAWA	Tadashi SUEHIRO
Yoshié BANSHO	Masazumi NAKAGAWA	Kenzi TAMARU
Hidehiro GOTÔ	Koji NAKANISHI	Takeo WATASE
Yoshimasa HIRATA	Shigeo OKUMURA	Iwao YASUMORI
Kenichi HONDA	Kazuo SAITO	Tsuneo YOSHINO
Sunao IMANISHI	Naoyasu SATA	Koshiro YOSHIOKA

(Continued from outside cover)

Organic and Biological

Quinones. I. The Syntheses of Acetyl-*p*-benzoquinone Derivatives and 2-Acetylnaphthoquinone . . . . . E. KUROSAWA 300
Studies on Antibiotics and Related Substances. XII. Syntheses of 10-Oxo-11-dodecenoic Acid and 11-Oxo-12-tridecenoic Acid, Antitumor Substances. . . . . M. KINOSHITA and S. UMEZAWA 308
On Oxazolo[5 : 4-b]tropones . . . . . T. NOZOE, K. DOI and K. KITAHARA 312
Alkylation of Sodio-2,3-dimethylindole and Sodio-tetrahydrocarbazole in Non-polar Solvent . . . . . M. NAKAZAKI 334
Non-benzenoid Aromatic Heterocycles. IV. An Attempted Synthesis of Indolo[3,2-b]indole : A Hetero-pentalene . . . . . H. KATO and M. OHTA 357
Intramolecular Hydrogen Bonding in α-Keto and α-Alkoxycarboxylic Acids. III. Comparison of the Spectra in the Carbonyl Region with Those in the O-H Stretching Region . . . . . M. ŌKI and M. HIROTA 374
Intramolecular Hydrogen Bonding in α-Keto and α-Alkoxycarboxylic Acids. IV. Electronic Effect in Aryloxyacetic Acids. . . . . M. ŌKI and M. HIROTA 378
Synthesis and Physical Properties of Normal Higher Primary Alcohols. III. Synthesis of Normal Higher Primary Alcohols of Even Carbon Numbers from Dodecanol to Hexatriacontanol . . . . . A. WATANABE 398
The Competitive Reduction of Nitrobenzene and para-Substituted Nitrobenzenes with Nickel Catalysts. . . . . A. SUGIMORI 407

Short Communications

Radiolysis of Crystalline Oxalate Complexes . . . . . A. SUGIMORI and G. TSUCHIHASHI 449
Steric Effects of ortho-Groups on Hydrogen Bond Formation in Phenol Derivatives as Studied by Nuclear Magnetic Resonance . . . . . I. YAMAGUCHI 451
New Stable Olefin Complexes of Cobalt(I). . . . . A. NAKAMURA and N. HAGIHARA 452
The Absolute Configuration of Rotenone . . . . . M. NAKAZAKI and H. ARAKAWA 453
On Some Dark-colored Chlorocuprates(I, II) and Related Compounds. II. Magnetic Susceptibility and Color at Liquid Helium Temperatures. . . . . M. MORI 454
The Nuclear Magnetic Resonance Spectra of Some Aconite Bases: *Lucaconine and Lucidusculine* . . . . . A. SUZUKI, T. AMIYA and T. MATSUMOTO 455
The Interaction of a Surfactant with a Monolayer Studied by Radiotracer Method. . . . . R. SHIMOZAWA and R. MATUURA 457
Electron Spin Resonance Study on Photolysis of Acetone and Benzophenone . . . . . K. KUWATA and K. HIROTA 458
Reaction of Tetraphenyl Titanate with Amines. . . . . T. YOSHINO, I. KIJIMA and M. OCHI 459

Über die Kupfersalze der ω-Amino-säuren. III. Über die Kristallstruktur von Kupfersalz des β-Alanins

Von Ken-ichi TOMITA

(Eingegangen am 23. Juli, 1960)

In Teil II[1] wurde die Kristallstruktur des Kupferglycinmonohydrates dargestellt. Als zweite Stufe der Versuchsmaterialien haben wir dasKupfersalz des β-Alanins gewählt und die Kristallstruktur dieses Materials mit Hilfe der röntgenographischen Methode untersucht. Nach der Feststellung dieser Kristallstruktur können wichtige Erkenntnisse, nicht nur über den Koordinationszustand des Cu Atomes, sondern auch über die molekulare Konfiguration des β-Alanins selbst[2], abgeleitet werden.

Wir würden uns auf die Kristallanalyse des Kupfersalzes des Isoserins, das ein Derivat von β-Alanin ist, weiter einlassen, aber diese Kristallstruktur ist so kompliziert, daß wir diese Analyse unterbrechen mussten. Trotzdem fügen wir am Ende dieser Abhandlung die kristallographischen Daten bei, weil diese Substanz sehr wichtig ist.

Experiment und Resultat

Darstellungsweise.—Das gereinigte, überschüssige Kupferhydroxyd wurde mit einer wässerigen Lösung von β-Alanin im Wasserbad etwa 2 Stunden erhitzt und filtriert. Beim nachherigem Einengen des tiefblauen Filtrates scheidet sich das Kupfersalz von β-Alanin als ein papierstreifenförmiger tiefblauer Kristall ab.

Wenn dieser Einkristall in der Atomsphäre liegen gelassen wird, verändert sich die Oberflächenfarbe zu hellblau. Dieses Ausbleichen beweist teilweise Entwässerung des Kristalles.

Die Mikroanalyse gibt folgende Resultate:

$Cu(C_3H_6NO_2)_2+6H_2O$ (Mol. Gew. 347.81)

Ber.: C, 20.72; H, 6.96; N, 8.06; H_2O, 31.08; Cu, 18.28. Gef.: C, 21.31; H, 7.02; N, 8.06; H_2O, 31.77; Cu, 18.12%.

Mit Hilfe der Schwebemethode (Benzoläthylendibromid Gemisch) ergibt sich ein spezifisches Gewicht von 1.50.

Gitterkonstante.—Mittels Rotation- und Weissenberg-Aufnahmen um [100] und [010] mit Cu$K\alpha$-Strahlung wurde die Intensität jeder Reflexion nach der sogenannten "multiple film method" aus vier Filmen im Vergleich zu einer gewöhnlichen Intensitätsskala bestimmt; die Schnittflächeneinheit des gebrauchten Einkristalls ist ungefähr 0.1×0.2 mm bei $(0kl)$-Reflexionen und ungefähr 0.8×1.2 mm bei $(h0l)$-Reflexionen. Das Verhältnis der relativen Intensitäten von stärkster zu schwächster Reflexion war ungefähr 1500 : 1 für $(0kl)$-Reflexion und 700 : 1 für $(h0l)$-Reflexion.

Wir nahmen keine Notiz von der Absorption, aber auf die Kompensation des primären Extinktioneffekts wurde der genaue g-Wert angewandt ($g=6.76\times10^{-4}$), der aus der Formel

$$I_r=I_o/(1-gI_o)$$

gerechnet wurde, wobei I_o die beobachtete Intensität und I_r die reale Intensität zeigt.

Die gesamten unabhängigen Zahlen der Äquator-Reflexionen, welche in der Ausbreitungskugel enthalten sind, sind 182 für [100]-Projektion und 133 für [010]-Projektion, während die beobachteten Zahlen 132 bzw. 125. Für die Bestimmung der Raumgruppe wurden die Auslöschungsgesetze für $(0kl)$, $(1kl)$ und $(h0l)$-Reflexionen benützt.

Die gefundenen Gitterkonstanten sind wie folgt:

$a=5.46$ Å, $b=7.71$ Å, $c=18.11$ Å,
$\beta=92°$ (Monoklinisches System).
Die Zahl der Moleküle pro Elementarzelle; $z=2$.
Raumgruppe: $C_{2h}^5-P2_1/c$.

Strukturbestimmung und Betrachtung

Die Raumgruppe $C_{2h}^5-P2_1/c$ hat ein symmetrisches Zentrum auf dem Anfangspunkt; wenn das Molekül die allgemeine Lage einnimmt, ist die Zahl der Moleküle in der Elementarzelle vier. Beim Kupfersalz des β-Alanins, beträgt jedoch diese Zahl nur zwei; hierzu muss das Cu-Atom die spezielle Lage in der Elementarzelle, d. h., den Anfangspunkt, einnehmen, und die um das Cu-Atom koordinierten zwei Moleküle des β-Alanins haben daher selbstverständlich eine trans Konfiguration. Unmittelbar darnach wurde eine vorläufige Fouriersynthese um [100] und [010]-Projektionen kalkuliert, wobei die Vorzeichen jeder Reflexion nur mit den Parametern des Cu-Atoms berechneten Strukturfaktoren durchgeführt wurden. Aus den vielen Maxima, die sich in Fourier-projektionen um [100] und [010] zeigen, wurden einige, die gleiche z-Parameterwerte haben, gewählt und in Hinsicht auf den Valenzwinkel und die interatomaren Abstände wurden einige weitere schnittweise

1) K. Tomita und I. Nitta, diese Zeitschrift, **34**, 286 (1961).

2) Die Strukturanalyse von β-Alanin wurde schon ungefähr 1948 von Herrn Dr. M. Katayama durchgeführt, aber bis heute ist dieses Resultat noch nicht veröffentlicht worden.

TABELLE I.

Atomart	x/a	y/b	z/c
Cu	0.000	0.000	0.000
C_1^I	−0.185	−0.025	0.158
C_2^I	0.065	−0.118	0.185
C_3^I	0.187	−0.228	0.130
O_1^I	−0.205	0.005	0.095
O_2^I	−0.325	0.005	0.206
O_3^I	0.187	0.280	0.040
O_4^I	0.450	0.322	0.172
O_5^I	−0.258	0.445	0.060
N^I	0.278	−0.135	0.058

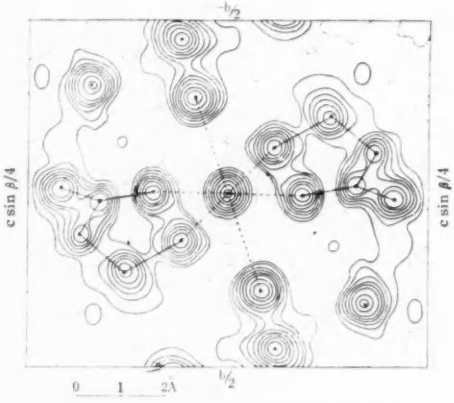

Abb. 1. Elektronendichteprojektion nach [100].
Das puntkierte Niveau der Kurven geht durch $1e/Å^2$ und die Kurve gleicher Elektronendichte liegen um $1e/Å^2$ auseinander, ausser im Kupfermaximum, wo die Äquidistanz $5e/Å^2$ beträgt.

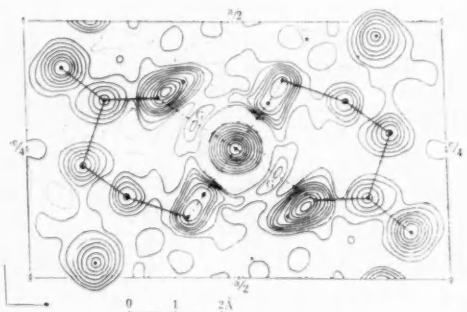

Abb. 2. Elektronendichteprojektion nach [010].
Das punktierte niedrigste Niveau der Kurven liegt bei $2e/Å^2$ und die Kurven gleicher Elektronendichte liegen um $1e/Å^2$ auseinander, ausser im Kupfermaximum, wo die Äquidistanz $5e/Å^2$ beträgt.

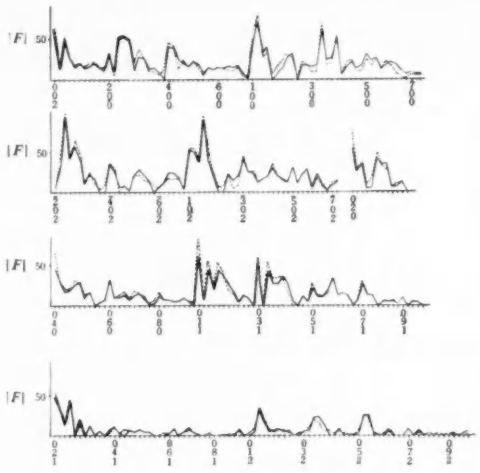

Abb. 3. Graphisches Vergleich der beobachteten und berechneten F-Werte.
(——: $|F_o|$, ------: $|F_c|$)

Fouriersynthesen unternommen. Zur Berechnung der Strukturamplituden wurde die Atomstreukurve für Cu nach Berghuis et al.[3] und für C, N und O nach McWeeny[4] angewandt. In Tabelle I sind die gefundenen Parameterwerte jedes Atoms zusammengestellt. Die letzte Elektronendichteprojektion nach [100] wird in Abb. 1, und nach [010] in Abb. 2 gezeigt, die ein weiteres Maximum G um das zentrale Cu-Atom vorweist; es scheint, daß dieses letztere Maximum von Abbruchs- oder Absorptionseffekt abhängt. In Abb. 3 sind die graphischen Vergleiche der beobachteten und berechneten F-Werte zusammengestellt. Die gefundenen isotropischen Temperaturfaktoren nach [100] und [010] betragen je 3.9 und 2.4, und für die [100]-Projektion wurde ein Zuverlässigkeitsindex R von 0.19 berechnet und für die [010]-Projektion von 0.22, wobei die Kalkulation über alle Reflexionen in der Ausbreitungskugel durchgeführt wurde.

Aus der schematischen Projektion der Atomschwerpunkte (Abb. 4) kann man auch die interatomaren Abstände und Bindungswinkel ersehen. Wie Abb. 4 deutlich zeigt, haben die um das zentrale Cu-Atom koordinierten vier Atome der zwei β-Alanin Moleküle (d. h., O_1^I, O_1^{II}, N^I und N^{II}) in Beziehung zu dem zentralen Metallatom eine plane trans Konfiguration; um das zentrale Metallatom wurde ein ungefähr planes gleichseitiges Viereck mit O_1^I, O_1^{II}, N^I und N^{II} gebildet und zwei Sauerstoffatome des Kristallwassermoleküls (d. h., O_1^I und

3) J. Berghuis, IJ. M. Haanappel, M. Potters, B. O. Loopstra, C. H. MacGillavry und A. L. Veenendaal, *Acta Cryst.*, **8**, 478 (1955).
4) R. McWeeny, ibid., **4**, 513 (1951).

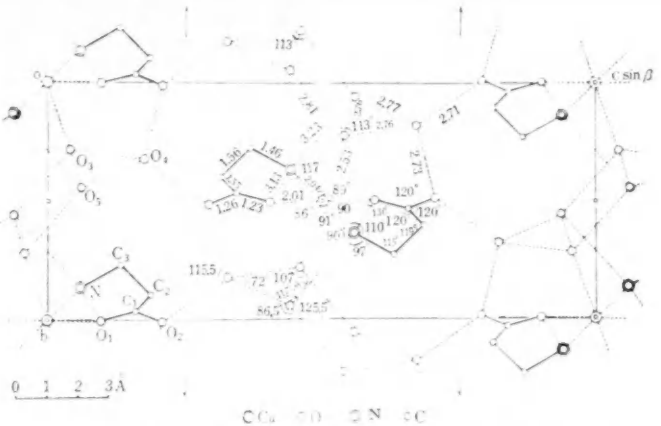

Abb. 4. Schematische Projektion der Atomschwerpunkte nach [100].

Tabelle 2a.

Verbindung	Cu—O	Cu—N	Cu—O (H_2O)
Cu-Ameisensäure Tetrahydrat[5]	{2.00Å {2.01	—	2.36Å
Cu-Prolin Dihydrat[6]	2.03	1.99	2.52
Cu-Glycin Monohydrat[1]	{1.93 {1.95	{1.98 {1.99	2.39
Cu-β-Alanin Hexahydrat	2.01	2.04	2.53

Tabelle 2b.

Verbindung	O—H···O	Typus
Cu-Ameisensäure Tetrahydrat[5]	{2.82Å	Wasser-Carboxyl
	{2.74, 2.78	Wasser-Wasser
Cu-Prolin Dihydrat[6]	2.94, 3.00	Wasser-Carboxyl
Ni-Glycin Dihydrat[7]	2.72, 2.72	Wasser-Carboxyl
Cu-Glycin Monohydrat[1]	2.75, 2.84	Wasser-Carboxyl
Cu-β-Alanin Hexahydrat	{2.71, 2.73	Wasser-Carboxyl
	{2.76, 2.76 {2.77, 2.81	Wasser-Wasser

Tabelle 2c.

Verbindung	N—H···O	Typus
Glycin[8]	{2.77, 2.85, {2.95, 3.07	Amino-Carboxyl
dl-Alanin[9]	{2.80, 2.84, {2.88	Amino-Carboxyl
Cu-Prolin Dihydrat[6]	2.86	Imino-Carboxyl
Ni-Glycin Dihydrat[7]	2.96, 3.13	Amino-Carboxyl
Cu-Glycin Monohydrat[1]	{2.97, 3.01 {3.01	Amino-Carboxyl
	2.97	Amino-Wasser
Cu-β-Alanin Hexahydrat	3.13	Amino-Carboxyl
	3.23	Amino-Wasser

5) R. Kiriyama, H. Ibamoto und K. Matso, ibid., **7**, 482 (1954).

O_3^{II}) nehmen zur gleichen Zeit die auf- und abgehenden Spitzen eines Oktaeders ein, das um das Cu-Atom gebildet wurde. Mit den übrigen vier Kristallwassermolekülen wurden die verschiedene Bindungen zwischen jedem Komplexmolekül in Form von Wasserstoffbrücken, d. h., N—H···O oder O—H···O, gebracht.

Es ist auch sehr interessant, die molekulare Struktur von β-Alanin selbst zu erkennen; Die NH_2- und COO-Gruppen des β-Alanin Moleküls haben eine sogenannte gauche Konfiguration in Beziehung zu der αC—βC Bindung. (Der Winkel zwischen der durch C_1^I, C_2^I und C_3^I und der durch C_1^I, C_2^I und N^I gebildeten Ebene ergab ungefähr 70°.) Bis heute wurde das Resultat über die Struktur des β-Alanins noch nicht veröffentlicht[2], aber wenn das Molekül des β-Alanins im Fall von Komplexbildung die gleiche molekulare Form als im freien Zustand beibehält, kann man daraus schliessen, dass es eine gauche Konfiguration hat.

Zum Schluss wird der Vergleich zwischen den verschiedenen interatomaren Abständen im Kupfersalz des β-Alanins mit denjenigen in anderen begleitenden Substanzen dargestellt (Tabelle 2a, 2b und 2c). Beim Kupfersalz der ω-Aminosäuren ist der Cu—O Abstand etwas kürzer als der Cu—N Abstand, während der Cu—O Abstand bei dem Kupfersalze des Prolins im Gegenteil etwas länger als der Cu—N Abstand ist. Wie in Tabelle 2b und 2c deutlich gezeigt wird, sind die O—H···O Abstände zwischen Wassermolekül und Car-

6) A. M. Mathieson und H. K. Welsh, ibid., **5**, 599 (1952).
7) A. J. Stosick, *J. Am. Chem. Soc.*, **67**, 365 (1945).
8) R. E. Marsh, *Acta Cryst.*, **11**, 654 (1958).
9) J. Donohue, *J. Am. Chem. Soc.*, **72**, 949 (1950).

boxylgruppe bei dem Kupfersalz des β-Alanins etwas kürzer als bei dem Kupfersalz des Glycins, aber die ersteren N—H···O Abstände sind etwas länger als die letzteren. Damit kann man vermuten, dass bei Kristallbildung des Kupfersalzes des Glycins die O—H···O und N—H···O Waserstoffbindungen zugleich die grössere Rolle spielen, während bei Kristallbildung von Kupfersalz des β-Alanins grösstenteils nur bei der O—H···O Wasserstoffbindung durchgeführt wird.

Kristallographische Daten von Kupferisoserintrihydrat

$CuC_3H_5NO_4 \cdot 3H_2O$ (Mol. Gew. 229.67)

Ber.: C, 16.33; H, 5.02; N, 6.35; H_2O, 24.48; Cu, 28.81. Gef.: C, 16.11; H, 4.92; N, 6.49; H_2O, 21.91; Cu, 28.50%.

Gitterkonstanten:

$a = 7.06$ Å, $b = 22.47$ Å, $c = 15.77$ Å, $\beta = 109°43'$.

Gefundene Dichte:

1.88 g/cc (Schwebemethode).

Die Zahl der Moleküle pro Elementarzelle: $z = 12$.

Raumgruppe: $C_{2h}^5 - P2_1/c$ (Monoklinisch).

Bei dieser Raumgruppe ist die Zahl der Moleküle in jeder Elementarzelle vier, wenn das Molekül die allgemeine Lage einnimmt.

Demnach sind in diesem Kristall drei kristallographisch verschiedenartige Moleküle, jeder für sich vier, vorhanden.

Meinem verehrten Lehrer, Herrn Professor Dr. I. Nitta, danke ich herzlich für wertvolle Anregungen und für seine stete Unterstützung bei der Durchführung dieser Arbeit. Dabei sei auch Herrn Dr. Y. Sasada für seine hilfreichen Ratschläge gedankt.

Chemisches Institut
Naturwissenschaftliche Fakultät
Universität Osaka
Nakanoshima Osaka

Quinones. I. The Syntheses of Acetyl-p-benzoquinone Derivatives and 2-Acetylnaphthoquinone

By Eturo Kurosawa

(Received August 8, 1960)

Acetyl-*p*-benzoquinone derivatives are expected to show interesting chemical and biological properties, owing to the presence of an acetyl carbonyl group conjugated to quinone double bond. However, only acetyl-*p*-benzoquinone has been reported in the literature[1].

An attempt was made as described below to synthesize several acetyl-*p*-benzoquinone derivatives, e. g., 2-methyl-5-acetyl-*p*-benzoquinone (acetyltoluquinone), 2, 3-dimethyl-5-acetyl-*p*-benzoquinone (acetyl-*o*-xyloquinone) and 2-acetyl-1, 4-naphthoquinone by the oxidation of corresponding acetylhydroquinone derivatives with silver oxide.

Acetylhydroquinone has been synthesized by several methods: viz., i) by the action of zinc chloride on hydroquinone in glacial acetic acid[2], ii) by the Fries migration of hydroquinone diacetate[3], and iii) by the action of acetyl chloride on hydroquinone dimethyl ether in the presence of aluminum chloride followed by demethylation[1]. But because of the complicated procedures or low yield, these methods did not give good results.

It has been found that these acetylhydroquinone derivatives are obtained in good yield as a result of the action of boron trifluoride on hydroquinone derivatives in glacial acetic acid[4]. Acetylation was carried out by the saturation of boron trifluoride to the suspension of hydroquinone derivatives in excess glacial acetic acid. 2-Acetylhydroquinone (III, R=R′=H) was obtained directly by this method from hydroquinone (I, R=R′=H) in an almost quantitative yield. But in the cases of 2-methyl- and 2, 3-dimethylhydroquinone and naphthohydroquinone, there were obtained mono- or diacetates of corresponding acetyl derivatives. For example, acetylation of 2-

1) T. Irie and E. Kurosawa, presented at the 7th Annual Meeting of the Chemical Society of Japan, Tokyo, April, 1954; M. C. Kloetzel, R. P. Dayton and B. Y. Abadir, *J. Org. Chem.*, **20**, 38 (1955); N. N. Vorozhtsov and V. P. Makaev, *D. I. Statei obschei Khim. Akad. Nauk, U. S. S. R.*, **1**, 553 (1953).

2) M. Nencki and W. Schmidt, *J. Prakt. Chem.*, **23**, 546 (1881).

3) "Organic. Syntheses," Vol. 28, New York (1948), p. 42; R. D. Desai and C. K. Mavani, *Proc. Indian Acad. Sci.*, **29A**, 267 (1949); P. S. Rao and K. L. Gakhar, ibid., **30A**, 327 (1949).

4) E. Kurosawa, *J. Chem. Soc. Japan, Pure Chem. Sec.* (*Nippon Kagaku Zasshi*), **78**, 312 (1957).

methylhydroquinone (I, R=H, R'=CH_3) afforded pale yellow crystals, then after several recrystallizations from dilute ethanol, colorless crystals were obtained. This material melted at 112°C and exhibited no coloration with ferric chloride in ethanol.

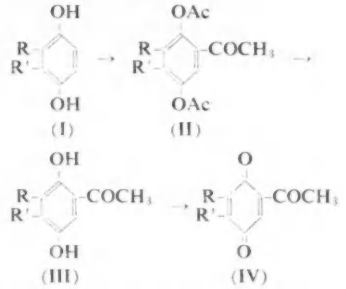

After saponification of this diacetate (II, R=H, R'=CH_3) with aqueous sodium hydroxide containing a small amount of sodium hydrosulfite, 2-methyl-5-acetylhydroquinone (III, R=H, R'=CH_3) was obtained; it melted at 145°C. Similarly, there was obtained 2, 3-dimethyl-5-acetylhydroquinone diacetate (II, R=R'=CH_3), m. p. 98°C, which was hydrolyzed to corresponding hydroquinone (III, R=R'=CH_3), m. p. 151°C. In the case of acetylation of naphthohydroquinone, 2-acetyl-4-acetoxynaphthol (V, R=$COCH_3$), m. p. 101°C, was obtained and it was hydrolyzed to 2-acetylnaphthohydroquinone (V, R=H).

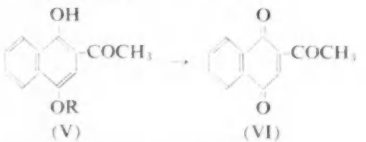

2-Methyl-5-acetylhydroquinone was oxidized quantitatively to 2-methyl-5-acetyl-*p*-benzoquinone (IV, R=H, R'=CH_3) by being shaken with silver oxide and anhydrous potassium carbonate in dry benzene. When 2, 3-dimethyl-5-acetylhydroquinone was oxidized under the same conditions, an oily product was obtained. It gave the stimulative odor characteristic to quinone derivative and it was easily reduced to 2, 3-dimethyl-5-acetylhydroquinone by shaking its chloroform solution with aqueous sodium hydrosulfite. In infrared spectrum, this compound showed the band attributed to quinone carbonyl at 1640 cm^{-1} as shown in Fig. 1, but no band in the region of about 3300 cm^{-1}. Similarly, 2-acetylnaphthohydroquinone was oxidized to 2-acetyl-1, 4-naphthoquinone (VI), m. p. 83~84°C, in good yield.

2-Acetyl-*p*-benzoquinone and 2-methyl-5-acetyl-*p*-benzoquinone have the bands attributed to quinone carbonyl at 1645 cm^{-1} and 1635 cm^{-1}

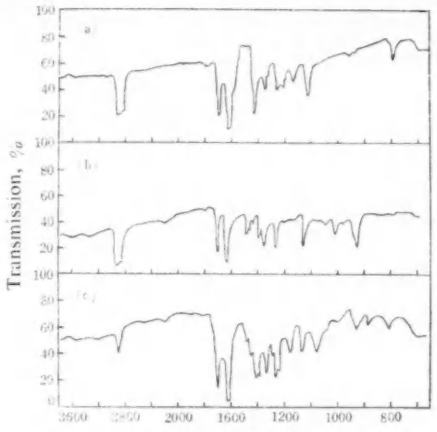

Fig. 1. IR spectra.
(a) Acetylbenzoquinone (Nujol)
(b) Acetyltoluquinone (Nujol)
(c) Acetyl-*o*-xyloquinone (direct)

in infrared spectrum as shown in Fig. 1. Likewise, 2, 3-dimethyl-5-acetyl-*p*-benzoquinone and 2-acetyl-1, 4-naphthoquinone have the bands attributed to quinone carbonyl at 1640 cm^{-1} and 1662 cm^{-1}, respectively. In general, it has been reported[5], that *p*-benzoquinone has the band attributed to quinone carbonyl at 1663 cm^{-1}; when the substituent is a negative group as chlorine or bromine, the quinone carbonyl band shifts to a higher frequency, and when the substituent is positive, the band shifts to a lower frequency. The position of the absorption maximum can be qualitatively interpreted by the sum of I-effect and M-effect. Contrary to expectation that acetyl-*p*-benzoquinone derivatives would show the band attributed to quinone carbonyl at a higher frequency than that of *p*-benzoquinone, due to the influence of the acetyl carbonyl group, these compounds show the bands at a considerable lower frequency as shown in Fig. 1.

These results indicate the existence of a large M-effect in the molecules of acetyl-*p*-benzoquinone derivatives. For the confirmation of this fact, the author attempted to find the relationship between the frequency of quinone carbonyl in infrared spectrum and the other properties of quinone derivatives. L. J. Bellamy[6] reported the existence of a straight lineal relationship between the sum of electronegativity of substituents of ethylene derivatives and frequency of CH_2-deformation (δCH_2), and between the molecular refractions of

5) P. Yates, M. I. Ardao and L. F. Fieser, *J. Am. Chm. Soc.*, **78**, 650 (1956).
6) L. J. Bellamy, *J. Chem. Soc.*, **1955**, 4221.

functional derivatives and frequencies of the carbonyl band of carboxylic acids. The author gave attention to the oxidation-reduction potential of quinone derivatives which is one of the important properties of these compounds. It has been suggested that certain quinones, e.g., ubiquinone, play a part in the oxidation-reduction process of living matter[7] and the feature of the reactions is interpreted with the oxidation-reduction potential[8].

The oxidation-reduction potentials and the frequencies of quinone carbonyl bands of some benzoquinone derivatives are listed in Table I. When the oxidation-reduction potentials are plotted against the frequency of quinone carbonyl bands, the resulting curve is a nearly straight line as shown in Fig. 2.

This result indicates that the hypsochromic shift of the quinone carbonyl band resultant from the effect of the substituent linearly depends on the elevation of oxidation-reduction potential of the quinones.

TABLE I. CARBONYL FREQUENCIES AND OXIDATION-REDUCTION POTENTIALS OF BENZOQUINONE DERIVATIVES

Benzoquinone	Frequency cm^{-1} [a]		Potential V.[b]
	in CS_2	Nujol	
Chlorobenzoquinone	1678		0.736[c]
Benzoquinone	1668	1663	0.711
Toluquinone	1663	1663	0.656
o-Xyloquinone	1660	1660	0.588
p-Xyloquinone	1660	1668	0.597
m-Xyloquinone	1657	1653	0.592
Thymoquinone	1660		0.589[c]
Pseudocumoquinone	1657*	1650	0.536
Duroquinone	1642	1639	0.471
Ubiquinone[d]	1653		0.542

a) P. Yates, M. I. Ardao and L. F. Fieser, *J. Am. Chem. Soc.*, **78**, 650 (1956).
b) See Ref. 8.
c) Conant and Fieser, *J. Am. Chem. Soc.*, **45**, 2194 (1923).
d) J. F. Pennock, R. Ruegg, U. Schwieter and O. Wiss, *Helv. Chim. Acta*, **41**, 3243 (1958).
* Inflection.

TABLE II. CARBONYL FREQUENCIES AND OXIDATION-REDUCTION POTENTIALS OF ACETYL-*p*-BENZOQUINONE DERIVATIVES

Benzoquinone	Frequency, cm^{-1}		Potential V.
	in CS_2	Nujol	
Acetylbenzoquinone	1668	1645	0.564
Acetyltoluquinone	1662	1645	0.539
Acetyl-*o*-xyloquinone	1654	1640	0.504

7) R. H. Thomson, "Naturally Occurring Quinones", Butterworths Scientific Publications, London (1957), p. 1; W. Mansfield Clark, "Oxidation-Reduction Potentials of Organic Systems", The Williams and Wilkins Company, Baltimore (1960).
8) Fausto Ramirez, et al., *J. Am. Chem. Soc.* **81**, 4338 (1959).

TABLE III. CARBONYL FREQUENCIES AND OXIDATION-REDUCTION POTENTIALS OF 1,4-NAPHTHOQUINONE DERIVATIVES

Substituent	Frequency, cm^{-1} in CCl_4	Potential V.[a]
2-Chloro-	1684	0.510
2-Bromo-	1686	0.509
2,3-Dichloro-	1687	0.498
None	1675	0.483
2-Methyl-	1670	0.422
2,3-Dimethyl-	1660	0.340
2,6-Dimethyl-	1668	0.405
2,7-Dimethyl-	1673	0.407
2-Methoxy-	1660	0.369

a) W. Mansfield Clark, "Oxidation-Reduction Potentials of Organic Systems", The Williams & Wilkins Company, Baltimore (1960), p. 376.

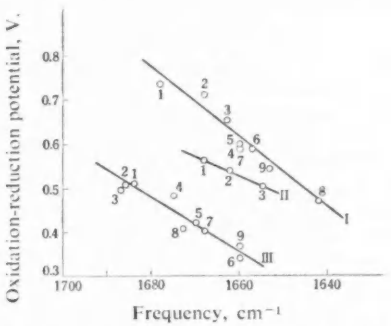

Fig. 2. Carbonyl frequency vs. oxidation-reduction potential.
I: Benzoquinone derivatives (in CS_2)
1. Chlorobenzoquinone
2. Benzoquinone
3. Toluquinone
4. *o*-Xyloquinone
5. *p*-Xyloquinone
6. *m*-Xyloquinone
7. Thymoquinone
8. Duroquinone
9. Ubiquinone
II: Acetylbenzoquinone derivatives (in CS_2)
1. Acetylbenzoquinone
2. Acetyltoluquinone
3. Acetyl-*o*-xyloquinone
III: Naphthoquinone derivatives (in CCl_4)
1. 2-Chloronaphthoquinone
2. 2-Bromonaphthoquinone
3. 2,3-Dichloronaphthoquinone
4. Naphthoquinone
5. 2-Methylnaphthoquinone
6. 2,3-Dimethylnaphthoquinone
7. 2,6-Dimethylnaphthoquinone
8. 2,7-Dimethylnaphthoquinone
9. 2-Methoxynaphthoquinone

The author determined the oxidation-reduction potentials of acetylbenzoquinone derivatives by the polarographic method. The buffer solution used was that of Smith et al.[9] The results, given in Table II and Fig. 2, show that these acetyl benzoquinone derivatives have relatively low potentials, but the quinone carbonyl frequencies are slightly higher than the other benzoquinone derivatives as compared with the potentials.

In general, the effect of substituents upon the oxidation-reduction potential has not been interpreted sufficiently, but in this case, the following explanation is possible. When the substituent of benzoquinone derivative gives a fairly large inductive effect in comparison with the M-effect against quinone carbonyl, a straight linear relationship between quinone-carbonyl frequency in the infrared spectrum and oxidation-reduction potential exists as shown in Fig. 2.

In the case of naphthoquinone and anthraquinone, however, relatively high frequencies of quinone carbonyl-bands against the oxidation-reduction potentials were observed as shown in Table III and Fig. 2. This fact is interpreted as due to the influence of the M-effect of an aromatic ring against quinone carbonyl.

Similarly, it is possible that in the cases of acetylbenzoquinone derivatives, deviation from the above linear relationship, as shown in Fig. 2, may be interpreted as due to the fairly large M-effect of the acetyl group against quinone carbonyl in comparison with the inductive effect.

From these results, it is expected that the interesting properties may be gained about acetylquinone derivatives by reason of the low oxidation-reduction potential and the lack of substituent in β-position toward quinone carbonyl and acetyl carbonyl.

Further investigation concerning the effect of the substituent upon the oxidation-reduction potential and the reactivity of acetylbenzoquinone derivatives is in progress.

Experimental

2-Methyl-5-acetylhydroquinone. — Methylhydroquinone (5 g.) was suspended in glacial acetic acid (30 cc.) and warmed on a water bath. Boron trifluoride was passed into the mixture. The suspension slowly dissolved and a red color appeared. The saturation of boron trifluoride afforded a clear red solution which was heated for further 5 hr. on a water bath. The reaction mixture was then poured into ice water. The crystals thus separated (crude product) were collected by filtration and dried. After repeated recrystallizations from dilute ethanol, colorless needles were obtained, m. p. 112°C. (Found: C, 62.35; H, 5.78%). This material was found to be identical with 2-methyl-5-acetylhydroquinone diacetate[10] by use of the mixed melting point method.

The above crude product was treated with 2 N sodium hydroxide containing a small amount of sodium hydrosulfite for half an hour and then the alkaline solution was neutralized with 2 N hydrochloric acid. The crystals thus obtained were filtered and recrystallized from dilute ethanol. 2-Methyl-5-acetylhydroquinone was obtained as yellow needles, m. p. 145°C. (Found: C, 65.10; H, 6.17%).

2-Methyl-5-acetylbenzoquinone. — 2-Methyl-5-acetylhydroquinone (5 g.), anhydrous potassium carbonate (5 g.) and freshly prepared silver oxide (15 g.) were shaken in dry benzene (50 cc.) for 5 min. at 40°C. The reaction mixture was filtered and the solids were shaken with fresh benzene. On evaporation of the combined solution under reduced pressure, orange yellow crystals were obtained. After sublimation in vacuo or recrystallization from carbon disulfide, this substance melted at 79.5°C, yield 94%.

Found: C, 65.90; H, 4.95. Calcd. for $C_9H_8O_3$: C, 65.85; H, 4.88%.

2,3-Dimethyl-5-acetylhydroquinone. — *o*-Xylohydroquinone (5 g.) was suspended in glacial acetic acid (30 cc.) and warmed on a water bath. Boron trifluoride was passed into the mixture. The suspension slowly dissolved and a yellow color appeared. After saturation of boron trifluoride, the reaction mixture was heated for further 5 hr. on a water bath. After the solution was poured into ice water, the resulting crystals (crude product) were collected and dried. After repeated recrystallizations from dilute ethanol, colorless needles were obtained, m. p. 97~98°C. This material exhibited no coloration with ferric chloride in ethanol and gave positive result to the iodoform test; by the mixed melting point method, it was found to be identical with 2,3-dimethyl-5-acetylhydroquinone diacetate (see below).

The above crude product was treated with 2 N alcoholic sodium hydroxide for 5 min. and then the alkaline solution was neutralized with 2 N hydrochloric acid. The crystals thus obtained were recrystallized from dilute ethanol. Yellow needles were obtained, m. p 151°C, yield 5.9 g. (91%).

Found: C, 66.83; H, 6.92. Calcd. for $C_{10}H_{12}O_3$: C, 66.67; H, 6.67%.

This material exhibited green coloration with ferric chloride in ethanol and a positive result to the iodoform test.

Acetylation of 2,3-Dimethyl-5-acetylhydroquinone. —2,3-Dimethyl-5-acetylhydroquinone (0.5 g.) was refluxed for 2 hr. in acetic anhydride (2 cc.). The solvent was removed under reduced pressure and the residue was sublimated in vacuo. Diacetate m. p. 97~98°C, was obtained as colorless needles.

Found: C, 63.64; H, 5.94. Calcd. for $C_{14}H_{16}O_5$: C, 63.64; H, 6.06%.

9) L. I. Smith, I. M. Kolthoff, S. Wawzonek and P. M. Ruoff, *J. Am. Chem. Soc.*, **63**, 1018 (1941).

10) R. D. Desai and C. K. Mavani, *Proc. Indian Acad. Sci.*, **29A**, 269 (1949).

2,4-Dinitrophenylhydrazone of 2,3-Dimethyl-5-acetylhydroquinone. — 2, 3-Dimethyl-5-acetylhydroquinone and 2,4-dinitrophenylhydrazine reacted in ethanol in the presence of a few drops of concentrated sulfuric acid. Crystals deposited were collected and recrystallized from butanol. Orange red needles were obtained, m. p. 271°C.

Found: C, 53.26; H, 4.55. Calcd. for $C_{16}H_{16}O_6N_4$: C, 53.33; H, 4.45%.

2,3-Dimethyl-5-acetylbenzoquinone. — 2,3-Dimethyl-5-acetylhydroquinone (5 g.), anhydrous potassium carbonate (5 g.) and freshly prepared silver oxide (15 g.) were shaken in dry benzene (50 cc.) for 5 min. at 35°C. The reaction mixture was filtered and the solid was shaken with fresh benzene. On evaporation of combined solution under reduced pressure, 2,3-dimethyl-5-acetylbenzoquinone was obtained in yellow brown oily state, yield 92%.

Found: C, 67.52; H, 5.68. Calcd. for $C_{10}H_{10}O_3$: C, 67.41; H, 5.62%.

2-Acetylnaphthohydroquinone. — Naphthohydroquinone (5 g.) was suspended in glacial acetic acid (30 cc.) and under water cooling, boron trifluoride was passed into the suspension. Under heat evolution, hydroquinone dissolved slowly and a clear red-brown solution was obtained. After saturation with boron trifluoride the reaction mixture was immediately poured into ice water. The orange red product (crude product) was filtered; after repeated recrystallizations from dilute ethanol, it melted at 101°C.

Found: C, 68.96; H, 5.00. Calcd. for $C_{14}H_{12}O_4$: C, 68.85; H, 4.93%.

In the infrared spectrum, this material has the bands attributed to OH at 3300 cm^{-1} (broad), acetate carbonyl at 1750 cm^{-1} and carbonyl (bonded) at 1630 cm^{-1}. It exhibited greenish blue coloration with ferric chloride in ethanol solution and a positive result to the iodoform test.

The above crude product was dissolved in 2 N aqueous sodium hydroxide containing a small amount of sodium hydrosulfite. After 20 min., the insoluble materials were filtered off, the solution was neutralized with 2 N hydrochloric acid and the resulting crystals collected by filtration. After repeated recrystallizations from dilute ethanol, yellow crystals were obtained, m.p. 206~208°C, yield 3.5 g. (56%).

Found: C, 70.92; H, 4.96. Calcd. for $C_{12}H_{10}O_3$: C, 71.29; H, 4.96%.

This material exhibited yellow brown coloration with ferric chloride in an ethanol solution and a positive result to the iodoform test. In the infrared spectrum, it has the bands attributed to OH at about 3300 cm^{-1} (bonded) and acetyl carbonyl at 1618 cm^{-1} (bonded.).

2-Acetylnaphthoquinone[11]**.** — 2-Acetylnaphthohydroquinone (1 g.), anhydrous potassium carbonate (1 g.) and freshly prepared silver oxide (3 g.) were shaken in dry benzene at 40°C for 15 min. The reaction mixture was filtered and the solvent was removed under reduced pressure. The residue was recrystallized from light petroleum; golden yellow needles were obtained, m. p. 83~84°C, yield 0.84 g. (85%). (Found: C, 71.85; H, 3.87%).

Determinations of Oxidation-Reduction Potential by Polargroaphic Method. — Oxidation-reduction potential measurement was carried out by preparing 0.001 M solution of quinone derivatives in a buffer solution containing 0.1 N sodium acetate and 0.1 N acetic acid in 50% ethanol at pH 5.4. In order to find the standard normal hydrogen electrode the potentials were calculated for pH of zero, using 0.246 V. as the standard potential of the saturated calomel electrode.

The author wishes to thank Professor Tosi Irie of Hokkaido University for his kind guidance throughout this work.

Department of Chemistry
Faculty of Science
Hokkaido University, Sapporo

11) P. Friedländer, *Ber.*, **28**, 1950 (1895).

Interaction Polarization of the Hydrogen Bonded Complexes. II

By KO KIMURA and Ryoichi FUJISHIRO

(Recieved August 22, 1960)

An increase of the molecular polarization due to hydrogen bonding reported by Sutton et al.[1], by Tsubomura[2] and also by the present authors[3] is one of variations of dielectric properties arising from the molecular interaction. Many obstacles are present in the precise determination of the molecular polarizations for the hydrogen bonded complexes from the measurements of dielectric constants, specific volumes and refractive indexes of ternary solutions (proton donors, proton acceptors and inert solvents). The most important point is

1) J. R. Hulett, J. A. Pegg and L. E. Sutton, *J. Chem. Soc.*, **1955**, 3901.
2) H. Tsubomura, This Bulletin, **31**, 435 (1958).
3) K. Kimura and R. Fujishiro, ibid., **32**, 433 (1959).

whether or not Debye's equation holds even approximately in ternary solutions, because the measurements are carried out in such solutions that the interaction between proton donors and proton acceptors can take place. This problem will be discussd elsewhere. In so far as polarization values for the complexes are calculated by the use of Debye's equation, we must devise a way to make the difference as small as possible between the dielectric constant of a pure solvent and that of a ternary solution containing large quantities of a proton acceptor. Otherwise the polarization values obtained from observed dielectric constants and specific volumes are not reliable because of the solvent effect. In order to make the dielectric constants of ternary solutions with high concentrations of proton acceptors as low as possible, it is necessary to use nonpolar proton acceptors such as *p*-dioxane and bipyridyl. For example, it follows that when we want to investigate the polarization value of the phenol + pyridine complex, examination of the phenol + bipyridyl complex instead of the phenol + pyridine complex itself is more reasonable from consideration of the solvent effect.

In the previous paper, the dielectric measurements were carried out for some of the OH···O hydrogen bonded systems by using benzene as an inert solvent, and the analysis was performed based on a model with the covalent character of the hydrogen bonds[4]. This report describes first the results of dielectric measurements for the OH···N hydrogen bonded systems such as benzyl alcohol + bipyridyl, benzyl alcohol + triethylamine, phenol + bipyridyl and phenol + triethylamine by exactly the same procedure as in the previous report, and secondly the correlation between the dielectric data and the infrared spectra.

Experimental

Materials used in this work were purified by the method described in Weissberger's text-book[5]. Benzene was used as a solvent throughout this work. It was frozen three times after being shaken with concentrated sulfuric acid and with dilute sodium hydroxide, dried over phosphorous pentoxide, and then fractionally distilled through a "Heli-Pack" column. Benzyl alcohol was purified by shaking with aqueous potassium hydroxide solution and extracting with ether, which had been freed from peroxides. The extract was treated with saturated sodium hydrogen sulfite solution and dried over potassium carbonate. After the removal of ether, benzyl alcohol was dried over lime and distilled under reduced pressure. α,α'-Bipyridyl (the special grade made by Wako Pure Chemicals Co., Ltd.) was dried in a desiccator and used without further purification. Its melting point was 70.5°C. The measurements of dielectric constants ε, refractive indexes n and specific volumes v were carried out at 25°C with the apparatus already reported[4].

Results

The results of the measurements of ε, n^2 and v for the four ternary systems i.e., benzyl alcohol + α,α'-bipyridyl + benzene, benzyl

TABLE I. POLARIZATION DATA AND FORMATION CONSTANTS OF THE HYDROGEN BONDED COMPLEXES

Benzyl alcohol + α,α'-Bipyridyl (The weight per cent of α,α'-bipyridyl is 4.011.)		Benzyl alcohol	
$\varepsilon = 2.2988 + 3.36\,w$			
$n^2 = 2.2555 + 0.07\,w$			
$v = 1.13442 - 0.163\,w$			
P'	98.7 cc.		
K	5.5 l./mol.		
P_1	102.6 cc.	P	93.8 cc.
R_D	32.4 cc.	R_D	32.5 cc.
μ_1	1.85 D	μ	1.73 D
Benzyl alcohol + Triethylamine (The weight per cent of triethylamine is 9.300, or 29.95.)			
$\varepsilon = 2.3025 + 5.70\,w$		$\varepsilon = 2.3512 + 6.18\,w$	
$n^2 = 2.2104 + 0.156\,w$		$n^2 = 2.1411 + 0.240\,w$	
$v = 1.16696 - 0.282\,w$		$v = 1.21583 - 0.347\,w$	
P'	145.6 cc.	P'	157.9 cc.
K	2.9 l./mol.	K	2.91./mol.
P_1	168.2 cc.	P_1	167.0 cc.
R_D	30.8 cc.	R_D	31.4 cc.
μ_1	2.57 D	μ_1	2.57 D
Phenol + α,α'-Bipyridyl (The weight per cent of α,α'-bipyridyl is 2.527.)		Phenol	
$\varepsilon = 2.2900 + 4.80\,w$			
$n^2 = 2.2512 + 0.168\,w$			
$v = 1.13811 - 0.259\,w$			
P_1	108.7 cc.		
K	55 l./mol.		
P_1	111.7 cc.	P	84.6 cc.
R_D	27.2 cc.	R_D	27.6 cc.
μ_1	2.03 D	μ	1.67 D
Phenol + Triethylamine (The weight per cent of triethylamine is 28.35.)			
$\varepsilon = 2.3430 + 10.54\,w$			
$n^2 = 2.1459 + 0.380\,w$			
$v = 1.21204 - 0.424\,w$			
P'	214.2 cc.		
K	83.8 l./mol.		
P_1	214.8 cc.		
R_D	28.0 cc.		
μ_1	3.02 D		

4) C. A. Coulson and U. Danielsson, *Arkiv Fysik*, **8**, 239, 245 (1954); H. Tsubomura, This Bulletin, **27**, 445 (1954).
5) A. Weissberger et al., "Organic Solvents", Interscience Publishers, New York (1955).

TABLE II

	$\Delta\mu_T$	$\Delta\mu_D$	[III]	$\Delta\nu$	
Benzyl alcohol + bipyridyl	0.19D	0.19D	1.6%	240 cm^{-1}	a)
Benzyl alcohol + triethylamine	1.17	1.17	10	400	b)
Phenol + bipyridyl	0.48	0.39	3.4	480	c)
Phenol + triethylamine	1.54 (1.00)*	1.45	13	600	d)
Benzyl alcohol + dioxane	0.10	0.10	0.7	110	e)
Phenol + dioxane	0.29	0.21	1.5	250	f)

* This value reported by Sutton et al.[1] was calculated by the use of the formula $P=\sum f_i p_i$.

a) Measurements for the ethanol + pyridine system were carried out by the present authors with a Perkin-Elmer model 21 spectrophotometer.

b) C. H. Huggins and G. C. Pimental, *J. Phys. Chem.*, **60**, 1615 (1956).

c) N. Fuson, P. Pineau and M-L. Josien, *J. Chem. Phys.*, **55**, 454 (1958).

d) Measurements were carried out by the present authors with a Perkin-Elmer model 21 spectrophotometer.

e) N. D. Coggeshall and E. L. Saier, *J. Am. Chem. Soc.*, **73**, 5414 (1951).

f) H. Tsubomura, *J. Chem. Phys.*, **24**, 927 (1956).

alcohol + triethylamine + benzene, phenol + α,α'-bipyridyl + benzene and phenol + triethylamine + benzene, are expressed in Table I by formulae relating ε, n^2 and v to w, respectively, where w represents the weight fraction of the proton donors. The calculation of the molecular polarizations from these experimental data was performed according to the method described in the previous paper[5]. Polarization values P' thus obtained are also shown in Table I, together with those for the corresponding binary systems already reported i. e., benzyl alcohol + benzene and phenol + benzene. P' will contain the polarization for the free proton donor as well as that for the complex. If the fraction of the proton donor existing in the form of the complex in the limit $w\rightarrow 0$ is estimated by the use of the formation constant K of the complex, the true polarization value P_1 for the complex is determined by both the polarization value P for the free proton donor and P'. The formation constants of the complexes tabulated in Table I are either taken from literatures or measured by the present authors. As K for the benzyl alcohol + α,α'-bipyridyl complex is expected to be of the same order as that for the ethanol + pyridine complex, we measured the ultraviolet spectra[6] of the latter system by using *n*-heptane as a solvent, and determined K from the variation of the intensity of the $n\rightarrow\pi$ electronic transition of pyridine[7] due to the addition of ethanol. K for the benzyl alcohol + triethylamine complex is reported to be about 2.9 l./mol.[8] by the measurement of infrared absorptions. When the content of triethylamine is 9.30 or 29.95 weight per cent, P_1 is calculated to be 168.2 cc. or 167.0 cc. The difference 1.2 cc. between these two values is attributable to the solvent effect. On the other hand, one can deduce both K and P_1 from P's in two concentrations of triethylamine. The calculated values of K and P_1 are 3.2 l./mol. and 166.2 cc., respectively. This result indicates the fact that the reliable association constant can be obtained in the case of the complexes of the small K and large $\Delta P=P_1-P$. As K for the phenol + α,α'-bipyridyl complex, we used the formation constant for the phenol + pyridine[9] determined by the measurement of infrared absorptions. The value of K for the phenol + triethylamine complex is reported to be about 83.8 l./mol.[10] by the measurement of ultraviolet absorptions.

If we assume that the distortion polarization does not vary with complex formation and is equal to the molecular refraction R_D at the sodium D line, then we can calculate the permanent dipole moment μ_1 for the proton donor forming the complex. This assumption is not always reasonable, because it is conceivable to ascribe ΔP to an increase of the atomic polarization. However, we shall carry out tentatively the analysis of experimental data under the assumption that ΔP arises from the intermolecular charge transfer. The vector subtraction of the dipole moment μ of the free proton donor from μ_1 gives the increment of the dipole moment due to complex formation. The results of the vector calculations are summarized in Table II.

6) Ultraviolet absorption spectra were measured with a Beckman model DU spectrophotometer.

7) G. J. Brealey and M. Kasha, *J. Am. Chem. Soc.*, **77**, 4462 (1955).

8) G. M. Barrow and E. A. Yerger, ibid., **76**, 5247 (1954).

9) N. Fuson, P. Pineau and M-L. Josien, *J. chim. phys.*, **55**, 454 (1958).

10) S. Nagakura and M. Gouterman, *J. Chem. Phys.*, **26**, 881 (1957).

Discussion

It is generally believed that the hydrogen bond is not only of the electrostatic, but also of the covalent character. If the hydrogen bond is somewhat of the covalent character, structure III among the following three

(I) O H···Y

(II) O^- H^+···Y

(III) O^-···H−Y^+

will play a relatively important role. Then the observed increment of the dipole moment $\Delta\vec{\mu}_T=\vec{\mu}_1-\vec{\mu}$ is considered to be due to the contribution of structure III in the case of benzyl alcohol + triethylamine, whereas in the phenol + triethylamine system, polarization of π-electrons of phenol will, to a certain extent, arise owing to the lone pair field of triethylamine. This induced moment will be of the magnitude of 0.16 D, as estimated from the detailed description for the phenol + dioxane system. In systems such as phenol + triethylamine, therefore, the vector subtraction of 0.16 D from $\Delta\mu_T$ gives the average increment of the dipole moment due to the contribution of the structure III. Furthermore, in the case of phenol + bipyridyl, it must be considered that polarization of π-electrons will be induced in pyridine owing to the proton field of phenol. This calculation is very difficult, and we could not estimate this value. The increase of the dipole moment $\Delta\mu_D$ arising from delocalization in this system, therefore, may be smaller than the tabulated $\Delta\mu_D$ which gives the upper limit.

If we estimate the O···Y distance from the shift of the wave number of the OH stretching vibration[11], the electric moment for structure III is evaluated. Moreover, when we suppose that the ratio of the weight of structure I to that of structure II is the same as in a free state, then we can estimate the contribution of structure III from the increment of the dipole moment. The results thus obtained are shown for all systems in Table II. The large contribution of structure III means the weakening of the OH bond, which is reflected on the decrease of the force constant of the OH bond, and hence leads to a decrease in the wave number of the OH stretching vibration. The wave number shift $\Delta\nu$ of the OH stretching vibration has often been correlated with the strengths of the hydrogen bonds. Therefore, we may expect the correlation of $\Delta\nu$ with the weight of structure III. The observed $\Delta\nu$'s for the OH stretching vibration are given in the last column in Table II. The weight of structure III is plotted against $\Delta\nu$ in Fig 1. The four complexes lie on a straight line except benzyl alcohol + triethylamine and phenol + triethylamine, but the latter two complexes show extraordinarily great values for the weight of structure III in spite of the small $\Delta\nu$. If the spectroscopic results are correct, it seems that there are some questions about the above-mentioned treatment of the dielectric data. This is because it is natural to expect that the weight of structure III varies continuously with $\Delta\nu$. However, it has already been found by Barrow[12] that when pyridine and triethylamine are used as proton acceptors, the latter shows a character considerably different from that of the former. He distinguished acetic acid + pyridine from acetic acid + triethylamine, and called the former and the latter the hydrogen bonded complex and the hydrogen bonded ion pair, respectively. If we accept the idea suggested by Barrow, the hydrogen bonded complex belongs to a different category from the hydrogen bonded ion pair, that is to say, there is a distinct boundary between the former and the latter. The dielectric data suggest this idea, but it seems difficult to understand even qualitatively that benzyl alcohol + triethylamine is of the ion pair character without showing an intermediate character. This point will be discussed elsewhere in near future.

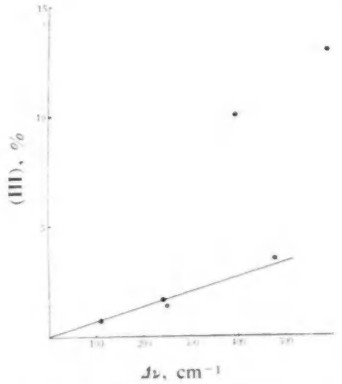

Fig. 1. The correlation of the weight of the structure III with $\Delta\nu$.

Summary

The dielectric measurements were carried out for benzyl alcohol + α,α'-bipyridyl, benzyl alcohol + triethylamine, phenol + α,α'-bipyridyl and phenol + triethylamine by using

11) K. Nakamoto, M. Margoshes and R. E. Rundle, *J. Am. Chem. Soc.*, **77**, 6480 (1955).

12) G. M. Barrow, ibid., **78**, 5802 (1956).

benzene as a solvent, and the polarization value for each system was calculated. The additional moments due to complex formation were evaluated, as in the previous paper, from both the polarization data and the spectroscopically determined formation constants. Then the weight of structure III was estimated and correlated with the wave number shift $\Delta\nu$ of the OH stretching vibration.

The authors wish to express their thanks to Dr. M. Momotani and Mr. M. Shiro of the Momotani Juntenkan Co., Ltd. for their kind permission to use an infrared spectrometer. The expense of this work has been partly defrayed by a grant from the Ministry of Education.

Department of Chemistry
Faculty of Science
Osaka City University
Kita-Ku, Osaka

Studies on Antibiotics and Related Substances. XII. Syntheses of 10-Oxo-11-dodecenoic Acid and 11-Oxo-12-tridecenoic Acid, Antitumor Substances[1]

By Mitsuhiro KINOSHITA and Sumio UMEZAWA

(Received August 18, 1960)

A recent publication[2] from this laboratory described the syntheses and antitumor activities of some methylene derivatives of ketocarboxylic acids, among which the calcium salt of 4-keto-5-hexene-1-carboxylic acid was found to have low toxicity as well as strong activity. The present paper is concerned with an extension of this work and presents the syntheses and antitumor activities of two higher members of even- and odd-numbered carbon acids of the above mentioned series. The syntheses have been worked out as shown in the accompanying chart.

$HO_2C(CH_2)_7CO_2C_2H_5$ → $Br(CH_2)_7CO_2C_2H_5$
I II

→ $CH_3CO\cdot CH\cdot(CH_2)_7CO_2C_2H_5$ → IVa
$CO_2C_2H_5$
III

$CH_3CO(CH_2)_nCO_2H$
IVa, IVb

→ $HCl\cdot(CH_3)_2N(CH_2)_2CO(CH_2)_nCO_2H$
Va, Vb

→ $HCl\cdot(CH_3)_2N(CH_2)_2CO(CH_2)_nCO_2CH_3$
VIa, VIb

→ $I(CH_3)_3N(CH_2)_2CO(CH_2)_nCO_2CH_3$
VIIa, VIIb

→ $CH_2=CHCO(CH_2)_nCO_2CH_3$
VIIIa, VIIIb

→ $CH_2=CHCO(CH_2)_nCO_2H$
IXa, IXb

IVa, Va, VIa, VIIa, VIIIa, IXa: $n=9$;
IVb, Vb, VIb, VIIb, VIIIb, IXb: $n=8$

11-Oxo-12-tridecenoic Acid (IXa).—Ethyl 9-bromononanoate (II) was prepared from ethyl hydrogen sebacate by the method[3] used for methyl 5-bromovalerate. The bromoester was converted into 13-(dimethylamino)-11-oxotridecanoic acid hydrochloride (Va) by the sequence of acetoacetic ester condensation, decarboxylation and the Mannich reaction. The methyl ester VIa of the Mannich base hydrochloride was converted into its free base and then to the methiodide VIIa. Thermal degradation of the methiodide afforded the desired methylene derivative VIIIa in a yield of 75.5%. Hydrolysis of the ester VIIIa with hydrochloric acid in acetone afforded 11-oxo-12-tridecenoic acid IXa.

The ultraviolet absorptions of VIIIa and IXa in methanol solution showed peaks at 210, 317~318 and 210, 317 mμ, respectively, suggesting the presence of α, β-unsaturated ketone group (Fig. 1). The infrared absorption characteristics of VIIIa and IXa were just as expected,

1) Presented at the 13th Annual Meeting of the Chemical Society of Japan, Tokyo, April 1960.
2) M. Kinoshita and S. Umezawa, This Bulletin, **33**, 1075 (1960).
3) C. F. H. Allen and C. W. Wilson, "Organic Syntheses," Coll. Vol. 3 (1955), p. 579.

showing the presence of double bond, conjugated carbonyl and carboxyl groups (Fig. 2 and Fig. 3).

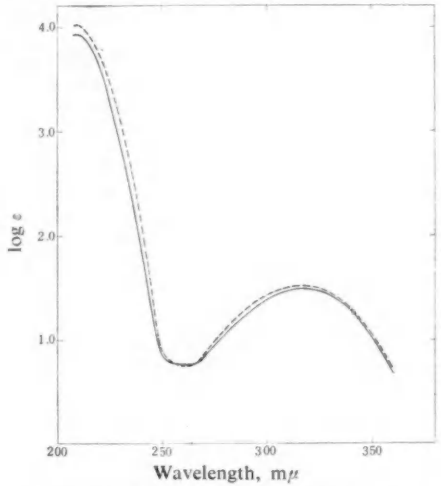

Fig. 1. Ultraviolet absorption spectra of methyl 11-oxo-12-tridecenoate (VIIIa) (----) and 11-oxo-12-tridecenoic acid (IXa) (——) in methanol.

Ozonolysis of the unsaturated keto-acid IXa gave formaldehyde, indicating the presence of a terminal methylene group.

As described above, 11-oxo-12-tridecenoic acid was obtained when the hydrolysis of methyl 11-oxo-12-tridecenoate (VIIIa) with hydrogen chloride in acetone was followed by adjustment of pH to feebly alkaline with a saturated solution of sodium bicarbonate and by removal of acetone at 60~65°C. However, it has been found that 13-chloro-11-oxotridecanoic acid was obtained by a similar procedure except that acetone was removed under cooling at about 5°C. On being treated with an aqueous acetone solution of sodium bicarbonate at 60~65°C, the saturated chloro derivative afforded IXa.

10-Oxo-11-dodecenoic Acid (IXb). — 12-(Dimethylamino)-10-oxododecanoic acid hydrochloride (Vb) was prepared from 10-oxo-undecanoic acid which had been described by J. Cason[4]. An analogous sequence of reactions as described above in the synthesis of IXa has been applied to yield the title compound.

Both 11-oxo-12-tridecenoic acid and 10-oxo-11-dodecenoic acid have been found to possess antitumor and antifungal activities. These compounds showed rather higher toxicity in

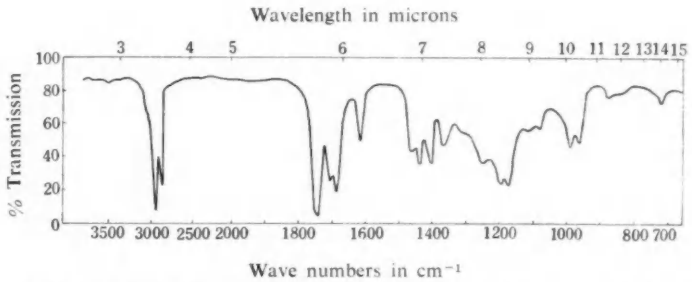

Fig. 2. Infrared absorption spectrum of methyl 11-oxo-12-tridecenoate (VIIIa) (liquid).

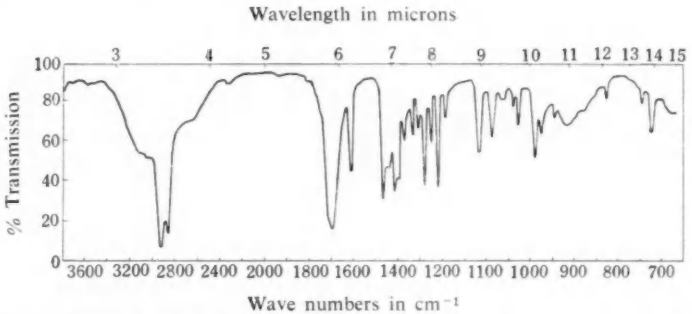

Fig. 3. Infrared absorption spectrum of 11-oxo-12-tridecenoic acid (IXa) (Nujol).

4) J. Cason, *J. Am. Chem. Soc.*, **68**, 2078 (1946).

comparison with 4-keto-5-hexene-1-carboxylic acid, which was previously reported[2].

Experimental

Ethyl 9-Bromononanoate (II).—This preparation was carried out according to the method used for methyl 5-bromovalerate[3]. Ethyl hydrogen sebacate (139 g.) was dissolved in a solution of potassium hydroxide (40 g.) in water (1.8 l.). A solution of silver nitrate (103 g.) in water (1.2 l.) was added under stirring. The precipitate of ethyl silver sebacate was collected, washed with methanol (400 ml.) and dried in a vacuum desiccator overnight. The silver salt was finely powdered, sieved through a 60-mesh screen and again dried in vacuo at 100°C over phosphorus pentoxide for 15 hr.; yield 183 g. (90%). To a stirred suspension of the dried salt in dry carbon tetrachloride (238 ml.) was added dry bromine (27.2 ml.) over a 45-min. period, and then the mixture was refluxed for 1 hr. on a water bath. The resulting mixture was filtered to remove silver bromide, which was washed with warm carbon tetrachloride (68 ml.). The filtrate was washed with 10% sodium carbonate and dried over sodium sulfate. The filtration followed by the removal of the solvent afforded a crude product of the title compound boiling at 148.5~151.8°C (9.8 mmHg), yield 80.1 g. (50% based upon ethyl hydrogen sebacate). Redistillation of the product gave an analytical sample, b. p. 147.5~148.5°C (8.9 mmHg), n_D^{20} 1.4622.

Found: C, 50.02; H, 8.14; Br, 30.35. Calcd. for $C_{11}H_{21}O_2Br$: C, 49.81; 7.94; Br, 30.19%.

Ethyl 10-Oxoundecane-1, 9-dicarboxylate (III).—A solution of sodioacetoacetic ester was prepared from sodium (7.75 g.), absolute ethanol (135 ml.) and ethyl acetoacetate (43.9 g.). Ethyl 9-bromononanoate (II) was added at 40~45°C under stirring in a 45 min. period and then the mixture was refluxed on a water bath for 2 hr. After filtration of sodium bromide, the filtrate was concentrated under reduced pressure. Distillation of the residue gave ethyl 10-oxoundecane-1,9-dicarboxylate, b. p. 173~191°C (5 mmHg), yield 62.3 g. (58.8%). Redistillation gave an analytical sample; b. p. 188.5~191.4°C (1.8 mmHg), n_D^{20} 1.4051.

Found: C, 64.80; H, 9.68. Calcd. for $C_{17}H_{30}O_5$: C, 64.94; H, 9.62%.

11-Oxododecanoic Acid (IVa).—A mixture of ethyl 10-oxoundecane-1,9-dicarboxylate (14.6 g.), 35% hydrochloric acid (26.3 ml.) and glacial acetic acid (50 ml.) was refluxed in an oil bath (125~130°C) for 1.5 hr. After cooling, the mixture was extracted with five 40 ml. portions of ether. The extract was evaporated to yield a crude solid of the title compound. Recrystallization from petroleum benzine (45~80°C) gave 82.5 g. (82.5%) of crystals. Repeated recrystallization from the same solvent gave an analytical sample, m. p. 62.8~63.7°C[5].

Found: C, 67.36; H, 10.08. Calcd. for $C_{12}H_{22}O_3$: C, 67.25; H, 10.35%.

5) J. Cason et al. recently reported m. p. 61~61.5°C of this compound which was prepared by an alternative method; see J. Cason and D. J. McLeod, *J. Org. Chem.*, 23, 1499 (1958).

13-(Dimethylamino)-11-oxotridecanoic Acid Hydrochloride (Va).—A mixture of 10-oxododecanoic acid (IV) (5.0 g.) and dimethylamine hydrochloride (1.9 g.) was heated at 110~115°C. To a resulting melt was added paraformaldehyde (0.7 g.) and the mixture was stirred at 105°C for 45 min. Evaporation under reduced pressure to remove moisture gave a solid, which was recrystallized from absolute ethanol to afford fine needles of 13-(dimethylamino)-11-oxotridecanoic acid hydrochloride, m. p. 145.0~146.5°C, yield 2.15 g. (31.2%). Repeated recrystallization from the same solvent gave an analytical sample, m. p. 145.5~146.5°C.

Found: C, 58.72; H, 9.70; N, 4.59. Calcd. for $C_{15}H_{30}O_3NCl$: C, 58.54; H, 9.83; N, 4.56%.

Methyl 13-(Dimethylamino)-11-oxotridecanoate Hydrochloride (VIa).—A mixture of 13-(dimethylamino)-11-oxotridecanoic acid hydrochloride (Va) (3.85 g.) in absolute methanol (40 ml.) was saturated with dry hydrogen chloride and allowed to stand overnight. Removal of the solvent under reduced pressure afforded the title compound as colorless fine needles, yield 3.85 g. (96.3%). An analytical pure sample was obtained by recrystallization from absolute methanol-ether followed by fractional sublimation under reduced pressure; m. p. 105~107°C.

Found: C, 59.44; H, 9.55; N, 4.28. Calcd. for $C_{16}H_{32}O_3NCl$: C, 59.67; H, 9.95; N, 4.38%.

Methyl 13-(Dimethylamino)-11-oxotridecanoate Methiodide (VIIa).—The crude methyl 13-(dimethylamino)-11-oxotridecanoate hydrochloride (2.55 g.) was triturated with water (3 ml.) and 50% aqueous potassium carbonate solution (5.5 ml.). The separated oil was extracted with eight 10 ml. portions of ether. After the extract was dried with fused potassium acetate, the ether was removed by distillation to give the crude crystalline solid of methyl 13-(dimethylamino)-11-oxo-tridecanoate melting at 22.0~23.0°C. Yield, 2.04 g. (90.4%). The product (2.0 g.) was dissolved in a mixture of absolute benzene (8.5 ml.) and absolute acetone (4.3 ml.) and to the solution was added methyl iodide (9.64 ml.) rapidly. The reaction was exothermic and immediately afforded a crystalline methiodide VIIa, which was washed with benzene-acetone (2:1); m. p. 142.5~144.8°C, yield, 3.05 g. (89.8%).

Found: C, 47.99; H, 7.59 N, 3.34. Calcd. for $C_{17}H_{34}O_3NI$: C, 47.79; H, 7.96; N, 3.28%.

Methyl 11-Oxo-12-tridecenoate (VIIIa).—A sample of the above methiodide VIIa (3.0 g.) was placed in a small distillation flask and heated at 164°C in an oil bath under highly reduced pressure (0.005 mmHg). The colorless crystals of methyl 11-oxo-12-tridecenoate were obtained in a receiver cooled in a dry ice-methanol bath; 1.27 g. (75.7%). Microdistillation gave an analytical sample; b. p. 85~90°C (bath temperature) (0.002 mmHg), m. p. 7.5~8.5°C.

Found: C, 69.88; H, 10.14. Calcd. for $C_{14}H_{24}O_3$: C, 69.96; H, 10.07%.

Maxima in the ultraviolet absorption spectrum were observed in methanol at 210 and 317~318 mμ with ε 10,360 and 32.8, respectively. The infrared absorption spectrum with liquid film showed maxima at 1747 (ester C=O), 1692 (conjugated C=O) and 1618 cm^{-1} (C=C).

11-Oxo-12-tridecenoic Acid (IXa). — A solution of methyl-11-oxo-12-tridecenoate (VIIIa) (1.100 g.) in acetone (30 ml.) and 35% hydrochloric acid (5 ml.) was kept at 20°C for 20 hr. The solution was cooled in an ice bath and adjusted to pH 8.2~8.4 with a saturated solution of sodium bicarbonate (35 ml.) and with solid sodium bicarbonate (9 g.). After removal of acetone by distillation at 60~65°C, the solution was shaken with two 10 ml. portions of ether to remove any unreacted ester. The water-layer was adjusted to pH 1.8~2.0 with 3 N hydrochloric acid and extracted with five 10 ml. portions of ethyl acetate. After the extract was dried over sodium sulfate, the ethyl acetate was distilled off under reduced pressure to yield a crude product of 11-oxo-12-tridecenoic acid (IXa), which was crystallized from petroleum benzine (b. p. 45~80°C); yield 588 mg. (57.3%), m. p. 57.5~61.0°C. An analytical sample was prepared by fractional vacuum sublimation, m. p. 61.0~62.0°C. The substance gave a negative iodoform reaction. Maxima in the ultraviolet absorption spectrum were observed at 210 and 317 mμ with ε 8575 and 30.5 in methanol, respectively. The infrared absorption spectrum in Nujol showed maxima at 1700 (C=O) and 1616 cm^{-1} (C=C).

Found: C, 68.58; H, 9.97. Calcd. for $C_{13}H_{22}O_3$: C, 68.99; H, 9.80%.

Ozonolysis of IXa.—A solution of IXa (100 mg.) in ethyl acetate (5 ml.) was treated with an approximately 2% (by weight) ozone-oxygen mixture at 0°C at a rate of 500 ml./min. for 2 hr. The resulting solution was mixed with water (5 ml.) and zinc dust (150 mg.) and the mixture was refluxed for 30 min. The reaction mixture was filtered while hot into a solution of methone (150 mg.) in ethanol (5 ml.). Dilution with 10 ml. of water afforded the needles of formaldehyde methone, m. p. 187~189°C; yield 22 mg. (17.1%). Admixing with an authentic specimen of formaldehyde methone showed no change of melting point.

13-Chloro-11-oxotridecanoic Acid.—A solution of methyl 11-oxotridecenoate (VIIIa) (1.0 g.) in acetone (30 ml.) and 35% hydrochloric acid (5 ml.) was kept at 20°C for 20 hr. The solution was cooled in an ice-bath and adjusted to pH 8.2~8.4 with a saturated solution of sodium bicarbonate (35 ml.) and with solid sodium bicarbonate (9 g.). After removal of acetone under reduced pressure at 5°C, the resulting solution was shaken with two 10 ml. portions of ether to remove any unchanged ester. The water layer was adjusted to pH 1.8~2.0 with 3 N hydrochloric acid and extracted with five 10 ml. portions of ethyl acetate. After the extract was dried over sodium sulfate, the solvent was distilled off in vacuo. The residue was crystallized from petroleum benzine (b. p. 45~80°C) to afford colorless fine plates of 13-chloro-11-oxotridecanoic acid; yield 639 mg. (58.4%), m. p. 58.5~61.0°C. They were recrystallized twice from petroleum benzine, m. p. 61.0~61.8°C. The substance gave a positive Beilstein's test. Admixing with a sample of IXa showed depression of melting point (m. p. 53.0~59.5°C). Only one maximum in the ultraviolet absorption spectrum was observed in methanol at 280 mμ (ε 47.0), which indicated a normal carbonyl group. The infrared absorption spectrum in Nujol showed a normal carbonyl band at 1710 cm^{-1}.

Found: C, 59.18; H, 9.01; Cl, 13.56. Calcd. for $C_{13}H_{23}O_3Cl$: C, 59.36; H, 8.74; Cl, 13.50%.

To a solution of the above product (850 mg.) in water (60 ml.) and acetone (60 ml.) was added an excess amount of sodium bicarbonate. Acetone was remorved by distillation at 60~65°C. The residue was processed by the same procedure as that used for the preparation of IXa to afford 655 mg. (89.7%) of IXa, m. p. 57.5~60.7°C. Admixing with a sample of IXa showed no change of melting point.

12-(Dimethylamino)-10-oxododecanoic Acid Hydrochloride (Vb).—A mixture of 10-oxoundecanoic acid[4] (IVb) (9.60 g.) and dimethylamine hydrochloride (3.93 g.) was heated at 110°C. To the resulting melt was added paraformaldehyde (1.44 g.) and the mixture was stirred at 105°C for 45 min. Evaporation under reduced pressure to remove moisture gave a solid which was crystallized from absolute ethanol (24 ml.) and absolute acetone (24 ml.) to afford the crystals of 12-(dimethylamino)-10-oxododecanoic acid hydrochloride; yield 3.55 g. (25.2%), m. p. 138~139.5°C. From the mother liquor 0.3 g. of the additional crop was obtained, m. p. 137~139°C. The total yield was 27.3%. An analytical sample was obtained by repeated recrystallization from ethanol, m. p. 138.5~139.5°C.

Found: C, 57.17; H, 9.63; N, 4.85. Calcd. for $C_{14}H_{28}O_3NCl$: C, 57.23; H, 9.60; N, 4.77%.

Methyl 12-(Dimethylamino)-10-oxododecanoate Methiodide (VIIb). — A mixture of 12-(dimethylamino)-10-oxododecanoic acid hydrochloride (Vb) (4.5 g.) and absolute methanol (46 ml.) was saturated with dry hydrogen chloride and allowed to stand overnight. The solvent was removed by distillation under reduced pressure to afforded a crude product of methyl 12-(dimethylamino)-10-oxododecanoate hydrochloride, which was triturated with water (5.7 ml.) and 50% aqueous potassium carbonate solution (10.4 ml.). The separated oil was extracted with eight 18 ml. portions of ether. After the extract was dried over fused potassium acetate, the ether was removed by distillation to give colorless prisms of methyl 12-(dimethylamino)-10-oxododecanoate (VIb) melting at 34.0~35.5°C; yield 1.7 g. (40.5%). The crude free ester (1.7 g.) was dissolved in a mixture of absolute benzene (7.5 ml.) and absolute acetone (4.8 ml.) and to the solution was added methyl iodide (8.5 g.). The reaction was exothermic and immediately afforded a crystalline methiodide (VIIb), which was washed wth benzene-acetone (2:1); m. p. 173°C (decomp., sintered at 141~142°C); yield 2.2 g. (34.7% based upon Vb).

Found: C, 45.97; H, 7.78; N, 3.80. Calcd. for $C_{16}H_{32}O_3NI$: C, 46.49; H, 7.80; N, 3.39%.

Methyl 10-Oxo-11-dodecanoate (VIIIb). — A sample of methiodide VIIb (2.20 g.) was placed in a small distillation flask and heated at 164°C in an oil bath under highly reduced pressure (0.005 mmHg). Colorless crystals of methyl 10-oxo-11-dodecenoate (VIIIb) were obtained in a receiver cooled in a dry ice-methanol bath; yield 1.02 g. (84.5%). Microdistillation gave an analytical sample, b. p. 95°C (bath temperature) (0.005 mmHg),

m. p. 12.2~13.2°C. Maxima in the ultraviolet absorption spectrum were observed in methanol at 209 and 317 mμ, with ε 9730 and 39.2, respectively. The infrared absorption spectrum in liquid film showed maxima at 1747 (ester C=O), 1692 (conjugated C=O), 1620 cm^{-1} (C=C).

Found: C, 69.26; H, 9.65. Calcd. for $C_{10}H_{22}O_3$: C, 68.99; H, 9.80%.

10-Oxo-11-dodecenoic Acid (IXb).—A solution of methyl 10-oxo-11-dodecenoate (VIIIb) (1.112 g.) in acetone (36 ml.) and 35% hydrochloric acid (6 ml.) was kept at 21°C for 21 hr. The solution was cooled in an ice-bath and adjusted to pH 8.2~8.4 with a saturated solution of sodium bicarbonate (42 ml.) and with solid sodium bicarbonate (9 g.). After removal of acetone by distillation at 65°C the solution was shaken with two 10 ml. portions of ether to remove any unchanged ester. The water-layer was adjusted to pH 1.8~2.0 with 3 N hydrochloric acid and extracted with five 10 ml. portions of ethyl acetate. After the extract was dried over sodium sulfate, ethyl acetate was distilled off under reduced pressure to yield a crude product of 10-oxo-11-dodecenoic acid (IXb) (850 mg.) melting at 47~53.5°C, which was recrystallized from petroleum benzine (b. p. 45~80°C); yield 548 mg. (51%), m. p. 56.0~56.8°C. It gave a negative iodoform reaction. Maxima in the ultraviolet absorption spectrum were observed in methanol at 209~210 and 321 mμ with ε 8660 and 27.9, respectively. The infrared absorption spectrum in Nujol showed maxima at 1702 (C=O) and 1615 cm^{-1} (C=C).

Found: C, 67.76; H, 9.36. Calcd. for $C_{12}H_{20}O_3$: C, 67.89; H, 9.50%.

Bioassays.—It is interesting to find that both 11-oxo-12-tridecenoic acid (IXa) and 10-oxo-11-dodecenoic acid (IXb) possess antitumor and antifungal activities. The minimum necessary concentrations of both IXa and IXb for the anti-HeLa cell effect were 125 mcg./ml. Against cells of Ehrlich cartinoma, IXa and IXb had potencies of 1.3 and 1.4 units/mg. (in terms of sarkomycin potency) by cylinder plate method, respectively. The daily intraperitoneal injection of 125 mcg. of IXa and IXb inhibited the ascites increase and prolonged the survival period of mice bearing ascities type of Ehrlich cartinoma by intraperitoneal route. Intravenous acute toxicity tests of IX and IXb in mice indicated the same LD_{50} dose of 670 mcg./mouse.

Both IXa and IXb completely inhibited the growth of *Trichophyton mentagrophytes* and *Penicillium chrysogenum* in a concentration of 7.8 mg./ml., but had comparatively weak activities against other fungi and bacteria tested.

Summary

1) 11-Oxo-12-tridecenoic acid (IXa) has been prepared from ethyl 9-bromononanoate (II) via 11-oxododecanoic acid (IVa) and the corresponding Mannich base Va.

2) 10-Oxo-11-dodecenoic acid (IXb) has been prepared from 10-oxoundecanoic acid (IVb) via the corresponding Mannich base Vb.

3) It has been found that IXa and IXb possess antitumor and antifugal activities.

The authors are indebted to Dr. H. Umezawa, National Institute of Health, Tokyo, for antitumor assays. Analyses of compounds were performed by Mr. S. Nakada of this laboratory. This work has been supported in part by the Cancer Research Grant of the Ministry of Education and by a grant from the Research Society of Microbiological Chemistry, to which the authors' thanks are due.

Department of Applied Chemistry
Faculty of Engineering
Keio University
Koganei-shi, Tokyo

On Oxazolo[5 : 4-b]tropones[1]

By Tetsuo Nozoe, Kozo Doi* and Kazuo Kitahara**

(Received August 29, 1960)

In the course of trying to prepare a pyridotropolone from 3-aminotropolone (I), it has been found that the condensation product of the aminotropolone and ethyl ethoxymethylenemalonate is not the anticipated vinylaminotropolone (II) but the dihydro-oxazolotropone (III), and that the latter III results in fission to form the oxazolotropone (IV) and ethyl malonate on pyrolysis[2]. An analogous observation has also been found in the

* Present address: The Chemical Research Institute of Non-Aqueous Solution, Tohoku University, Sendai.
** Present address, The Research Laboratory, Tokyo Tanabe Pharmaceutical Co., Tokyo.

1) This work in part was presented at the Tohoku Local Meeting of the Chemical Society of Japan, June, 1956.
2) T. Nozoe, K. Doi and K. Kitahara, This Bulletin, to be published.

condensation product of *o*-aminophenol and ethoxymethylenemalonate[3]. The structure of the oxazolotropone (IV) was elucidated, at that time, from the similarity of its ultraviolet absorption to that of 2-methyloxazolo[5 : 4-b]-tropone (V) which had been obtained from the reaction of the aminotropolone and acetic anhydride[4].

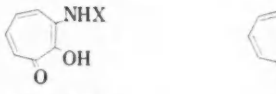

I: X=H
VI: X=CHO

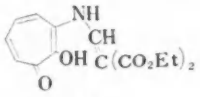

II

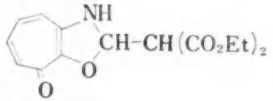

III

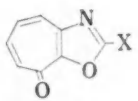

IV: X=H
V: X=CH_3

In this communication the present authors will deal with some reactions of the oxazolotropone (IV) and its derivatives, and with the condensation products of the aminotropolone and benzaldehydes in relation to the subject.

Oxazolo[5:4-b]tropone (IV) was also prepared readily by application of methods analogous to those used for the preparations of benzoxazole from *o*-aminophenol to the aminotropolone. Thus, IV was obtained easily on heating the aminotropolone and formamide[5] and on heating 3-formylaminotropolone (VI) in a sealed tube[6].

There have been known to date besides IV, the following oxazolotropones: 2-methyloxazolo-[5 : 4-b]tropone[4] (V) and its bromo derivatives, 2-methyloxazolo[4 : 5-b]tropone[7] (VII), and 2-methyloxazolo[5 : 4-b]benzo[d]tropone[8] (VIII). Recently preparations of 2-methyloxazolo[5 : 4-b]tropones from several diaminotropolones and acetic anhydride have been reported[9].

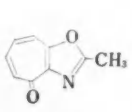

VII

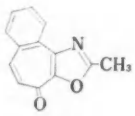

VIII

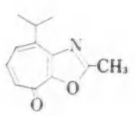

IX

Nicholls and Tarbell[8] assigned the absorption maxima at 1617 and 1567 cm^{-1} in the infrared spectrum of VIII to the tropone carbonyl and the conjugated C=N stretching vibration, respectively. The oxazolotropone (IV) has maxima at 1635 and 1588 cm^{-1}, and has a further sharp maximum at 3120 cm^{-1}, which is probably considered to originate in the CH vibration of the oxazole ring of IV, because a corresponding absorption is absent in the 2-methyloxazolotropones (V, VII and VIII); benzoxazole has also a maximum at 3125 cm^{-1}, whereas 2-methylbenzoxazole lacks this absorption[10].

It had been reported that 3-amino-4-isopropyltropolone affords a monoacetate of m. p. 70.5~73°C on being heated with acetic anhydride[11]. This monoacetate, however, was found to be an oxazolotropone (IX) because of the close resemblance of its ultraviolet absorption to that[2] of IV.

Oxazolotropone (IV), similarly to benzoxazole, was readily hydrolyzed by dilute acid or alkali to form 3-aminotropolone (I). In either case, the formylaminotropolone (V) was not isolated as the intermediate of the reaction.

It has been known that tropolone methyl ethers react with liquid ammonia to give 2-aminotropones. Oxazolotropone (IV) is also regarded as a methyl ether analogue of tropolone and an examination, therefore, was directed to find a possibility of formation of 1, 3-diazaazulene derivative from IV.

When oxazolotropone (IV) was allowed to stand in liquid ammonia overnight, there was obtained the aminotropolone (I) as an ammonolysis product. The 2-methyloxazolotropone (V) resulted in formation of I and additional acetamide on being treated in the same way as the above. The reaction mechanism is probably interpreted as follows:

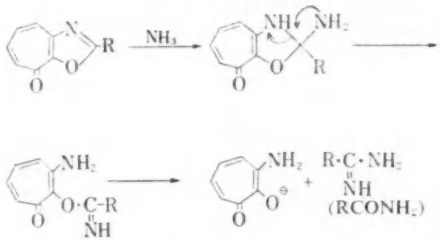

The proposed machanism seems to be endorsed by the following facts: a) While tropolone acetate was ammonolyzed under the same

3) T. Nozoe and K. Doi, ibid., to be published.
4) Y. Kitahara, *Science Repts. Tohoku Univ., Ser. I*, 40, 83 (1956).
5) S. Niementowski, *Ber.*, 30, 3064 (1897).
6) A. Ladenburg, ibid., 10, 1124 (1877).
7) A. W. Johnson and M. Tisler, *J. Chem. Soc.*, 1955, 1841.
8) C. A. Nicholls and D. S. Tarbell, *J. Am. Chem. Soc.*, 74, 4935 (1951).
9) T. Nozoe, Y. Kitahara, K. Doi and M. Takahashi, *Bull. Chem. Research Inst. Non-Aqueous Solns.*, Tohoku Univ., 9, 7 (1959).
10) H. M. Randall, R. G. Fowler, N. Fuson and J. R. Dangl, "Infrared Determination of Organic Molecules", Van Nostrand, New York (1949), p. 214.
11) T. Nozoe, Y. Kitahara, E. Kunioka and K. Doi, *Proc. Japan Acad.*, 26, 38 (1950).

condition to give tropolone and acetamide, 3-acetylaminotropolone was recovered unreacted. b) While the dibenzoyl compound of the aminotropolone was also ammonolyzed readily to give the *N*-benzoylaminotropolone and benzamide under the same condition, the former was recovered likewise in an unreacted state. These facts suggest that the formation of *O*-acylated compound as an intermediate occurs in the respective reaction of the oxazolotropone and liquid ammonia. The cleavage of this kind of oxazole ring recalls the reaction of imino ethers and ammonia resulting in the formation of the corresponding alcohol and amidine[12].

In the subsequent papers[2,3], the authors are to discuss a ring-chain tautomerism between aromatic vinylamines possessing a hydroxyl group in the ortho position and oxazoline derivatives. According to Sachs and Brunetti[13], the reaction product of *o*-aminophenol and 2,4-dinitrobenzaldehyde exists in the form of 2-(2,4-dinitrophenyl)benzoxazoline in place of the expected 2,4-dinitrobenzylidene-*o*-aminophenol. It seems to be very interesting to find whether such a fact would also be applicable to the condensation products of the aminotropolone (I) and benzaldehydes.

Unlike 5-aminotropolone[14], 3-aminotropolone (I) did not give any reaction product when heated with benzaldehyde. Even on being heated with more reactive *p*-nitrobenzaldehyde at 150°C for one hour, a condensation product was not obtained. This difficulty, however, was overcome easily by the use of caustic alkali in the reaction. When an equimolar mixture of the aminotropolone, respective benzaldehyde and sodium hydroxide was heated in methanol, the azomethine derivative (X, XI and XII) could be readily prepared. These products showed red coloration with ferric chloride test and hydrolyzed readily to form the aminotropolone (I) with water or aqueous alcohol. These facts mean that they do not exist in the form of their ring-tautomers of XIII. The same reaction of the aminotropolone and *p*-nitrobenzaldehyde afforded 2-(*p*-nitrophenyl)oxazolotropone (XIV), the structure of which was assumed from the fact that it agreed with a reaction product of the aminotropolone and *p*-nitrobenzoyl chloride.

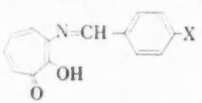

X: X=H
XI: X=Cl
XII: X=OCH_3

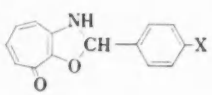

XIII

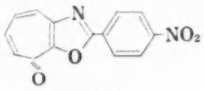

XIV

While the reaction of the aminotropolone and benzoyl chloride in pyridine produced a mixture of the dibenzoylated and *N*-benzoylated compounds, the reaction of the aminotropolone and *p*-nitrobenzoyl chloride under the same condition resulted in the formation of the oxazolotropone (XIV), which showed no coloration with ferric chloride. An oxazole ring formation in the reaction with benzaldehydes or benzoyl chlorides seems to be more rapid in the case of the aminotropolone (I) than in the case of *o*-aminophenol[15].

Experimental

The ultraviolet absorptions were measured in methanol solution with a Beckman model DU spectrophotometer. The infrared absorption was measured on potassium bromide disk with a Perkin-Elmer model 21 infrared spectrometer, using a rock salt prism.

Oxazolo[5:4-b]tropone (IV).—a) 3-Aminotropolone (I, 0.28 g.) and formamide (1 ml.) was heated under reflux at 220°C. Benzene (2 ml.) was added to the reaction mixture at room temperature and the residual solid was collected. It gave IV (0.1 g.), m. p. and mixed m. p.[2] 150~151°C, after sublimation in vacuo following recrystallization from benzene. b) A mixture of the aminotropolone (I, 1.4 g.) and 80% formic acid (30 ml.) was heated under reflux for 3 hr. The evaporated residue of the solvent was crystallized from ethanol to give 3-formylaminotropolone (VI, 1.2 g.) as yellow prisms, m. p. 167~168°C (reported[4] m. p. 168~169°C). When VI (0.3 g.) in a sealed tube was heated on an oil bath of 250°C for 30 min., the oxazolotropone (IV, 0.1 g.) was obtained.

Hydrolysis of the Oxazolotropone (IV).—A mixture of IV (30 mg.) and 3 N hydrochloric acid (1 ml.) or 2 N sodium hydroxide (1 ml.) was heated at 50°C for 30 min. Neutralization of the reaction mixture gave 3-aminotropolone (I), m. p. and mixed[4] m. p. 97~98°C.

2-Methyl-4-isopropyloxazolo[5:4-b]tropone (IX).—A mixture of 3-amino-4-isopropyltropolone[11] (30 mg.) and acetic anhydride (1 ml.) was heated under reflux for one hour. The evaporated residue of the solvent, after sublimation in vacuo following crystallization from petroleum ether (b. p. 40~60°C), gave the oxazolotropone (IX) as colorless prisms, undepressed on admixture with an authentic sample which had been reported[11] to be a monoacetate of the aminotropolone.

Found: C, 69.82; H, 6.21; N, 7.35. Calcd. for $C_{11}H_{11}O_2N$: C, 69.82; H, 5.86; N, 7.40%. λ_{max}^{MeOH} mμ (log ε): 245 (4.51), 320 (3.91)

12) J. Houben et al., *J. prakt. Chem.*, **105**, 12 (1922).

13) F. Sachs and W. Brunetti, *Ber.*, **40**, 3230 (1907).

14) T. Nozoe, S. Seto et al., *Proc. Japan Acad.*, **27**, 426 (1951).

15) R. D. Desai, *J. Chem. Soc.*, **1934**, 1186.

Ammonolysis of the Oxazolotropone (IV).—A solution of IV (0.7 g.) in liquid ammonia (50 ml.) was allowed to stand in a pressure bottle for 24 hr. at room temperature. Ammonia was allowed to evaporate, the residue was washed out with methanol (50 ml.), and the evaporated residue of the solvent was crystallized from benzene to give the aminotropolone (I, 0.53 g.).

Ammonolysis of the 2-Methyloxazolotropone (V).—A solution of V (0.5 g.) in liquid ammonia (50 ml.) was allowed to stand for 3 days at room temperature. The residual solid of evaporation of ammonia, afer recrystallization from dilute methanol, afforded the aminotropolone (I, 0.3 g.). The evaporated residue of the mother-liquor, after chromatographic purification (alumina—benzene) following crystallization from petroleum ether (b. p. 40~60°C), gave acetamide (50 mg.) of m. p. 80~81°C.

Ammonolysis of Tropolone Acetate.—A solution of tropolone acetate (0.4 g.), which prepared according to Doering's description[16], in liquid ammonia (40 ml.) was allowed to stand overnight at room temperature. The evaporated residue of ammonia was dissolved in water, the residual solution was acidified with dilute hydrochloric acid, and extracted with chloroform (20 ml.). The extract, after re-extraction with dilute alkali followed by evaporation in vacuo, gave acetamide (50 mg.). The alkaline extract, after acidification with dilute hydrochloric acid, and after being extracted with chloroform and subsequent evaporation of the solvent, gave tropolone (0.27 g.). The result similar to the above has been recently reported by Sato[17]. An experiment on ammonolysis of 3-acetylaminotropolone under the same condition ended in the recovery of unreacted material.

Condensation of 3-Aminotropolone (I) and Benzaldehydes.—To a solution of I (0.28 g.), respective benzaldehyde (0.02 mol.) and methanol (5 ml.), was added a solution of sodium hydroxide (80 mg.) in water (0.5 ml.), and the mixture was heated under reflux for 30 min. Then the reaction mixture was diluted with water (10 ml.), neutralized with acetic acid, and extracted with chloroform (30 ml.). The evaporated residue of the solvent was crystallized from a suitable solvent to give:

3-Benzylideneaminotropolone (X): yellow leaflets (chloroform), m. p. 142~143°C,

Found: N, 6.19. Calcd. for $C_{14}H_{11}O_2N$: N, 6.22%.

3-p-Chlorobenzylideneaminotropolone (XI): yellow prisms (chloroform), m. p. 124~125°C,

Found: N, 5.68. Calcd. for $C_{14}H_{10}O_2NCl$: N, 5.40%.

3-Anisylideneaminotropolone (XII): yellow prisms (benzene), m. p. 110~111°C.

Found: N, 5.34. Calcd. for $C_{15}H_{13}O_3N$: N, 5.49%.

All of the three reaction products showed red coloration with alcoholic ferric chloride and hydrolyzed easily to form the aminotropolone (I) on being shaken with water or aqueous alcohol.

2-*p*-Nitrophenyloxazolo[5 : 4-b]tropone (XIV).—a) A solution of sodium hydroxide (0.1 g.) in water (0.5 ml.) was added to a solution of the aminotropolone (I, 0.35 g.), *p*-nitrobenzaldehyde (0.4 g.) and methanol (5 ml.), and heated under reflux for 30 min. The reaction mixture, treated as above, afforded the oxazolotropone (XIV, 0.2 g.) as yellow needles, m. p. 251~252°C. It did not show any coloration with ferric chloride.

Found: C, 62.69; H, 3.01; N, 10.45. Calcd. for $C_{14}H_8O_4N_2$: C, 62.69; H, 3.12; N, 10.51%. λ_{max}^{MeOH} mμ (log ε): 265 (4.44), 374 (4.06).

b) A mixture of the aminotropolone (0.14 g.), *p*-nitrobenzoyl chloride (0.19 g.), and pyridine (4 ml.) was stirred for one hour at room temperature. It was then diluted with water (10 ml.) and the residual solid was collected. Recrystallization of it from nitrobenzene gave the above XIV, m. p. and mixed m. p. 251~252°C.

Benzoylation of 3-Aminotropolone (I).—A solution of I (0.14 g.), benzoyl chloride (0.14 g.) and pyridine (2 ml.) was stirred for 20 min. at room temperature, then diluted with water (10 ml.), and the residual solid (0.19 g.) of m. p. 150~152°C, was collected. Its fractional recrystallization from a mixture of benzene and methanol afforded 3-benzoylaminotropolone benzoate from the less soluble portion, and 3-benzoylaminotropolone from the more soluble portion,

3-Benzoylaminotropolone Benzoate: pale yellow leaflets, m. p. 174°C, which showed no coloration with ferric chloride.

Found: C, 73.29; H, 4.40; N, 4.07. Calcd. for $C_{21}H_{15}O_4N$: C, 73.29; H, 4.38; N, 4.06%.

3-Benzoylaminotropolone: pale yellow needles, m.p. 146°C, which showed red coloration with ferric chloride.

Found: C, 69.62; H, 4.72; N, 6.00. Calcd. for $C_{14}H_{11}O_3N$: C, 69.70; H, 4.59; N, 5.80%.

When a mixture of the dibenzoylated compound (0.5 g.) and liquid ammonia (60 ml.) was allowed to stand for 7 days at room temperature, 3-benzoylaminotropolone and benzamide were obtained by treatment similar to the above description.

The authors express their gratitude to Messrs. K. Kato, S. Ohyama, A. Iwanaga and S. Azumi for microanalyses, and to Mr. Y. Ikegami for the infrared spectral measurement.

Department of Chemistry
Faculty of Science
Tohoku University
Katahira-cho, Sendai

16) W. von E. Doering and L. H. Knox, *J. Am. Chem. Soc.*, **73**, 828 (1951).
17) T. Sato, *J. Chem. Soc. Japan, Pure Chem. Sec. (Nippon Kagaku Zasshi)*, **80**, 1058 (1959).

Colloid Chemical Studies on Starching Materials. III. Dynamic Viscosity and Dynamic Rigidity of Starch Solutions

By Masayuki NAKAGAKI* and Kazuko MURAGISHI

(Received August 18, 1960)

In recent years, anomalous flow properties of colloidal systems have been investigated extensively in the field of rheology, in which the flow property is explained by a combination of rigidities and viscosities. Examples of the combination frequently used are so called Maxwell's model and Voigt's model. Even for fluid, it is required to presuppose some rigidity element to explain its flow property on the basis of these models. The existence of a kind of rigidity may be understood by considering the fact that the so-called structural viscosity of a solution can be explained by assuming a kind of yield value, as shown in a previous paper of this series on dilute solutions of polyvinyl alcohol[1].

In the present paper, starch solutions, also known to show structural viscosity, are examined by a rheometer to obtain the frequency dependencies of dynamic rigidity and dynamic viscosity, and an attempt is made to explain these by Maxwell's and Rouse's model.

Experimental

Rheometer.—A top-drive coaxial rheometer was used. Details of the rheometer were described by Nakagawa and Seno[2]. The sample to be studied was put in the gap between the coaxial internal and external cylinders. The radius of the internal cylinder r_1 was 2.00 cm. and that of the external cylinder r_2 was 2.50 cm. The depth l of the immersion of the internal cylinder was 15.0 cm., which was equal to the height of the cylinder. The moment of inertia I of the internal cylinder was 3005 g. cm^2. The internal cylinder was hung by a quenched steel wire whose diameter was 1.0 mm., and whose length was 92.5 cm. The torsional constant of the wire determined from the period of the free torsional oscillation, k, was 0.90×10^5 dyne cm.

At the top of the wire, a sinusoidal torsional oscillation was applied and the oscillation of the internal cylinder was recorded on a photographic paper as a Lissajous' figure obtained by combining perpendicularly the oscillation of the internal cylinder and the oscillation at the top of the wire. The Lissajous' figure thus obtained was an ellipse.

The dynamic viscosity η and the dynamic rigidity G are calculated by the equations:

$$\left.\begin{aligned}\eta &= \frac{R}{4\pi l}\left(\frac{1}{r_1^2}-\frac{1}{r_2^2}\right)=47.8\times10^{-5}\times R(\text{poises})\\ G &= \frac{K}{4\pi l}\left(\frac{1}{r_1^2}-\frac{1}{r_2^2}\right)=47.8\times10^{-5}\times K(\text{dyne/cm}^2)\end{aligned}\right\} \quad (1)$$

where R and K are the quantities to be determined experimentally by using the equations:

$$\left.\begin{aligned}R &= k\sin\phi/\omega p\\ K &= k(\cos\phi/p-1)+I\omega^2\end{aligned}\right\} \quad (2)$$

Here, the lag angle ϕ and the amplitude ratio p are to be obtained by the analysis of the photographic picture, and ω is the angular frequency. The latter is defined by

$$\omega=2\pi/T_f \quad (3)$$

where T_f is the period of oscillation. All experiments were made in a thermostat at 30°C.

A Check of the Rheometer by Using Distilled Water.—Distilled water is an example of so-called Newtonian liquid, for which $G=0$ and $K=0$. All the Lissajous' figures obtained for distilled water by the present rheometer were linear, which give $\sin\phi=0$ and $R=0$. This means that the viscosity of distilled water was too small to be detected by this apparatus, that is $\eta=0$. Since $\sin\phi=0$ and $\cos\phi=1$ for distilled water, Eq. 2 can be simplified to

$$1/p=1-(I/k)\omega^2 \quad (4)$$

Therefore the relation between $1/p$ and ω^2 should be expressed by a straight line which intersects with the ordinate at $1/p=1$ and has an inclination of -0.0333 according to the values of I and k given above. In Fig. 1, the experimental values are shown by open circles, while the theoretical relation give by Eq. 4 is shown by a straight line. The agreement is fairly good. Apparent values of the rigidity G of distilled water calculated from the experimental values of p will give the experimental error. The error in the worst case was about 18 dyne/cm^2 (for $\omega=11.5$).

Materials and Preparation of Pastes.—The materials used were potato starch, sweet potato starch, and rice starch of pharmaceutical grade. The starch, dried in a desiccator and weighed accurately, was put in a flask, water was added, and it was heated at 90°C for 30 min. stirring with a glass rod inserted through a hole in a rubber stopper fitted loosely to the flask. For the heating, the temperature of a water bath was raised gradually from room temperature to boiling, and kept boiling

* Present address: Faculty of Pharmacy, Koyto University, Sakyo-ku, Kyoto.

1) M. Nakagaki and A. Shimazaki, This Bulletin, **29**, 60 (1956).

2) T. Nakagawa and M. Seno, ibid., **29**, 471 (1956).

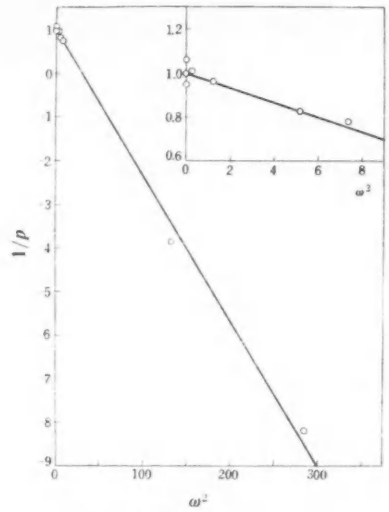

Fig. 1. Distilled water.

for 30 min. The temperature in the flask was 90°C when the bath water was boiling. Then, the flask was placed in cold water for cooling. The paste was used for the measurement immediately after it was cooled, and the measurement was finished in the same day.

Results and Discussion

The values of the dynamic viscosity η and the dynamic rigidity G thus obtained are shown in the following figures. Fig. 2 is for 3% potato starch paste, Fig. 3 is for 5% potato starch paste, Fig. 4 is for 5% sweet potato

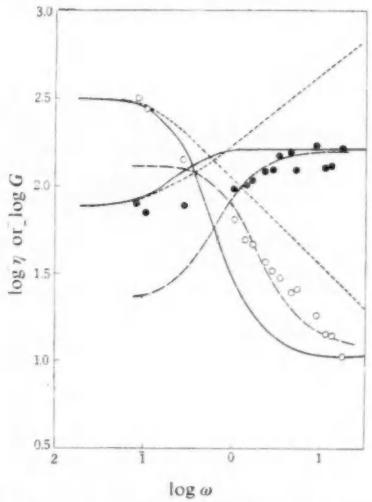

Fig. 2. $\eta(\bigcirc)$ and $G(\bullet)$ of 3% potato starch paste.

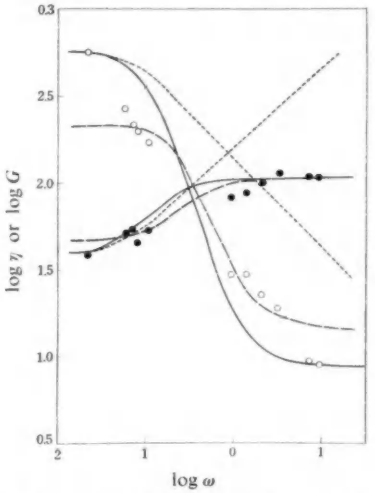

Fig. 3. $\eta(\bigcirc)$ and $G(\bullet)$ of 5% potato starch paste.

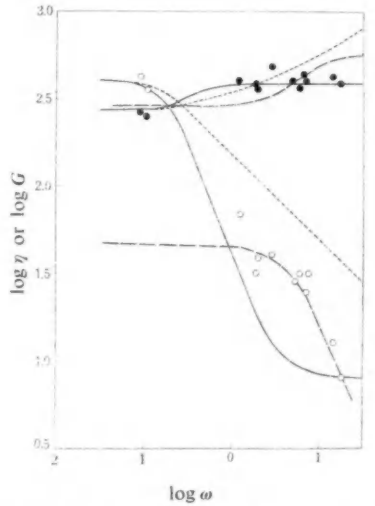

Fig. 4. $\eta(\bigcirc)$ and $G(\bullet)$ of 5% sweet potato starch paste.

starch paste, and Fig. 5 is for 5% rice starch paste. In these figures, the abscissa is $\log \omega$, while the ordinate is $\log \eta$ for open circles and is $\log G$ for closed circles.

For all these pastes, the dynamic viscosity decreased and the dynamic rigidity increased with the increase of the frequency. This is, as is well known, the usual viscoelastic behavior. To describe the viscoelastic behavior, Maxwell's four element model is often used. By this model the frequency dependence of

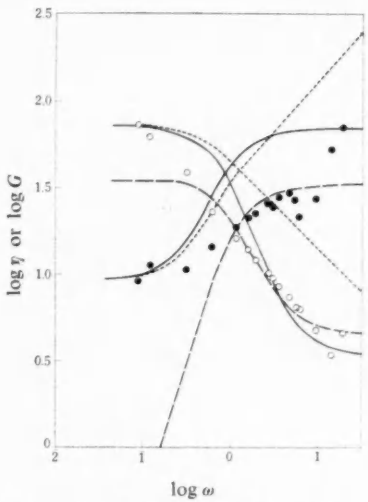

Fig. 5. η_i(○) and G(●) of 5% rice starch paste.

the dynamic viscosity and the dynamic rigidity are expressed by the equations,

$$\eta_i = \eta_{i2}/(1+\tau_2^2\omega^2) + \eta_{i3} \tag{5}$$

$$G = G_1 + G_2\tau_2^2\omega^2/(1+\tau_2^2\omega^2) \tag{6}$$

where, η_{i2}, η_{i3}, G_1 and G_2 are constants, and τ_2 is also a constant called relaxation time, and is given by the relation,

$$\tau_2 = \eta_{i2}/G_2 \tag{7}$$

An attempt was made to see how well these equations can explain the experimental results.

In order to find out the values of the parameters, G_1, G_2, η_{i2}, η_{i3} and τ_2, attaching importance equally to both η_i and G, the following procedure was at first used. By using Eqs. 5, 6 and 7,

$$\left.\begin{aligned} \eta_i &= B - \tau_2 G \\ B &= \eta_{i3} + \eta_{i2} + \tau_2 G_1 \end{aligned}\right\} \tag{8}$$

can be derived. Therefore, if one plots experimental values of η_i and G of the same ω value on the ordinate and the abscissa, respectively, one should obtain a linear relationship and one can determine the value of B and τ_2. Then, by plotting experimentally obtained η_i and $(B-\tau_2 G)$ on the ordinate (these quantities are not necessarily equal with each other because of experimental errors and any deviation from Maxwell's model), and $1/(1+\tau_2^2\omega^2)$ on the abscissa, one should again obtain another linear relationship which gives the value of η_{i2} and η_{i3}. The parameter G_1 is obtained from these values on the basis of the second equation of Eq. 8. Thus, one should be able to determine the values of all the parameters, η_{i2}, η_{i3}, G_1, G_2, and τ_2. However, the experimental data seemed not to agree with Maxwell's model in the present case, because two expected linear relationships were not exactly satisfied. By trying, however, to draw straight lines to satisfy the experimental plots as far as possible, the values of the parameters were determined, as shown in lines called I in Table I. Calculated values of $\log\eta_i$ and $\log G$ by using these values are shown in Figs. 2—5 with broken curves. It is seen that these curves partially satisfy the experimental plots but not in the whole range of the frequency.

The second method to determine the parameter values of Maxwell's four element model was used as follows, according to the experience that most curves in the previous case were already almost horizontal in the larger and smaller range of $\log\omega$. Eqs. 5 and 6 show that

$$\left.\begin{aligned} &\eta_i(\tau_2\omega \ll 1) = \eta_{i2} + \eta_{i3} \\ &\eta_i(\tau_2\omega \gg 1) = \eta_{i3} \\ &G(\tau_2\omega \ll 1) = G_1 \\ &G(\tau_2\omega \gg 1) = G_1 + G_2 \end{aligned}\right\} \tag{9}$$

On the basis of these equations, it was assumed that the experimental values of η_i and G for the smallest ω are $(\eta_{i2}+\eta_{i3})$ and G_1, respectively, and those for the largest ω are η_{i3} and (G_1+G_2). The values of the parameters thus obtained

TABLE I. PARAMETERS IN MAXWELL'S FOUR ELEMENT MODEL
(in c. g. s. units)

Starch	Concentration	No.	G_1	G_2	η_{i2}	η_{i3}	τ_2
Potato	3%	I	22.5	129	120	13.0	0.933
		II	78.5	83.1	303	10.6	3.65
Potato	5%	I	45.3	60.0	200	15.0	3.33
		II	38.8	66.2	550	8.82	7.55
Sweet potato	5%	I	290	287	43.2	3.17	0.150
		II	268	120	411	8.01	3.43
Rice	5%	I	0.32	32.6	30.5	4.60	0.937
		II	9.21	59.6	67.6	3.41	1.13

are cited in line II of Table I. By using these values, solid curves in Figs. 2—5 were obtained. Comparing these curves with experimental plots, it is seen that $\log \eta$ decreases with the increase of $\log \omega$ more slowly in experimental plots than in Maxwell's model, and that $\log G$ increases at greater values of $\log \omega$ in experimental plots than in Maxwell's model. Moreover, it is by no means guaranteed experimentally that $\log \eta$ and $\log G$ curves are almost horizontal in the larger and smaller ranges of $\log \omega$.

Considering that these two attempts were not successful, it may be concluded that the viscoelastic behavior of starch paste can not be explained by Maxwell's four element model. Then, Rouse's model was examined. Rouse[3] studied the viscoelastic properties of high polymer solution and obtained theoretical equations. Neglecting the viscosity of solvent, η_s, because it is far smaller than the viscosity of paste, the equations are:

$$\left.\begin{aligned} \eta &= \eta_0 f_1(\tau\omega) \\ f_1 &= (6/\pi^2) \sum_{p=1}^{N} [p^2/(p^4+\tau^2\omega^2)] \end{aligned}\right\} \quad (10)$$

and

$$\left.\begin{aligned} G &= (6/\pi^2)(\eta_0/\tau) f_2(\tau\omega) \\ f_2 &= \sum_{p=1}^{N} [\tau^2\omega^2/(p^4+\tau^2\omega^2)] \end{aligned}\right\} \quad (11)$$

The values of f_1 and f_2 are given in Rouse's paper. These equations are essentially a modification of Maxwell's theory. On comparing these equations with experimental data, it turned out to be necessary to introduce a constant G_0 into Eq. 11 to give

$$G = G_0 + (6/\pi^2)(\eta_0/\tau) f_2(\tau\omega) \quad (12)$$

Referring the results of the second method of Maxwell's four element model (the line II in Table I), the value of η_0 should be equal to $(\eta_2+\eta_3)$ and G_0 to G_1 in order to satisfy the experimental values for small ω values. If it is further assumed that the value of τ is equal to τ_2 of the second method, the dotted curves in Figs. 2—5 are obtained. Values of both $\log \eta$ and $\log G$ thus calculated from Eqs. 10 and 12, respectively, are in all cases greater than experimental values. If the value of τ is to be changed to improve the agreement between the calculated values and the experimental values, the value of τ should be larger for $\log \eta$ (to shift the theoretical curves toward the left), and smaller for $\log G$ (to shift the curves to the right). Therefore, Rouse's equation can not explain both $\log \eta$ and $\log G$ simultaneously by using a common set of η_0, G_0, and τ. The other feature of Rouse's curves to be mentioned here is that $\log \eta$ decreases with the increase of $\log \omega$ too slowly and $\log G$ increases too rapidly, if they are compared with the experimental data. This difficulty will be removed if one assumes that there are large aggregates of polymer molecules with large values of η_0 and G_0 in a paste under small frequency and that the aggregates change to smaller ones of smaller η_0 and G_0 with the increase of the frequency. Such an assumption of the structural change of paste with the frequency will be discussed in detail in a following paper of this series.

Comparing the values of parameters in the line II of Table I, it is seen that the rigidity of sweet potato starch paste is much greater than potato starch paste, and both the rigidity and viscosity of rice starch paste are smaller than those of potato and sweet potato starch pastes. These are comparisons for pastes prepared by heating at 90°C for 30 min. The viscoelastic properties of starch paste would change by changing the method of preparation, so that the above stated results do not exclude an expectation that rice starch paste would have larger η and G values than potato starch paste if the pastes are cooked at a higher temperature for a longer time.

The authors wish to thank Dr. Tsurutaro Nakagawa for his kind advice concerning the construction of the rheometer. The authors also thank Dainihon Ink Manufacturing Co. for supporting this project.

Summary

The frequency dependences of dynamic viscosity and dynamic rigidity of (3 and) 5% starch pastes were measured by using a top-drive coaxial rheometer for potato starch, sweet potato starch and rice starch at 30°C. The results were compared with Maxwell's four element model and Rouse's model. Neither fit the experimental results. A structural change of the paste depending on the frequency was suggested.

Faculty of the Science of Living
Osaka City University
Nishi-ku, Osaka

3) P. E. Rouse, *J. Chem. Phys.*, **21**, 1272 (1953).

Dielectric Investigation on Coals. V. Microwave Dielectric Constant

By Kazuo CHITOKU and Keniti HIGASI

(Received August 25, 1960)

Dielectric methods have been applied to the study of coals during these several years[1-4]. In the laboratory of the present writers[1,2] measurements were made directly on polished coal plates as well as on mixtures of coal powder and paraffin-wax, and a frequency range from 300 c./sec. to 50 Mc./sec. was employed. In contrast to the work by Groenewege et al.[3,4], special attention was paid to the frequency dependence of dielectric constants and losses of coals. In the present paper new and more complete information will be given which was obtained by use of a wider frequency range including a microwave measurement at 4.28 cm. wavelength. Representative coals were kindly selected and provided for this measurement by Dr. H. Honda, Resources Research Institute of Japan.

Experimental Apparatus and Method

The dielectric measurement at the microwave frequency of 7000 Mc./sec. was made by use of the transmission method developed by von Hippel and others[5,6]. The block diagram of the apparatus is shown in Fig. 1.

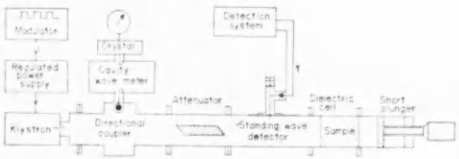

Fig. 1. Block diagram of the apparatus for measuring dielectric constant and loss at 7000 Mc./sec.

The complex dielectric constant $\varepsilon^* = \varepsilon' - j\varepsilon''$ is given by

$$\varepsilon' - j\varepsilon'' = \frac{(1/\lambda_c)^2 - (\gamma_2 d/2\pi d)^2}{(1/\lambda_c)^2 + (1/\lambda_g)^2} \qquad (1)$$

where λ_c and λ_g are the cut-off wavelength and the wavelength in the air-filled guide, respectively. γ_2 is the complex propagation factor of the coal sample and d is the thickness of the sample. For determining $\gamma_2 d$ of the sample, the standing wave ratio $E_{\min.}/E_{\max.}$ and the distance from the sample

TABLE I. MICROWAVE DIELECTRIC CONSTANT OF COAL MIXTURE ESTIMATED BY THE METHOD OF DAKIN AND WORKS[7]

No.	Specimen	Thickness cm.	Dielectric constant (Short)	(Open)	(Values taken)
1	Taihei	0.41	2.845	2.840	
		1.40	2.87	2.85	2.86
2	Tempoku	0.40	3.15	2.85	
		1.40	2.946	2.84	2.89
3	Nakago-kaso	0.415	2.757	2.85	
		1.415	2.908	2.802	2.86
4	Nakago	0.410	2.837	2.789	
		0.310	2.884	2.854	2.81
5	Kasima	0.415	2.620	2.688	
		0.910	2.726	2.692	
		1.305	2.692	2.653	2.67
6	Pocahontas (USA)	0.40	2.926	2.720	
		1.40	2.887	2.683	2.79
7	Hutago	0.40	2.908	2.695	
		1.40	2.690	2.670	2.68
8	Yubari	0.40	2.923	2.700	
		0.82	2.763	2.622	
		1.40	2.680	2.365	2.69
9	Hasima	0.405	2.802	2.660	
		0.305	2.940	2.722	2.73
10	Kamati	0.92	2.800	2.765	
		1.40	2.812	2.765	2.79
11	Yatake	0.40	2.930	2.700	
		1.40	2.796	2.738	2.77
12	Onuki	0.405	2.910	2.735	
		1.310	2.854	2.730	2.79
	Paraffin	0.415	2.230	2.285	
		0.320	2.302	2.248	2.26

1) a) I. Miyasita, R. Miura and K. Higasi, This Bulletin, **28**, 148 (1955); b) I. Miyasita and K. Higasi, ibid., **30**, 513 (1957); c) K. Higasi, I. Miyasita and Y. Ozawa, ibid., **30**, 546 (1957). d) I. Miyasita, K. Higasi and M. Kugo, ibid., **30**, 550 (1957); e) K. Higasi, Y. Higasi and I. Miyasita, ibid., **30**, 556 (1957); f) K. Higasi, *Kagaku*, **27**, 148 (1957); g. K. Higasi and Y. Higasi, ibid., **27**, 630 (1957).

2) a) I. Miyasita, *Bull. Res. Inst. Appl. Elec. Hokkaido Univ., (Oyodenki Kenkyujo Iho)*, **5**, 123 (1953); b) I. Miyasita, ibid., **6**, 117 (1954); c) I. Miyasita, ibid., **7**, 17 (1955); d) I. Miyasita, ibid., **9**, 122 (1957).

3) M. P. Groenewege, J. Schuyer and D. W. van Krevelen, *Fuel*, **34**, 339 (1955).

4) D. W. van Krevelen and J. Schuyer, "Coal Science", Elsevier Publ. Co., Amsterdam (1957).

5) S. Roberts and A. R. von Hippel, *J. Appl. Phys.*, **17**, 610 (1946).

6) A. R. von Hippel, "Dielectrics and Waves", John Wiley and Sons, New York, N. Y., (1954); A. R. von Hippel, "Dielectric Materials and Applications", John Wiley and Sons, New York, N. Y., (1954).

7) T. W. Dakin and C. N. Works, *J. Appl. Phys.*, **18**, 789 (1947).

Table II. Chemical analysis of coal

No.	Specimen	Moisture	Ash	Dry-ash-free basis				
				C%	H	O	N	S
1	Taihei	12.86	5.84	65.10	4.93	28.43	0.93	0.62
2	Tempoku	12.80	1.52	70.37	4.74	23.79	1.10	0
3	Nakago-kaso	11.19	4.75	70.92	4.65	23.59	0.73	0.11
4	Nakago	13.32	3.96	74.33	5.26	19.29	0.95	0.17
5	Kasima	4.11	5.02	77.94	6.07	12.62	0.65	2.72
6	Pocahontas (USA)	2.09	2.59	82.79	6.02	8.86	2.01	0.32
7	Hutago	1.54	2.31	83.16	6.31	8.81	1.56	0.16
8	Yubari	1.13	2.67	84.85	6.16	7.20	1.78	0.01
9	Hasima	1.24	2.09	86.59	5.56	6.48	1.22	0.15
10	Kamati	1.05	2.47	89.47	4.61	3.43	1.84	0.65
11	Yatake	1.11	2.74	89.55	4.86	3.07	1.88	0.64
12	Onuki	1.68	1.80	91.16	3.97	2.56	1.78	0.53

boundary to the position $E_{min.}$ were measured[6]. The ambiguity in finding $\gamma_2 d$ can be avoided by carrying out both open and short circuit measurements by the standard method. Further, as the samples treated here had low dielectric losses the simplification due to Dakin and Works[7] could be introduced into the calculation. Values of ε' obtained independently in this manner by open and short circuit methods were compared with each other (see Table I). A weighted mean value is taken for each sample.

The sample material which was made of coal powder and paraffin-wax was prepared in the form having the exact dimension required by the size of the wave guide, the possible error being ± 0.05 mm. (see Fig. 1).

The measurement at the frequency range between 1~20 kc./sec. was made by a low frequency bridge (Yokogawa BV-z-103) (see Ref. 2 for further information.). For the frequency range between 1~50 Mc./sec. a Q-meter (Yokogawa CA-102) was used. In order to compare the values of dielectric constants obtained by three different apparatuses, the absolute determination of dielectric constants becomes necessary. For this purpose, standard reference materials of dielectric constants provided by the Government Electrotechnical Laboratory, Tokyo, were measured with the apparatuses described above and compared with the results on coals. The maximum error in the dielectric constant is believed to be 5% and reliability in values of dielectric losses are somewhat lower but the latter are not so important in the interpretation as dielectric constants. All the measurements were carried out at room temperature.

Experimental Materials

All the coal specimens examined in these experiments were kindly provided by Dr. H. Honda, Resources Research Institute, Japan. The chemical analyses of the samples are given in Table II. The paramagnetic susceptibility has been examined by the present writers for the following specimens[8]: No. 4, 0.40; No. 8, 0.28; No. 11, 1.23; No. 12, 3.90 10^{-5} c. g. s. electromagnetic units per gram.

On account of its exceptionally high dielectric constant, water is the greatest cause of error in the dielectric measurement. Great care was taken to eliminate any traces of moisture contained in the samples. The coal samples were reduced into powder form below 200 mesh and strongly dried by heating at 105°C and reduced pressure of 10^{-2} mmHg for 30 hr.

About 26 g. of dried powder of coal thus obtained was mixed with 20 g. of melted paraffin-wax, cooled in a mold and cut carefully into a shape suitable for the measurement. The volume percent of coal in the mixture was estimated for each sample by measuring the densities of coal and paraffin-wax. The properties of solid paraffin-wax used are: density 0.914/24°C, m. p. 58.5~60°C, dielectric constant 2.29/1 Mc., 2.26/7000 Mc. and $\tan\delta$ 0.000/1 kc.~7000 Mc.

Results

Dielectric constants ε' and $\tan\delta$ obtained for the coal mixture are recorded in Table III.

In order to determine the value of the dielectric constant of a coal from that of a mixture, Böttcher's equation[1,9,10] was employed, in which ε', ε_1' and ε_2' are the dielectric constant

$$\frac{\varepsilon'-\varepsilon_1'}{3\varepsilon'} = v_2 \frac{\varepsilon_2'-\varepsilon_1'}{\varepsilon_2'+2\varepsilon'} \qquad (2)$$

of the mixture, the paraffin-wax and coal particles, respectively and v_2 is the volume fraction of the coal particle in the mixture. The value ε_2' for each specimen of coal thus obtained is shown in parentheses below that for the mixture.

8) H. Honda, K. Chitoku, Y. Yokozawa and K. Higasi, This Bulletin, **31**, 891 (1958).

9) C. J. F. Böttcher, *Rec. trav. chim.*, **64**, 47 (1945); C. J. F. Böttcher, "The Theory of Electric Polarisation", Elsevier, Amsterdam (1952), p. 417.

10) Y. Zyomoto, *J. Fuel Soc. Japan*, (*NenryoKyokaishi*), **37**, 248 (1958).

TABLE III. DIELECTRIC CONSTANTS (ε') AND LOSS TANGENT (UNIT: 10^{-4}) OF COAL MIXTURES MEASURED AT FREQUENCIES 1 kc./sec.~7000 Mc./sec. AND DIELECTRIC CONSTANTS OF COALS ESTIMATED (ε_2')

No. (Specimen)	Vol. % of coal		1 kc.	3 kc.	10 kc.	20 kc.	1 Mc.	3 Mc.	50 Mc.	7000 Mc.
1	40.1	ε'	3.17	3.17	3.19	3.19	3.06	3.03	3.01	2.86
		ε_2'	(4.75)	(4.75)	(4.82)	(4.82)	(4.51)	(4.44)	(4.38)	(3.95)
		tan ϑ	238	169	113	83	92	101	108	142
2	49.0	ε'	3.26	3.21	3.21	3.21	3.19	3.18	3.14	2.89
		ε_2'	(4.45)	(4.32)	(4.32)	(4.32)	(4.35)	(4.34)	(4.24)	(3.66)
		tan ϑ	91	67	58	72	72	84	127	158
3	46.0	ε'	3.21	3.23	3.22	3.22	3.12	3.10	3.08	2.86
		ε_2'	(4.48)	(4.53)	(4.51)	(4.51)	(4.33)	(4.29)	(4.24)	(3.69)
		tan ϑ	64	72	61	49	68	76	95	134
4	48.0	ε'	3.09	3.10	3.09	3.05	3.10	3.09	3.08	2.81
		ε_2'	(4.07)	(4.09)	(4.07)	(3.97)	(4.17)	(4.16)	(4.14)	(3.50)
		tan ϑ	83	64	50	61	52	53	67	99
5	47.4	ε'	2.89	2.89	2.89	2.89	2.78	2.78	2.77	2.67
		ε_2'	(3.59)	(3.59)	(3.59)	(3.59)	(3.40)	(3.42)	(3.39)	(3.18)
		tan ϑ	32	58	55	40	39	37	50	92
6	48.4	ε'	2.87	2.87	2.81	2.81	2.81	2.81	2.79	2.79
		ε_2'	(3.52)	(3.52)	(3.38)	(3.38)	(3.45)	(3.46)	(3.41)	(3.44)
		tan ϑ	229	143	138	97	44	41	48	70
7	50.4	ε'	2.85	2.79	2.79	2.79	2.79	2.79	2.78	2.68
		ε_2'	(3.42)	(3.29)	(3.29)	(3.29)	(3.35)	(3.36)	(3.34)	(3.14)
		tan ϑ	106	65	43	47	22	25	31	59
8	49.6	ε'	2.77	2.77	2.77	2.77	2.76	2.76	2.76	2.69
		ε_2'	(3.26)	(3.26)	(3.26)	(3.26)	(3.30)	(3.31)	(3.31)	(3.18)
		tan ϑ	68	10	26	22	17	19	16	51
9	49.5	ε'	2.84	2.84	2.84	2.84	2.77	2.77	2.77	2.73
		ε_2'	(3.42)	(3.42)	(3.42)	(3.42)	(3.32)	(3.34)	(3.34)	(3.27)
		tan ϑ	66	75	81	65	25	21	33	75
10	47.2	ε'	2.83	3.87	2.89	2.89	2.81	2.81	2.80	2.79
		ε_2'	(3.45)	(3.55)	(3.60)	(3.60)	(3.48)	(3.49)	(3.47)	(3.47)
		tan ϑ	67	120	46	23	19	21	21	25
11	45.9	ε'	2.85	2.86	2.86	2.86	2.84	2.83	2.82	2.77
		ε_2'	(3.54)	(3.57)	(3.57)	(3.57)	(3.59)	(3.58)	(3.56)	(3.46)
		tan ϑ	152	68	72	48	21	18	13	26
12	40.0	ε'	3.19	3.05	3.05	3.05	2.89	2.89	2.87	2.79
		ε_2'	(4.83)	(4.37)	(4.37)	(4.37)	(3.98)	(4.00)	(3.94)	(3.73)
		tan ϑ	886	563	311	192	60	37	21	40
Paraffin[a)]		ε_1	2.34	2.34	2.34	2.34	2.29	2.28	2.28	2.26

a) Values of ε_1 used in calculating ε_2 by Eq. 2.

Dielectric Constant and Oxygen Content.— Dielectric constants obtained at 1 kc./sec. and 7000 Mc./sec. are plotted against oxygen content (Fig. 2). Intermediate frequency dielectric constants lie between the two curves.

Dielectric constants decrease sharply at first but increase regularly with increase in oxygen content after reaching a minimum at about 8%. From functional group analysis of coal it has been found that the amounts of hydroxyl groups, carboxyl groups, carbonyl groups and methoxyl groups increase with oxygen content[11]. Among them, the hydroxyl group is regarded as the most important*. From the infrared analysis, the absorption band at 3.0 μ is ascribed to the existence of associated OH and NH bonds[12]. One might infer from these

11) M. Ihnatowicz, *Prace Glownego Inst. Gornictwa* (Katowice) *Komun.*, 125 (1952); L. Blom, L. Edelhausen and D. W. van Krevelen, *Fuel*, **36**, 135 (1957) cited by Ref. 3, p. 217.

* According to private communication from Dr. H. Honda, functional analysis gives the following data. No. 2, Tempoku: O, 23.79%; O_{OH}: 10.3%; O_{COOH}, 0.4%. No. 6, Pocahontas: O, 8.86%; O_{OH}, 2.4%; O_{COOH}, 0.5%. No. 8, Yubari: O, 7.20%; O_{OH}, 0%; O_{COOH}, 0.9%. No. 10, Kamati: O, 3.43%; O_{OH}, 0%; O_{COOH}, 0%.

12) C. G. Cannon and G. B. B. Sutherland, *Trans. Faraday Soc.*, **41**, 279 (1945) and others; see Ref. 3, p. 185.

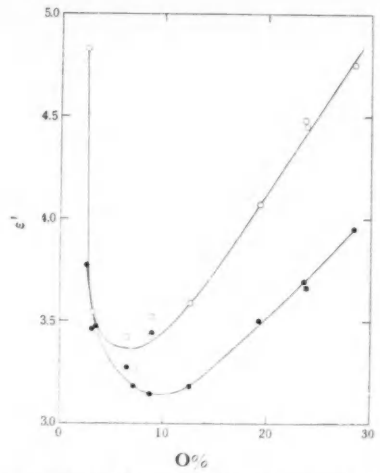

Fig. 2. Dielectric constants of coals (ε_2') at frequencies 1 kc./sec. and 7000 Mc./sec. and oxygen content (dry-ash-free basis).
—○— 1 kc. —●— 7000 Mc.

pieces of evidence that polar groups which are closely associated with the oxygen content are mainly responsible for the dielectric constant of coal containing more than 10% oxygen. This seems parallelled by the fact that dielectric constants of polymers increase with the amount of polar groups contained in them[13,14]. Indeed, coals generally speaking are a sort of high-polymers having some polar groups.

Dielectric Constant and Carbon Content. — Dielectric constants obtained at three frequencies, 1 kc./sec., 1 Mc./sec. and 7000 Mc./sec. are plotted against carbon content (Fig. 3). For the sake of comparison, optical dielectric constants as defined by the refractive index n and the absorption index k for visible light of the wavelength 5460 Å.

$$\varepsilon_\infty = n^2(1-k^2) \qquad (3)$$

are plotted as dotted lines in the same graph. The optical measurement is due to Huntjens and van Krevelen[15]. There are available other optical measurements[16], but they are not recorded here in order to prevent the figure from becoming overcrowded with points.

From a glance at Fig. 3, it will be seen that in the region C 85~89% all the dielectric constants, at audio, radio and microwave frequencies converge so that they become almost identical to each other. The plotted curve for

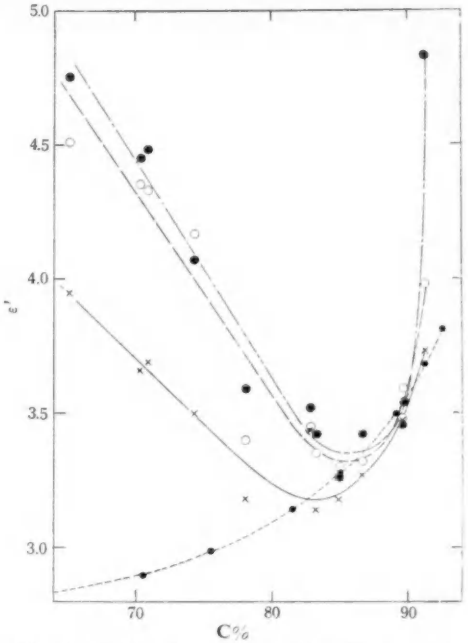

Fig. 3. Dielectric constants of coals (ε_2') at various frequencies and carbon contents of coals.
—•— 1 kc.
—○— 1 Mc.
—×— 7000 Mc.
----●---- van Krevelen $n^2(1-k^2)$

optical dielectric constants lies between these three curves. This is probably anomalous, but it must be remembered that optical dielectric constants were obtained for coals of different origins**. It may be reasonable to assume that microwave values in this region are almost identical with the optical dielectric constant.

With the decrease in carbon content (less than 80%) the difference between the optical and the microwave dielectric constants becomes significant. It was unexpected that there should be such a large difference between these values in this region. If this difference is due to the rotation of polar groups, these groups must have a small size[14]. One might infer from this that the perticular polar groups responsible for this phenomenon are hydroxyl groups situated at the periphery of the aromatic system, because the internal rotation of non-associated OH groups around the C–O axis will be least sterically hindered.

Fischer found that diphenyl ether has an anomalously small relaxation time[17]. Recently

13) R. M. Fuoss, *J. Am. Chem. Soc.*, **63**, 369 (1941).
14) C. P. Smyth, "Dielectric Behavior and Structure", McGraw-Hill Book Co., Inc., New York, N. Y., 1955.
15) F. J. Huntjens and D. W. van Krevelen, *Fuel*, **33**, 88 (1954).
16) D. G. Murchison, *Brennstoff Chem.*, **39**, 47 (1958); S. R. Broadbent and A. J. Shaw, *Fuel*, **34**, 385 (1955).

** In fact, Broadbent and Shaw[16] gave smaller optical dielectric constants than van Krevelen.
17) E. Fischer, *Z. Elektrochem.*, **53**, 16 (1949).

an explanation has been given for this observation as arising from the internal rotation of the two benzene rings around C–O axes[18]. Coal is sometimes considered as built up of aromatic ring complexes linked through oxygen or non-aromatic bridges containing oxygen atoms[19]. Possibly these units might provide certain contributions to the microwave dielectric constant, if a particular type of internal rotation is to occur. But roughly speaking the hydroxyl group will be mainly responsible for this effect.

It would be a matter of speculation to estimate dipole moments for coals. However, if coal may be regarded as a supercooled liquid[3], the Onsager equation for liquids may be used for this purpose[16,17]. Further, on account of the low dielectric constant, the Debye equation will give practically the same moment values the Onsager equation[13]. It can be shown that the dipole moment μ for the unit having the molecular volume M/d is

$$\mu = A\left[(\varepsilon_2' - \varepsilon_\infty)\frac{M}{d}\right]^{1/2} \qquad (4)$$

where A for Debye equation is

$$A^2 = \frac{27kT}{4\pi N(\varepsilon_2' + 2)(\varepsilon_\infty + 2)}, \qquad (5)$$

in which k is Boltzman constant, N is Avogadro constant and T is the absolute temperature. Further, at room temperature, $T = 298°C$

$$A^2 = \frac{0.147 \times 10^{-36}}{(\varepsilon_2' + 2)(\varepsilon_\infty + 2)} \quad \text{Debye}$$

In similar way it can be shown that

$$A^2 = \frac{0.147 \times 10^{-36}(2\varepsilon_2' + \varepsilon_\infty)}{3\varepsilon_2'(\varepsilon_\infty + 2)^2} \quad \text{Onsager}$$

There exist no reliable data for the molecular weight of coal. According to van Krevelen and Schuyer[3] the average molecular weight is in the vicinity of 2500. We shall assume an arbitrary molecular volume $M/d = 2000$ for the purposes of the present calculation. For coal with a density of 1.3, this assumption gives a molecular weight of 2600.

Regarding the static dielectric constant ε_2' in Eq. 1 we shall use values obtained at frequency of 1 kc. Optical dielectric constants ε_∞ are calculated by Eq. 3 using van Krevelen's data, which are supposed to be somewhat higher than those of the coals considered here; the estimated dipole moment is consequently slightly smaller than the actual moment. Further, the A value for the Debye equation will be used in the calculation of the moment. The result is shown in Table IV.

TABLE IV. DIPOLE MOMENTS OF COALS (μ) FOR THE MOLECULAR VOLUME ($M/d = 2000$)

No.	Specimen	C%	ε_2'/1 kc.	ε_∞	μ, D
1	Taihei	65.10	4.75	2.85	4.1
2	Tempoku	70.37	4.45	2.90	3.8
3	Nakago-kaso	70.92	4.48	2.91	3.8
4	Nakago	74.33	4.07	2.96	3.3
5	Kasima	77.94	3.59	3.05	2.4
6	Pocahontas (USA)	82.79	3.52	3.20	1.8
7	Hutago	83.16	3.42	3.21	1.5
8	Yubari	84.85	3.26	3.28	0
9	Hasima	86.59	3.42	3.36	~0
10	Kamati	89.47	3.45	3.53	0
11	Yatake	89.55	3.54	3.54	0
12	Onuki	91.16	4.83	3.68	—

As an example we shall consider a dipole moment 3.8 D obtained for specimen No. 2 Tempoku brown coal. If this magnitude of moment arises only from OH groups which have complete freedom of rotation around C–O axis, the number of OH groups in a volume 2000 cc. will be estimated by

$$\mu^2_{obs} = n \cdot \mu^2_{OH} \qquad (6)$$

where μ_{obs} and μ_{OH} are moments observed and that of the OH group respectively. Putting $\mu_{obs} = 3.8$ D and $\mu_{OH} = 1.56$ D[20] we obtain $n = 5.9$; there are about 6 OH groups capable of rotation.

On the other hand, functional analysis reveals that this particular coal specimen has a hydroxyl (phenolic) percentage of 10.3%. In molecular volume $M/d = 2000$ ($d = 1.41$), this gives 291 g. oxygen, that is 18 OH groups. Therefore, one may conclude that about one-third of the total OH groups can rotate freely. The hydroxyl percentage chemically determined does not represented the amount of OH group actually existing in coal. There is no strong reason for supposing that a certain fraction of OH groups has complete freedom of rotation while another fraction has not and that other polar groups can not make a contribution to dielectric constant. In fact, the estimation of the dipole moment described above and its related discussion has only qualitative significance.

Summary

1. Using the transmission method, resonance method and bridge method, dielectric constants

18) K. Higasi and C. P. Smyth, to be published in *J. Am. Chem. Soc.*
19) S. G. Ward, *J. Inst. Fuel*, 21, 80 (1947); cited in Ref. 3, p. 207.
20) Y. Kurita and M. Kubo, This Bulletin, 27, 364 (1954). This is not the moment of OH group moment itself but the component of the phenolic OH moment perpendicular to the C–O axis.

and losses are measured on paraffin-wax mixtures of twelve specimens of coal ranging from C 65 to 92%.

2. Dielectric constants of coals are estimated for these coals by means of Böttcher's equation.

3. The relation between dielectric constant and oxygen content is discussed and it is shown that polar groups contribute to dielectric constant.

4. From the comparison with optical dielectric constant, the motion of dipoles in coals in the electric field can be discussed. Rough estimates of dipole moments are also given.

The present writers wish to thank Dr. H. Honda for his cooperation in this work and also Dr. H. Baba for his assistance in performing the calculation of microwave dielectric constants.

Research Institute of Applied Electricity
Hokkaido University, Sapporo

Polarographic Behavior of Vanadium and Iron in Thiocyanate

By G. S. Deshmukh and J. P. Srivastava

(Received June 13, 1960)

Thiocyanate has been used extensively as a complexing agent for a number of cations. Meite's[1] observation that iron (III) is reduced in a medium composed of 0.7 M KCNS, 0.02 M sulfuric acid and 0.004% gelatin with a half-wave potential >0.0 volt is contradicted by the data of the "Polarographic spectra"[2] giving $E_{1/2}$ vs. S. C. E. as −0.2 volt. The condition for the latter observation has not been defined.

Direct estimation of VO^{2+} based on the catalytic action of the ion on potassium chlorate and potassium iodide reaction has been developed recently by Shiokawa[3]. Polarographic characteristics of vanadyl ion showed that it is reducible or oxidizable depending on the nature of the complex formed with the supporting electrolyte[4]. Syrokomskiĭ and Nazareva[5] devised a new type of coulometer to effect anodic oxidation of VO^{2+} to VO^{3+} which is titrable with Mohr's salt solution.

Preliminary investigations showed that thiocyanate in presence of mineral acids is capable of reducing vanadium(V) to lower valency states. Vanadium(V) and thiocyanate solution when mixed together developed the green coloration characteristics of trivalent vanadium ion, which on raising the acidity of the solution turned blue. The intermediate green state was initially mistaken to be vanadium green, corresponding to molybdenum blue, and was found to be very stable even on prolonged exposure to air. Spectrophotometric studies revealed that it is only the mixture of vanadium(V) and vanadium(IV). This conclusion was further confirmed when the green solution was shaken with isobutyl alcohol. The solution separated into two layers; the yellow aqueous layer and blue tetravalent vanadium in the organic layer.

The present communication reports in detail a study of polarographic behavior of vanadium (IV) thus obtained and iron(III) in potassium thiocyanate. Appropriate conditions for the simultaneous determination of the two elements in presence of each other have also been described.

Experimental

Leeds and Northrup Electrochemograph Type E was used for recording the polarograms in conjunction with an external saturated calomel reference electrode connected through an agar-potassium chloride bridge to the electrolysis cell. The temperature was maintained throughout at 25±0.1°C. A Beckman zeromatic pH meter was used for measuring the pH of the solutions. The dropping mercury electrode had $m^{2/3}t^{1/6}$ value of 2.414 $mg^{2/3}/sec^{1/2}$ with open circuit.

Vanadyl sulfate solution was prepared by dissolving the reagent grade vanadium pentoxide in dilute sulfuric acid and reducing it by sulfur dioxide. Excess of sulfur dioxide was boiled off and the solution standardized against potassium permanganate. Iron solution was obtained by dissolving a weighed quantity of "A. R. ferric ammonium sulfate" in distilled water. This was

1) L. Meites, "Polarographic Technique", Interscience Publishers, New York, N. Y. (1955), p. 269.
2) L. Meites, loc. cit Front and back lining papers.
3) T. Shiokawa, *J. Chem. Soc. Japan, Pure Chem. Sec. (Nippon Kagaku Zasshi)*, **70**, 418 (1950).
4) I. M. Kolthoff and J. J. Lingane, "Polarography", Vol. II, Interscience Publishers, New York, N. Y. (1952), p. 449.
5) V. S. Syrokomskii and T. I. Nazareva, *Zhur. Anal. Khim.*, **6**, 15 (1951).

also standardized against potassium permanganate. All other chemicals used were of reagent grade.

Results and Discussion

Characteristics of Polarographic Waves.—A number of vanadium(IV) and iron(III) polarograms were recorded at different pH values. It was observed that vanadium(IV) gets reduced at and below pH≈3. The two reduction stages of vanadium(IV) are well developed when the pH of the solution was below 2.0 but above 1.5. Further increase in acidity shifted the half-wave potentials of the first wave towards positive potentials. The wave was completely obliterated below a pH of 0.5. In less acidic solutions (between pH 2.0~3.5), the first wave was drawn out and ill defined. Iron polarograms also were well defined below pH 3.0 but the $E_{1/2}$ ($E_{1/2}$ = −0.17 volt vs. S. C. E. in 1.0 M potassium thiocyanate containing 0.005% gelatin at pH 1) was not much affected by the pH of the solution (cf. Table I).

Thiocyanate concentration had considerable effect on the half-wave potential of vanadium. While the first wave was shifted towards negative potentials with increasing thiocyanate concentration, the $E_{1/2}$ of the second wave moved to more positive potentials. The polarograms of iron were also shifted towards negative potentials by the increased concentrations of the supporting electrolyte. The shift in both the cases i. e., the first wave of vanadium and the polarograms of iron, towards negative potentials with the increasing thiocyanate concentrations may possibly be attributed to the superimposition of the anodic wave of thiocyanate. During the course of experiments it was further observed that the half-wave potential of the iron wave was dependent not only on the thiocyanate concentrations but also on the iron and thiocyanate ratio. Conjugating it with the previous observation that the $E_{1/2}$ of iron polarograms remain unaffected by the pH of the solution, it may

TABLE I. EFFECT OF pH ON VANADIUM AND IRON POLAROGRAMS

Solution No.	pH of solun.	$E_{1/2}$ of vanadium polarograms, volt vs. S. C. E.		$E_{1/2}$ of iron polarograms, volt vs. S. C. E.
		1st wave	2nd wave	
1	0.5	−0.20	−0.57	−0.20
2	0.8	−0.21	−0.57	−0.18
3	1.1	−0.23	−0.56	−0.18
4	1.3	−0.25	−0.56	−0.18
5	1.5	−0.27	−0.57	−0.18
6	1.8	−0.30	−0.57	−0.17
7	2.0	−0.32	−0.57	
8	2.5	Not defined	−0.57	
9	3.0	Not reducible	−0.57	−0.17
10	3.6	Not reducible		

TABLE II. EFFECT OF SUPPORTING ELECTROLYTE'S CONCENTRATION ON VANADIUM AND IRON POLAROGRAMS

Solution No.	Thiocyanate concentration M	$E_{1/2}$ of vanadium polarograms, volt vs. S. C. E.		$E_{1/2}$ of iron polarograms, volt vs. S. C. E.
		1st wave	2nd wave	
1	5.0	−0.30	−0.49	−0.31
2	3.75	−0.28	−0.51	−0.29
3	2.50	−0.24	−0.53	−0.26
4	1.25	−0.25	−0.56	−0.20
5	1.00	−0.25	−0.56	−0.17
6	0.50	—	−0.57	−0.15
7	0.25	Washed off	−0.58	−0.15

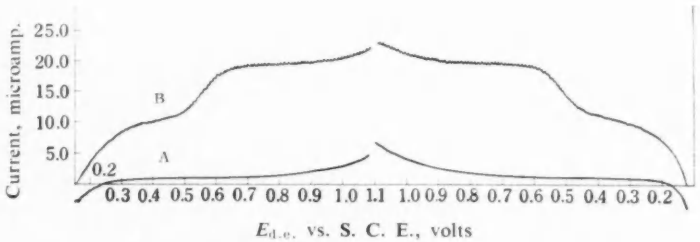

Fig. 1. Direct and reverse vanadium (2.19 mM) polarograms

Temperature 25±0.1°C — Recorder damping 2.0
Drop time 3.33 sec. — Recorder range 50 μA
Gelatin concn. 0.005% — pH of solution 1.6

Waves	Zero line	$E_{1/2}$ of 1st wave	$E_{1/2}$ of 2nd wave
A	0.0	Blank	—
B	2.5	−0.21	−0.537

be concluded that over the pH range studied a series of iron thiocyanate complexes are formed depending on the iron : thiocyanate ratio. Shifting of the second wave of vanadium towards more positive potentials with increasing thiocyanate concentrations suggest that the V(II)–NCS complex apparently has a lower dissociation constant than the V(III)–NCS complex (cf. Table II).

A study of the typical polarogram and its log plot shows that the vanadium waves are reversible (Fig. 1). The polarogram was obtained with a mixture of 2.19 mM vanadyl sulfate and 1.0 M potassium thiocyanate and 0.005% gelatin as maximum suppressor. In agreement with the general equation

$$E_{d.e.} = E_{1/2} - \frac{0.059}{n} \log \frac{i}{i_d - i}$$

the plot of $E_{d.e.}$ vs. $\log \frac{i}{i_d - i}$ is a straight line. The slope of 0.07 volt for the second wave suggests one electron transfer in reduction. As both the waves of vanadium have the same height, it was concluded that vanadium gets reduced first to vanadium(III) and finally to vanadium(II).

Iron polarograms exhibit only one reduction stage, and thus suggest the possibility of only one electron change. $E_{1/2}$ for iron reduction could not be assigned due to its dependence both on iron as well as on thiocyanate concentration but under the most restricted conditions of 2.00 mM iron and 1.0 M thiocyanate with 0.005% gelatin as maximum suppressor the $E_{1/2}$ observed was −0.17 volt vs. S. C. E.

The average $E_{1/2}$ for 2.19 mM vanadyl sulfate in 1.0 M potassium thiocyanate and 0.005% gelatin as maximum suppressor at pH 1.5 was found to be −0.21 volt, and to be −0.54 volt for the first and second wave respectively.

Under the conditions defined, a series of vanadium(IV) polarograms were run to plot the calibration curve. All the wave heights for the first wave were read from the plots at −0.45 volt and the corresponding values for the residual current were deducted to obtain the i_d for vanadium(IV) alone. The wave heights for the second stage reduction were calculated by extrapolating the plateau of the two waves.

The values of I obtained for different concentrations (cf. Table III) show that the reduction for both the waves are diffusion controlled. A linear concentration-current relationship is also followed by iron polarograms. The wave heights for iron polarograms were obtained by taking the difference of the actual and residual wave height at the same potential i. e., at −0.45 volt.

Table III. Diffusion current constant for vanadium polarograms

Solution No.	Concentration of vanadium mM	$I(I=i_d/cm^{2/3}\ t^{1/6})$ of vanadium waves	
		1st wave	2nd wave
1	0.438	1.43	1.65
2	0.876	1.42	1.65
3	1.09	1.42	1.65
4	1.31	1.42	1.65
5	1.75	1.42	1.66
6	2.19	1.42	1.65
7	2.62	1.42	1.65
8	3.5	1.42	1.66
9	3.94	1.42	1.65
10	4.38	1.42	1.65

The effect of different cations on vanadium polarograms was also studied. Cobalt and manganese do not interfere with the polarogram. Nickel and chromium(III) develop their own waves at more negative potentials but the diffusion current plateau for vanadium is not appreciably distorted. The presence of molybdenum(VI) and tungsten(VI) is detrimental as these ions deteriorate the vanadium waves, thus making the measurement of diffusion current practically impossible. Cupric ion has a typical effect of shifting the vanadium waves to more negative potentials. This results in the formation of only one wave which is probably the resultant of the waves comprising the wave heights due to Cu^{2+} and both the vanadium waves. The presence of nitrates, chlorides, bisulfates and ammonium ions has no effect on vanadium polarograms. None of these above mentioned ions except molybdenum and tungsten affect the iron polarograms. Molybdenum and tungsten completely distort the wave.

Recommended Procedure of Analysis.—The appropriate amount of unknown solution to give a final vanadium concentration above 0.4 mM and iron concentration above 0.5 mM is mixed with potassium thiocyanate. The overall potassium thiocyanate concentration is maintained at 1.0 M. The acidity of the solution is adjusted to pH 1.5 with hydrochloric acid and the mixture allowed to stand for 15 min. During this period vanadium(V) gets reduced to vanadium(IV). The appearance of violet color (being a mixture of blue due to vanadium(IV) and blood-red due to iron(III) thiocyanate) indicates the completion of the reduction. This solution when polarographed exhibits a two-step reduction, the first being the composite wave due to the reductions of iron(III) to iron(II) and vanadium(IV) to vanadium(III), and the second one being due to the degradation of vanadium(III) to vanadium(II). In order to derive the vanadium

content of the solution, the wave height of the second stage reduction is measured by extrapolating the plateaus and reading it from the calibration curve.

On subtracting the height of the first wave of vanadium as read from the calibration curve for the corresponding value of vanadium obtained previously, from that of the composite wave (the polarogram of the mixed iron and vanadium solution), the contribution due to iron alone is calculated. In the procedure adopted, wave heights of iron and vanadium polarograms are appreciable, only if the concentrations of corresponding elements are above the prescribed limit, i. e., 0.5 mM and 0.4 mM respectively.

TABLE IV. SIMULTANEOUS DETERMINATION OF IRON AND VANADIUM

Solution No.	Vanadium added mM	Vanadium recovered, mM	Iron added, mM	Iron recovered mM
1	0.438	0.438	0.4	0.42
2	0.87	0.87	0.8	0.81
3	1.31	1.33	1.2	1.21
4	1.75	1.79	1.6	1.62
5	2.19	2.21	2.0	2.0
6	2.62	2.66	2.4	2.4
7	3.16	3.16	2.8	2.82
8	3.50	3.50	3.2	3.18
9	3.94	4.10	3.6	3.6
10	4.38	4.42	4.01	4.01

Values obtained by the above procedure are reported in Table IV. It may be seen that the results are within the limits of experimental error. The method provides a convenient procedure for the simultaneous determination of iron and vanadium contents and may suitably be adopted to the analysis of vanadium steels provided copper(II), molybdenum(VI), and tangsten(VI) are sequestered.

The authors wish to express their sincere thanks to Professor S. S. Joshi for his advice and to Dr. G. B. Singh, Head of the Chemistry Department, for facilities during the course of this study. The financial aid by the Government of India to one of us (J. P. S.) is also gratefully acknowledged.

Chemical Laboratories
Banaras Hindu University
Varanasi-5

The Thermal Decomposition of Dimethyl Ether in the Presence of Hydrogen Sulfide

By Naomi IMAI and Osamu TOYAMA

(Received August 23, 1960)

The catalytic action of hydrogen sulfide on the thermal[1] as well as photochemical[2] chain decomposition of acetaldehyde has been studied in this laboratory, and its catalytic effect has been attributed to the reactions between methyl radicals and hydrogen sulfide molecules and between hydrosulfide radicals and acetaldehyde molecules, both taking place faster than the reaction between methyl radicals and acetaldehyde molecules. Methanethiol was also found to have an analogous catalytic action on the thermal decomposition of acetaldehyde[3].

Dimethyl ether has been known to decompose thermally by a chain mechanism involving methyl radicals[4-6] and its decomposition may therefore be expected to be catalyzed by hydrogen sulfide like that of acetaldehyde. In the present work the kinetics of the thermal decomposition of dimethyl ether in the presence of hydrogen sulfide has been studied in the temperature range 360 to 440°C and compared with the results obtained in the absence of hydrogen sulfide.

Experimental

Materials. — Dimethyl ether was prepared by dehydration of methyl alcohol by concentrated sulfuric acid at 80°C, decarbonated and dried by potassium hydroxide and calcium chloride, and purified by bulb-to-bulb distillation. Hydrogen sulfide was

1) N. Imai and O. Toyama, unpuhlished work.
2) N. Imai and O. Toyama, This Bulletin, 33, 1120 (1960).
3) N. Imai and O. Toyama, ibid., 33, 1408 (1960).
4) F. O. Rice and K. F. Herzfeld, *J. Am. Chem. Soc.*, 56, 284 (1934).
5) S. W. Benson, *J. Chem. Phys.*, 25, 27 (1956).
6) S. W. Benson and P. V. S. Jain, ibid., 31, 1008 (1959).

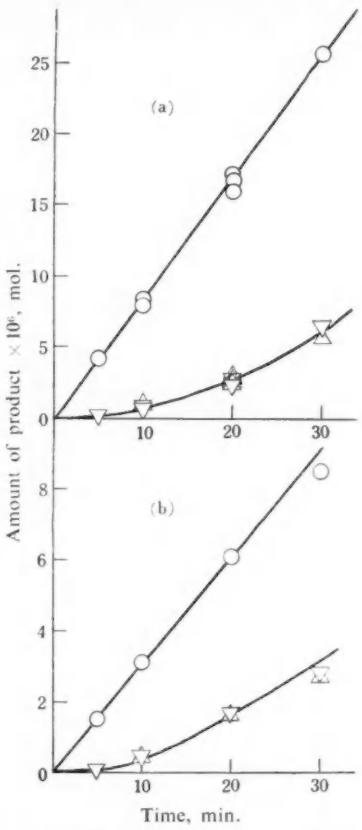

Fig. 1. Dependence of amount of product on reaction time. ○, CH_4; ▽, CO; △, H_2. (a) $[CH_3OCH_3]=2.13\times10^{-6}$ mol. cc^{-1}, $[H_2S]=0$, 440°C; (b) $[CH_3OCH_3]=2.32\times10^{-6}$, $[H_2S]=1.64\times10^{-6}$ mol. cc^{-1}, 380°C.

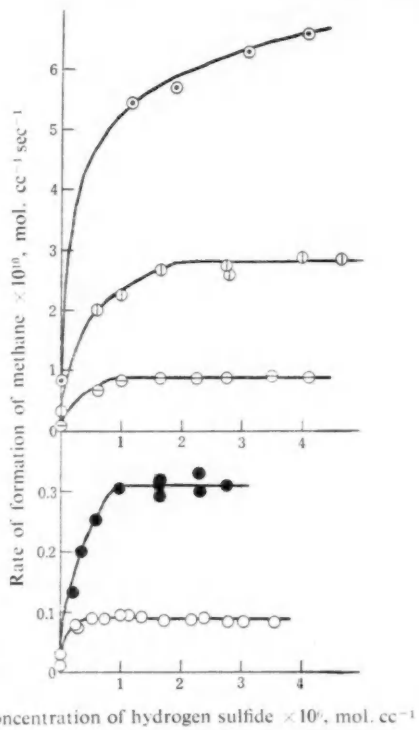

Fig. 3. Dependence of the rate of decomposition in the presence of hydrogen sulfide on its concentration. ○, $[CH_3O\cdot CH_3]=2.39\times10^{-6}$ mol. cc^{-1}, 360°C; ●, $[CH_3OCH_3]=2.32\times10^{-6}$ mol. cc^{-1}, 380°C; ⊖, $[CH_3OCH_3]=2.25\times10^{-6}$ mol. cc^{-1}, 400°C; ⓣ, $[CH_3OCH_3]=2.19\times10^{-6}$ mol. cc^{-1}, 420°C; ⊙, $[CH_3OCH_3]=2.13\times10^{-6}$ mol. cc^{-1}, 440°C.

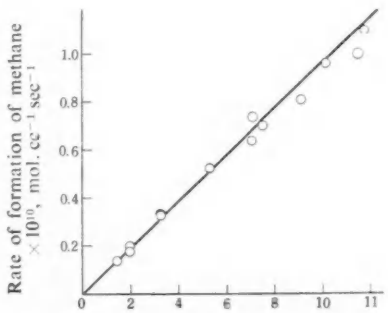

Fig. 2. Dependence of the rate of decomposition of the ether alone on its concentration at 420°C.

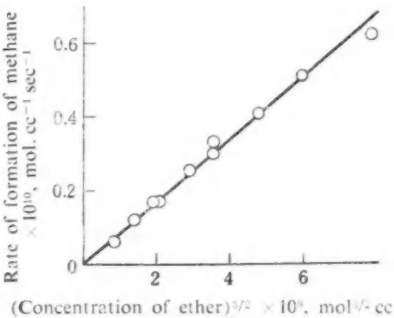

Fig. 4. Dependence of the rate of the decomposition of ether on its concentration in the presence of 2.32×10^{-6} mol. cc^{-1} of hydrogen sulfide at 380°C.

TABLE I. PYROLYSIS OF DIMETHYL ETHER IN THE ABSENCE AND PRESENCE OF HYDROGEN SULFIDE

Temp. °C	Initial concentration $\times 10^6$ mol./cc.		Reaction time min.	Amount of product $\times 10^6$ mol.		
	CH_3OCH_3	H_2S		CH_4	CO	H_2
360	2.39	0	100	0.79	0.082	—
		0	100	0.81	0.073	—
		0.263	30	2.32	0.187	—
		0.287	30	2.17	0.17	—
		0.527	30	2.64	0.23	—
		0.742	30	2.60	0.31	—
		1.00	30	2.78	0.38	—
		1.13	30	2.80	0.40	—
		1.36	30	2.96	0.48	—
		1.72	40	3.35	0.65	—
		2.18	30	2.55	0.46	—
		2.39	40	3.51	0.74	—
		2.78	40	3.28	0.72	—
		3.04	30	2.46	0.43	—
		3.57	30	2.43	0.44	—
380	2.32	0	50	1.51	0.067	—
		0	100	2.86	0.186	—
		0	100	2.92	0.21	—
		0.204	20	2.6	0.38	—
		0.344	20	3.9	0.40	—
		0.580	20	4.9	0.66	—
		0.975	5	1.49	0.099	—
		1.64	5	1.51	0.11	—
		1.64	10	3.1	0.49	0.46
		1.64	20	6.1	1.72	1.62
		1.64	30	8.5	2.83	2.7
		2.32	10	3.25	0.50	—
		2.32	20	5.88	1.62	1.3
		2.76	10	3.00	0.54	—
	0.91	2.32	20	1.21	0.237	—
	1.25		20	2.32	0.676	—
	1.53		20	3.28	0.76	0.6
	1.63		20	3.33	0.78	—
	2.03		20	4.94	1.06	0.9
	2.32		10	3.25	0.50	—
	2.32		20	5.88	1.60	1.3
	2.83		20	8.00	1.90	1.7
	3.27		20	10.0	2.46	1.7
	3.94		10	6.13	0.97	—
400	2.25	0	50	4.61	0.34	—
		0	100	8.86	1.03	1.1
		0.61	12	7.9	1.06	1.2
		1.00	10	8.1	1.35	1.4
		1.65	10	8.3	1.64	1.5
		2.25	20	16.9	5.68	5.4
		2.75	10	8.6	1.72	1.5
		3.49	10	8.8	2.08	2.1
		4.12	10	8.6	2.09	1.9

Table I (Continued)

420	1.27	0	30	4.00	0.376	—
	1.55	0	30	5.13	0.48	0.5
	1.56	0	30	5.79	0.68	0.5
	2.19	0	20	6.36	0.504	0.5
	2.19	0	40	12.8	1.72	1.5
	3.02	0	30	15.3	1.86	2.1
	3.67	0	30	18.6	2.31	1.6
	3.69	0	30	21.5	3.0	3.0
	3.83	0	30	20.4	2.14	2.6
	4.35	0	30	26.5	3.49	3.2
	4.68	0	20	18.8	5.02	2.2
	5.05	0	20	20.0	2.30	2.2
	5.16	0	20	21.4	2.24	1.7
	2.19	0.59	5	9.72	1.64	1.8
		1.00	5	11.0	2.02	2.0
		1.65	5	13.0	3.0	2.8
		2.73	5	13.4	3.16	3.2
		2.78	5	12.6	3.02	2.9
		3.99	5	14.0	3.9	3.5
		4.64	5	13.9	3.68	3.8
440	2.13	0	5	4.10	0.28	—
		0	10	7.9	0.70	1.0
		0	10	8.3	0.91	—
		0	20	15.9	2.42	2.4
		0	20	16.7	2.74	2.8
		0	20	17.1	2.5	2.5
		0	30	25.6	6.5	5.6
		1.15	2	10.6	1.69	1.1
		1.88	2	11.1	2.19	2.3
		3.08	2	12.3	2.34	2.5
		4.08	2	12.8	2.69	2.9

prepared by dropping water on aluminum sulfide in an evacuated vessel, dried by passing through a trap at −78°C and purified by bulb-to-bulb distillation. The cupric oxide used in analysis was a commercial sample.

Apparatus.—The apparatus used in the present work is similar to that described previously[3]. The reaction vessel is a glass cylinder of about 162 cc. capacity.

Procedure.—Required quantities of dimethyl ether and hydrogen sulfide were mixed and left at room temperature for about 30 min. before pyrolysis, and then introduced into the reaction vessel which had already been kept at the experimental temperature. After an appropriate time of reaction, usually corresponding to less than five per cent decomposition, the reaction mixture was expanded into an analytical system. Methane and carbon monoxide in products were analyzed quantitatively in the same way as described previously[7]. Hydrogen was oxidized by cupric oxide at 260°C to water vapor and the amount of the latter was determined from its pressure by an oil manometer. As it was found that the adsorption of the water on the glass wall led to incorrect estimates of hydrogen, calibration was made with known amounts of hydrogen. The amounts of hydrogen thus corrected seem to be still not very accurate. When the amount of hydrogen formed by the decomposition was very small, it was not determined.

Results and Discussion

In Table I are listed the amounts of methane, carbon monoxide and hydrogen formed by the decomposition of dimethyl ether both in the absence and in the presence of hydrogen sulfide at various conditions. It has been well known that dimethyl ether decomposes thermally according to the following stoichiometric equations[6,8,9].

$$CH_3OCH_3 \rightarrow CH_4 + CH_2O$$

$$CH_2O \rightarrow CO + H_2$$

It is shown in Table I that, even in the presence of hydrogen sulfide, the amount of

7) N. Imai and O. Toyama, This Bulletin, 33, 652 (1960).

8) P. J. Askey and C. N. Hinshelwood, *Proc. Roy. Soc.*, A115, 251 (1927).

9) E. Leifer and H. C. Urey, *J. Am. Chem. Soc.*, 64, 994 (1942).

carbon monoxide formed is always equal to that of hydrogen within the experimental error and is always less than 30% of that of methane. Fig. 1 shows plots of the amounts of methane, carbon monoxide and hydrogen against the time obtained from series of runs (a) in the absence and (b) in the presence of hydrogen sulfide under otherwise constant conditions. It is seen in the figure that the rate of formation of methane remains constant for 30 min. during which 7.4 (a) and 2.3 (b) % of the ether have decomposed, while those of carbon monoxide and hydrogen increase with time. These observations indicate that carbon monoxide and hydrogen are produced by the decomposition of formaldehyde as represented by the above equation in the presence of hydrogen sulfide as well as in its absence.

It is generally agreed that the main feature of the thermal decomposition of dimethyl ether can be explained by the following chain mechanism[1].

$$CH_3OCH_3 \rightarrow CH_3 + OCH_3 \quad (1)$$

$$OCH_3 + CH_3OCH_3 \rightarrow CH_3OH + CH_3OCH_2 \quad (2)$$

$$CH_3 + CH_3OCH_3 \rightarrow CH_4 + CH_3OCH_2 \quad (3)$$

$$CH_3OCH_2 \rightarrow CH_2O + CH_3 \quad (4)$$

$$CH_3 + CH_3 \rightarrow C_2H_6 \quad (5)$$

The steady state equations derived from this scheme yield the rate equation

$$-\mathrm{d}[CH_3OCH_3]/\mathrm{d}t = R_{CH_4} = k_1^{1/2}k_3k_5^{-1/2}\,[CH_3OCH_3]^{3/2} \quad (I)$$

in general agreement with experimental results obtained by various workers[6,8,9]. Also in this work, the rate of decomposition of the ether alone was found to be proportional to the 3/2 power of the concentration of dimethyl ether at 420°C as seen in Fig. 2. From the slope of the straight line in the figure, the value of $k_1^{1/2}k_3k_5^{-1/2}$ was obtained. At other temperatures, values of $k_1^{1/2}k_3k_5^{-1/2}$ were calculated from the concentration of ether and the rate of formation of methane, making use of Eq. I. They are listed in Table II.

TABLE II. VALUES OF $k_1^{1/2}k_3k_5^{-1/2}$ AND $k_1^{1/2}k_7k_8^{-1/2}$

Temp. °C	$k_1^{1/2}k_3k_5^{-1/2}\times10^3$ ($mol^{1/2}\,cc^{1/2}\,sec^{-1/2}$)	$k_1^{1/2}k_7k_8^{-1/2}\times10^5$ ($mol^{1/2}\,cc^{1/2}\,sec^{-1/2}$)
360	0.223	0.240
380	0.855	0.847 0.864[a]
400	2.73	2.60
420	9.68	8.75
440	28.8	

a) Obtained from a series of runs with varied ether concentrations and a constant hydrogen sulfide concentration (Fig. 4).

Now in the presence of a sufficient amount of hydrogen sulfide, the reactions of methyl and methoxyl radicals with hydrogen sulfide may be so much faster than those with dimethyl ether, that the latter reactions may be neglected compared to the former. Hence reaction 2 may be replaced by reaction 2′ and reaction 3 by reactions 6 and 7.

$$OCH_3 + H_2S \rightarrow CH_3OH + HS \quad (2')$$

$$CH_3 + H_2S \rightarrow CH_4 + HS \quad (6)$$

$$HS + CH_3OCH_3 \rightarrow H_2S + CH_3OCH_2 \quad (7)$$

If, in addition, the concentration of hydrosulfide radicals is much higher than that of methyl radicals, the chain will terminate by reaction 8, reaction 5 being negligible compared to reaction 8.

$$HS + HS \rightarrow \text{products} \quad (8)$$

The above chain mechanism consisting of reactions 1, 2′, 6, 7, 4 and 8 leads to the following rate equation.

$$-\mathrm{d}[CH_3OCH_3]/\mathrm{d}t = R_{CH_4} = k_1^{1/2}k_7k_8^{-1/2}[CH_3OCH_3]^{3/2} \quad (II)$$

If the chain is sufficiently long, it is readily shown that in the steady state

$$k_6[CH_3][H_2S] = k_7[HS][CH_3OCH_3]$$

or

$$[HS]/[CH_3] = (k_6/k_7)([H_2S]/[CH_3OCH_3]) \quad (III)$$

Therefore, when the quantity in the right-hand side of Eq. III is very large, the rate of decomposition will be represented by Eq. II.

Fig. 3 shows the dependence of the rate of formation of methane on the concentration of hydrogen sulfide at varied temperatures. The rate increases with the increase in the concentration of hydrogen sulfide, until it attains a constant value. Fig. 4 shows that the rate of formation of methane in the presence of 2.32×10^{-6} mol. cc^{-1} of hydrogen sulfide at 380°C is proportional to the 3/2 power of the concentration of the ether. Both Figs. 3 and 4 thus indicate that Eq. II holds when the ratio $[H_2S]/[CH_3OCH_3]$ is large. Values of $k_1^{1/2}k_7k_8^{-1/2}$ determined from the constant values of the rate in Fig. 3 and from the slope of the straight line in Fig. 4 are listed in Table II together with those of $k_1^{1/2}k_3k_5^{-1/2}$. The fairly good agreement of the two values of $k_1^{1/2}k_7k_8^{-1/2}$ at 380°C obtained by different methods shows again the validity of Eq. II.

The values given in Table II lead to the following Arrhenius expressions:

$$k_1^{1/2}k_3k_5^{-1/2} = 10^{15.16\pm0.13}\times\exp\{-(54{,}500\pm400)/\boldsymbol{RT}\}\ \mathrm{mol}^{-1/2}\,\mathrm{cc}^{1/2}\,\mathrm{sec}^{-1/2}$$

$$k_1^{1/2}k_3k_5^{-1/2}=10^{15.26\pm0.24}\times\exp\{-(51{,}800\pm700)/\boldsymbol{RT}\}$$
$$\mathrm{mol}^{-1/2}\,\mathrm{cc}^{1/2}\,\mathrm{sec}^{-1/2}$$

The expression for $k_1^{1/2}k_3k_5^{-1/2}$ shows a good agreement with that of $10^{15.11}\exp(-55{,}600/\boldsymbol{RT})$ $\mathrm{mol}^{-1/2}\,\mathrm{cc}^{1/2}\,\mathrm{sec}^{-1/2}$ obtained by Benson and Jain[9] who studied the thermal decomposition of dimethyl ether in the temperature range from 490 to 550°C.

The expression of $k_1^{1/2}k_3k_5^{-1/2}$ divided by that of $k_1^{1/2}k_7k_8^{-1/2}$ yields

$$(k_3/k_7)(k_5/k_8)^{1/2}=0.8\exp(-2{,}700/\boldsymbol{RT})$$

Assuming k_3/k_5 to be unity, $k_3/k_7=0.8\exp(-2{,}700/\boldsymbol{RT})$ and hence $E_7=E_3-2.7$ kcal./mol., E's denoting activation energies. The result seems reasonable since hydrosulfide radicals have been shown to be more reactive towards organic molecules than methyl radicals. Reported values of E_3 are 8.4[10], 9.5[11] and 10.0[12] kcal./mol. and that of A_3 is of the order of 10^{11} $\mathrm{mol}^{-1}\,\mathrm{cc.\,sec}^{-1}$. If we accept the intermediate value of 9.5 kcal./mol. for E_3, it follows that

$$k_7=10^{11}\exp(-6{,}800/\boldsymbol{RT})\ \ \mathrm{mol}^{-1}\,\mathrm{cc.\,sec}^{-1}$$

The present authors found previously that $k_8=10^{11}\exp(-2{,}600/\boldsymbol{RT})$[7]. The combination of these yields

$$k_8/k_7=\exp(4{,}200/\boldsymbol{RT})$$

It follows therefore that k_8/k_7 is much greater than unity at experimental temperatures although it decreases with the rise of temperature. This accounts for the fact that Eq. II holds even when the ratio $[H_2S]/[CH_3OCH_3]$ in Eq. III is not very large and that, the higher the temperature, the greater is the ratio $[H_2S]/[CH_3OCH_3]$ where Eq. II begins to be applicable, as seen in Fig. 3.

Benson and Jain have argued that the activation energy of the initial step, E_1, of 92 kcal./mol., obtained from their value of $E_{overall}=(1/2)E_1+E_3-(1/2)E_5=55.6$ kcal./mol. combined with $E_3=9.5$ kcal./mol., is too large compared with $E_1=81$ kcal./mol. obtained by Rice and Johnston[13], who decomposed dimethyl ether in the temperature range from 1010 to 1150°K and determined E_1 by an antimony mirror removal method. In order to explain this discrepancy, they suggest that the chain terminates not only by reaction 5 but also by reactions 9 and 10

$$CH_3+CH_2OCH_3\rightarrow C_2H_5OCH_3 \qquad (9)$$
$$2CH_2OCH_3\rightarrow (CH_3OCH_2)_2 \qquad (10)$$

and that reaction 4 is not unimolecular but bimolecular

$$CH_2OCH_3+\mathbf{M}\rightarrow CH_2O+CH_3+\mathbf{M} \qquad (4')$$

The rate of decomposition is then expressed as

$$-\mathrm{d}[CH_3OCH_3]/\mathrm{d}t=\frac{k_1^{1/2}k_3k_5^{-1/2}}{1+(k_{10}/k_5)^{1/2}(k_5/k_{4'})}[CH_3OCH_3]^{3/2}$$

Since $E_{10}=E_5=0$, $E_3=9.5$ and $E_{4'}=19$ kcal./mol.[12], the denominator of the overall rate constant decreases with temperature. This situation, they believe, explains the overall activation energy greater than $(1/2)E_1+E_3-(1/2)E_5$.

However, if $E_1=81$ kcal./mol. and consequently $(1/2)E_1+E_3-(1/2)E_5=50$ kcal./mol. as they assume, $E_3-E_7=-1.8$ kcal./mol., i.e., $E_3<E_7$ and the catalysis such as shown by Eq. II cannot be expected to take place[14]. The interpretation given by Benson and Jain must therefore be regarded as incompatible with the results obtained in the present work. On the other hand, the agreement between the two overall A factors in the absence and presence of hydrogen sulfide seems to support the idea that $k_{overall}=k_1^{1/2}k_3k_5^{-1/2}$, since it is probable that $A_3=A_7$ and $A_5=A_8$. The discrepancy between the overall activation energy in the pyrolysis of the ether alone and those of elementary reactions may therefore be attributed to the error in the estimation of E_1. Baughan et al.[15] estimated E_1 as 87 kcal./mol.

As seen in Table I, the time required to produce a definite amount of methane in the absence of hydrogen sulfide is about ten times as great as that in its presence, but the ratio of the amount of carbon monoxide to that of methane, compared with the same amount of the latter, is far less sensitive to the presence of hydrogen sulfide. This indicates that the decomposition of formaldehyde is also catalyzed by hydrogen sulfide. Kodama, Takezaki and Fujie[16] suggested that in the pyrolysis of dimethyl ether, formaldehyde decomposes by the following chain processes:

$$CH_3+CH_2O\rightarrow CH_4+CHO$$
$$CHO\rightarrow CO+H$$
$$H+CH_3OCH_3\rightarrow H_2+CH_3OCH_2$$
$$CH_3OCH_2\rightarrow CH_2O+CH_3$$

10) M. K. Phibbs and B. B. Darwent, *Can. J. Research*, **B28**, 395 (1950).
11) A. F. Trotman-Dickenson and E. W. R. Steacie, *J. Chem. Phys.*, **19**, 329 (1951).
12) R. A. Marcus, B. B. Darwent and E. W. R. Steacie, ibid., **16**, 983 (1948), recalculated in Ref. 11.
13) F. O. Rice and W. R. Johnston, *J. Am. Chem. Soc.*, **56**, 214 (1934).
14) Whether reaction 4 may be unimolecular or bimolecular, Eq. II holds when reactions 5, 9 and 10 are neglected compared with reaction 8.
15) E. C. Baughan, M. G. Evans and M. Polanyi, *Trans. Faraday Soc.*, **37**, 377 (1941).
16) S. Kodama, Y. Takezaki and R. Fujie, *J. Chem. Soc. Japan, Pure Chem. Sec.* (*Nippon Kagaku Zasshi*), **72**, 892 (1951).

In the presence of hydrogen sulfide, this scheme may be modified as follows:

$$HS + CH_2O \rightarrow H_2S + CHO$$
$$CHO \rightarrow CO + H$$
$$H + H_2S \rightarrow H_2 + HS$$

Summary

Dimethyl ether has been decomposed thermally in the presence and absence of hydrogen sulfide over the temperature range 360~440°C. The rate of decomposition is enhanced by the presence of hydrogen sulfide, but the rate law is unchanged, i.e., the rate is proportional to the 3/2 power of the ether concentration, irrespective of the presence of hydrogen sulfide.

The catalytic action of hydrogen sulfide is satisfactorily explained by the steps, $CH_3 + H_2S \rightarrow CH_4 + HS$ (6), $HS + CH_3OCH_3 \rightarrow H_2S + CH_3OCH_2$ (7) and $CH_3OCH_2 \rightarrow CH_2O + CH_3$ (4). Overall rate constants in the absence and presence of hydrogen sulfide are represented by $10^{15.16}\exp(-54{,}500/RT)$ and $10^{15.26}\exp(-51{,}800/RT)$ mol.$^{-1/2}$ cc$^{1/2}$ sec$^{-1/2}$ respectively. The combination of these gives $k_3/k_7 = 0.8\exp(-2{,}700/RT)$, where k_3 refers to the reaction $CH_3 + CH_3OCH_3 \rightarrow CH_4 + CH_3OCH_2$ (3). If, therefore, the activation energy of reaction 3 is 9.5 kcal./mol. as reported by Trotman-Dickenson and Steacie, that for reaction 7 is 6.8 kcal./mol. The results obtained indicate that the decomposition of the formaldehyde formed intremediately is also catalyzed by hydrogen sulfide.

Department of Applied Chemistry
College of Engineering
University of Osaka Prefecture
Sakai, Osaka

Alkylation of Sodio-2, 3-dimethylindole and Sodio-tetrahydrocarbazole in Non-polar Solvent

By Masao NAKAZAKI

(Received September 26, 1960)

In the previous paper[1], the formation of 11-alkyltetrahydrocarbazolenines (IV) and 9-alkyltetrahydrocarbazoles (III) by the alkylation of tetrahydrocarbazole (I) with sodium amide and alkyl halides in liquid ammonia was reported.

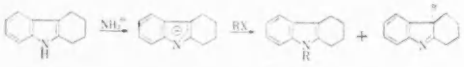

I II III IV

III a R = $CH_2C_6H_5$ IV a R = $CH_2C_6H_5$
b R = CH_2–CH=CH_2 b R = CH_2–CH=CH_2
c R = CH_3 c R = CH_3

The ratio of the yield of 11-alkyltetrahydrocarbazolenines (IV) to 9-alkyltetrahydrocarbazoles (III) was found to be affected by the halides employed: benzyl chloride gave the highest ratio and was followed by ally bromide, isopropyl iodide and methyl iodide.

The same sort of "ambident" alkylation[2,3] to give 1-alkyl-2, 3-dimethylindoles (VII) and 3-alkyl-2,3-dimethylindolenines (VIII) was observed in the alkylation of 2, 3-dimethylindole (V) in liquid ammonia with sodium amide and alkyl halides, and the ratio of *C*-alkyl/*N*-alkyl products were also found to depend on the nature of alkyl halides in the same sequence as that demonstrated in the alkylation of tetrahydrocarbazole. On the other hand, the alkylation of sodio-indole (IX) in non-polar solvent (benzene or without solvent) was studied by Funakubo[4], who reported the preparation of

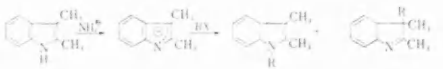

V VI VII VIII

VII a R = CH_3 VII a R = $CH_2C_6H_5$
b R = CH_2–CH=CH_2
c R = CH_3

1) M. Nakazaki and S. Isoe, *J. Chem. Soc. Japan, Pure Chem. Sec.* (*Nippon Kagaku Zasshi*), **76**, 1159 (1955).
2) M. Nakazaki, This Bulletin, **32**, 838 (1959).
3) The Grignard complex of I and V give 11-alkyltetrahydrocarbazolenines(IV) and 3-alkyl-2,3-dimethylindolenines (VIII) respectively, and there can be found no formation of *N*-substituted derivatives. T. Hoshino, *Ann.*, **500**, 35 (1932); B. Witkop, *J. Am. Chem. Soc.*, **72**, 614 (1950); Ref. 1.
4) E. Funakubo, *J. Chem. Soc. Japan, Pure Chem. Sec.* (*Nippon Kagaku Zasshi*), **48**, 652 (1927). Cf. R. Weisberger, *Ber.*, **42**, 3520 (1910).

N-alkyl indoles (X) (methyl, ethyl, *n*-propyl, isopropyl, allyl, *n*-butyl, isobutyl and isoamyl) by this method.

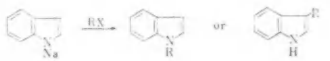

IX X XI

a $R=CH_2-CH=CH_2$
b $R=CH_2C_6H_5$
c $R=C(C_6H_5)_3$
d $R=CH_2COOC_2H_5$

But on our repetition of his experiment[1], his *N*-allylindole picrate (m. p. 169~170°C) turned out to be the picrate of recovered indole, and from the mother liquor was isolated another picrate (m. p. 105~106°C) which was established to be identical with the picrate of 3-allylindole (XIa)[5] prepared by the Grignard synthesis.

Kubota also found another example of β-alkylation of sodio-indole in non-polar solvent when he obtained 3-benzyl(XIb)[6], 3-triphenylmethyl-indole (XIc)[7] and ethyl β-indoleacetate (XId)[8] by heating a suspension of sodio-indole in dry benzene with benzyl chloride, triphenylmethyl chloride and ethyl chloroacetate respectively.

Unfortunately these authors did not dare to examine their alkylation method for 2, 3-disubstituted indoles, and this contribution is concerned with the alkylation of sodio-2, 3-disubstituted indoles in non-polar solvent as a natural extension of our alkylation studies in liquid ammonia.

Tetrahydrocarbazole (I) and 2, 3-dimethylindole (V) were chosen as representatives of 2, 3-disubstituted indoles, because various 11-alkyltetrahydrocarbazlenines (IV), 3-alkyl-2, 3-dimethylindolenines (VIII) and *N*-alkyl derivatives III and VII have been prepared by our hands[1,2] and their structures were firmly established.

The general procedure carried out in our alkylation study was as follows: to a suspension of sodium amide in liquid ammonia (prepared in situ), a solution of indole derivatives (I or V) in toluene was added and the liquid ammonia was evaporated at room temperature. After residual ammonia was expelled by heating the solution up to the boiling point of toluene, a solution of halide in toluene was added under refluxing with stirring. The separation of indolenine derivatives and *N*-alkyl derivatives was worked out by the conventional method as in the case of alkylation in liquid ammonia.

The same directing effect of the alkylation reagents was confirmed in this alkylation in non-polar solvent; i. d. with benzyl chloride and allyl bromide, sodio-tetrahydrocarbazole afforded 11-alkyltetrahydrocarbazolenines (IV) predominantly, whereas with methyl iodide, *N*-methyl derivative was the sole product isolated; 2, 3-dimethyl-indole gave only indolenine derivatives VIII with benzyl chloride and allyl bromide, but with methyl iodide, *N*-methyl derivative VIIa accompanied with a small amount of indolenine derivative VIIIc.

It is noteworthy to compare these results with the directing effects of alkylation reagents in the alkylation of sodium salt of 2, 6-disubstituted phenols (XII) in non-polar solvent, which was studied strenuously by Curtin and his collaborators[9] recently.

To explain their observation that benzyl chloride and ally bromide give predominantly the *C*-alkyl derivative(6-alkyl-2, 6-dimethyl-2, 4-cyclohexadienone) XIII, whereas methyl iodide gives XIV with a trace of XIII, various factors which seem to control the direction of alkylation were considered, however, no decisive conclusion seems have to have been reached. We have proposed a reasonable mechanism to explain the marked directing effect of benzyl

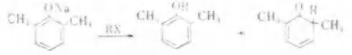

XII XIV XIII

and ally halides in the alkylation of tetrahydrocarbazole in liquid ammonia, but this can not be advanced to rationalize the ambident alkylations in non-polar solvent without further experimental supports.

Studies of alkylation of 2, 6-dimethylphenol in liquid ammonia are now in progress in our laboratory, and should be the subject of a subsequent communication.

Experimental

Alkylation of Tetrahydrocarbazole (I).—*1) With Benzylchloride.*—A mixture of 5 g. of tetrahydrocarbazole and 100 cc. of toluene was added to a suspension of sodium amide in lipuid ammonia

5) Authentic *N*-allylindole (b. p. 114~116°C/6 mmHg., picrate: m. p. 79~79.5°C) was prepared by the alkylation of indole in liquid ammonia with sodium amide and allyl bromide. Ref. 1.

6) T. Kubota, *J. Chem. Soc. Japan, Pure Chem. Sec.* (*Nippon Kagaku Zasshi*), **59**, 407 (1938).

7) T. Kubota and I. Mita, ibid., **59**, 409 (1936). This 3-triphenylmethyl-indole was found to be identical with the compound which had been prepared by E. Funakubo and T. Hirotani (*Ber.*, **69**, 2123 (1936)) by the reaction of the Grignard complex of indole with triphenylmethyl chloride and had been assigned the structure of *N*-triphenylmethyl derivative by them.

8) T. Kubota, Japan Pat., 166925 (1934).

9) D. Y. Curtin et al., *J. Am. Chem. Soc.*, **79**, 3156 (1957); **80**, 1391, 4339, 6016 (1958); *J. Org. Chem.*, **23**, 9 (1958).

prepared from 0.5 g. of sodium and 200 cc. of liquid ammonia. The liquid ammonia was evaporated at room temperature and the resulting suspension of sodio-tetrahydrocarbazole in toluene was refluxed in order to expel the last trace of ammonia. A solution of 4 g. of benzyl chloride in 20 cc. of toluene was added dropwise. After the solution was stirred and refluxed for 1.5 hr., the toluene was distilled with steam, and the residue was extracted with ether. The ether solution was washed with 2 N hydrochloric acid to separate the basic and neutral fractions.

N-Benzyltetrahydrocarbazole (IIIa): — The ethereal extract was washed with water twice and dried over anhydrous sodium sulfate. Removal of the solvent gave a semisolid which was washed with petroleum ether-ether to give 0.5 g. of recovered tetrahydrocarbazole. The washing was concentrated to afford a pale yellow oil, which was distilled in vacuo, 0.4 g. b. p. 170~180°C/2 mmHg (literature[1]: b. p. 195°C/2 mmHg). The picrate was recrystallized from ethanol to give red needles which melted at 110~111°C, alone and admixed with an authentic sample of *N*-benzyltetrahydrocarbazole (m. p. 110~111°C).

Found: N, 11.49. Calcd. for $C_{19}H_{19}N \cdot C_6H_3O_7N_3$: N, 11.42%.

11-Benzyltetrahydrocarbazolenine (IVa):—After the acidic solution was washed with ether, 4 N sodium hydroxide solution was added to precipitate the basic material which was extracted with ether.

The extract was washed with water and dried over anhydrous sodium sulfate. The solvent was removed to give a semisolid which was filtered free from viscous mother liquor. The crystals were recrystallized from ethanol-water to afford prisms melting at 84~85°C, which was found identical with 11-benzyltetrahydrocarbazolenine by the mixed melting point determination with an authentic specimen (literature: m. p. 85~86°C[1]). The picrate was recrystallized from ethanol to give yellow prisms, m. p. 176~177.5°C (literature: 176~177°C[1]). The mixed melting point with an authentic specimen was 176~177.5°C.

Found: N, 11.53. Calcd. for $C_{19}H_{19}N \cdot C_6H_3O_7N_3$: N, 11.42%.

2) With Allyl Bromide. — To a suspension of sodio-tetrahydrocarbazole in toluene prepared from 200 cc. of liquid ammonia, 0.7 g. of sodium, 5 mg. of ferric nitrate, 5 g. tetrahydrocarbazole (I) and 100 cc. of toluene, as described previously, a solution of 4 g. of ally bromide in 20 cc. of toluene was added dropwise with stirring and refluxing in a period of 2 hr. After the reaction mixture was refluxed for an additional 5 hr., the solvent was removed by steam distillation and the residue was extracted with ether. The neutral and basic fractions were separated as described above.

N-Allyltetrahydrocarbazole(IIIb):—From the neutral fraction, 0.5 g. of tetrahydrocarbazole was recovered (m. p. 110~116°C). The residue was distilled in vacuo to afford a viscous pale yellow liquid, b. p. 125~128°C/2 mmHg (literature[1]: b. p. 157°C/3 mmHg). The picrate was recrystallized to give red needles melting at 76~77°C, which were found to be identical with the picrate of *N*-allyltetrahydrocarbazole by the mixed melting point determination with an authentic sample, m. p. 76~77°C[1].

Found: N, 13.05. Calcd. for $C_{15}H_{17}N \cdot C_6H_3O_7N_3$: N, 12.73%.

11-Allyltetrahydrocarbazolenine (IVb): — The basic fraction gave 2.0 g. of crystals which were recrystallized from petroleum ether to afford 11-allyltetrahydrocarbazolenine, m. p. 54~56°C, identified by the mixed melting point determination with an authentic sample (literature[1]: m. p. 57~58°C). The picrate was recrystallized from ethanol to give yellow prisms, m. p. 139~142°C, the identity of which with the picrate of 11-allytetrahydrocarbazolenine was established by the mixed melting point determination with an authentic sample (literature[1]: m. p. 142~143°C).

Found: N, 12.94. Calcd. for $C_{15}H_{17}N \cdot C_6H_3O_7N_3$: N, 12.72%.

3) With Methyl Iodide. — The alkylation with methyl iodide was carried out following the general procedure described above. A solution of 8 g. of methyl iodide in 40 cc. of toluene was added dropwise during 6 hr. in a suspension of sodio-tetrahydrocarbazole (0.02 mol.) on toluene prepared from 200 cc. of liquid ammonia, 0.7 g. of sodium, 3.4 g. of sodium and 80 cc. of toluene. After the usual work up, the basic and neutral fractions were separated.

N-Methyltetrahydrocarbazole (IIIc): — The vacuum distillation of the neutral fraction gave 1.4 g. of viscous pale yellow oil, b. p. 124~126°C/2 mmHg. The picrate was recrystallized from ethanol to give brown-red needles melting at 109~112°C. The mixed melting point with an authentic specimen[1] (m. p. 113~114°C) was 109~112°C.

Found: N, 13.79. Calcd. for $C_{13}H_{15}N \cdot C_6H_3O_7N_3$: N, 13.52%.

The Basic Fraction: — Removal of the ether afforded an amber yellow solid which was sparingly soluble in dilute sodium hydroxide, dilute hydrochloric acid, ethanol and ether respectively add could not be converted into crystalline picrate. This substance was not studied further.

Alkylation of 2, 3-Dimethylindole (V).—*1) With Benzylchloride*:—A solution of 5 g. of 2,3-dimethylindole (V) in 100 cc. of toluene was added dropwise into a suspension of sodium amide in liquid ammonia prepared from 200 cc. of liquid ammonia, 1 g. of sodium and 5 mg. of ferric nitrate. The liquid ammonia was evaporated and the remaining mixture was refluxed with stirring. To the reaction mixture, a solution of 5.3 g. of benzyl chloride in 20 cc. of toluene was added and refluxing with stirring was continued for 8 hr. After the reaction mixture was worked up as described in the alkylation of tetrahydrocarbazole, the basic and the neutral fractions were separated.

2, 3-Dimethyl-3-benzylindolenine (VIIIa):—Removal of the solvent afforded 4.6 g. of a solid, which was recrystallized from petroleum ether to give crystals melting at 48~49°C, alone and admixed with an authentic specimen (m. p. 48~49°C[10]).

The picrate was recrystallized from ethanol to give

10) M. Nakazaki, S. Isoe and K. Tanno, *J. Chem. Soc. Japan, Pure Chem. Sec.* (*Nippon Kagaku Zasshi*), **76**, 1262 (1955).

yellow prisms, m. p. 137～139°C, the mixed melting point of which with an authentic sample[10] was found 137～140°C.

Found: N, 12.20. Calcd. for $C_{17}H_{17}N \cdot C_6H_3O_7N_3$: N, 12.06%.

The Neutral Fraction: — A small amount of 2,3-dimethylindole was recovered, but the search for *N*-benzyl derivative was fruitless.

2) With Allyl Bromide.—Using 5 g. of allyl bromide, the alkylation was carried out exactly as the procedure described above.

2,3-Dimethyl-3-allylindolenine (VIIIb): — The crude basic fraction (1 g.) was distilled in vacuo to give a yellow liquid, b. p. 125～128°C/12 mmHg. The picrate was recrystallized from ethanol to afford yellow needles m. p. 158～160°C, the mixed melting point with an authentic sample[2] (m. p. 156～157°C) showed 159～160°C.

Found: N, 13.65. Calcd. for $C_{13}H_{15}N \cdot C_6H_3O_7N_3$: N, 13.52%.

Neutral Fraction: — The crude neutral fraction (2 g.) was distilled in vacuo to give two fractions: 1. 1.4 g. b. p. 100～125°C/2 mmHg. which was proved as 2,3-dimethylindole recovered, 2. 0.5 g. b. p. 125～130°C/2 mmHg which did not give crystalline picrate and was not studied further.

3) With Methyl Iodide. — The alkylation was carried out using 12 g. of methyl iodide, and the basic and neutral fractions were separated as described above.

2,3,3-Trimethylindolenine (VIIIc):—The crude basic fraction (1.1 g.) was distilled in vacuo to give 0.4 g. of VIIIc, b. p. 80°C/1 mmHg, the characteristic odor of which resembles that of jasmin. The picrate was recrystallized from ethanol to afford yellow needles melting at 158°C, which was found identical with the picrate of 2,3,3-trimethylindolenine (literature[2]: m. p. 158°C) by the mixed melting point determination.

Found: N, 14.54. Calcd. for $C_{11}H_{13}N \cdot C_6H_3O_7N_3$: 14.43%.

1,2,3-Trimethylindole (VIIa): — From the neutral fraction, a small amount of 2,3-dimethylindole was recovered by recrystallization from petroleum ether. The mother liquor, after removal of the solvent, was distilled in vacuo to give 1.1 g. of yellow liquid, b. p. 90～93°C/2 mmHg (literature[2]: b. p. 117～120°C/6 mmHg). The picrate was recrystallized from ethanol to afford brownish-black needles, m. p. 145～147°C which was not depressed on admixing with an authentic specimen[2] of the picrate of 1,2,3-trimethylindole (m. p. 148～149°C).

Found: N, 14.70. Calcd. for $C_{11}H_{13}N \cdot C_6H_3O_7N_3$: N, 14.43%.

The author is very grateful to Mr. Sachio Itaba for his technical assistance.

Institute of Polytechnics
Osaka City University
Kita-ku, Osaka

Microwave Spectrum and Molecular Structure of Monochloroacetonitrile, CH_2ClCN

By Kaname WADA, Yoshikazu KIKUCHI, Chi MATSUMURA, Eizi HIROTA and Yonezo MORINO

(Received September 5, 1960)

Since the structure of the monochloroacetonitrile molecule CH_2ClCN is similar to that of propargyl chloride $CH_2ClC{\equiv}CH$, it is of some interest to compare the structure of the two molecules with each other in detail. In particular, the C—Cl bond length is important in the respect because it will give some information concerning the electronic structure of the molecule. The quadrupole coupling constant of chlorine nucleus is also important for discussing the nature of the C—Cl bond.

When the present investigation was coming nearly to the end, a paper was published by Graybeal on the structure of the CH_2ClCN molecule by the microwave absorption spectrum[1]. But his result seems to involve a number of unreliable data and moreover only two isotopic species, $CH_2{}^{35}ClCN$ and $CH_2{}^{37}ClCN$, were used in his study. The molecular structure and the molecular constants obtained in the present paper would be more reliable than those by Graybeal.

Experimental

The rotational spectra of monochloroacetonitrile, $CH_2{}^{35}ClCN$, $CH_2{}^{37}ClCN$, $CD_2{}^{35}ClCN$, and $CD_2{}^{37}ClCN$, were observed at room temperature by using the recording microwave spectrometer with a 100 Kc. Stark modulation described in the previous paper[2]. The microwave was supplied by klystrons,

1) J. D. Graybeal, *J. Chem. Phys.*, **32**, 1258 (1960).
2) E. Hirota and Y. Morino, This Bulletin, to be published.

TABLE I. OBSERVED AND CALCULATED CENTER FREQUENCIES

	$CH_2^{35}ClCN$		$CH_2^{37}ClCN$		$CD_2^{35}ClCN$		$CD_2^{37}ClCN$	
	obs.	calcd.	obs.	calcd.	obs.	calcd.	obs.	calcd.
a-Type								
$2_{1,2}\rightarrow 3_{1,3}$	17545	17544.20			17190.80	17190.34	16832.86	16833.12
$3_{0,3}\rightarrow 4_{0,4}$	23966.23	23968.50						
$3_{1,3}\rightarrow 4_{1,4}$	23385.72	23388.83			22914.78	22914.49		
$4_{1,4}\rightarrow 5_{1,5}$	29227.24	29230.41	28611.54	28612.16	28633.16	28633.68	28038.14	28039.38
$5_{1,5}\rightarrow 6_{1,6}$	35065.78	35068.33	34324.38	34326.95	34346.03	34346.84	33636.16	33634.53
b-Type								
$1_{0,1}\rightarrow 1_{1,0}$	22422.50	22422.48	22332.96	22332.97				
$3_{0,3}\rightarrow 3_{1,2}$	23192.78	23191.36	23074.41	23074.49	17585.67	17584.56		
$4_{0,4}\rightarrow 4_{1,3}$	23821.51	23820.40			18304.48	18304.23	18187.47	18185.99
$5_{0,5}\rightarrow 5_{1,4}$	24625	24623.42			19234.33	19232.49		
$6_{0,6}\rightarrow 6_{1,5}$	25614.88	25612.08	25409	25405.55	20389.63	20387.74	20192.84	20191.62
$7_{0,7}\rightarrow 7_{1,6}$	26801	26799.24	26549	26547.20	21791.27	21790.80	21541.20	21540.40
$8_{0,8}\rightarrow 8_{1,7}$	28201	28199.58	27894	27892.79	23465.04	23463.98	23148.64	23147.47
$9_{0,9}\rightarrow 9_{1,8}$	29831	29828.87	29458	29457.20	25429.58	25429.40	25034.94	25033.99
$10_{0,10}\rightarrow 10_{1,9}$	31706	31703.42	31253	31255.89	27708.01	27706.52	27222.44	27219.00
$11_{0,11}\rightarrow 11_{1,10}$	33842	33839.15	33303	33304.09	30318.90	30308.94		
$12_{0,12}\rightarrow 12_{1,11}$					33273.50	33239.82	32562.24	32531.71
$13_{0,13}\rightarrow 13_{1,12}$							35734.94	35655.44
$0_{0,0}\rightarrow 1_{1,1}$	28120.10	28120.11	27912.08	27912.07				
$1_{0,1}\rightarrow 2_{1,2}$	33818.58	33817.76	33492.20	33491.20				
$4_{0,4}\rightarrow 4_{1,3}$	23821.51	23820.40						
$5_{1,5}\rightarrow 6_{0,6}$	15794.49	15800.49	15038.47	15042.88				
$6_{1,6}\rightarrow 7_{0,7}$	22551.95	22559.80						
$11_{2,10}\rightarrow 12_{1,11}$	16468.89	16502.57	14790.03	14823.01				

TABLE II. ROTATIONAL CONSTANTS AND ASYMMETRY PARAMETERS

	$CH_2^{35}ClCN$	$CH_2^{37}ClCN$	$CD_2^{35}ClCN$	$CD_2^{37}ClCN$
A	25271.30 Mc./sec.	25122.52 Mc./sec.	19494.88 Mc./sec.	19377.44 Mc./sec.
B	3151.01	3081.13	3119.94	3051.63
C	2848.80	2789.56	2780.81	2724.15
b_P	-6.78471×10^{-3}	-6.57069×10^{-3}	-1.02490×10^{-2}	-9.92993×10^{-3}

Varian X-12 and X-13, and the frequency was multiplied by a silicon crystal. The frequency range covered was 15000 Mc./sec. to 35000 Mc./sec.

The deuterated samples were prepared as follows: a mixture of the normal monochloroacetonitrile, heavy water and a trace of anhydrous sodium carbonate was kept on a hot water bath for a day and then distilled out. The infrared absorption spectrum showed neither the C-H stretching nor the CH_2 deformation bands.

Results

Monochloroacetonitrile is a nearly prolate symmetric top molecule and both a- and b-type transitions were observed. The transitions of the b-type Q-branch, $J_{0,J}\rightarrow J_{1,J-1}$, were most easily identified because of their characteristic hyperfine patterns due to the quadrupole moment of the chlorine nucleus ($I=3/2$) and confirmed by plotting the values of $A-(B+C)/2$ and $b_P=(C-B)/(2A-B-C)$. For CH_2ClCN a-type, and b-type R-branch transitions and for CD_2ClCN a-type R-branch transitions were also measured. The observed center frequencies are given in Table I.

The rotational constants of CH_2ClCN were determined by using the transitions, $0_{0,0}\rightarrow 1_{1,1}$, $1_{0,1}\rightarrow 1_{1,0}$, and $3_{0,3}\rightarrow 3_{1,2}$. Unfortunately none of these transitions were measured for CD_2ClCN and the rotational constants were determined by using relatively low-J transitions. The values are listed in Table II. The center frequencies calculated by using these constants are compared with the observed ones in Table I. (a rigid rotor calculation).

For $CH_2^{35}ClCN$ rough estimation of centrifugal effect is made (Table III) by assuming the expression for a symmetric top molecule, $-D_J J^2(J+1)^2-D_{JK}J(J+1)K_{-1}^2-D_K K_{-1}^4$. The transitions used for determining the centrifugal constants are $4_{0,4}\rightarrow 4_{1,3}$, $5_{1,5}\rightarrow 6_{1,6}$, $5_{1,5}\rightarrow 6_{0,6}$, $6_{1,6}\rightarrow 7_{0,7}$, and $11_{2,10}\rightarrow 12_{1,11}$. The center frequencies calculated with the centrifugal distortion correction are compared with the observed

Table III. Effect of the centrifugal distortion for $CH_2{}^{35}ClCN$

($D_J = 0.004399$ Mc./sec., $D_{JK} = -0.02340$ Mc./sec., $D_K = 0.3398$ Mc./sec.)

	ν_{rigid}	$D_{corr.}$	$\nu_{corr.}$	$\nu_{obs.}$
$2_{1,2} \rightarrow 3_{1,3}$	17544.20	−0.33	17543.87	17545
$3_{0,3} \rightarrow 4_{0,4}$	23968.50	−1.13	23967.37	23966.23
$3_{1,3} \rightarrow 4_{1,4}$	23388.83	−0.94	23387.89	23385.72
$4_{1,4} \rightarrow 5_{1,5}$	29230.41	−1.97	29228.44	29227.24
$5_{1,5} \rightarrow 6_{1,6}$	35068.33	−3.52	35064.81	35065.78
$1_{0,1} \rightarrow 1_{1,0}$	22422.48	−0.29	22422.19	22422.50
$3_{0,3} \rightarrow 3_{1,2}$	23191.36	−0.06	23191.30	23192.78
$4_{0,4} \rightarrow 4_{1,3}$	23820.40	0.13	23820.53	23821.51
$5_{0,5} \rightarrow 5_{1,4}$	24623.42	0.36	24623.78	24625
$6_{0,6} \rightarrow 6_{1,5}$	25612.08	0.64	25612.72	25614.88
$7_{0,7} \rightarrow 7_{1,6}$	26799.24	0.97	26800.21	26801
$8_{0,8} \rightarrow 8_{1,7}$	28199.58	1.35	28200.93	28201
$9_{0,9} \rightarrow 9_{1,8}$	29828.87	1.77	29830.64	29831
$10_{0,10} \rightarrow 10_{1,9}$	31703.42	2.23	31705.65	31706
$11_{0,11} \rightarrow 11_{1,10}$	33839.15	2.75	33841.90	33842
$0_{0,0} \rightarrow 1_{1,1}$	28120.11	−0.31	28119.80	28120.10
$1_{0,1} \rightarrow 2_{1,2}$	33817.76	−0.34	33817.42	33818.58
$4_{0,4} \rightarrow 4_{1,3}$	23820.40	0.12	23820.52	23821.51
$5_{1,5} \rightarrow 6_{0,6}$	15800.49	−4.16	15796.33	15794.49
$6_{1,6} \rightarrow 7_{0,7}$	22559.80	−6.63	22553.17	22551.95
$11_{2,11} \rightarrow 12_{1,11}$	16502.57	−34.01	16468.56	16468.89

Table IV. Molecular constants of monochloroacetonitrile

(Graybeal's values are also given for comparison.)

Present

Calculated

C—Cl 1.7815 Å, C—H 1.0881 Å, H···H 1.7812 Å, ∠CCCl 111°29′, ∠CCH 107°27′, $\Delta = 0.2194$ amu Å^2, $\chi_{aa} = -32.8$ Mc./sec., $\chi_{bb} = -7.2$ Mc./sec.

Assumed

C—C 1.458 Å, C—N 1.158 Å, ∠CCN 180°,

Graybeal

Calculated

C—Cl 1.767 Å, C—C 1.472 Å, H···H 1.728 Å, ∠CCCl 111°24′, $\chi_{aa} = -30.45$ Mc./sec., $\chi_{bb} = -7.73$ Mc./sec.,

Assumed

C—H 1.070 Å, C—N 1.158 Å, ∠CCN 180°, ∠CCH 109°30′.

ones in Table III. It is seen that the discrepancy found in the rigid rotor calculation is largely reduced, even for high-J transitions.

Since only two hydrogen atoms are located above and below the symmetry plane, the distance between them r is given by[2]

$$r = [(I_a + I_b - I_c + \Delta)/m]^{1/2}$$

where Δ is a quantity similar to the inertia defect and m is the mass of hydrogen or deuterium atom. The values of Δ and r (Table IV) were determined by means of the method of least-squares using the four equations given by the four isotopic species.

The number of the rotational constants obtained is twelve. Four of them are used in obtaining the hydrogen to hydrogen distance, hence there remain eight constants for determining the other structural parameters, d_{C-C}, d_{C-Cl}, d_{C-H}, $d_{C\equiv N}$, ∠CCCl, ∠CCH, and ∠CCN. Since isotopes of carbon and nitrogen atoms were not available, none of these parameters could be determined. The C–C bond length adjacent to the triple bond is usually about 1.458 Å, and the C≡N bond length in cyano group is reported for a number of molecules to be 1.158 Å[3]. The assumption of the linear structure for the C—C≡N group may not influence the other structural parameters. Thus the following values were assumed: $d_{C-C} = 1.458$ Å,

3) C. C. Costain and B. P. Stoicheff, *J. Chem. Phys.*, 30, 777 (1959).

TABLE V. COMPARISON OF THE CENTER FREQUENCIES ($CH_2^{35}ClCN$) GIVEN BY GRAYBEAL AND BY THE PRESENT AUTHORS

	obs.		calcd.	
	Graybeal	Present	Graybeal*	Present**
a-Type				
$2_{1,2}\leftarrow 3_{1,3}$	17550	17545	17549.40	17550.06
$3_{0,3}\leftarrow 4_{0,4}$	23974	23966.23	23975.39	23975.42
$3_{2,2}\leftarrow 4_{2,3}$	24002		24003.65	24003.66
$3_{3,1}\leftarrow 4_{3,2}$	24011		24012.09	24012.11
$3_{3,0}\leftarrow 4_{3,1}$	24011		24012.21	24012.23
$3_{2,1}\leftarrow 4_{2,2}$	24036		24034.28	24034.28
b-Type				
$5_{1,5}\leftarrow 6_{0,6}$	15794.54	15794.49	15794.54	15795.07
$10_{1,10}\leftarrow 9_{2,7}$	16347.33		16347.34	16337.31
$11_{2,10}\leftarrow 12_{1,11}$	16469.00	16468.89	16469.00	16467.53
$6_{1,6}\leftarrow 7_{0,7}$	22554.00	22551.95	22553.57	22555.14
$4_{0,4}\leftarrow 4_{1,3}$	23829.80	23821.51	23830.09	23830.39

* Values cited from Graybeal's paper. No corrections for centrifugal effects.

** Values calculated by using the rotational constants given by Graybeal. No corrections for centrifugal effects.

$d_{C\equiv N}=1.158$ Å, and $\angle CCN=180°$. The remaining five parameters were determined by the method of least-squares using the values of A and B, as shown in Table IV.

Nuclear quadrupole coupling constant is calculated for $CH_2^{35}ClCN$ from the transitions $1_{0,1}\leftarrow 1_{1,0}$, $3_{0,3}\leftarrow 3_{1,2}$, and $6_{0,6}\leftarrow 6_{1,5}$, and given in Table IV. If the electronic charge distribution about the C—Cl bond is assumed to be cylindrical, the quadrupole coupling constant along the C—Cl bond axis is −80 Mc./sec. The value is consistent with that observed in the solid state, 76.25 Mc./sec.[4] The hyperfine structures due to the nitrogen nucleus were not resolved.

Discussion

A quite normal value 1.7815 Å is obtained for the C—Cl bond length, which is very close to the value obtained for propargyl chloride, 1.780 Å[2], hence it is sure that neither a double bond structure nor an ionic structure contributes so much to the electronic configuration in the ground state of this molecule.

The center frequencies measured by Graybeal[4] are shown in Table V. Some of them are confirmed by the present investigation within the experimental error, but others show a definite discrepancy. Graybeal calculated the center frequencies by using the rotational constants given in Table VI. However, some of them are also in error by as much as 10 Mc./sec. It is found that the δ expansion formula he used[5] is insufficient for calculating the energy of the rotational states with J as high as ten. As a result his values of A are larger than the present ones by about 13 Mc./sec. (Table VI). On the other hand the constants of the present paper reproduce the

TABLE VI. COMPARISON OF THE ROTATIONAL CONSTANTS (IN Mc./sec) OBTAINED BY GRAYBEAL AND BY THE PRESENT AUTHORS

	$CH_2^{35}ClCN$		$CH_2^{37}ClCN$	
	Graybeal	Present	Graybeal	Present
A	25284.77	25271.30	25135.17	25122.52
B	3151.61	3151.01	3081.77	3081.13
C	2849.90	2848.80	2790.84	2789.56

frequencies of low-J transitions in good agreement with the observed ones. If the centrifugal distortion is taken into account, the rotational constants given in the present paper would account even for high-J transitions (Table III).

Graybeal reported the C—Cl bond length to be 1.767 Å and the C—C bond length to be 1.472 Å (Table IV). If isotopic species of carbon or nitrogen atoms were not available as in his study, it would be difficult to determine these two parameters separately. The correction due to the inertia defect has not been taken in the H···H distance obtained by Graybeal, thus the structure of the CH_2 group reported by him is not reliable.

The value of the quadrupole coupling constant of chlorine nucleus is observed to be −80 Mc./sec., which is slightly higher than that of propargyl chloride (−75.8 Mc./sec.)[2]

4) J. D. Graybeal and C. D. Cornwell, *J. Phys. Chem.*, **62**, 483 (1958).

5) Graybeal used likely the expansion formula given by King, Hainer and Cross [*J. Chem. Phys.*, **11**, 27 (1943)].

or of ethyl chloride (−70.07 Mc./sec.)[6]. This fact may be accounted for by the presence of the electronegative cyano group, since this reduces the ionic structure of the C—Cl bond. The present value of the quadrupole coupling constant of chlorine nucleus would be more reasonable than Graybeal's value −76.36 Mc./sec., since the (absolute) value obtained in the vapor phase is usually larger than that in the solid phase by several megacycles and the coupling constant of monochloroacetonitrile is 76.25 Mc./sec. in the solid state.

6) R. S. Wagner and B. P. Dailey, ibid., **26**, 1588 (1957).

The authors wish to express their sincere thanks to Dr. Makoto Shima, Institute for Physical and Chemical Research, for supplying them with heavy water. The expenses for this research were defrayed from the Scientific Research Encouragement Grant of the Ministry of Education to which the authors' thanks are also due.

Department of Chemistry
Faculty of Science
The University of Tokyo
Hongo, Tokyo

Microwave Spectrum of Propargyl Halides. I. Molecular Structure, Dipole Moment, and Quadrupole Coupling Constant of Propargyl Chloride

By Eizi Hirota and Yonezo Morino

(Received September 5, 1960)

The C—Cl bond length in propargyl chloride $CH_2ClC \equiv CH$ was found by Pauling, Gordy and Saylor[1] to be 1.82±0.02 Å. It is remarkably longer than C—Cl lengths observed in a number of other aliphatic chlorides. However, the value obtained in the previous paper[2], 1.7802 Å, was close to the usual C—Cl bond length.

The present paper will include the observation and the analysis of rotational spectra of two other isotopic species, $CH_2{}^{35}ClC{\equiv}CD$ and $CH_2{}^{37}ClC \equiv CD$, and will give a molecular structure more reliable than the previous one.

Experimental

The spectrometer used was similar to that reported by Shimoda, Nishikawa and Itoh[3]. A 100 Kc. sine wave modulation was used. The microwave was generated by klystrons, 2K26, 2K25, 8V77, X-12, and X-13, and the frequency was multiplied by a silicon crystal. The frequency range covered was from 7000 Mc./sec. to 36000 Mc./sec. An X-band absorption cell of 3 m. in length was employed, and the Stark electrode was supported by Teflon tape grooved at its center. The spacing between the electrode and the cell was not measured, but the calibration was made by observing the Stark effect of the $J=1\rightarrow 2$ lines of carbonyl sulfide $^{16}O^{12}C^{32}S$ at 24325.94 Mc./sec.[4]. The vacuum system was designed in such a way that the sample flew continuously through the cell, its pressure being estimated by a Pyrani gauge. The cell was cooled with dry ice when necessary. The frequency of microwave was measured by the technique developed by Shimoda[5]. The out-put power of microwave was detected by another silicon crystal and fed into a narrow band amplifier tuned with 100 Kc./sec. and then detected by a phase-sensitive detector. The signal was amplified by a low-frequency amplifier and observed on a cathode ray oscilloscope or on a recorder. The ultimate sensitivity was about $5\times 10^{-9}\,cm^{-1}$ when the recorder was used[6].

Propargyl chloride was synthesized by Dr. T. Shimozawa by the chlorination of propargyl alcohol[7]. The deuterated species $CH_2ClC{\equiv}CD$ was obtained by mixing normal propargyl chloride with heavy water which was made slightly alkaline by adding a small quantity of anhydrous sodium carbonate.

Results

Rotational Spectra and Rotational Constants. —Propargyl chloride is a nearly prolate symmetric top, and the a- and b- axes are in the

1) L. Pauling, W. Gordy and J. H. Saylor, *J. Am. Chem. Soc.*, **64**, 1753 (1942).
2) E. Hirota, T. Oka and Y. Morino, *J. Chem. Phys.*, **29**, 444 (1958).
3) K. Shimoda, T. Nishikawa and T. Itoh, *J. Phys. Soc. Japan*, **9**, 974 (1954).
4) S. A. Marshall and I. Weber, *Phys. Rev.*, **105**, 1502 (1957).
5) K. Shimoda, *J. Phys. Soc. Japan*, **9**, 378 (1954).
6) C. Matsumura, E. Hirota and Y. Morino, This Bulletin, to be published.
7) T. Chiba, T. Shimozawa, I. Miyagawa and Y. Morino, This Bulletin, **30**, 223 (1957).

TABLE I. OBSERVED AND CALCULATED FREQUENCIES OF THE SPECTRA IN THE GROUND VIBRATIONAL STATE (Mc./sec.)*

	$CH_2{}^{35}ClC{\equiv}CH$		$CH_2{}^{37}ClC{\equiv}CH$		$CH_2{}^{35}ClC{\equiv}CD$		$CH_2{}^{37}ClC{\equiv}CD$	
	Obs.	Calcd.	Obs.	Calcd.	Obs.	Calcd.	Obs.	Calcd.
a-Type								
$2_{0,2}\rightarrow 3_{0,3}$	17559.47	17559.49	17194.93	17195.16	16494.03	16494.16	16153.62	16153.69
$2_{1,2}\rightarrow 3_{1,3}$	17117.51	17117.56	16769.44	16767.89	16085.85	16085.84	15758.59	15758.66
$2_{1,1}\rightarrow 3_{1,2}$	18023.22	18023.67	17643.00	17644.90	16919.85	16922.17	16567.43	16567.27
$3_{0,3}\rightarrow 4_{0,4}$	23397.48	23397.50					21526.20	21525.66
$3_{1,3}\rightarrow 4_{1,4}$	22819.59	22819.50			21444.19	21444.31	21008.84	21008.26
$3_{1,2}\rightarrow 4_{1,3}$	24028.26	24027.56	23520.91	23520.66				
$3_{2,2}\rightarrow 4_{2,3}$	23429.2$_0$	23428.80						
$3_{2,1}\rightarrow 4_{2,2}$	23460.52	23460.76						
$4_{0,4}\rightarrow 5_{0,5}$	29222.29	29222.55	28617.83	28618.03	27452.20	27452.01	26887.05	26886.87
$4_{1,4}\rightarrow 5_{1,5}$	28518.24	28518.16	27936.00	27936.02	26800.23	26779.84	26255.39	26255.11
$4_{2,3}\rightarrow 5_{2,4}$	29281.78	29281.64	28672.8	28673.52	27504.77	27504.40	26936.60	26936.20
$4_{2,2}\rightarrow 5_{2,3}$	29345.7$_0$	29345.55			27560.52	27560.76	26988.42	26989.13
$4_{3,1}\rightarrow 5_{3,2}$, $4_{3,2}\rightarrow 5_{3,3}$	29302.15	29302.58	28694.4	28693.31	27523.16	27523.20	26953.83	26954.03
$4_{1,3}\rightarrow 5_{1,4}$			29394.00	29394.71	28193.52	28193.40		
b-Type								
$2_{0,2}\rightarrow 2_{1,1}$					21067.5	21067.11		
$3_{0,3}\rightarrow 3_{1,2}$					21495.43	21495.16	21364.7	21365.02
$4_{0,4}\rightarrow 4_{1,3}$	22921.58	22921.47						
$5_{0,5}\rightarrow 5_{1,4}$	23727.87	23726.87			22816.32	22817.10		
$6_{0,6}\rightarrow 6_{1,5}$	24719.31	24719.17	24508.91	24508.92	23728.20	23729.56	23520.15	23521.57
$7_{0,7}\rightarrow 7_{1,6}$	25911.16	25911.93	25656.94	25657.54	24822.98	24825.12	24575.30	24577.65
$8_{0,8}\rightarrow 8_{1,7}$	27319.22	27320.31	27011.07	27012.77	26114.84	26117.23	25819.24	25822.33
$9_{0,9}\rightarrow 9_{1,8}$	28958.40	28960.73	28587.43	28590.16	27615.44	27620.62	27263.97	27269.54
$0_{0,0}\rightarrow 1_{1,1}$	27077.01	27077.01	26868.46	26868.46	26008.25	26008.25	25797.49	25797.49
$7_{1,7}\rightarrow 8_{0,8}$	29132.01	29130.87						
$11_{2,10}\rightarrow 12_{1,11}$	17442.95	17435.36						
$12_{2,11}\rightarrow 13_{1,12}$	25079.7	25072.4						

* The centrifugal distortion is assumed to be $-D_{JK}J(J+1)K^2-D_JJ^2(J+1)^2$, with $D_{JK}=-0.057$ Mc./sec. and $D_J=0.0021$ Mc./sec.

TABLE II. ROTATIONAL CONSTANTS AND PRINCIPAL MOMENT OF INERTIA IN THE GROUND VIBRATIONAL STATE*

	$CH_2{}^{35}ClC{\equiv}CH$	(Calcd.)**	$CH_2{}^{37}ClC{\equiv}CH$	(Calcd.)**	$CH_2{}^{35}ClC{\equiv}CD$	(Calcd.)**	$CH_2{}^{37}ClC{\equiv}CD$	(Calcd.)**
A	24299.28	(24300.75)	24146.48	(24144.91)	23396.70	(23396.74)	23238.18	(23236.39)
B	3079.77	(3080.72)	3013.80	(3014.82)	2890.33	(2890.24)	2828.85	(2828.84)
C	2777.73	(2778.31)	2721.98	(2722.64)	2611.55	(2611.56)	2559.31	(2550.40)
b_P	-7.06709×10^{-3}		-6.85720×10^{-3}		-6.75178×10^{-3}		-6.56026×10^{-3}	
I_a	20.80436		20.93601		21.60694		21.75433	
I_b	164.146		167.739		174.904		178.705	
I_c	181.994		185.722		193.575		197.526	

* Rotational constants are given in Mc./sec. and principal moments of inertia in amu Å^2. Conversion factor 505531 Mc./sec. amu Å^2 is used.

** Values are calculated by using the set of structure parameters (I) given in Table V.

symmetry plane. Thus the dipole moment has components along the a- and b-axes, and transitions of both a- and b-types are observed. The observed spectra are listed in Table I, where center frequencies are given. The assignment is made mainly by the b-type Q-branch series, $J_{0,J}\rightarrow J_{1,J-1}$. The quadrupole hyperfine structure due to chlorine atom is of some use to check the assignment.

The b-type Q-branch series mentioned above give the rotational constants $[A-(B+C)/2]$ and the asymmetry parameters b_P, whereas the constants $B+C$ and $B-C$ are obtained by measuring the a-type R-branch lines. The

$0_{0,0} \rightarrow 1_{1,1}$ lines are important since their frequencies are equal to $A+C$. The rotational constants and the asymmetry parameters are given in Table II, where the moments of inertia are calculated by using the conversion factor 505531 Mc./sec. amu Å^2. The frequencies calculated by using these rotational constants are compared with the observed ones in Table I.

In the course of searching, the spectra of two excited vibrational states were found. By comparing their intensities with those of the ground state, one is assigned to the CCCl bending mode and the other to one of the C—C≡C bending modes. The center frequencies and the rotational constants derived from them are listed in Table III.

Table III. Observed and calculated frequencies of the spectra and rotational constants in the excited vibrational states ($CH_2^{35}ClC{\equiv}CH$) (Mc./sec.)

	State I (δCCCl)		State II (δCC≡C)	
	Obs.	Calcd.	Obs.	Calcd.
$2_{0,2} \rightarrow 3_{0,3}$	17597.0	17592.7	17545.4	17545.4
$0_{0,0} \rightarrow 1_{1,1}$	27230.76	27230.8		
$6_{0,6} \rightarrow 6_{1,5}$	24926.32	24926.7		
$7_{0,7} \rightarrow 7_{1,6}$	26141.31	26142.4		
$8_{0,8} \rightarrow 8_{1,7}$	27576.77	27578.2	27184.66	27185.2
$9_{0,9} \rightarrow 9_{1,8}$			28809.18	28810.5
$A(\alpha_i)$	24450.2	(−150.9)	24214.6	(84.7)
$B(\beta_i)$	3088.1	(−8.3)	3076.09	(3.68)
$C(\gamma_i)$	2780.6	(−2.9)	3776.60	(1.13)
b_P	-7.14570×10^{-3}		-7.03413×10^{-3}	

Structure Analysis. — The structure of propargyl chloride is specified by eight parameters: C—Cl, C—C, C≡C, methylenic C—H, and acetylenic C—H bond lengths, and CCCl, HCH and CCH bond angles, the C—C≡C—H group being assumed to be linear. The distance between two hydrogen atoms in methylene group is directly given by the quantity $[(I_a+I_b-I_c)/m_H]^{1/2}$. The four kinds of isotopic species give fairly close values for the distance, as shown in Table IV. However, as Laurie pointed out[8], the inertia defect Δ makes this distance short and the angle HCH apparently small. Since the data on the isotopic molecules for which deuterium is substituted in the methylene group were not available, it was difficult to see how much the inertia defect was. If the value is assumed to be 0.2194 amu Å as found for chloroacetonitrile[9], the distance H···H becomes 1.7715 Å. In the following the molecular structure is calculated by assuming Δ equal to zero or 0.2194 amu Å^2.

8) V. W. Laurie, *J. Chem. Phys.*, **28**, 704 (1958).
9) K. Wada, Y. Kikuchi, C. Matsumura, E. Hirota, and Y. Morino, This Bulletin, **34**, 337 (1961).

Table IV. The hydrogen to hydrogen distance in methylene group

	$I_a-I_b+I_c$ (amu Å^2)	H···H (Å)
$CH_2^{35}ClC{\equiv}CH$	2.956	1.712_3
$CH_2^{37}ClC{\equiv}CH$	2.953	1.711_4
$CH_2^{35}ClC{\equiv}CD$	2.936	1.706_5
$CH_2^{37}ClC{\equiv}CD$	2.933	1.705_6

The inertia defect arises from the zero-point vibration, and it is accepted from the case of water molecule[10] that the contribution of low-frequency vibrations to inertia defect is larger than those of high-frequency ones. The CCCl and C—C≡C bending modes are mentioned as the low-frequency vibrations in propargyl chloride, and the rotational constants are obtained in the excited states of these two vibrations as stated above. It is interesting to see how much the inertia defect and the distance H···H are changed if the rotational constants are corrected for these two vibrations. The corrected rotational constants, A', B', and C', are given by

$$A' = A_0 + (1/2)(\alpha_1+\alpha_2)$$

$$B' = B_0 + (1/2)(\beta_1+\beta_2)$$

and

$$C' = C_0 + (1/2)(\gamma_1+\gamma_2)$$

where α_1, β_1, γ_1 and α_2, β_2, γ_2 denote the changes of rotational constants due to the two vibrations. Their observed values are 24266.2 Mc./sec., 3077.5 Mc./sec. and 2776.8 Mc./sec., respectively. The H···H distance, 1.738 Å, calculated by using A', B' and C' is in fact fairly larger than that obtained by A_0, B_0 and C_0, 1.709 Å, but still smaller than 1.772 Å which was obtained by assuming Δ = 0.2194 amu Å^2.

The parameters other than the H···H distance, seven in number, are to be determined by the remaining eight constants. Not all parameters can be determined by the present data, hence several assumptions are necessary. It is recognized that the C≡C bond length is relatively constant, irrespective of the attached groups. The value 1.207 Å is assumed for this length[11,12]. The acetylenic C—H bond length makes a small contribution to the rotational constants, hence the value 1.06 Å is assumed for this distance without strong influence upon other parameters to be obtained[12]. The lengths, C—H and C—D, are assumed to be the same. The groups C—C≡C and C—C≡N are usually considered linear, though the detailed investigations gave slightly bent structures[13]. Here the

10) B. T. Darling and D. M. Dennison, *Phys. Rev.*, **57**, 128 (1940). See also Ref. 8.
11) G. Herzberg and B. P. Stoicheff, *Nature*, **175**, 79 (1955).
12) C. C. Costain and B. P. Stoicheff, *J. Chem. Phys.*, **30**, 777 (1959).
13) C. C. Costain and J. R. Morton, ibid., **31**, 389 (1959); E. Hirota and Y. Morino, This Bulletin, **33**, 158, 705 (1960).

linear structure is also assumed. Two additional assumptions are the methylenic C—H bond length equal to 1.09 Å and the CCH bond angle equal to 111°30′. These two parameters, especially the latter, affect considerably the rotational constant A, in spite of the light weight of a hydrogen atom. Hence some precaution must be taken for selecting the assumed values for these parameters.

First, the inertia defect is set equal to zero. The methylenic C—H bond length and the CCH bond angle are assumed to be 1.09 Å and 111°30′, respectively. The eight rotational constants, A and C for each isotopic molecule, are used to determine the C—Cl and the C—C bond lengths, and the CCCl bond angle. They are found to be 1.7800 Å, 1.4582 Å, and 112°9′, respectively (Table V). If the bond lengths C—Cl and C—C become longer, both A and C decrease, on the other hand the A increases and the C decreases with the increase of the CCCl angle. Thus the determination of the CCCl angle is definite, but it is somewhat difficult to determine two bond lengths separately. Still it is feasible to obtain fairly good results for the two bond lengths. The fitting of the calculated constants with the observed is carried out by the least-squares method, the mean deviation is 0.00051 Å for the C—Cl bond length, 0.00062 Å for the C—C bond length, and 0.54′ for the CCCl bond angle. If the assumed value for the C≡C length, 1.207 Å, is in error by 0.01 Å, the C—Cl is changed by 0.001 Å, the C—C by 0.007 Å, and the CCCl by 2.5′.

TABLE V. STRUCTURE PARAMETERS UNDER VARIOUS ASSUMPTIONS

Set	Assumption I amu Å²	Assumption ∠CCH	Result C—Cl Å	Result C—C Å	Result ∠CCCl
I	0	111°30′	1.7800	1.4582	112°9′
II_a	0.2194	107°30′	1.7728	1.4766	111°43′
II_b	0.2194	109°30′	1.7768	1.4724	111°45′
II_c	0.2194	111°30′	1.7808	1.4690	111°44′

Other assumptions
C≡C 1.207 Å
C—H (methylenic) 1.09 Å
C—H=C—D (acetylenic) 1.06 Å
C—C≡C—H(D) linear

In the second place, the inertia defect is assumed to be 0.2194 amu Å². This value is borrowed from the result for the chloroacetonitrile molecule. An analysis by the least-squares method is carried out by using three values for the CCH angle, 107°30′, 109°30′ and 111°30′. The methylenic C—H length is fixed to 1.09 Å. As stated above, the HCH angle becomes 108°42′, a quite reasonable value. The results obtained for the C—Cl and the C—C lengths, and the CCCl angle are listed in Table V. The CCCl bond angle is relatively independent of the values assumed for the CCH angle; however, the two bond lengths are varied by 0.008 Å. It is difficult to say which case is the most reasonable, but the length of the C—C bond adjacent to the triple bond is reported about 1.460 Å in a number of related molecules[11,12]. In this respect the case 111°30′ for the CCH angle is the most favorable, where the C—C length is 1.4690 Å. It is yet by no means clear whether or not the assumed value for the inertia defect is reasonable. It is felt that the inertia defect slightly less than 0.2194 amu Å² is more reasonable, since the C—C bond length then becomes somewhat shorter than 1.4690 Å. The parameter values, which are considered the most reasonable at present, are given in the last column of Table VI, where errors are attached by taking into account the zero-point vibration, inadequacy of the assumed parameters, and so on.

TABLE VI. MOLECULAR STRUCTURE

C—Cl	1.780±0.003 Å
C—C	1.465±0.007 Å
CCCl	111°50′±20′
HCH	108°42′±1°
CCH	111°30′±1°30′

Assumptions
C≡C 1.207 Å
C—H (methylenic) 1.09 Å
C—H(D) (acetylenic) 1.06 Å
C—C≡C—H(D) linear

Quadrupole Coupling Constant of Chlorine Atom. — The chlorine nuclear quadrupole coupling constant is determined by measuring the hyperfine structure of eight rotational transitions of the most abundant species $CH_2{}^{35}ClC{\equiv}CH$. By the lack of accidental degeneracy in rotational energy only the two components of the coupling constant, χ_{aa} and χ_{bb}, are obtained. The least-squares method gives $\chi_{aa}=-30.4$ Mc./sec. and $\chi_{bb}=-7.5$ Mc./sec. The hyperfine structures calculated by using these values are compared with the observed ones in Table VII.

A similar analysis is carried out on the hyperfine structures of eight transitions of $CH_2{}^{35}ClC{\equiv}CD$, but it is found that the values −28.2 Mc./sec. and −9.7 Mc./sec., which are

TABLE VII. HYPERFINE STRUCTURES OF THE CHLORINE NUCLEAR QUADRUPOLE COUPLING CONSTANT (Mc./sec.)

Transition	$F'' \rightarrow F'$		$CH_2{}^{35}ClC{\equiv}CH$			$CH_2{}^{35}ClC{\equiv}CD$		
			Obs.	Calcd.*	Calcd.−Obs.	Obs.	Calcd.**	Calcd.−Obs.
$2_{12}\rightarrow3_{13}$	7/2	9/2	+1.08	+1.09	+0.01	+1.08	+1.05	−0.03
	5/2	7/2	−0.88	−0.83	+0.05	−0.57	−0.74	−0.17
	3/2	5/2	−2.34	−2.28	+0.06	−2.56	−2.25	+0.31
	1/2	3/2	−0.28	−0.36	−0.08			
$3_{21}\rightarrow4_{22}$	9/2	11/2	+0.97	+1.05	+0.08			
	7/2	9/2	−1.82	−1.85	−0.03			
	5/2	7/2	−0.74	−0.81	−0.07			
	3/2	5/2	+2.08	+2.09	+0.01			
$3_{13}\rightarrow4_{14}$	9/2	11/2				+0.80	+0.98	+0.18
	7/2	9/2				−0.07	−0.13	−0.06
	5/2	7/2				−1.00	−1.17	−0.17
$3_{03}\rightarrow3_{12}$	7/2	7/2				+5.63	+5.26	−0.34
	5/2	5/2				+1.58	+1.58	0.00
	9/2	9/2				−2.92	−2.63	+0.29
	3/2	3/2				−6.52	−6.31	+0.21
$4_{04}\rightarrow4_{13}$	9/2	9/2	+4.51	+4.52	+0.01			
	7/2	7/2	+1.95	+2.03	+0.08			
	11/2	11/2	−2.40	−2.59	−0.19			
	5/2	5/2	−5.16	−5.08	−0.08			
$5_{05}\rightarrow5_{14}$	11/2	11/2	+4.07	+4.23	−0.16	+4.29	+4.37	+0.08
	9/2	9/2	+2.38	+2.29	−0.09	+2.15	+2.37	+0.22
	13/2	13/2	−2.69	−2.65	+0.04	−2.55	−2.73	−0.18
	7/2	7/2	−4.45	−4.59	−0.14	−4.61	−4.73	−0.12
$6_{06}\rightarrow6_{15}$	13/2	13/2	+4.21	+4.10	−0.11	+4.24	+4.25	+0.01
	11/2	11/2	+2.65	+2.49	−0.16	+2.67	+2.57	−0.10
	15/2	15/2	−2.94	−2.74	+0.20	−2.92	−2.83	+0.09
	9/2	9/2	−4.45	−4.35	−0.10	−4.51	−4.50	+0.01
$7_{07}\rightarrow7_{16}$	15/2	15/2	+4.02	+4.06	+0.04	+4.10	+4.21	+0.11
	13/2	13/2	+2.67	+2.66	−0.01	+2.67	+2.75	+0.08
	17/2	17/2	−2.84	−2.84	0.00	−2.86	−2.95	−0.09
	11/2	11/2	−4.25	−4.25	0.00	−4.30	−4.40	−0.10
$8_{08}\rightarrow8_{17}$	17/2	17/2	+4.10	+4.08	−0.02	+4.30	+4.23	−0.07
	15/2	15/2	+2.85	+2.82	−0.03	+2.98	+2.92	−0.06
	19/2	19/2	−3.02	−2.97	+0.05	−3.09	−3.08	+0.01
	13/2	13/2	−4.24	−4.23	+0.01	−4.51	−4.38	+0.12
$9_{09}\rightarrow9_{18}$	19/2	19/2	+4.06	+4.14	+0.08	+4.30	+4.29	−0.01
	17/2	17/2	+2.98	+2.98	0.00	+3.13	+3.09	−0.04
	21/2	21/2	−3.06	−3.11	−0.05	−3.22	−3.22	0.00
	15/2	15/2	−4.21	−4.26	−0.05	−4.46	−4.42	+0.04

* $\chi_{aa}=-30.4$ Mc./sec. and $\chi_{bb}=-7.5$ Mc./sec. are used.
** $\chi_{aa}=-28.2$ Mc./sec. and $\chi_{bb}=-9.7$ Mc./sec. are used.

calculated from coupling constants of $CH_2{}^{35}ClC{\equiv}CH$ by transforming the principal axes, explain the hyperfine structures sufficiently well.

If the values of χ_{aa} and χ_{bb} were accurate, the rotation of the principal axes due to the deuterium substitution might give the asymmetry parameter, but the present data do not warrant such a procedure. On the other hand, the second-order effect observed for the bromine nuclear quadrupole hyperfine structure of rotational spectra of propargyl bromide $CH_2BrC{\equiv}CH$ indicated that the asymmetry parameter was small[14]. The values of χ_{aa} and χ_{bb} obtained above give $\chi_{bond}=-75.8$ Mc./sec., under the assumption of the cylindrical symmetry of charge distribution about the C—Cl bond. The result is consistent with the value in the solid state, 71.6246 Mc./sec.[15]

Dipole Moment. — The dipole moment has two components; one along the a-axis and the other along the b-axis. The Stark effect of the $0_{0,0}\rightarrow1_{1,1}$ transition of $CH_2{}^{35}ClC{\equiv}CH$ is measured to obtain the two components of the

14) Y. Kikuchi, E. Hirota and Y. Morino, *J. Chem. Phys.*, **31**, 1139 (1959); This Bulletin, **34**, 348 (1961).

15) T. Shimozawa, T. Chiba, I. Miyagawa and Y. Morino, ibid., to be published.

dipole moment. The presence of the chlorine nuclear quadrupole moment makes the Stark effect complicated, but it is possible to analyze the Stark effect of the $0_{0,0}\rightarrow 1_{1,1}$ transition, since the J number associated is small[16].

The quadrupole energy of the state $1_{1,1}$ is small, hence the weak, the intermediate, and the strong field cases are successively met with the increase of the Stark electric field. The quadrupole energy is zero for the state $0_{0,0}$.

The calculation of the Stark effect and the quadrupole effect is carried out by taking the wave function, $|IJ\tau M_J M_I>$, as the basis. The matrix elements of the Hamiltonian for the Stark effect H_E are diagonal in M_J and M_I, but they connect different rotational states. The state $0_{0,0}$ couples with states $1_{0,1}$ and $1_{1,1}$, and the state $1_{1,1}$ with states $1_{1,0}$, $2_{1,2}$, $0_{0,0}$, $2_{2,0}$ and $2_{0,2}$ by the Hamiltonian H_E. The differences in rotational energies are greater than the Stark or quadrupole energies, so that the second-order perturbation is sufficient to calculate the Stark effect[17]. Thus, it is reduced to the form;

$$\sum_{J'\tau'} \frac{|(IJ\tau M_J M_I|H_E|IJ'\tau' M_J M_I)|^2}{E_{J\tau}-E_{J'\tau'}} = (\alpha+\beta M_J^2)\varepsilon^2$$

where ε is the Stark field strength, and α and β are constants depending upon the rotational constants, the rotational quantum numbers, and the dipole moment.

The Hamiltonian for the quadrupole energy, H_Q, has matrix elements, diagonal as well as nondiagonal with respect to M_J and M_I. Matrix elements between different rotational states are ignored, since the first-order perturbation is sufficient enough to treat the quadrupole energy. The matrix elements appropriate at present are as follows:

$$\begin{aligned}
&(IJ\tau M_J M_I|H_Q|IJ\tau M_J' M_I')\\
&=P[3M_I^2-I(I+1)]\,[3M_J^2-J(J+1)]\\
&\qquad (M_J'=M_J,\ M_I'=M_I)\\
&=P[3/2+3M_I M_J+3(M_I\mp 1)(M_J\pm 1)]\\
&\quad\times\{[I(I+1)-M_I(M_I\mp 1)]\\
&\quad\times[J(J+1)-M_J(M_J\pm 1)]\}^{1/2}\\
&\qquad (M_J'=M_J\pm 1,\ M_I'=M_I\mp 1)\\
&=P(3/2)\{[J(J+1)-M_J(M_J\pm 1)]\\
&\quad\times[J(J+1)-(M_J\pm 1)(M_J\pm 2)]\\
&\quad\times[I(I+1)-M_I(M_I\mp 1)]\\
&\quad\times[I(I+1)-(M_I\mp 1)(M_I\mp 2]\}^{1/2}\\
&\qquad (M_J'=M_J\pm 2,\ M_I'M_I\mp 2)
\end{aligned}$$

where P is given by

$$\begin{aligned}
P=\{&\chi_{aa}[J(J+1)+E(\kappa)-(\kappa+1)(\partial E(\kappa)/\partial\kappa)]\\
&+2\chi_{bb}(\partial E(\kappa)/\partial\kappa)\\
&+\chi_{cc}[J(J+1)-E(\kappa)\\
&+(\kappa-1)(\partial E(\kappa)/\partial\kappa)]\}/\\
&[4J(J+1)(2J-1)(2J+3)I(2I-1)]
\end{aligned}$$

which is reduced for the state $1_{1,1}$ to

$$P(1_{1,1})=-(1/60)\chi_{bb}$$

Secular determinant for the state $1_{1,1}$ factors into three groups, corresponding to $M_F=M_J+M_I=5/2$, $3/2$ and $1/2$, respectively. Secular determinants are all doubly degenerate. The case $M_F=5/2$ is the simplest, since the wave function belonging to $M_F=5/2$ is $|M_J, M_I>=|1, 3/2>$ or $|-1, -3/2>$. The secular equation is

$$3P+(\alpha+\beta)\varepsilon^2-W=0$$

The two pairs of wave functions, $\{|\pm 1, \pm 1/2>, |0, \pm 3/2>\}$, belong to $M_F=3/2$ and give rise to a two-dimensional secular equation:

$$\begin{vmatrix} -3P+(\alpha+\beta)\varepsilon^2-W & 3\sqrt{6}\,P \\ 3\sqrt{6}\,P & -6P+\alpha\varepsilon^2-W \end{vmatrix}=0$$

The wave functions corresponding to $M_F=1/2$ are $|\pm 1, \mp 1/2>$, $|0, \pm 1/2>$ and $|\mp 1, \pm 3/2>$, and the secular equation is

$$\begin{vmatrix} 3P+(\alpha+\beta)\varepsilon^2-W & -3\sqrt{6}\,P & 6\sqrt{3}\,P \\ -3\sqrt{6}\,P & 6P+\alpha\varepsilon^2-W & 0 \\ 6\sqrt{3}\,P & 0 & -3P+(\alpha+\beta)\varepsilon^2-W \end{vmatrix}=0$$

If the field strength ε is equal to zero, the secular equations give the following energy states:

$W_1=3P$	$F=5/2$,	$M_F=5/2$
$W_{21}=3P$	$5/2$,	$3/2$
$W_{22}=-12P$	$3/2$,	$3/2$
$W_{31}=3P$	$5/2$,	$1/2$
$W_{32}=-12P$	$3/2$,	$1/2$
$W_{33}=15P$	$1/2$,	$1/2$

Here the representation $|IFM_I M_F>$ rather than $|IJM_I M_J>$ is good. There are only two states $|F, M_F>=|3/2, 1/2>$ and $|3/2, 3/2>$ possible in the rotational state $0_{0,0}$. Since the selection rule is $\Delta M_F=0$, transition to the state W_1 is forbidden and two pair states W_{21} and W_{31}, and W_{22} and W_{32} are degenerate, there are three hyperfine lines. If the Stark field increases so that the Stark energies $\alpha\varepsilon^2$ or $\beta\varepsilon^2$ are larger than P, the strong field case is apropppriate. The secular determinantes described above give the following states:

16) F. Coester, *Phys. Rev.*, **77**, 454 (1950).
17) S. Golden and E. B. Wilson, Jr., *J. Chem. Phys.*, **16**, 669 (1948).

$$W_1=(\alpha+\beta)\varepsilon^2+3P \quad M_J=1, \quad M_I=3/2$$
$$W_{21}=(\alpha+\beta)\varepsilon^2-3P \quad 1, \quad 1/2$$
$$W_{22}=\alpha\varepsilon^2-6P \quad 0, \quad 3/2$$
$$W_{31}=(\alpha+\beta)\varepsilon^2+3P \quad 1, \quad 3/2$$
$$W_{32}=\alpha\varepsilon^2+6P \quad 0, \quad 1/2$$
$$W_{33}=(\alpha+\beta)\varepsilon^2-3P \quad 1, \quad 1/2$$

This case can be expressed by the representation $|IJM_IM_J>$. The rotational state $0_{0,0}$ involves two states $|M_J, M_I>=|0, 1/2>$ and $|0, 3/2>$. Two transitions to the states $W_{21}(M_J=0, M_I=3/2)$ and $W_{22}(M_J=0, M_I=1/2)$ are allowed by the selection rules, $\Delta M_J=0$ and $\Delta M_I=0$.

The solutions for the intermediate case are obtained by solving the secular determinants given above. Eigenfunctions are obtained to calculate the transition probabilities. The change of the hyperfine patterns with the electric field, the frequencies and the intensities, is given in Fig. 1.

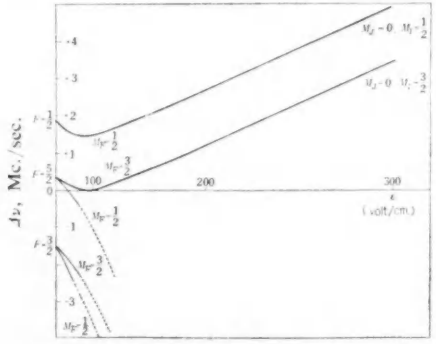

Fig. 1. Stark effect of the $0_{0,0}\rightarrow 1_{1,1}$ transition ($CH_2{}^{35}ClC{\equiv}CH$).

It is interesting to note that the transition to the state W_{21} in case $\varepsilon=0$ shifts first to lower frequency with increasing electric field, stops at some field strength ε_0, and then moves to a higher frequency. The observed intensity reduces to zero at ε_0, because the Stark modulation is used for the measurement. This is also the case for the transition to the state W_{33} at $\varepsilon=0$. The case $M_F=3/2$ is considered. The solutions are obtained by solving the secular equation, that is

$$W^{\pm}=-(1/2)\,[9P-(2\alpha+\beta)\varepsilon^2] \pm[(1/4)(3P+\beta\varepsilon^2)^2+54P^2]^{1/2}$$

The line mentioned above corresponds to the transition to the state W^+ and its frequency is given by

$$\nu=(W^++\alpha_0\varepsilon^2)/h$$

where $-\alpha_0\varepsilon^2$ is the Stark effect of the state $0_{0,0}$. Then the electric field ε_0, at which the Stark effect of the line changes its sign from minus to plus, is given by

$$\varepsilon_0{}^2=(P/\beta)\{-3-[216(2\alpha_0+2\alpha+\beta)^2/[\beta^2-(2\alpha_0+2\alpha+\beta)^2]]^{1/2}\}$$

The constants, α_0, α and β, are functions of two components of dipole moments, μ_a and μ_b. The Stark effect of the strong field case gives $\alpha_0+\alpha+\beta$ and ε_0 thus obtained provides another information on α_0, α and β.

The two components thus found are $\mu_a=0.98_3$ D and $\mu_b=1.36_0$ D, and the total moment $\mu_t=1.68$ D. There are four choices for the direction of the dipole moment, but it seems most plausible that the negative direction of the dipole moment lies between the C–Cl and the C—C≡C—H bonds, at an angle of $16\pm7°$ from the former. The total dipole moment 1.68 D is compared favorably with the value obtained by the dielectric constant measurement, 1.65 D[f].

Discussion

Pauling, Gordy and Saylor[1] explained the long C—Cl bond length by assuming a resonance structure $Cl{-}CH_2{=}C{=}C^+{-}H$, but the present result clearly shows that it is unnecessary to consider such a resonance structure. The C—Cl bond was found to be a normal value of 1.780 Å. In addition to this, the resonance structure given above predicts a small quadrupole coupling constant and a large dipole moment. These are not found in the present data either. Laurie and Lide observed the C—Cl bond length in 1-chloro-2-butyne to be

TABLE VIII. COMPARISON OF MOLECULAR STRUCTURES

	Propargyl chloride $CH_2ClC{\equiv}CH$	Methyl chloride CH_3Cl	Ethyl chloride CH_3CH_2Cl
C—Cl (Å)	1.780[a]	1.781[b]	1.7785[c]
C—C (Å)	1.465[a]	—	1.5495[c]
χ_{bond} (Cl^{35}) (Mc./sec.)	−75.8[a]	−74.740[c]	−70.07[c]
μ (D)	1.68[a]	1.869[d]	2.05[f]

a) The present paper.
b) S. L. Miller, L. C. Aamodt, G. Dousmanis, C. H. Townes and J. Kraitchman, *J. Chem. Phys.*, **20**, 1112 (1952).
c) S. Geschwind, R. Gunther-Mohr and C. H. Townes, *Phys. Rev.*, **81**, 288 (1951).
d) R. G. Shulman, C. H. Townes and B. P. Dailey, ibid., **78**, 145 (1950).
e) R. S. Wagner and B. P. Dailey, *J. Chem. Phys.*, **26**, 1588 (1957).
f) C. P. Smyth, "Dielectric Behavior and Structure" McGraw-Hill Book Co., New York, N. Y. (1955), p. 269.

1.79$_6$ Å[18]. The data were, however, not sufficiently accurate and in addition the presence of internal rotation complicated the problem.

It is of some help to compare the constants of the propargyl chloride molecules with those of some other molecules. Table VIII shows such a comparison, where methyl and ethyl chlorides are taken as reference substances.

The authors are greatly indebted to Professor K. Shimoda, Mr. H. Hirakawa, and their coworkers at the Department of Physics for their advice in constructing the apparatus. They should like to thank Mr. T. Oka who collaborated with them in the early stage of this investigation. They wish also to express their sincere thanks to Dr. M. Shima, Institute for Physical and Chemical Research, for supplying them with heavy water. The expenses for this research were defrayed from the Scientific Research Encouragement Grant of the Ministry of Education to which the authors' thanks are also due.

Department of Chemistry
Faculty of Science
The University of Tokyo
Hongo, Tokyo

18) V. W. Laurie and D. R. Lide, Jr., ibid., **31**, 939 (1959).

Microwave Spectrum of Propargyl Halides. II. Molecular Structure and Second-Order Quadrupole Effect of Propargyl Bromide

By Yoshikazu KIKUCHI, Eiji HIROTA and Yonezo MORINO

(Received September 5, 1960)

In the previous papes[1] the C—Cl distance in propargyl chloride was reported to be close to the usual C-Cl bond length, 1.780±0.002 Å. The determination of the C—Br length in propargyl bromide is also of interest to obtain an additional assurance to the conclusion obtained in the previous paper.

An anomaly due to accidental degeneracy in rotational energy has been observed in bromine nuclear quadrupole hyperfine structure of some b-type Q-branch transitions[2]. The deviation from the first-order theory amounted to several megacycles. An analysis using the second-order perturbation has enabled us to know the direction of the principal axes and principal values of the quadrupole coupling constant of the bromine atom. It was found that the direction of the largest principal value of the coupling constants coincided with that of the C—Br bond and the asymmetry parameter was very small*.

1) E. Hirota and Y. Morino, This Bulletin, **34**, 341 (1961).
2) Preliminary account is given in the paper, Y. Kikuchi, E. Hirota and Y. Morino, *J. Chem. Phys.*, **31**, 1139 (1959).
* Recently the microwave spectrum of ethyl iodide was measured by Kasuya and Oka[3], They found a hyperfine structure of the iodine atom deviating from the first-order theory.
3) T. Kasuya and T. Oka, *J. Phys. Soc., Japan*, **15**, 296 (1960).

Experimental

The spectra of propargyl bromide, $CH_2{}^{79}BrC{\equiv}CH$, $CH_2{}^{81}BrC{\equiv}CH$, $CH_2{}^{79}BrC{\equiv}CD$ and $CH_2{}^{81}BrC{\equiv}CD$, were observed by a Stark modulation spectrometer described in the previous paper. The two isotopic species of bromine have almost equal natural abundance, hence no special preparation was necessary. The deuterated samples were obtained by the method used for the preparation of deuterated propargyl chloride.

Results

Rotational Spectra and Rotational Constants. —Propargyl bromide is also a nearly prolate symmetric top, similar to the chloride. The symmetry plane includes a- and b-axes, hence a- as well as b-type transitions are expected to be observed.

Table I gives the observed center frequencies. Preliminary assignment is based on frequencies expected for the assumed structure and hyperfine patterns. Transitions of a-type R-branch, $J_{1,J} \rightarrow J+1_{1,J+1}$, split into four lines and are easily identified by their characteristic hyperfine structures. The assignment of b-type Q-branch transitions is confirmed by plotting the asymmetry parameter b_P versus the quantity $A-(B+C)/2$.

The rotational constants and the asymmetry

TABLE I. OBSERVED AND CALCULATED CENTER FREQUENCIES (Mc./sec.)

Transition	$CH_2{}^{79}BrC{\equiv}CH$		$CH_2{}^{81}BrC{\equiv}CH$		$CH_2{}^{79}BrC{\equiv}CD$		$CH_2{}^{81}BrC{\equiv}CD$	
	Obs.	Calcd.	Obs.	Calcd.	Obs.	Calcd.	Obs.	Calcd.
a-Type								
$6_{0,6}\rightarrow 7_{0,7}$	29035.53	29035.59	28843.44	28843.46	27359.91	27359.92	27178.13	27178.01
$6_{1,6}\rightarrow 7_{1,7}$	28460.66	28460.76	28275.01	28274.95	26820.29	26820.65	26644.31	26644.52
$6_{1,5}\rightarrow 7_{1,6}$	29721.56	29721.58	29520.15	29520.46		28001.53	27811.32	27811.37
$6_{2,5}\rightarrow 7_{2,6}$	29099.90	29099.97	28906.35	28906.25	27419.44	27419.53	27235.99	27236.07
$6_{2,4}\rightarrow 7_{2,5}$	29171.76	29171.81	28976.40	28976.40	27485.36	27485.50	27301.11	27300.52
$5_{0,5}\rightarrow 6_{0,6}$	24903.78	24904.57	24739.83	24739.50		23466.94		23310.34
$5_{1,5}\rightarrow 6_{1,6}$	24399.30	24399.29	24240.00	24239.93	22993.25	22993.14	22841.84	22841.79
$5_{1,4}\rightarrow 6_{1,5}$	25479.55	25480.30	25308.40	25307.79		24005.60		23842.20
$4_{1,4}\rightarrow 5_{1,5}$	20335.98	20335.82	20203.04	20202.97	19163.99	19163.81		19037.41
$3_{1,3}\rightarrow 4_{1,4}$	16270.72	16270.71	16164.26	16164.38	15332.75	15332.94	15231.60	15231.63
b-Type								
$13_{0,13}\rightarrow 13_{1,12}$	28406.9	28414.0	28270.2	28275.0	26945.4	26945.9	26815.7	26816.0
$12_{0,12}\rightarrow 12_{1,11}$	26906.93	26911.78	26791.33	26794.45	25545.00	25545.56	25435.05	25435.40
$11_{0,11}\rightarrow 11_{1,10}$	25563.6	25566.2	25466.9	25468.0	24290.1	24290.0	24197.6	24197.4
$10_{0,10}\rightarrow 10_{1,9}$	24367.0	24368.6	24286.7	24287.3	23171.6	23171.9	23095.0	23094.6
$9_{0,9}\rightarrow 9_{1,8}$	23309.9	23310.7	23243.9	23243.9	22184.3	22183.7	22120.1	22119.7
$8_{0,8}\rightarrow 8_{1,7}$	22384.6	22384.2	22330.7	22330.0	21318.0	21317.9	21265.6	21265.4
$7_{0,7}\rightarrow 7_{1,6}$	21578.3	21581.5	21538.3	21538.0				
$6_{0,6}\rightarrow 6_{1,5}$	20896.0	20895.5	20861.7	20861.0				
$5_{0,5}\rightarrow 5_{1,4}$	20319.5	20319.8	20292.9	20292.7				
$9_{1,9}\rightarrow 10_{0,10}$	26159.13	26164.36	25854.17	25860.54				

TABLE II. ROTATIONAL CONSTANTS, ASYMMETRY PARAMETERS, AND CENTRIFUGAL DISTORTION CONSTANTS

		$CH_2{}^{79}BrC{\equiv}CH$	$CH_2{}^{81}BrC{\equiv}CH$	$CH_2{}^{79}BrC{\equiv}CD$	$CH_2{}^{81}BrC{\equiv}CD$
A	obs.	21010.0 ± 3 Mc./sec.	20986.5 ± 3 Mc./sec.	20045.8 ± 3 Mc./sec.	20021.0 ± 3 Mc./sec.
	calcd.	21012.0	20987.9	20047.3	20022
B	obs.	2169.31 ± 0.2	2154.37 ± 0.2	2043.49 ± 0.2	2029.28 ± 0.2
	calcd.	2169.41	2154.51	2043.06	2028.96
C	obs.	1989.09 ± 0.2	1976.34 ± 0.2	1874.70 ± 0.2	1862.50 ± 0.2
	calcd.	1989.19	1976.44	1874.36	1862.27
	b_P	-4.7600×10^{-3}	-4.7045×10^{-3}	-4.6662×10^{-3}	-4.6136×10^{-3}
	D_J	0.001 Mc./sec.	0.001 Mc./sec.	0.001 Mc./sec.	~0 Mc./sec.
	D_{JK}	−0.0455	−0.0432	−0.0505	−0.0460

TABLE III. THE HYDROGEN TO HYDROGEN DISTANCE IN METHYLENE GROUP (Å)

	$CH_2{}^{79}BrC{\equiv}CH$	$CH_2{}^{81}BrC{\equiv}CH$	$CH_2{}^{79}BrC{\equiv}CD$	$CH_2{}^{81}BrC{\equiv}CD$
r(H···H)	1.7098	1.7108	1.7092	1.7084

parameters are given in Table II, and the frequencies calculated by using these constants are compared with the observed ones in Table I. A rough correction is made for the centrifugal distortion by assuming the expression $-D_J J^2(J+1)^2 - D_{JK} J(J+1)K^2$. The observed values of D_J and D_{JK} are given in Table II.

Structure Analysis.—The number of structural parameters is the same as that of the chloride. Again the H···H distance in methylene group is given by

$$r(\mathrm{H\cdots H}) = [(I_a + I_b - I_c)/m_{\mathrm{H}}]^{1/2} \qquad (1)$$

The values for the four isotopic species given in Table III are close to each other, their average being 1.7096 Å. The eight constants are left to calculate other structural parameters. Since the mass ratio of two bromine isotopes ^{79}Br and ^{81}Br is almost equal to unity and the bromine atom is located so close to the a-axis, the data are not sufficient to calculate seven parameters. The following values are assumed: methylene C—H is equal to 1.090 Å, ∠CCH to 111°30′, C≡C to 1.207 Å, and acetylene C—H to 1.060 Å. The acetylene C—H and C—D bond lengths are assumed to be equal. The linearity of the group C—C≡C—H is again assumed. By means of the method of least-squares the

bond lengths C—Br and C—C and the bond angle CCBr are found to be 1.9415 Å, 1.4549 Å, and 111°59′, respectively.

Thus far, the effect of inertia defect is ignored, but, as mentioned in the previous paper, the results given above for the three parameters do not change appreciably even by taking account of the inertia defect. In addition, since the weight of a bromine atom is more than twice as great as that of a chlorine atom, errors in the parameters C—Br and ∠CCBr may be small. The results are given in Table IV.

TABLE IV. MOLECULAR STRUCTURE

C—Br	1.9415 Å	H···H*	1.7096 Å
C—C	1.4549 Å	∠CCBr	111°59′

Assumed values

C—H (methylene) 1.090 Å

C—H, C—D (acethylene) 1.060 Å

C≡C	1.207 Å	∠CCH	111°30′

* Correction for the inertia defect is not made.

Second-Order Quadrupole Effect. — Theory[4] indicates that the quadrupole energy is expressed as follows, averaging over rotational states of an asymmetric molecule

$$E_Q=(IJ\tau F|H_Q|IJ\tau F)+\sum_{J'\tau'}\frac{|(IJ\tau F|H_Q|IJ'\tau'F)|^2}{E_{J\tau}-E_{J'\tau'}} \tag{2}$$

Usually the difference in rotational energies $E_{J\tau}-E_{J'\tau'}$, is much larger than the quadrupole energy hence the second terms may be omitted. For a nearly prolate symmetric top the first-order energy

$$(IJ\tau F|H_Q|IJ\tau F)=\frac{1}{J(J+1)}\{\chi_{aa}[3K_{-1}^2-J(J+1)-3\sum_n(n-1)C_nb_P^n-\sum_n nC_nb_P^{n-1}]-2\chi_{bb}\sum_n nC_nb_P^{n-1}\}\cdot\boldsymbol{f}(IJF) \tag{3}$$

is a good approximation for the quadrupole energy, where $\chi_{ff}=eQ\partial^2V/\partial f^2$, $f=a$, b and c are molecule-fixed axes chosen as the principal axes of inertia, and $\boldsymbol{f}(IJF)$ is Casimir's function. However, if rotational energies $E_{J\tau}$ and $E_{J'\tau'}$ are almost degenerate, the second-order terms can not be ignored. The matrix elements have been derived by Bragg[5]:

$$(IJ\tau F|H_Q|IJ+A\tau'F)=\boldsymbol{g}_\alpha(IJF)(J\tau M_J=J|\chi_{ZZ}|J+A\tau'M_J=J) \tag{4}$$

where $\chi_{ZZ}=eQ\partial^2V/\partial Z^2$ (Z is a space-fixed axis), $\alpha=0$, ±1, ±2, and

$$\boldsymbol{g}_0=[3C(C+1)-4I(I+1)J(J+1)]\div[8I(2I-1)J(2J-1)] \tag{5a}$$

$$\boldsymbol{g}_1=[F(F+1)-I(I+1)-J(J+2)]\times[(I+J+F+2)(I-J+F)\times(J-I+F+1)(J+I-F+1)]^{1/2}\div\{8I(2I-1)J[(2J+1)]^{1/2}\} \tag{5b}$$

$$\boldsymbol{g}_2=[(I+J+F+2)(I+J+F+3)(I-J+F-1)\times(I-J+F)(J-I+F+1)(J-I+F+2)\times(I+J-F+1)(I+J-F+2)]^{1/2}\div\{16I(2I-1)[(2J+1)(J+1)]^{1/2}\} \tag{5c}$$

where $C=F(F+1)-I(I+1)-J(J+1)$. The $(J|J-1)$ and $(J|J-2)$ elements may be determined from equations given above by the Hermitian property of H_Q. The tensor component χ_{ZZ} is expressed in terms of direction cosines Φ_{Zf} and χ_{aa}, etc., the components of eQq tensor referred to the principal axes a, b and c. The result is

$$\chi_{ZZ}=(\Phi_{Za}^2-\Phi_{Zc}^2)\chi_{aa}+(\Phi_{Zb}^2-\Phi_{Zc}^2)\chi_{bb}+2\Phi_{Za}\Phi_{Zb}\chi_{ab}+2\Phi_{Zb}\Phi_{Zc}\chi_{bc}+2\Phi_{Zc}\Phi_{Za}\chi_{ca} \tag{6}$$

The asymmetric top wave functions as well as direction cosines belong to the representation of the four group[6]. Thus the matrix element of χ_{ZZ} is zero unless the direct product of the representation of the two rotational states is equal to that of Φ_{Zf} $\Phi_{Zf'}$. Table V gives the symmetry of the direction cosines and the wave functions.

The rotational wave function for a slightly asymmetric top molecule is approximately given by

$$\Psi_K^{(1)}=S_K+\alpha S_{K-2}+\beta S_{K+2} \tag{7}$$

where S_K is Wang's symmetric top wave function, and the coefficients α and β are given by Lide[7]. For propargyl bromide the wave function of this type is sufficient to calculate the second-order quadrupole energy, since the asymmetry parameter of the molecule is small.

Transitions of b-type Q-branches are observed to split into four lines by the quadrupole effect of bromine nucleus. For transitions of high J the first-order theory predicts that the splitting $\nu_4-\nu_3$ is equal to $\nu_2-\nu_1$, but the deviation was observed, in particular, for the transition $12_{0,12}\rightarrow12_{1,11}$ (Table VI).

In applying the second-order theory described above the energies of the states which couple with the states $12_{0,12}$ and $12_{1,11}$ are first calculated. The result is shown in Tables VII

4) See, for example, M. W. P. Strandberg, "Microwave Spectroscopy", Methuen & Co., Ltd., London (1954), Chapter IV.

5) J. K. Bragg, *Phys. Rev.*, **74**, 533 (1948). See also G. Racah, ibid., **62**, 438 (1942).

6) G. W. King, R. M. Hainer and P. C. Cross, *J. Chem. Phys.*, **11**, 27 (1943).

7) D. R. Lide, Jr., ibid., **20**, 1761 (1952).

TABLE V. SYMMETRY OF DIRECTION COSINES AND WAVE FUNCTIONS

Direction cosine	K_{-1}	K_1		E	C_2^a	C_2^b	C_2^c
Φ_{Za}^a, Φ_{Zb}^b, Φ_{Zc}^c	e	e	A	1	1	1	1
$\Phi_{Zc}\Phi_{Zb}$, Φ_{Za}	e	o	B_a	1	1	−1	−1
$\Phi_{Zc}\Phi_{Za}$, Φ_{Zb}	o	o	B_b	1	−1	1	−1
$\Phi_{Za}\Phi_{Zb}$, Φ_{Zc}	o	e	B_c	1	−1	−1	1

TABLE VI. LINE SEPARATIONS OF HYPERFINE STRUCTURES OF b-TYPE Q-BRANCH LINES

Transition	$CH_2^{79}BrC{\equiv}CH$			$CH_2^{81}BrC{\equiv}CH$			$CH_2^{79}BrC{\equiv}CD$			$CH_2^{81}BrC{\equiv}CD$		
	$\nu_2-\nu_1$	$\nu_3-\nu_2$	$\nu_4-\nu_3$	$\nu_2-\nu_1$	$\nu_3-\nu_2$	$\nu_4-\nu_3$	$\nu_2-\nu_1$	$\nu_3-\nu_2$	$\nu_4-\nu_3$	$\nu_2-\nu_1$	$\nu_3-\nu_2$	$\nu_4-\nu_3$
$13_{0,13}\rightarrow13_{1,12}$	4.14	41.43	6.99	3.30	35.04	5.40	3.71	43.70	7.69	3.04	36.60	6.09
$12_{0,12}\rightarrow12_{1,11}$	10.47	40.59	~0	6.81	33.48	1.71	8.55	42.58	2.42	6.25	35.15	2.80
$11_{0,11}\rightarrow11_{1,10}$	6.51	38.97	4.98	5.52	32.37	4.29	6.87	40.80	5.21	5.59	33.88	4.50
$10_{0,10}\rightarrow10_{1,9}$	6.51	37.95	5.58	5.52	31.23	4.86	7.06	39.36	6.54	5.76	33.34	4.82
$9_{0,9}\rightarrow9_{1,8}$	7.32	36.36	6.51	5.76	30.39	5.37	7.74	38.38	6.86	6.21	31.42	5.84
$8_{0,8}\rightarrow8_{1,7}$	7.65	35.28	7.29	6.72	29.49	6.24	8.29	36.83	8.09	6.94	31.03	6.49
$7_{0,7}\rightarrow7_{1,6}$	4.89	40.74	2.37	4.35	34.74	2.10						
$6_{0,6}\rightarrow6_{1,5}$	9.99	34.05	8.49	8.46	28.26	7.65						
$5_{0,5}\rightarrow5_{1,4}$	16.08			13.9	28.0							

TABLE VII. STATES COUPLING WITH $12_{0,12}$ AND THEIR ENERGY DIFFERENCES IN Mc./sec.

State	$E(12_{0,12})-E(J'\tau')$			
	$CH_2^{79}BrC{\equiv}CH$	$CH_2^{81}BrC{\equiv}CH$	$CH_2^{79}BrC{\equiv}CD$	$CH_2^{81}BrC{\equiv}CD$
$10_{0,10}$	95006.7	94384.4	89533.3	88939.3
$10_{2,8}$	18110.3	17554.3	16109.0	15586.0
$11_{2,10}$	−26955.9	−27223.1	−26370.1	−26616.9
$12_{2,10}$	−78067.2	−77973.8	−74500.4	−74405.1
$13_{2,12}$	−130783.8	−130361.7	−124203.3	−123792.9
$14_{0,14}$	−111267.7	−110542.5	−104862.6	−104170.4
$14_{2,12}$	−191185.0	−190324.8	−181064.9	−180239.9
$10_{1,10}$	80545.6	79884.1	75641.6	75014.2
$11_{1,10}$	23982.4	23756.1	22405.3	22188.0
$12_{1,12}$	−12875.3	−12928.3	−12397.7	12444.1
$13_{1,12}$	−82010.7	−81522.4	−77457.7	−76994.7
$14_{1,14}$	−122480.5	−121820.7	−115690.4	−115056.0

TABLE VIII. STATES COUPLING WITH $12_{1,11}$ AND THEIR ENERGY DIFFERENCES IN Mc./sec.

State	$E(12_{1,11})-E(J'\tau')$			
	$CH_2^{79}BrC{\equiv}CH$	$CH_2^{81}BrC{\equiv}CH$	$CH_2^{79}BrC{\equiv}CD$	$CH_2^{81}BrC{\equiv}CD$
$10_{1,9}$	97547.1	96888.9	91904.6	91277.9
$10_{3,7}$	−49195.1	−49830.0	−48378.4	−48962.1
$11_{1,11}$	62763.7	62276.3	59067.8	58608.9
$11_{3,9}$	−94962.1	−95291.8	−91501.1	−91794.0
$12_{3,9}$	−144934.8	−144930.2	−138584.9	−138559.3
$13_{3,13}$	−38752.5	−38579.1	−36601.2	−36429.1
$13_{1,11}$	−199018.7	−198653.7	−189544.5	−189175.5
$14_{1,13}$	−114429.1	−113658.5	−107812.3	−107078.5
$14_{3,11}$	−257371.4	−256614.8	−244522.1	−243780.1
$10_{2,9}$	45646.4	44958.5	42227.2	41581.5
$11_{0,11}$	76446.2	76005.1	72226.3	71807.5
$11_{2,9}$	−962.0	−1324.9	−1668.2	−2005.4
$12_{2,11}$	−49895.0	−49948.2	−47797.5	−47838.1
$13_{0,13}$	−26703.6	−26470.8	−24983.3	−24758.8
$13_{2,11}$	−105599.8	−105254.7	−100246.0	−99909.3
$14_{2,13}$	−162004.1	−161313.4	−153434.4	−152765.8

TABKE IX. HYPERFINE STRUCTURES OF a-TYPE R-BRANCH LINES (Mc./sec.)

$J''\tau''\leftarrow J'\tau'$	$F''\leftarrow F'$	$CH_2{}^{79}BrC\equiv CH$		$CH_2{}^{81}BrC\equiv CH$		$CH_2{}^{79}BrC\equiv CD$		$CH_2{}^{81}BrC\equiv CD$	
		Calcd.	Obs.	Calcd.	Obs.	Calcd.	Obs.	Calcd.	Obs.
$6_{1,6}-7_{1,7}$	15/2−17/2	−1.99	−2.00	−1.63	−1.52	−0.91	−1.76	−1.63	−1.59
	13/2−15/2	−0.29	−0.26	−0.24	−0.22	−0.30	−0.19	−0.26	−0.16
	9/2−11/2	+1.26	+1.11	+1.03	+0.90	+1.23	+1.10	+1.05	+0.98
	11/2−13/2	+2.95	+3.04	+2.42	+2.31	+2.84	+2.70	+2.43	+2.30
$5_{1,5}-6_{1,6}$	13/2−15/2	−2.65	−2.59	−2.17	−2.17	−2.54	−2.54	−2.17	−2.10
	11/2−13/2	−0.15	−0.19	−0.12	−0.10	−0.16	−0.08	−0.15	−0.12
	7/2− 9/2	+1.65	+1.62	+1.36	+1.30	+1.62	+1.55	+1.39	+1.34
	9/2−11/2	+4.15	+4.12	+3.40	+3.43	+4.00	+3.97	+3.41	+3.37
$4_{1,4}-5_{1,5}$	11/2−13/2	−3.76	−3.76	−3.08	−3.08	−3.61	−3.64	−3.08	
	9/2−11/2	+0.40	+0.31	+0.32	−0.31	+0.34	+0.11	+0.28	
	5/2− 7/2	+2.13	+2.32	+1.75	−1.80	+2.11	+2.01	+1.81	
	7/2− 9/2	+6.28	+6.11	+5.15	−5.14	+6.05	+6.41	+5.17	
$3_{1,3}-4_{1,4}$	9/2−11/2	−5.80	−5.72	−4.76	−4.90	−5.57	−5.55	−4.75	−4.76
	7/2− 9/2	+2.25	+2.26	+1.84	−1.87	+2.09	+2.23	+1.76	+1.90
	3/2− 5/2	+2.38		+1.95		+2.41		+2.08	
	5/2− 7/2	+10.43	+10.37	+8.55	−8.84	+10.06	+10.18	−8.59	+8.60

TABLE X. HYPERFINE STRUCTURES OF $12_{0,12}\leftarrow 12_{1,11}$ TRANSITION (Mc./sec.)

$J''\leftarrow J'$	$F''\leftarrow F'$	$CH_2{}^{79}BrC\equiv CH$		$CH_2{}^{81}BrC\equiv CH$		$CH_2{}^{79}BrC\equiv CD$		$CH_2{}^{81}BrC\equiv CD$	
		Calcd.	Obs.	Calcd.	Obs.	Calcd.	Obs.	Calcd.	Obs.
$12_{0,12}-12_{1,11}$	27/2−27/2	−30.54	−30.71	−23.50	−23.53	−29.92	−29.85	−23.71	−23.80
	25/2−25/2	−20.43	−20.24	−16.67	−16.72	−21.39	−21.30	−17.43	−17.55
	29/2−29/2	+20.39	+20.35	+16.71	+16.76	+21.36	+21.28	+17.47	+17.60
	23/2−23/2	+20.34	+20.35	+18.43	+18.47	+23.77	+23.70	+20.30	+20.40

TABLE XI. QUADRUPOLE COUPLING CONSTANTS OF THE BROMINE ATOM

	$CH_2{}^{79}BrC\equiv CH$	$CH_2{}^{81}BrC\equiv CH$	$CH_2{}^{79}BrC\equiv CD$	$CH_2{}^{81}BrC\equiv CD$
χ_{aa}	316 Mc./sec.	259 Mc./sec.	300 Mc./sec.	255 Mc./sec.
χ_{bb}	−16	−13	−8	−5
χ_{cc}	403	336	415	342
χ_{xx}	−286	−238	−295	−241
χ_{yy}	−301	−246	−292	−250
χ_{zz}	587	484	587	491
θ	33°48′	33°59′	34°49′	34°36′
θ'	34° 2′	33°58′	35° 7′	35° 3′
η	0.03	0.02	−0.01	0.02

TABLE XII. COMPARISON OF THE MOLECULAR CONSTANTS

Compound	r(C−Br)	eQ_q	
		^{79}Br	^{81}Br
Propargyl bromide	1.9415 Å	587 Mc./sec.	484 Mc./sec.
Methyl bromide	1.939 Å*	577.3**	482.4**
Ethyl bromide	1.9400 Å***	416.5***	349.1***

* J. W. Simmons and W. E. Anderson, *Phys. Rev.*, **80**, 338 (1950).
** A. H. Sharbaugh and J. Mattern, ibid., **75**, 1102 (1949).
*** R. S. Wagner, B. P. Dailey and N. Solimene, *J. Chem. Phys.*, **26**, 1593 (1957).

and VIII where the states are chosen by symmetry consideration.

It is to be noted that the state $11_{2,9}$ is nearly degenerate with the state $12_{1,11}$, while the energies of other states differ by more than 10000 Mc./sec. from that of the state $12_{0,12}$ or $12_{1,11}$. Since the symmetry of the state $11_{2,9}$ is B_a and that of the state $12_{1,11}$ B_b while that of $\Phi_{Za}\Phi_{Zb}$ is B_c as is given in Table V, the state $11_{2,9}$ couples with the state $12_{1,11}$ by the quadrupole Hamiltonian of the form $\Phi_{Za}\Phi_{Zb}\chi_{ab}$. This coupling is dominant in the second-order terms, thus the second-order energy is nearly proportional to $\chi_{ab}{}^2$. The other terms χ_{bc} and

χ_{ca} are equal to zero by the symmetry of the molecule.

The line separations given in Table VI, $\nu_2-\nu_1$ and $\nu_4-\nu_3$, are expressed as

$$\nu_2-\nu_1=K\chi_{aa}+L\chi_{bb}+M\chi_{ab}^2 + (\text{small terms involving } \chi_{aa}^2,\ \chi_{bb}^2 \text{ and } \chi_{aa}\chi_{bb}) \quad (8a)$$

$$\nu_4-\nu_3=K\chi_{aa}+L\chi_{bb}+N\chi_{ab}^2 + (\text{small terms involving } \chi_{aa}^2,\ \chi_{bb}^2 \text{ and } \chi_{aa}\chi_{bb}) \quad (8b)$$

where K, L, M and N are constants. In these expressions the first two terms are the first-order energies and the others are the second-order energies. It is to be noted that the first two terms are the same for both equations. In employing Eq. 7 the second-order terms of δ in the coefficients, α and β, are neglected. After appropriate correction is made for the last term, χ_{ab} is obtained by subtracting Eq. 8b from Eq. 8a. By substituting the value of χ_{ab} into Eq. 8a or 8b, a linear equation of χ_{aa} and χ_{bb} is obtained. Another linear relation is given by well-resolved a-type R-branch transitions (Table IX), for which the second-order effect seems to be small. From these relations χ_{aa} and χ_{bb} are calculated. The results are compared with the observed ones in Tables IX and XI.

By use of χ_{aa}, χ_{bb} and χ_{ab} the principal values of the χ-tensor and the directions of the principal axes (x, y and z) are determined without any assumptions. The θ designates the angle between the a- and z-axes and the θ' that between the direction of the C—Br bond and the a-axis. The two angles are found to agree within experimental errors. The asymmetry parameter η, which is given by $(\chi_{xx}-\chi_{yy})/\chi_{zz}$, is close to zero for the four isotopic species, where the x-axis is taken in the (ab) plane. The average value of η is $+0.015\pm0.013$.

Discussion

The C—Br bond length obtained, 1.9415 $\pm$0.005 Å, is close to the values usually observed in saturated hydrocarbon bromides. Table XII shows comparison of this value with those of methyl and ethyl bromides. It is to be noted that the values for the C—Br length in those three compounds are of the same order of magnitude within experimental errors.

The z-direction of the quadrupole coupling constant coincides with the direction of the C—Br bond within errors involved in the present experiment. It is a good confirmation of the current assumption usually made. The value of χ_{zz} is compared with those of methyl and ethyl bromides in Table XII. The three values of the coupling constant are also close to each other.

The authors wish to express their sincere thanks to Dr. Makoto Shima, Institute for Physical and Chemical Research, for supplying them with heavy water. The expenses for this research were defrayed from the Scientific Research Encouragement Grant of the Ministry of Education to which the authors' thanks are also due.

Department of Chemistry
Faculty of Science
The University of Tokyo
Hongo, Tokyo

Nuclear Magnetic Resonance Study of Hydrogen Bond in Salicylaldehyde

By Ichiro YAMAGUCHI

(Received August 7, 1960)

It is well accepted that a strong intramolecular hydrogen bond is formed between the hydroxyl and aldehyde groups in a salicylaldehyde molecule. This evidence was obtained by various molecular spectroscopic methods[1] and dipole moment measurements,[2] and some characteristic structures for this hydrogen-bonded system were suggested on the basis of these measurements. Nuclear magnetic resonance (NMR) measurement is expected to give further informations concerning the

1) a) M. Tsuboi, This Bulletin, **25**, 60 (1952); b) H. Yamada, ibid., **32**, 1051 (1959); c) A. E. Martin, *Nature*, **166**, 474 (1950); d) P. D. Simova and B. Skorchev, *Izvest. Bulgar. Akad. Nauk., Otdel. Fiz.-Mat. i Tekh. Nauki Ser. Fiz.*, **4**, 47 (1954).

2) a) H. Lumbroso and P. Rumpf, *Bull. soc. chim. France*, **1950**, 371; b) R. Mecke and A. Reuter, *Z. Naturforsch.*, **4a**, 368 (1949).

hydrogen bond in this molecule.

Compounds with intramolecular hydrogen bond so far well investigated by the NMR method are *o*-chlorophenol[3,4], *o*-bromophenol[5], and *o*-cresol[3,5]. The resonance field for the OH proton in these compounds was comparatively dependent on concentration in various solutions. This suggests that the intermolecular hydrogen bond in these compounds is easily disrupted by dilution of solutions. On the other hand, the intramolecular hydrogen bond in compounds such as *o*-nitrophenol or salicylaldehyde is so strong that it would scarcely form a intermolecular hydrogen bond. It is expected therefore that the OH lines of NMR for these compounds would not show remarkable concentration dependence[6].

In the present experiment, the measurement of the OH resonance shift in NMR spectrum of salicylaldehyde was carried out in solutions of several solvents with various concentrations. In addition to this, the concentration dependence of the resonance spectrum of the ring protons was also investigated.

Experimental

NMR measurements were made at 20°C with a Varian NMR spectrometer operating at 56.4 Mc./sec. Salicylaldehyde was a guaranteed grade reagent and used without further purification. Solvents chosen in this experiment were cyclohexane and carbon tetrachloride (inert solvents), and chloroform, methanol, benzene, acetone, ether and pyridine (proton donors and acceptors). These solvents were purified for eliminating extra lines in their NMR spectra.

The sweep rate was calibrated by taking the value of the chemical shift between the methyl group proton and the benzene ring proton in toluene as 4.90 p. p. m.[7] The value of chemical shift of each line was obtained referring to an external reference of water in a capillary, and the correction for bluk diamagnetic susceptibility was made. Solutions of twelve stages of concentrations between 0.05 and 0.95 mole fractions were prepared for each solvent.

Results and Discussion

Fig. 1a shows the concentration dependence of the chemical shifts for protons of salicylaldehyde in cyclohexane solution. The lowest curve was assigned to the OH proton by reasoning which will be described later. The next lowest is for the CHO proton. The resonance lines for the ring protons are very complex as shown later. However the corresponding magnetic fields are expressed by two lines for simplicity in the figure, showing decrease with decreasing concentration. The displacement of the lines to a higher field at higher concentration is caused by the interaction among benzene molecules. The decrease of the resonance field for the OH group on dilution seems to correspond to a charge migration from the proton to the ring. Most of the chemical

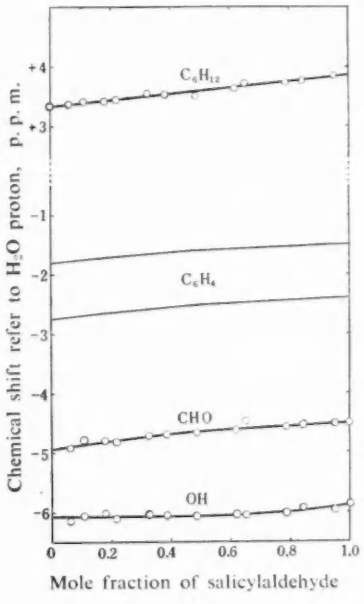

(a)

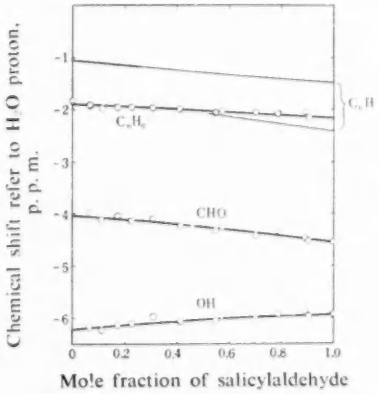

(b)

3) C. M. Huggins, G. C. Pimentel and J. N. Shoolery, *J. Phys. Chem.*, **60**, 1311 (1956).

4) I. Gränacher, *Helv. Phys. Acta*, **31**, 734 (1958); M. Martin and F. Hérail, *Compt. rend.*, **248**, 1994 (1954).

5) R. L. Batdorf, Ph. D. thesis, Univ. of Minnesota, 1955.

6) Puranik and Ramavataram observed the slight shift in the C=O vibrational frequency for salicylaldehyde in the presence of proton donor or acceptor group. This shift was attributed to the minute weakening of the intramolecular hydrogen bond. P. G. Puranik, *J. Chem. Phys.*, **23**, 761 (1955); K. Ramavataram, *Proc. Indian Acad. Sci.*, **45A**, 47 (1957).

7) N. F. Chamberlain, *Anal. Chem.*, **31**, 56 (1959).

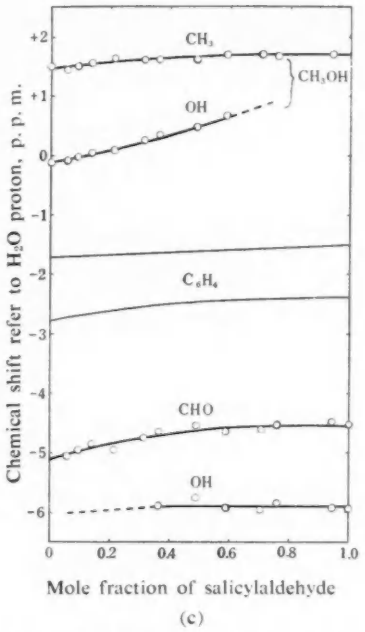

(c)

Fig. 1. Chemical shift diagrams of salicylaldehyde in several solutions;
(a) cyclohexane solution, (b) benzene solution, and (c) methanol solution.

shift diagrams observed for the other solutions have much the same feature as that for cyclohexane solution except for benzene and pyridine solutions.

Fig. 1b. shows the proton resonance in benzene solution. The field for the CHO group increases with decreasing concentration in contrast to the other observed solutions. This may be due to a hydrogen bond formation between the acidic proton in the CHO group and the π electron system of a solvent benzene molecule; the proton is located in a region where the effect of the benzene ring is diamagnetic as in the case of chloroform in benzene solution[8].

Fig. 1c. shows the chemical shift diagram for methanol solution. The OH proton resonance line of alcohol disappears in the concentrated region. The some is true for the OH proton of salicylaldehyde but in the dilute region. This implies the exchange of protons between OH group of alcohol and that of phenol. The broadening of these two lines over all the concentration range may also be an additional evidence for this exchange process. From the separation of the above two lines for both groups, the upper limit for the exchange rate was estimated as about 330 c. p. s. It is therefore probable that even a proton contributing to a strong intramolecular hydrogen bond formation is also able to exchange.

Fig. 2 shows the concentration dependence of the chemical shift of proton resonance lines for the OH group in various solutions. Batdorf[5] measured the chemical shift of the OH proton in various phenol derivatives in saturated solutions of acetone. He showed that among the OH lines for various phenol derivatives the OH line for salicylic acid derivatives appeared at the lowest field region (around -6 p. p. m. referring to water proton). The OH proton lines for the other phenol derivatives appeared at considerably higher fields than that for salicylaldehyde. In general, the OH line for phenol derivatives forming merely intermolecular hydrogen bond appears in the range of about -2 to -4 p. p. m. from the water proton line. Comparing these values with those for salicylic acid derivatives with intramolecular hydrogen bond, it may be said that the strength of the intramolecular hydrogen bond in salicylic acid derivatives is ranked to be considerably high.

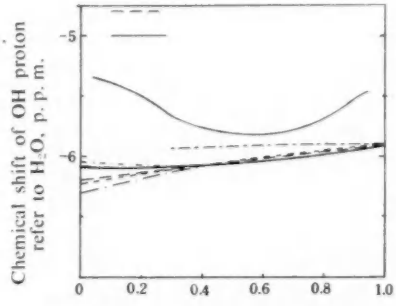

Fig. 2. OH proton resonance shift in salicylaldehyde of various solutions.
Solvent
- Cyclohexane
- Carbon tetrachloride
- Chloroform
- Methanol
- Benzene
- Acetone
- Pyridine

For various solutions observed, the concentration dependence of the OH lines are almost the same except pyridine solution which will be discussed later. This fact is somewhat surprising because it may suggest that the nature of the OH proton in salicylaldehyde is scarcely affected at all by the solvents with high hydrogen bond forming ability. The above fact also suggests that the intramolecular hydrogen

8) L. W. Reeves and W. G. Schneider, *Can. J. Chem.*, 35, 251 (1957).

bond in salicylaldehyde is considerably strong and does not allow a hydrogen bond to form with the other molecular species.

The resonance field of the OH proton is observed to decrease slightly as the concentration of the solution decreases. In general dilution of a phenol with some moderate solvent, intermolecularly hydrogen-bonded polymerized molecules dissociate to dimer molecules showing a decrease of the OH proton resonance field. However dissociation of dimerized ones to monomers shows an increase of the field. Thus, for intermolecularly hydrogen-bonded compounds the variation of the OH proton resonance field generally has a minimum, where the most effectively and strongly hydrogen-bonded species is seemed to form. In contrast to phenol, the field for the OH proton line of salicylaldehyde decreases monotonously with dilution of solution showing no increase even on extreme dilution. This suggests that the bonding becomes stronger as the concentration decreases and the hydrogen bond remains even in the solution of extremely low concentration. Therefore, for salicylaldehyde, the free single molecule with the intramolecular hydrogen bond is considered to be the most effectively hydrogen-bonded species. This result also suggests that in concentrated solutions there exist dimerized or polymerized molecules[9] which dissociate to monomer molecules on dilution. The broadening of the OH lines observed in concentrated range in almost all the solutions may be attributed to a rather slow exchange process of OH protons among several kinds of polymerized species.

An exceptional behavior of OH line was observed for pyridine solution. The curve in Fig. 2 shows apparently anomalous behavior. First, the resonance occurs at higher field than that for the other solutions. This may be ascribed to some change in its electronic configuration caused by interaction with a pyridine molecule. Secondly, the magnetic field decreases with decreasing concentration in concentrated range. This may arise from the same dissociation process as that the other solutions show and simultaneously from the formation of strong hydrogen bond between salicylaldehyde and pyridine. Thus the minimum resonance field appears at the equimolecular composition of the solution. The third is the increase of the curve in dilute range. This may be attributed to the formation of multiply hydrogen-bonded species with pyridine. This experimental result may suggest that the hydrogen bond between salicylaldehyde and pyridine is stronger than the intramolecular hydrogen bond in salicylaldehyde.

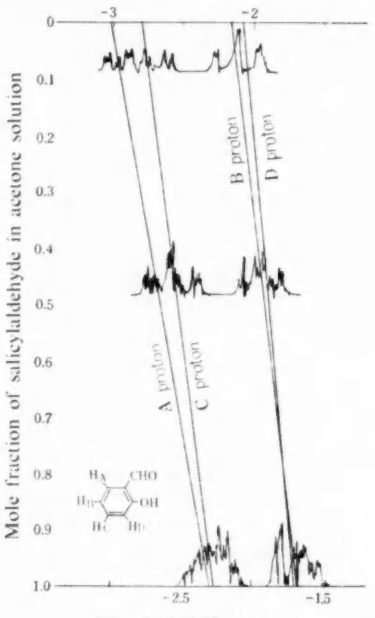

Fig. 3. Concentration dependent behavior of ring proton resonance lines of salicylaldehyde in acetone solution.

A remarkable solvent effect was also observed in the resonance spectra of ring protons, especially in the systems with proton donor or acceptor solvents. Although the spectrum of the ring protons could not be exactly analyzed, it was possible to assign the spectral lines to each proton by tracing the change in the spectral figure of the system on dilution. Fig. 3. shows an example of this solvent effect on the ring protons in acetone solution.

The whole spectrum of the ring protons displaces to lower field on dilution. This displacement is considered to arise from change in the interaction among benzene rings as mentioned previously. In a series of the spectra of solutions with different concentrations, the lines due to A proton (ortho to CHO group) and D proton (ortho to OH group) exhibit opposed dilution displacement to each other. The A proton lines displace to lower field while those of D to higher field on dilution relative to the displacement of the whole ring proton spectrum. Various effects may be attributed to these shift changes of dilution[10]. However, the essential feature to cause the

9) Simova and Skorchev also suggested the existence of dimerized molecules. See Ref. Id.

10) A. D. Buckingham, T. Schaefer and W. G. Schneider, *J. Chem. Phys.*, **32**, 1227 (1960).

spectral change, especially that for A and D protons, would probably be a charge migration in the molecule affected by the change in the hydrogen bonding situation of this molecule.

Summary

The concentration dependent behavior of the proton resonance spectra of salicylaldehyde in several solution systems were measured. The behavior of the OH resonance line for the solution systems showed the evidence of the existence of considerably strong intramolecular hydrogen bond in the molecule. The behavior of the ring proton spectrum on dilution suggested the occurrence of the charge migration in the ring affected by the change in the hydrogen bonding situation.

The author wishes to express his sincere thanks to Professor S. Fujiwara and Dr. A. Danno for their kind encouragement and suggestions on this work and also to Dr. H. Shimizu, N. Nakagawa and N. Hayakawa for their valuable discussions.

Radiation Application Division
Japan Atomic Energy Research Institute
Tokai Ibaraki-ken

Non-benzenoid Aromatic Heterocycles. IV[*1)] *. An Attempted Synthesis of Indolo[3, 2-b]indole : A Hetero-pentalene*

By Hiroshi KATO and Masaki OHTA

(Received September 19, 1960)

Since the proposal of pentalene (I) by Robinson[2] as a possible aromatic substance, it has been the subject of many studies. Although dibenzopentalene and a few other condensed pentalene derivatives have recently been synthesized (showing non-aromatic polyene properties), the synthesis of pentalene or even benzopentalene is still awaited, and the results of theoretical treatments on the stability of these compounds by several groups of workers are not in accordance[3].

It has been found that substitution of –C=C– groups in a conjugated compound by heteroatoms results in a system which shows properties of the original compound to a certain extent. These facts led the authors to attempt a synthesis of indolo[3, 2-b]indole (II) as a model of diazadibenzopentalene in order to add some experimental data concerning the stability of the proposed pentalene ring system[4]. As possible routes to indolo[3, 2-b]indole, intramolecular dehydration of 2-(*o*-aminophenyl)-indolone (III) or dehydrogenation of *N, N'*-dihydroindolo[3, 2-b]indole (dindole) (IV) may be considered. These two compounds, III and IV, have been prepared[5] by reduction of *o, o'*-dinitrobenzil by Raney nickel or by zinc and hydrochloric acid, respectively.

An attempted intramolecular condensation of 2-(*o*-aminophenyl)indolone has been briefly reported by Ruggli et al.[5], but as nothing has been described about the condensation reagent, the present authors tried to dehydrate it using a variety of condensation catalysts, none of which gave an identifiable product.

Next, the dehydrogenation of dindole was tried. When dindole was refluxed with chloranil in *n*-butanol, an intense violet coloration took place, but the color faded away gradually and tetrachlorohydroquinone was isolated from the reaction mixture. Neither, in this case, was the expected indolo[3, 2-b]indole, obtained, and an amorphous polymeric product was obtained. The elemental composition of this substance is not very far from $C_{14}H_{11}ON_2$. Attempts to isolate this colored substance were not successful, but the absorption curve of this substance in the visible region is quite similar to 2-(*o*-aminophenyl)indolone and the R_f value of this compound is the same as 2-(*o*-aminophenyl)-indolone. From these facts and the supplemental data described in the experimental

* Presented at the meeting of the Chemical Society of Japan, Tokyo, October, 1959.

1) Part III, H. Kato, T. Ogawa and M. Ohta, This Bulletin, **33**, 1468 (1960).

2) J. W. Armit and R. Robinson, *J. Chem. Soc.*, **1922**, 827.

3) Cf. for example, W. Baker and J. F. W. McOmie, "Non-benzenoid Aromatic Compounds" in "Progress in Organic Chemistry", Vol. 3, Butterworths Scientific Publications, London (1955), p. 44.

4) During the course of this investigation, a series of condensed azapentalenes have been prepared by Treibs. W. Treibs, *Naturwissenschaften*, **46**, 170 (1959).

5) P. Ruggli et al., *Helv. Chim. Acta*, **18**, 845 (1935).

part, it may be concluded that the colored compound is 2-(*o*-aminophenyl)indolone.

These experimental data, although negative, indicate that at least some interaction exists between the two compounds (IV and chloranil) and dehydrogenation has occurred in dindole. On the basis of these data, it seemed reasonable to assume that dehydrogenation of dindole gave indolo[3, 2-b]indole as an intermediate product, but this compound is so unstable that it took up traces of water present in butanol and gave 2-(*o*-aminophenyl)indolone. When rigidly dehydrated *n*-butanol was used as solvent, the beginning of coloration required a longer period and on addition of a small amount of water, the coloration took place at once. This fact also lends some support to the above described assumption.

During the course of this investigation, the authors have known that Treibs[6] also attempted dehydrogenation of dindole using many catalysts, but indolo[3, 2-b]indole was not prepared.

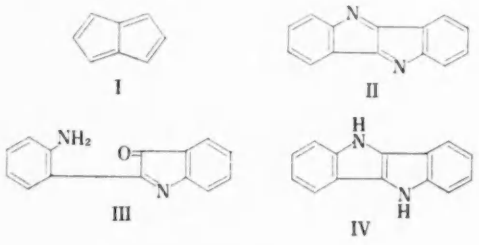

Experimental

Attempted Cyclodehydration of 2-(*o*-Aminophenyl) indolone.—2-(*o*-Aminophenyl)indolone[5] was treated with the following reagents under warming or at room temperature: polyphosphoric acid, concentrated sulfuric acid, acetic acid, triethylamine, and piperazine. Polyphosphoric acid and sulfuric acid gave a yellow amorphous substance, accompanied by the starting material. Acetic acid yielded a yellow polymeric substance, and in the case of triethylamine the starting material was recovered unchanged.

6) W. Treibs, private communication.

Reaction of Dindole with Chloranil.—a) A butanolic solution (30 ml.) of dindole[5] (0.5 g.) and chloranil (0.6 g.) was gently refluxed for four hours. At first a deep violet coloration took place, but it faded away gradually, and after four hours the solution became pale brown. The solvent was removed under reduced pressure and the residue was washed with ether and purified by chromatography (alumina-benzene). The yellow powder from the eluate was repeatedly recrystallized first from benzene-benzine and then from benzene giving yellow amorphous powder. It does not show a distinct melting point (about 300°C).

Found: C, 74.02; H, 4.40. Calcd. for $C_{14}H_{10}ON_2$: C, 75.65; H, 4.54%.

The ether washings in the above experiment were extracted with 10% aqueous sodium hydroxide and the aqueous layer was acidified which hydrochloric acid. The white crystals (0.47 g.) which separated out were recrystallized from acetic acid giving white needles, m. p. 234°C (in a sealed tube), undepressed on admixture with tetrachlorohydroquinone.

b) When chloranil or dindole alone was refluxed in *n*-butanol, no coloration took place, and chloranil gave no tetrachlorohydroquinone.

c) Dindole and chloranil was heated cautiously until the coloration took place, and the colored solution in situ was used for spectroscopic measurement. (λ_{max} 550 mμ; with a small shoulder at about 490 mμ; intensity unspecified). The shape of the curve in the visible region is the same with 2-(*o*-aminophenyl)indolone. Attempts to isolate this colored substance (by chromatography) were unsuccessful. The colored substance and 2-(*o*-aminophenyl)indolone gave the same spot in paper chromatography (R_f=0.95, solvent: butanol-pyridine-water, 4 : 1 : 2). This colored substance seemed a little more unstable than 2-(*o*-aminophenyl)indolone, but when 2-(*o*-aminophenyl)indolone was heated with chloranil in *n*-butanol, it decomposed rapidly to give a yellow solution.

d) When rigidly dehydrated *n*-butanol (freshly twice distilled) was used as solvent, the beginning of coloration was delayed and the intensity of the color was feeble and on addition of a small amount of water, the color was intensified immediately.

The authors are indebted to Mr. Asaji Kondo for microanalyses.

Laboratory of Organic Chemistry
Tokyo Institute of Technology
Meguro-ku, Tokyo

Normal Coordinate Treatment and Assignment of Infrared Absorption Bands of Polyvinyl Chloride

By Takehiko SHIMANOUCHI and Mitsuo TASUMI

(Received September 16, 1960)

In the analysis of infrared absorption spectra it is often of considerable importance to calculate the frequencies of the normal vibrations.

Recent developments in high-speed computers have made it possible to calculate the normal vibrations of complex molecules. We have calculated the frequencies of the polyvinyl chloride molecule using the force constants transferred from simple molecules. These results suggest a modification of the assignment proposed in former studies[1,2] and will be reported in the present paper.

Method of Calculation and Results

The normal coordinate treatment was carried out on assuming that the polyvinyl chloride molecule is syndyotactic and takes the extended zigzag form with the repeating unit made up of two monomer units. The unit cell for this structure is shown in Fig. 1. This model belongs to a group isomorphous with to the point group C_{2v}[1], and in Table I symmetry species, selection rules, and dichroic properties are given.

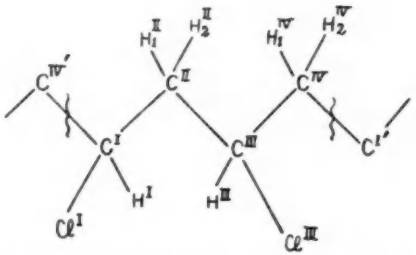

Fig. 1. Unit cell for syndyotactic structure of polyvinyl chloride.

TABLE I. SYMMETRY SPECIES, SELECTION RULES, AND DICHROISM FOR SYNDYOTACTIC POLYVINYL CHLORIDE*

C_{2v}	E	C_2	σ_v	σ_g	Number of frequencies	IR (Dichroism)	R
A_1	1	1	1	1	9	σ	active
A_2	1	1	−1	−1	7	inactive	active
B_1	1	−1	1	−1	9	σ	active
B_2	1	−1	−1	1	7	π	active

* As to the notation, see Ref. 1.

TABLE II. INTERNAL COORDINATES

Bond lengths;		Bond angles;			
R^{I}	C^{I}–C^{II}	θ^{I}	$C^{IV'}$–C^{I}–C^{II}	φ_1^{II}	C^{I}–C^{II}–H_1^{II}
R^{II}	C^{II}–C^{III}	θ^{II}	C^{I}–C^{II}–C^{III}	φ_2^{II}	C^{I}–C^{II}–H_2^{II}
R^{III}	C^{III}–C^{IV}	θ^{III}	C^{II}–C^{III}–C^{IV}	φ_3^{II}	C^{III}–C^{II}–H_1^{II}
R^{IV}	C^{IV}–$C^{I'}$	θ^{IV}	C^{III}–C^{IV}–$C^{I'}$	φ_4^{II}	C^{III}–C^{II}–H_2^{II}
r_1^{I}	C^{I}–Cl^{I}	θ^{I}	Cl^{I}–C^{I}–H^{I}	φ_1^{III}	C^{II}–C^{III}–H^{III}
r_2^{I}	C^{I}–H^{I}	θ^{II}	H_1^{II}–C^{II}–H_2^{II}	φ_2^{III}	C^{II}–C^{III}–Cl^{III}
r_1^{II}	C^{II}–H_1^{II}	θ^{III}	H^{III}–C^{III}–Cl^{III}	φ_3^{III}	C^{IV}–C^{III}–H^{III}
r_2^{II}	C^{II}–H_2^{II}	θ^{IV}	H_1^{IV}–C^{IV}–H_2^{IV}	φ_4^{III}	C^{IV}–C^{III}–Cl^{III}
r_1^{III}	C^{III}–H^{III}	φ_1^{I}	$C^{IV'}$–C^{I}–Cl^{I}	φ_1^{IV}	C^{III}–C^{IV}–H_1^{IV}
r_2^{III}	C^{III}–Cl^{III}	φ_2^{I}	$C^{IV'}$–C^{I}–H^{I}	φ_2^{IV}	C^{III}–C^{IV}–H_2^{IV}
r_1^{IV}	C^{IV}–H_1^{IV}	φ_3^{I}	C^{II}–C^{I}–Cl^{I}	φ_3^{IV}	$C^{I'}$–C^{IV}–H_1^{IV}
r_2^{IV}	C^{IV}–H_2^{IV}	φ_4^{I}	C^{II}–C^{I}–H^{I}	φ_4^{IV}	$C^{I'}$–C^{IV}–H_2^{IV}

1) S. Krimm and C. Y. Liang, *J. Polymer Sci.*, **22**, 95 (1956).

2) S. Narita, S. Ichinohe and S. Enomoto, ibid., **37**, 273, 281 (1959).

TABLE III. INTERNAL SYMMETRY COORDINATES

$$A_1 \quad S_1 = \frac{1}{2}(\Delta R^{I} + \Delta R^{II} + \Delta R^{III} + \Delta R^{IV})$$

$$S_2 = \frac{1}{2}(\Delta r_1^{II} + \Delta r_2^{II} + \Delta r_1^{IV} + \Delta r_2^{IV})$$

$$S_3 = \frac{1}{\sqrt{2}}(\Delta r_2^{I} + \Delta r_1^{III})$$

$$S_4 = \frac{1}{\sqrt{2}}(\Delta r_1^{I} + \Delta r_2^{III})$$

$$S_5 = \frac{1}{\sqrt{2}}(\Delta\Theta^{I} + \Delta\Theta^{III})$$

$$S_6 = \frac{1}{\sqrt{2}}(\Delta\Theta^{II} + \Delta\Theta^{IV})$$

$$S_7 = \frac{1}{\sqrt{2}}(\Delta\theta^{I} + \Delta\theta^{III})$$

$$S_8 = \frac{1}{\sqrt{2}}(\Delta\theta^{II} + \Delta\theta^{IV})$$

$$S_9 = \frac{1}{\sqrt{8}}(\Delta\varphi_1^{II} + \Delta\varphi_2^{II} + \Delta\varphi_3^{II} + \Delta\varphi_4^{II} + \Delta\varphi_1^{IV} + \Delta\varphi_2^{IV} + \Delta\varphi_3^{IV} + \Delta\varphi_4^{IV})$$

$$S_{10} = \frac{1}{\sqrt{8}}(\Delta\varphi_1^{II} - \Delta\varphi_2^{II} - \Delta\varphi_3^{II} + \Delta\varphi_4^{II} - \Delta\varphi_1^{IV} + \Delta\varphi_2^{IV} + \Delta\varphi_3^{IV} - \Delta\varphi_4^{IV})$$

$$S_{11} = \frac{1}{2}(\Delta\varphi_2^{I} + \Delta\varphi_4^{I} + \Delta\varphi_1^{III} + \Delta\varphi_3^{III})$$

$$S_{12} = \frac{1}{2}(\Delta\varphi_1^{I} + \Delta\varphi_3^{I} + \Delta\varphi_2^{III} + \Delta\varphi_4^{III})$$

Four redundancies are included among these coordinates.

$$A_2 \quad S_1 = \frac{1}{2}(\Delta R^{I} + \Delta R^{II} - \Delta R^{III} - \Delta R^{IV})$$

$$S_2 = \frac{1}{2}(\Delta r_1^{II} + \Delta r_2^{II} - \Delta r_1^{IV} - \Delta r_2^{IV})$$

$$S_3 = \frac{1}{\sqrt{2}}(\Delta\Theta^{II} - \Delta\Theta^{IV})$$

$$S_4 = \frac{1}{\sqrt{2}}(\Delta\theta^{II} - \Delta\theta^{IV})$$

$$S_5 = \frac{1}{\sqrt{8}}(\Delta\varphi_1^{II} + \Delta\varphi_2^{II} + \Delta\varphi_3^{II} + \Delta\varphi_4^{II} - \Delta\varphi_1^{IV} - \Delta\varphi_2^{IV} - \Delta\varphi_3^{IV} - \Delta\varphi_4^{IV})$$

$$S_6 = \frac{1}{\sqrt{8}}(\Delta\varphi_1^{II} - \Delta\varphi_2^{II} - \Delta\varphi_3^{II} + \Delta\varphi_4^{II} + \Delta\varphi_1^{IV} - \Delta\varphi_2^{IV} - \Delta\varphi_3^{IV} + \Delta\varphi_4^{IV})$$

$$S_7 = \frac{1}{2}(\Delta\varphi_2^{I} - \Delta\varphi_4^{I} - \Delta\varphi_1^{III} + \Delta\varphi_3^{III})$$

$$S_8 = \frac{1}{2}(\Delta\varphi_1^{I} - \Delta\varphi_3^{I} - \Delta\varphi_2^{III} + \Delta\varphi_4^{III})$$

One redundancy is included.

$$B_1 \quad S_1 = \frac{1}{2}(\Delta R^{I} - \Delta R^{II} - \Delta R^{III} + \Delta R^{IV})$$

$$S_2 = \frac{1}{2}(\Delta r_1^{II} - \Delta r_2^{II} + \Delta r_1^{IV} - \Delta r_2^{IV})$$

$$S_3 = \frac{1}{\sqrt{2}}(\Delta r_2^{I} - \Delta r_1^{III})$$

$$S_4 = \frac{1}{\sqrt{2}}(\Delta r_1^{I} - \Delta r_2^{III})$$

$$S_5 = \frac{1}{\sqrt{2}}(\Delta\Theta^{I} - \Delta\Theta^{III})$$

$$S_6 = \frac{1}{\sqrt{2}}(\Delta\theta^{I} - \Delta\theta^{III})$$

$$S_7 = \frac{1}{\sqrt{8}}(\Delta\varphi_1^{II} + \Delta\varphi_2^{II} - \Delta\varphi_3^{II} - \Delta\varphi_4^{II} - \Delta\varphi_1^{IV} - \Delta\varphi_2^{IV} + \Delta\varphi_3^{IV} + \Delta\varphi_4^{IV})$$

$$S_8 = \frac{1}{\sqrt{8}}(\Delta\varphi_1^{II} - \Delta\varphi_2^{II} + \Delta\varphi_3^{II} - \Delta\varphi_4^{II} + \Delta\varphi_1^{IV} - \Delta\varphi_2^{IV} + \Delta\varphi_3^{IV} - \Delta\varphi_4^{IV})$$

$$S_9 = \frac{1}{2}(\Delta\varphi_2^{I} + \Delta\varphi_4^{I} - \Delta\varphi_1^{III} - \Delta\varphi_3^{III})$$

$$S_{10} = \frac{1}{2}(\Delta\varphi_1^{I} + \Delta\varphi_3^{I} - \Delta\varphi_2^{III} - \Delta\varphi_4^{III})$$

One redundancy is incuded.

$$B_2 \quad S_1 = \frac{1}{2}(\Delta R^{I} - \Delta R^{II} + \Delta R^{III} - \Delta R^{IV})$$

$$S_2 = \frac{1}{2}(\Delta r_1^{II} - \Delta r_2^{II} - \Delta r_1^{IV} + \Delta r_2^{IV})$$

$$S_3 = \frac{1}{\sqrt{8}}(\Delta\varphi_1^{II} + \Delta\varphi_2^{II} - \Delta\varphi_3^{II} - \Delta\varphi_4^{II} + \Delta\varphi_1^{IV} + \Delta\varphi_2^{IV} - \Delta\varphi_3^{IV} - \Delta\varphi_4^{IV})$$

$$S_4 = \frac{1}{\sqrt{8}}(\Delta\varphi_1^{II} - \Delta\varphi_2^{II} + \Delta\varphi_3^{II} - \Delta\varphi_4^{II} - \Delta\varphi_1^{IV} + \Delta\varphi_2^{IV} - \Delta\varphi_3^{IV} + \Delta\varphi_4^{IV})$$

$$S_5 = \frac{1}{2}(\Delta\varphi_2^{I} - \Delta\varphi_4^{I} + \Delta\varphi_1^{III} - \Delta\varphi_3^{III})$$

$$S_6 = \frac{1}{2}(\Delta\varphi_1^{I} - \Delta\varphi_3^{I} + \Delta\varphi_2^{III} - \Delta\varphi_4^{III})$$

As only the vibrations in which corresponding atoms in all the unit cells move in phase are optically active for such high polymers, the calculation was done for these modes of vibration according to the method applied to polyethylene[3]. The internal coordinates and the internal symmetry coordinates used are given in Tables II and III. For the internal coordinates only the bond lengths and angles are taken and the angles of internal rotation about the C–C bond are excluded. Therefore, in this calculation the torsional vibrations of the zigzag chain are not considered, but this has comparatively little effect on the other calculated frequencies.

The potential field used is the Urey-Bradley type[4].

$$2V = K(\text{C–C})\sum_{R}(\Delta R)^2 + K(\text{C–H})_{\text{CHH}}\sum_{r_a}(\Delta r_a)^2 + K(\text{C–H})_{\text{CHCl}}\sum_{r_b}(\Delta r_b)^2$$

3) T. Shimanouchi and S. Mizushima, *J. Chem. Phys.*, **17**, 1102 (1949).

4) T. Shimanouchi, ibid., **17**, 245, 734, 848 (1949).

$$+K(\text{C-Cl})\sum_{r_c}(\Delta r_c)^2$$
$$+H(\text{C-C-C})\times(1.54)^2\sum_{\Theta}(\Delta\Theta)^2$$
$$+H(\text{H-C-H})\times(1.09)^2\sum_{\theta_a}(\Delta\theta_a)^2$$
$$+H(\text{H-C-Cl})\times(1.09)\times(1.77)\sum_{\theta_b}(\Delta\theta_b)^2$$
$$+H(\text{H-C-C})_{\text{CHH}}\times(1.09)\times(1.54)\sum_{\varphi_a}(\Delta\varphi_a)^2$$
$$+H(\text{H-C-C})_{\text{CHCl}}\times(1.09)\times(1.54)\sum_{\varphi_b}(\Delta\varphi_b)^2$$
$$+H(\text{Cl-C-C})\times(1.77)\times(1.54)\sum_{\varphi_c}(\Delta\varphi_c)^2$$
$$+F(\text{C}\cdots\text{C})\sum_{Q}(\Delta Q)^2+F(\text{H}\cdots\text{H})\sum_{q_a}(\Delta q_a)^2$$
$$+F(\text{H}\cdots\text{Cl})\sum_{q_b}(\Delta q_b)^2$$
$$+F(\text{H}\cdots\text{C})_{\text{CHH}}\sum_{q_c}(\Delta q_c)^2$$
$$+F(\text{H}\cdots\text{C})_{\text{CHCl}}\sum_{q_d}(\Delta q_d)^2$$
$$+F(\text{Cl}\cdots\text{C})\sum_{q_e}(\Delta q_e)^2+\text{linear terms}$$

where R, r_a, r_b, r_c, Θ, θ_a, θ_b, φ_a, φ_b, φ_c, Q, $q_a\cdots q_e$ represent the following bond lengths, bond angles, and interatomic distances indicated in parentheses.

$R(R^{\text{I}}, R^{\text{II}}, R^{\text{III}}, R^{\text{IV}})$
$r_a(r_1^{\text{II}}, r_2^{\text{II}}, r_1^{\text{IV}}, r_2^{\text{IV}})$
$r_b(r_2^{\text{I}}, r_1^{\text{III}})$
$r_c(r_1^{\text{I}}, r_2^{\text{III}})$
$\Theta(\Theta^{\text{I}}, \Theta^{\text{II}}, \Theta^{\text{III}}, \Theta^{\text{IV}})$
$\theta_a(\theta^{\text{II}}, \theta^{\text{IV}})$
$\theta_b(\theta^{\text{I}}, \theta^{\text{III}})$
$\varphi_a(\varphi_1^{\text{II}}, \varphi_2^{\text{II}}, \varphi_3^{\text{II}}, \varphi_4^{\text{II}}, \varphi_1^{\text{IV}}, \varphi_2^{\text{IV}}, \varphi_3^{\text{IV}}, \varphi_4^{\text{IV}})$
$\varphi_b(\varphi_2^{\text{I}}, \varphi_4^{\text{I}}, \varphi_1^{\text{III}}, \varphi_3^{\text{III}})$
$\varphi_c(\varphi_1^{\text{I}}, \varphi_3^{\text{I}}, \varphi_2^{\text{III}}, \varphi_4^{\text{III}})$
$Q(\text{C}^{\text{IV}'}\cdots\text{C}^{\text{II}}, \text{C}^{\text{I}}\cdots\text{C}^{\text{III}}, \text{C}^{\text{II}}\cdots\text{C}^{\text{IV}}, \text{C}^{\text{III}}\cdots\text{C}^{\text{I}'})$
$q_a(\text{H}_1^{\text{II}}\cdots\text{H}_2^{\text{II}}, \text{H}_1^{\text{IV}}\cdots\text{H}_2^{\text{IV}})$
$q_b(\text{H}^{\text{I}}\cdots\text{Cl}^{\text{I}}, \text{H}^{\text{III}}\cdots\text{Cl}^{\text{III}})$
$q_c(\text{C}^{\text{I}}\cdots\text{H}_1^{\text{II}}, \text{C}^{\text{I}}\cdots\text{H}_2^{\text{II}}, \text{C}^{\text{III}}\cdots\text{H}_1^{\text{II}}, \text{C}^{\text{III}}\cdots\text{H}_2^{\text{II}}, \text{C}^{\text{III}}\cdots\text{H}_1^{\text{IV}}, \text{C}^{\text{III}}\cdots\text{H}_2^{\text{IV}}, \text{C}^{\text{I}'}\cdots\text{H}_1^{\text{IV}}, \text{C}^{\text{I}'}\cdots\text{H}_2^{\text{IV}})$
$q_d(\text{C}^{\text{IV}'}\cdots\text{H}^{\text{I}}, \text{C}^{\text{II}}\cdots\text{H}^{\text{I}}, \text{C}^{\text{II}}\cdots\text{H}^{\text{III}}, \text{C}^{\text{IV}}\cdots\text{H}^{\text{III}})$
$q_e(\text{C}^{\text{IV}'}\cdots\text{Cl}^{\text{I}}, \text{C}^{\text{II}}\cdots\text{Cl}^{\text{I}}, \text{C}^{\text{II}}\cdots\text{Cl}^{\text{III}}, \text{C}^{\text{IV}}\cdots\text{Cl}^{\text{III}})$

For the first calculation we used the force constants transferred from polyethylene[3], 1, 2-dichloroethane[5], and 1, 1, 2, 2-tetrachloroethane[6]. These force constants are indicated as Set 1 in Table IV. The molecular constants assumed are also given in Table IV. From these values the characteristic values, L-matrix, potential energy distribution, and Jacobian $\partial(\nu_1\cdots\nu_k)/\partial(K_1\cdots K_n)$ were calculated with the use of the PC-1 computer built in the Department of Physics, The University of Tokyo. In the next calculation, taking into account the results of the first calculation and the observed values, we introduced the new force constants, Sets 2 and 3 given in Table IV, and repeated the calculation in the same way. In the case of Set 2 the force constants are adjusted so that the calculated frequencies show the best agreement with the observed values of polyvinyl chloride. Set 3 was obtained by modifying the former sets in such a way as to make the calculated frequencies correspond reasonably to the observations for deuterated polyvinyl chloride also.

The calculated frequencies are compared with the observed in Tables V and VI, in which the assignments of bands based on the calculated potential energy distribution are also given.

TABLE IV. FORCE CONSTANTS (in millidyn./Å)[a] AND INTRAMOLECULAR TENSION (κ) (in millidyn. Å)

		Set 1	Set 2	Set 3
1	K(C-C)	2.8[b]	3.10	3.00
2	K(C-H)$_{\text{CHH}}$	4.2[b]	4.15	4.15
3	K(C-H)$_{\text{CHCl}}$	3.90[d]	4.10	4.10
4	K(C-Cl)	1.81[c]	1.65	1.70
5	κ(-CHH-)	0.2[b]	0.21	0.20
6	κ(-CHCl-)	0.10[c]	0.10	0.10
7	H(C-C-C)	0.2[b]	0.20	0.20
8	H(H-C-H)	0.4[b]	0.36	0.38
9	H(H-C-C)$_{\text{CHH}}$	0.15[b]	0.09	0.12
10	H(H-C-Cl)	0.05[c]	0.06	0.06
11	H(H-C-C)$_{\text{CHCl}}$	0.15[c]	0.15	0.15
12	H(Cl-C-C)	0.10[c]	0.10	0.10
13	F(C···C)	0.3[b]	0.50	0.45
14	F(H···H)	0.1[b]	0.06	0.08
15	F(H···C)$_{\text{CHH}}$	0.4[b]	0.43	0.41
16	F(H···Cl)	0.80[c]	0.80	0.80
17	F(H···C)$_{\text{CHCl}}$	0.40[c]	0.45	0.45
18	F(Cl···C)	0.60[c]	0.50	0.55

Molecular constants
r(C-C)=1.54 Å, r(C-H)=1.09 Å, r(C-Cl)=1.77 Å.
All the bond angles=109°28′
a F' is assumed to be $-0.1F$.
b Transferred from polyethylene[3].
c Transferred from 1,2-dichloroethane[5].
d Transferred from 1,1,2,2-tetrachloroethane[6].

Discussion

Polyvinyl Chloride (PVC). — Of the three infrared active species, A_1, B_1 and B_2

5) S. Mizushima, I. Nakagawa, I. Ichishima and T. Miyazawa, ibid., 22, 1614 (1954).
6) K. Naito, I. Nakagawa, K. Kuratani, I. Ichishima and S. Mizushima, ibid., 23, 1907 (1955).

TABLE V. CALCULATED AND OBSERVED FREQUENCIES OF POLYVINYL CHLORIDE (in cm^{-1}) and assignments

Calcd. 1[a]	Calcd. 2[b]	Calcd. 3[c]	Obs.[d]		Assignment
2891	2969	2969	2967	w σ	CH str. (B_1), (A_1)
2880	2969	2968			
2921	2911	2905	2920	m σ	CH_2 antisym. str. (B_1), (B_2)
2919	2910	2905			
2905	2871	2873	2849	w σ	CH_2 sym. str. (A_1)
			2820	vvw σ	
1501	1425	1459	1427	s σ	CH_2 bend. (A_1)
1392	1340	1360	1381	vw π	CH_2 wag. (B_2)
1397	1343	1367	1352	vw σ	CH_2 wag. (B_1)
1225	1246	1245	1330	m σ	CH bend. (A_1)
1227	1245	1244	1250	s σ	CH bend. (B_1)
			1243	vvw σ	
1190	1210	1208	1228	w π	CH bend. (B_2)
			1197	w π	
1030	1063	1054	1125	vw π	CC str. (B_2)
1076	1103	1100	1096	m σ	CC str. (A_1), (B_1)
1028	1089	1071			
1016	976	993	963	m σ	CH_2 rock. (B_1)
1026	930	977	926	vw σ	CH_2 twist. (A_1)
874	832	849	833	w π	CH_2 rock. (B_2)
			693	m σ	
663	639	651	635	s σ	CCl str. (A_1)
			615	s σ	
639	624	633	603	w σ*	CCl str. (B_1)
			487	vw	
444	458	452	430	w	CCC def. (B_1)
343	328	338	363	w	CCl bend. (A_1)
313	294	303	315	vw	CCl bend. (B_2)
290	283	290			CCl bend. (B_1)
			182	w	torion (A_1, B_2)
			160	w	
			102	vw	

a Calculated from the force constants, Set 1.
b Calculated from the force constants, Set 2.
c Calculated from the force constants, Set 3.
d See Refs. 1, 2, 7—11.
* As to the dichroism of the 603 cm^{-1} band we shall report later.

should have parallel dichroism when the molecular chains are oriented along the stretching direction. As shown in Table V the observed parallel bands correspond reasonably to the calculated B_2 frequencies. The perpendicular bands, also, show good correspondence with the calculated A_1 and B_1 frequencies. The main points of the present assignment are summarized as follows:

1) Both of the two CH stretching frequencies which belong to the A_1 and B_1 species are assigned to the band at 2967 cm^{-1}. The former assignment[1] of the CH stretching mode (A_1) to the 2820 cm^{-1} band is improper because of the weak interaction between the two CH bonds. This is also the case for 1, 1, 2, 2-tetrachloroethane, in which the two CH bonds are situated nearer than in polyvinyl chloride. The CH stretching frequency of this compound appears only at 2990 cm^{-1} in infrared spectra and at 2989 cm^{-1} in Raman spectra[6].

2) Krimm and Liang[1] assigned the A_1 and B_1 CH bending modes to the bands at 1330 cm^{-1} and 1250 cm^{-1}, respectively, However, because of the weak interaction between the two CH bonds such great splitting can not be expected. This expectation is confirmed clearly by our calculation. The calculated Jacobian shows that both of these frequencies depend similarly on the force constants H(H-C-Cl), $H(\text{H-C-C})_{\text{CHCl}}$, F(H···Cl), $F(\text{H}\cdots\text{C})_{\text{CHCl}}$, and κ_{CHCl}, and it is impossible to separate them. The corresponding frequencies are found in 1, 1, 2, 2-tetrachloroethane at 1304 cm^{-1} (A_u)

TABLE VI. CALCULATED AND OBSERVED FREQUENCIES OF DEUTERATED POLYVINYL CHLORIDE (in cm^{-1}) AND ASSIGNMENTS

Calcd. 1[a]	Calcd. 3[b]	Obs.[c]	Assignment
2120 2111	2177 2169	2228 m σ	CD str. (A_1, B_1)
2164 2163	2151 2152	2159 vw σ	CD_2 antisym. str. (B_1, B_2)
2095	2090	2122 vw σ	CD_2 sym. str. (A_1)
1218	1225	1273 w σ	CC str.+CD_2 bend. (A_1)
1254	1261	1251 m π	CC str.+CD_2 wag. (B_2)
1170	1189	1112 s σ	CC str.+CD_2 wag. (B_1)
		1091 sh ?	
1024	1028	1041 sh σ	CD bend.+CC str. (B_1)
998	986	1017 vs σ	CD_2 bend.+CD bend. (A_1)
		958 sh σ	
938	930	937 s π ?	CD_2 wag.+CD bend. (B_2)
909	905	904 sh π ?	CD_2 rock.+CD_2 wag. (B_1)
844	858	886 vw ?	CD bend.+CD_2 bend. (A_1)
		836 w π ?	
806	807	806 w π	CD bend.+CD_2 wag.+CD_2 rock. (B_2)
820 805	822 771	787 s σ	CD bend.+CD_2 rock.+CCl str. (B_1) CD_2 twist.+CCl str. (A_1)
685	672	680 vw π	CD_2 rock. (B_2)
		628 m σ	
591	574	594 m σ	CCl str.+CD_2 twist. (A_1)
		573 w σ	
586	575	568 m σ	CCl str.+CD_2 rock. (B_1)
374	391		CCC def. (B_1)
330	322		CCl bend. (A_1)
279	272		CCl bend. (B_2)
260	260		CCl bend. (B_1)

a Calculated from the force constants, Set 1.
b Calculated from the force constants, Set 3.
c See Ref. 2.

and 1308 cm^{-1} (B_g) for the trans from, and at 1280 cm^{-1} (A) and 1243 cm^{-1} (B) for the gauche form. Even in the gauche form the splitting does not exceed 40 cm^{-1}. So, at first it seemed reasonable to assign the 1250 cm^{-1} band to both A_1 and B_1 CH bending modes and the 1330 cm^{-1} band to the CH_2 wagging mode (B_1). On the other hand the change of the dichroism observed for PVC films of varying degrees of stretching (which will be reported later) shows that the 1330 and 1250 cm^{-1} bands should belong to A_1 and B_1 species, respectively. This fact can be understood if we assume that strong coupling takes place between one of the CH bending modes and the CH_2 wagging or twisting mode, and the large splitting of frequencies occurs, though it is inconsistent with the results of our calculation. This deviation may be due to the incompleteness of the force constants given in Table IV. Ambiguity is still remaining as to this point; our final assignments are shown in Table V.

3) The bands at 1228, 963 and 833 cm^{-1} are assigned to CH bending (B_2), CH_2 rocking (B_1), and CH_2 rocking (B_2) frequencies, respectively, according to the results of the calculation. The 1228 cm^{-1} band was assigned by Krimm et al.[7] to the overtone of the 615 cm^{-1} band. However, this band remains definitely in the spectrum of the highly syndyotactic polymer for which the 615 cm^{-1} band is observed as a shoulder of the 693 cm^{-1} band. Kawasaki et al.[8] suggested that the very weak band found at 1243 cm^{-1} may be assignable to the overtone of the 615 cm^{-1} band.

4) The bands at 2820, 1197, 693 and 615 cm^{-1} are not assigned. The 693 cm^{-1} band is associated with the atactic structure and the 615 cm^{-1} band with the syndyotactic structure, which is not in the ordered configuration,

7) S. Krimm, A. R. Berens, V. L. Folt and J. J. Shipman, *Chem. & Ind.*, **1958**, 1512.
8) A. Kawasaki et al., *Abstr. of Symposium on the Infrared and Raman Spectroscopy (Tokyo)*, p. 41 (1959).

because they can not be observed for the sample prepared by radiation-induced polymerization of a urea-vinyl chloride complex[7,9-11]. The band at 1197 cm^{-1} seems to behave analogously, but in a less distinct manner.

5) The band at 926 cm^{-1} is only tentatively assigned to the CH_2 twisting frequency. It is known that for some vibrational modes, such as CH_3 rocking vibrations in ethane and CH_2 twisting vibrations in 1, 2-dichloroethane, the calculated frequencies deviate considerably from the observed[4,12-14]. Therefore, it may be undesirable to assign the 926 cm^{-1} band to the CH_2 twisting mode simply because it corresponds to the calculated value of 977 cm^{-1}. More detailed investigation of the intramolecular potential field seems to be necessary to settle this problem.

Deuterated Polyvinyl Chloride.—1) The infrared spectrum of deuterated PVC was reported by Enomoto et al.[2] Compared with the spectrum of normal PVC, it is quite complicated and hard to analyze, as many bands are found in the 800 cm^{-1} to 1300 cm^{-1} region. From the results of the present calculation and the observed dichroism tentative assignments are proposed for the main bands. The calculated potential energy distribution and L-matrix indicate that a strong coupling of two or more modes occurs for most bands of deuterated PVC. For example, for the calculated 858 cm^{-1} (A_1) vibration, in-phase coupling of the CD_2 and CD bending modes occurs while in the case of the calculated 986 cm^{-1} (A_1) vibration, out-of-phase coupling occurs. This is shown in Fig. 2. The in-phase mode is expected to be weak in intensity, and it probably corresponds to the very weak band at 886 cm^{-1}. The intensity of the out-of-phase mode is strong and it undoubtedly corresponds to the very strong band at 1017 cm^{-1}. A similar situation is found for the calculated 807 cm^{-1} (B_2) and 930 cm^{-1} (B_2) vibrations (see Fig. 3). The 930 cm^{-1} mode is expected to be strong and corresponds to the strong parallel band at 937 cm^{-1}, and the 807 cm^{-1} mode is weak and corresponds to the weak band at 806 cm^{-1}.

2) The bands at 594 cm^{-1} and 568 cm^{-1} are assigned to the CCl stretching frequencies (A_1 and B_1). These bands correspond to those at 635 cm^{-1} and 603 cm^{-1}, respectively, of normal PVC. Asahina and Enomoto[15] showed that the 628 cm^{-1} band disappears in the sample obtained by irradiation-induced polymerization of a urea-vinyl chloride-d_3 complex. Therefore, this band is the contribution of the atactic structure and corresponds to the 690 cm^{-1} band of normal PVC. The deuterated PVC prepared by Enomoto et al. was kindly made available to us. We measured the spectrum of this sample using a grating spectrometer (Perkin-Elmer Model 112G) and found a new band at about 573 cm^{-1}, which probably corresponds to the 615 cm^{-1} band of normal PVC. All four bands of deuterated PVC are perpendicular.

As stated above the observed infrared absorption bands, including their dichroism, can

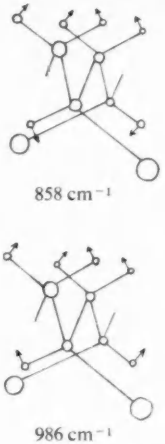

Fig. 2. Vibrational modes of 858 cm^{-1} and 986 cm^{-1}.

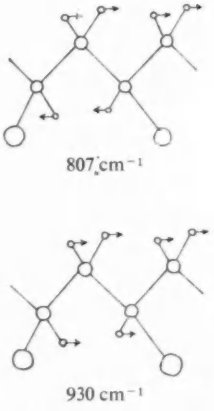

Eig. 3. Vibrational modes of 807 cm^{-1} and 930 cm^{-1}.

9) T. Shimanouchi, S. Tsuchiya and S. Mizushima, *J. Chem. Phys.*, **30** 1365 (1959).
10) T. Shimanouchi, S. Tsuchiya and S. Mizushima, *The High Polymer (Kobunshi)*, **8**, 202 (1959).
11) S. Krimm, A. R. Berens, V. L. Folt, and J. J. Shipman, *Chem. & Ind.*, **1959**, 433.
12) I. Nakagawa and S. Mizushima, *J. Chem. Phys.*, **21**, 2195 (1953).
13) I. Nakagawa, *J. Chem. Soc. Japan, Pure Chem. Sec. (Nippon Kagaku Zasshi)*, **74**, 848 (1953).
14) I. Nakagawa, ibid., **77**, 1030 (1956).
15) M Asahina and S. Enomoto, ibid., **81**, 1374 (1960).

be satisfactorily accounted for on the basis of the calculation of normal vibrations. This gives a further confirmation of the syndyotactic configuration for the crystalline part of polyvinyl chloride. The remaining important problem is to study the potential field more thoroughly, and for this purpose the comparative investigation of other polymers and related compounds will be indispensable.

We wish to thank Professor H. Takahashi for making available the PC-1 computer. Thanks are also due to Dr. K. Nambu and Mr. S. Enomoto, who kindly gave us various samples of polyvinyl chloride.

Department of Chemistry
Faculty of Science
The University of Tokyo
Hongo, Tokyo

Molecular Structure of Epibromohydrin and Glycidol by Electron Diffraction

By Masato IGARASHI

(Received September 26, 1960)

The molecular structure of ethylene oxide[1], propylene oxide and epichlorohydrin[2] has been studied previously by the electron diffraction method. As for the size of the CCO ring, the electron diffraction results have agreed almost perfectly with that of microwave spectrum study of ethylene oxide[3]. The C–C distance was 1.46±0.03 Å and the C–O distance were about 1.44 Å, whereas the values by microwave spectroscopy were 1.472 Å and 1.436 Å, respectively.

In propylene oxide and epichlorohydrin, the C–C (methyl) distance was about 1.52 Å and the angle between C–C (methyl) and CCO ring plane was about 58°. The chlorine atom in epichlorohydrin was the farthest apart from the CCO ring.

In the present paper the structures of epibromohydrin and glycidol are reported especially in regard to the configuration of the bromine atom and of the oxygen atom of alcohol in each molecule.

Experimental

Epibromohydrin was prepared according to the procedure described in "Organic synthesis"[4]. The boiling point was 61°C at 50 mmHg. Glycidol was prepared from glycerol monochlorohydrin by the procedure of Nef[5]. The boiling point was 52°C at 10 mmHg. The apparatus of electron diffraction and the procedures of experiment were the same as those of the previous reports[1,2]. Visual intensity curves are shown in Figs. 3 and 5.

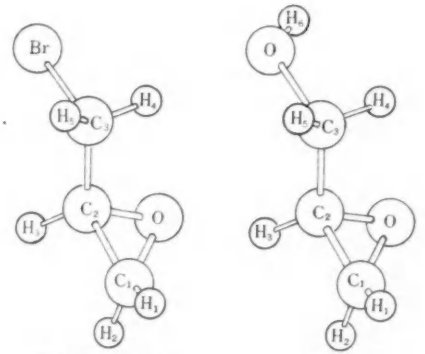

Fig. 1. Perspective pictures of epibromohydrin and glycidol.

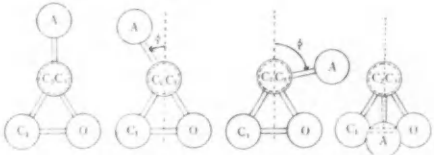

Fig. 2. Various configurations of epibromohydrin and glycidol showing internal rotations, which were projected along C_2-C_3 axis (cf. Fig. 1). A stands for bromine or oxygen atom. Hydrogen atoms are omitted for convenience.

Analysis

Radial distribution and theoretical intensity curves were calculated using the same formulas

1) M. Igarashi, This Bulletin, **26**, 330 (1953).
2) M. Igarashi, ibid., **28**, 58 (1955).
3) G. L. Cunningham, A. W. Boyd, R. J. Myer, W. D. Gwinn and W. I. Le Van, *J. Chem. Phys.*, **19**, 676 (1951).
4) Organic Synthesis, **14**, 42; **16**, 31.
5) J. U. Nef, *Ann.*, **335**, 231 (1904).

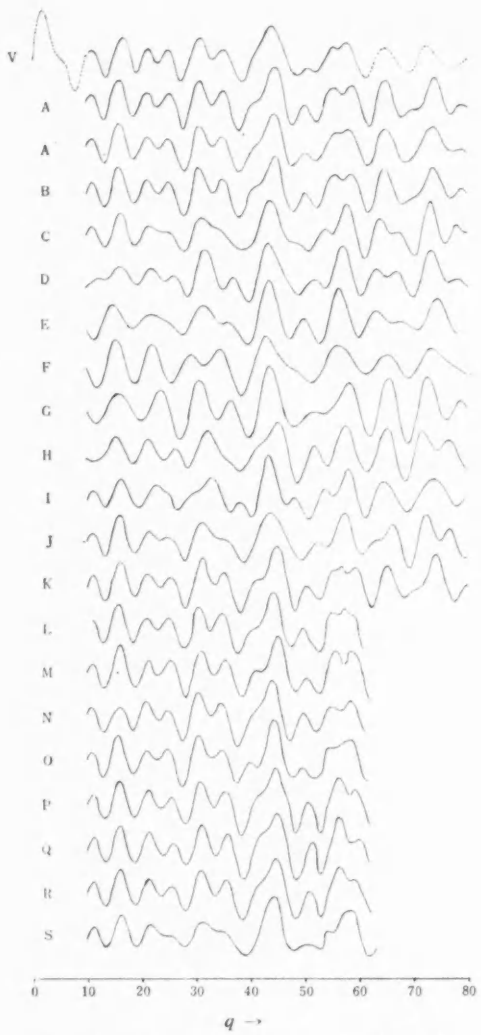

Fig. 3. Visual intensity curve (V) and theoretical intensity curves for the models from A to S (Table I) of epibromohydrin. Curve A′ is drawn using thermal factor $b_{ij}=0.0002$ instead of zero in curve A for the atomic pairs $C_1\cdots Br$ and $O\cdots Br$.

as before[2]. Making reference to the previous reports[1-3], some parameters of the molecular models for the theoretical intensity curves were assumed as follows: the CCO ring size and C–H distances adjacent, attached to the ring, are equal to those of ethylene oxide, the other C–H distances 1.09 Å, the angles C_2C_3Br and C_2C_3O are both 109.5°, and the angle between C_1C_2 and $C_3C_2H_3$ plane is 21° (Fig. 1). Other parameters such as C_2–C_3 distance and its inclination from the ring plane, C_3–Br and C_3–O distances, and the angles of internal rotation (Fig. 2) were examined.

Epibromohydrin.—The visual intensity curve in the region of $q=60\sim80$ was uncertain, therefore in the correlation method the maxima and minima in the region of $q=10\sim60$ were compared with the theoretical intensity curves, and radical distribution curves were calculated, using several different intensity values in the former region. On account of the damping factor $\exp(-aq^2)$ the positions of the peaks in radial distribution curves were not so much affected by the intensity in such a region. The radial distribution curve is nearly consistent with models A and K (Table I).

Molecular models for the theoretical intensity curves were constructed in the following ranges: C_2–C_3: 1.50∼1.58 Å, C_3–Br: 1.88∼1.96 Å, angle between C_2–C_3 and CCO ring: 45∼70°, rotational angle ϕ around C_2–C_3 axis: 0∼360° (Table I).

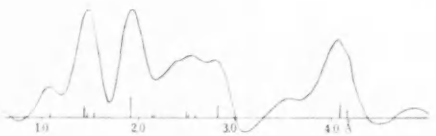

Fig. 4. Radial distribution curve of epibromohydrin. Vertical lines show the interatomic distances of model A.

The theoretical intensity curves of the models in which the rotational angles drawn in Fig. 2 are smaller than ±15° have features which resemble the observed. But as those having the other rotational angles are very far from the observed, these models can be rejected. C_2–C_3 and C_3–Br bond distances and the inclination of C_2–C_3 were examined mainly by the q_{calcd}/q_{obs} values (Table I).

The results are as follows: C_2–$C_3=1.53\pm0.03$ Å, C_3–$Br=1.91\pm0.02$ Å, angle between C_2–C_3 and CCO ring is 58±8°, rotational angle ϕ is 0±15°, i.e. the bromine atom is almost trans against the midpoint of C_1–O.

Glycidol.—Theoretical intensity curves of the models in which the rotational angles are about 0° and 80° have features which resemble the observed, although the maximum of the model of 80° at about $q=33$ is not predominant compared with that of 0° (Fig. 5). The models of the other ϕ values such as G, H, L and M may be excluded because the apperances of the intensity curves at about $q=30$ and 50 are very different in comparison with the observed.

The radial distribution curve RD_1 calculated using the visual intensity curve which is shown by the solid line in Fig. 5 and spliced by the

TABLE I. MODELS FOR EPIBROMOHYDRIN AND q_{calcd}/q_{obs} VALUES

Model	C_2–C_3 Å	C_3–Br Å	Inclination of C_2–C_3	Rotational angle, ϕ	Mean value of q_{calcd}/q_{obs}	Average deviation
A	1.54	1.92	58°	0°	0.993	0.015
B	1.54	1.92	58°	15°	0.996	0.017
C	1.54	1.92	58°	33°	—	—
D	1.54	1.92	58°	90°	—	—
E	1.54	1.92	58°	147°	—	—
F	1.54	1.92	58°	180°	—	—
G	1.54	1.92	58°	−147°	—	—
H	1.54	1.92	58°	−90°	—	—
I	1.54	1.92	58°	−33°	—	—
J	1.54	1.92	58°	−15°	0.998	0.015
K	1.50	1.92	58°	0°	1.003	0.015
L	1.58	1.92	58°	0°	0.991	0.015
M	1.54	1.88	58°	0°	1.005	0.019
N	1.54	1.96	58°	0°	0.986	0.015
O	1.54	1.92	45°	0°	0.987	0.015
P	1.54	1.92	65°	0°	0.998	0.019
Q	1.54	1.92	70°	0°	1.011	0.016
R	1.54	1.92	65°	15°	—	—
S	1.54	1.92	65°	33°	—	—

TABLE II. MODELS FOR GLYCIDOL AND q_{calcd}/q_{obs} VALUES

Model	C_2–C_3 Å	C_3–O Å	Inclination of C_2–C_3	Rotational angle, ϕ	Mean value of q_{calcd}/q_{obs}	Average deviation
A	1.54	1.43	58°	0°	0.998	0.016
B	1.50	1.40	58°	0°	1.005	0.020
C	1.54	1.46	58°	0°	0.992	0.022
D	1.58	1.43	58°	0°	—	—
E	1.50	1.43	58°	0°	1.005	0.013
F	1.50	1.43	58°	−15°	1.006	0.008
G	1.50	1.43	58°	−33°	—	—
H	1.50	1.43	58°	−60°	—	—
I	1.50	1.43	58°	−75°	—	—
J	1.50	1.43	58°	−80°	1.003	0.008
K	1.50	1.43	58°	−90°	1.010	0.005
L	1.50	1.43	58°	−120°	—	—
M	1.50	1.43	58°	180°	—	—
N	1.50	1.43	58°	33°	1.007	0.011
O	1.54	1.43	58°	−85°	0.998	0.007
P	1.50	1.40	58°	−85°	1.010	0.008
Q	1.54	1.46	58°	−85°	0.995	0.008
R	1.50	1.43	50°	0°	—	—
S	1.50	1.43	50°	85°	—	—
T	1.50	1.43	65°	0°	—	—
U	1.50	1.43	65°	85°	—	—

theoretical intensity of model E at small q values has a slight peak at about 3.0 Å, which might be regarded as a ghost and a somewhat larger peak at about 3.6 Å, which should correspond to the configuration $\phi=0°$.

But another radial distribution curve RD_2 calculated using the dashed intensity curve in the region of about $q=35$ instead of solid intensity curve and the theoretical intensity curve of model J at small q values in Fig. 5, shows a more predominant peak at about 3.0 Å which corresponds to the existence of the configuration of about $\phi=80°$ (Fig. 6).

Whether the configuration of the oxygen atom of alcohol is at about $\phi=0°$, or about $\phi=80°$, or at the both positions, could not be determined by the present visual method.

The parameters other than the internal rotation were examined in the following ranges: C_2–C_3: 1.50~1.58 Å, C_3–O: 1.40~1.46 Å, angle

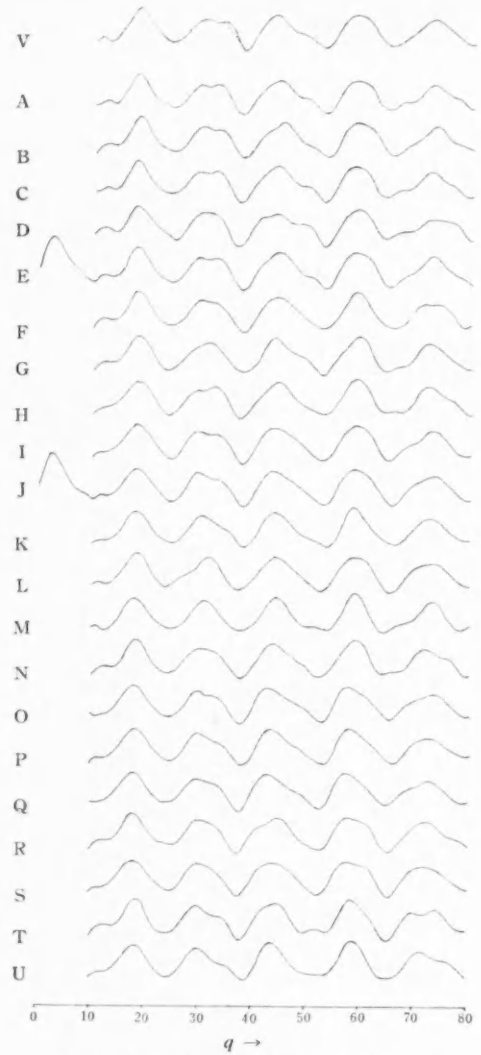

Fig. 5. Visual intensity curve (V) and theoretical intensity curves for the models from A to U (Table II) of glycidol.

between C_2–C_3 and CCO ring: 50~65° (Table II).

As the features of the theoretical intensity curves of the models in which C_2–C_3 inclinations against CCO ring plane are 50° and 65° are considerably different from the visual, both models can be excluded as inadequate. C_2–C_3 and C_3–O bond distances were examined mainly by the q_{calcd}/q_{obs} values (Table II). The results are as follows: C_2–C_3=1.53±0.03 Å, C_3–O=1.43±0.03 Å, angle between C_2–C_3 and CCO ring is 58±5°.

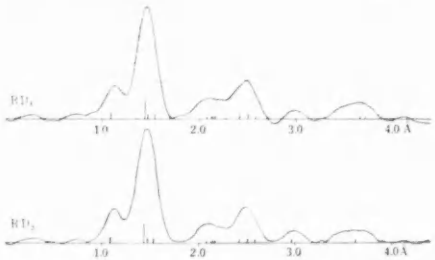

Fig. 6. Radial distribution curves of glycidol. Vertical lines show the interatomic distance of models A (RD_1) and O (RD_2).

Discussion

As mentioned in the previous report[2] about epichlorohydrin and the present report about epibromohydrin, chlorine and bromine atoms in these compounds are almost at the trans position against the midpoint of C_1–O, i.e. these atoms are fathest apart from the CCO ring.

Therefore it can be thought that there is a strong steric repulsion between chlorine atom or bromine atom and ethylene oxide ring.

If the same steric repulsion is present between oxygen atom of alcohol and ethylene oxide ring and moreover no intramolecular hydrogen bond between two oxygen atoms, the oxygen atom of alcohol will be at trans too. Contrarily, if there is a stronger intramolecular hydrogen bond than the steric repulsion, the oxygen atom of alcohol will be nearer to the oxygen atom in the ring than the trans position and ϕ will be equal to about 80°.

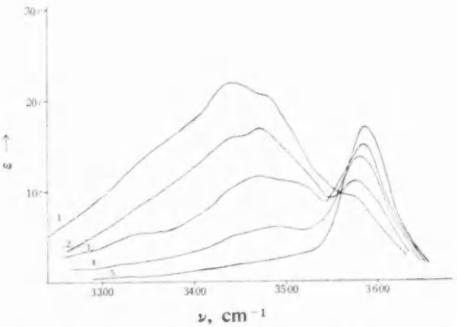

Fig. 7. Infrared absorption spectra of glycidol in carbon tetrachloride solutions. ε is molecular extinction coefficient, c is the concentration of satulated solution at room temperature and ν is wave number. Curves from (1) to (5) are absorption spectra of solutions of the following concentratrations; (1): c, (2): $1/2\,c$, (3): $1/5\,c$, (4): $1/18\,c$, (5): $1/54\,c$.

Unfortunately as the theoretical intensity curves of both the models rather resemble each other in the features which are characteristic of internal rotations, the above two cases could not be determined unambiguously.

However infrared absorption spectrums of glycidol in dilute carbon tetrachloride solutions using lithium fluoride prism did not show a deviation of O–H stretching vibration by which the intramolecular hydrogen bond can be recognized (Fig. 7). It may be supposed that in the vapor state at room temperature there exists no intramolecular hydrogen bond either, so the oxygen atom of alcohol will be almost at trans against the midpoint of C_1–O.

The author wishes to express his sincere gratitude to Professor A. Kotera for his guidance throughout this research and to Dr. K. Nukada and Miss. U. Maeda, Government Chemical Industrial Research Institute of Tokyo, for the infrared investigation of glycidol solution. He is also indebted to Mr. T. Wada for his help during the experiment.

Department of Chemistry
Faculty of Science
Tokyo University of Education
Koishikawa, Tokyo

An Electron Diffraction Investigation of the Molecular Structure of Ethylenimine

By Masato IGARASHI

(Received September 26, 1960)

In the three membered ring compounds such as cyclopropane, ethylene oxide, ethylene sulfide and ethylenimine, the isoelectronic groups $H_2C\langle$, $O\langle$, $S\langle$ and $HN\langle$ bear a resemblance to each other, so that the structural features for these molecules are identical except for these groups.

Since two sp hybrid atomic orbitals may not be at an angle less than 90° to each other, the bonding orbitals which constitute rings CCC, CCO, CCS and CCN can not point directly at each other, but they are bent, forming the "banana bond"[1].

Electron diffraction and microwave spectrum investigations have reported the molecular structures of these ring compounds in which the nuclear distances of C–C were in most cases shorter than the normal C–C single bond distance, 1.54 Å.

By the electron diffraction method, the C–C distances were 1.53±0.03 Å[2], 1.54 Å[3] and 1.515 ±0.02 Å[4] in cyclopropane, and 1.46±0.03 Å[5] in ethylene oxide. Further, by the microwave spectroscopy the C–C distance was 1.472 Å[6] in ethylene oxide, 1.492 Å[6] in ethylene sulfide and 1.480 Å[7] in ethylenimine respectively. The HCH angles have been found to be about 116°[4] and 117°[6,7], which are larger than the tetrahedral angle, 109.5°.

In this report the results of the electron diffraction study of ethylenimine by the sector-microphotometer method are described and compared with those of the microwave spectrum study[7] (Table I).

TABLE I. MOLECULAR STRUCTURE OF ETHYLENIMINE BY MICROWAVE SPECTROSCOPY[7]

C-C	1.480 Å	$\angle C_2NH$	112°
C-N	1.488 Å	$\angle CCH_2$	159°25′
C-H	1.083 Å	$\angle HCH$	116°41′
H-H	1.000 Å (assumed)		

Experimental

Ethylenimine was kindly furnished by Professor Y. Iwakura, Tokyo Institute of Technology; its boiling point was 55°C.

The electron diffraction instrument in the Department of Chemistry, Faculty of Science, the University of Tokyo[8] was used for the diffraction experiment. It incorporates with r^2-sector which

1) C. A. Coulson and W. E. Moffit, *Phil. Mag.*, **40**, 1 (1949).
2) L. Pauling and L. O. Brockway, *J. Am. Chem. Soc.*, **59**, 1223 (1937).
3) O. Bastiansen and O. Hassel, *Tids. Kjemi Bergvesen Met.*, **6**, 71 (1946).
4) H. Pfeiffer, Ph. D. thesis, California Institute of Technology, 1948.
5) M. Igarashi, This Bulletin, **26**, 330 (1953).
6) G. L. Cunningahm, A. W. Boyd, R. J. Mayer, W. D. Gwinn and W. I. LeVan, *J. Chem. Phys.*, **19**, 679 (1951).
7) T. E. Turner, V. C. Fiora, W. M. Kendrick and B. L. Hicks, ibid., **21**, 564 (1953); T. E. Turner, V. C. Fiora and W. M. Kendrick, ibid., **23**, 1966 (1955).
8) K. Kuchitsu, This Bulletin, **30**, 391 (1956).

is rotated rapidly during exposure. Diffraction photographs were obtained on Fuji Process Hard plates. During the diffraction experiment the liquid sample reservoir has been cooled by a freezing mixture of ice and sodium chloride to reduce the amount of the sample vapor. The camera length was 11.82 cm. and the wave length of electron was 0.0578 Å, which was determined by measuring the transmission patterns of a gold foil.

Two pairs of photographs of the exposures of 25 and 50 sec., and of 30 and 60 sec. were used for intensity measurement. The optical densities of these plates were measured by the microphotometer. The photographic plates were rotated rapidly around the center of the diffraction pattern while being scanned by the microphotometer.

Analysis

Optical densities of each pair of the diffraction photographs were converted to relative intensity by Karle's procedure[9]. A smooth background line was drawn through the intensity curve multiplied by q and molecular intensity curve $M(q)$ was obtained by the following formula

$$M(q) = (I_T - I_B)/I_B, \qquad (1)$$

where I_T is the total intensity and I_B is the background intensity.

Radial Distribution Curve. — The radial distribution carve was calculated from the molecular intensity curve $M(q)$ according to the following equation:

$$f(r) = \sum_{q=1}^{90} qM(q)\exp(-aq^2)\sin(\pi qr/10) \qquad (2)$$

where the value of a is chosen as 0.000284 to make the integrand of Eq. 2 converge rapidly and $q = (40/\lambda)\sin(\theta/2)$, where θ is the angle of scattering and λ is the wavelength of the electron beam. The intensity curve from $q = 0$ to $q = 18$ was spliced by the theoretical intensity curve calculated for an assumed model.

A few steps of successive approximation were made to get a reasonable background line which would satisfy Karle's criterion of non-negativeness in the radial distribution curve as closely as possible. The final molecular intensity curve is shown in Fig. 1 and the radial distribution curve in Fig. 2.

The radial distribution curve consists of three peaks at about 1.09 Å, 1.49 Å and 2.19 Å. The first peak is due to bonded C–H and N–H distances, the second to bonded C–C and C–N distances and the third to non-bonded N···cH, C···cH and C···NH distances. It is difficult to separate the first and the second peaks into two components and the third into three components respectively, because these component peaks overlap each other heavily. The first peak can be resolved into its components by three distinct sets of parameters (Fig. 3 and Table II). Sets A and C are the extreme cases for the differences between C–H and N–H

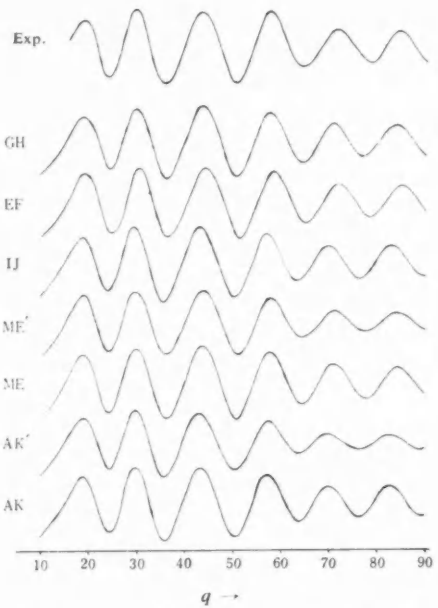

Fig. 1. Experimental and theoretical intensity curves.

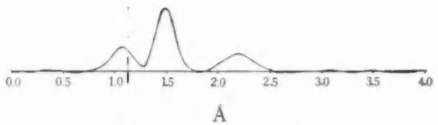

Fig. 2. The radial distribution curve.

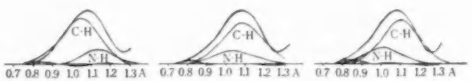

Fig. 3. Analysis of the first peak of the radial distribution curve.

TABLE II. ANALYSIS OF THE FIRST PEAK OF RADIAL DISTRIBUTION CURVE

Set	Atomic pair	Equilibrium distance, Å	Mean amplitude, Å
A	C–H	1.05	0.065
	N–H	1.14	0.03
B	C–H	1.09	0.075
	N–H	1.04	0.07
C	C–H	1.11	0.06
	N–H	1.01	0.04

9) J. Karle and I. L. Karle, *J. Chem. Phys.*, **18**, 957, 963 (1950).

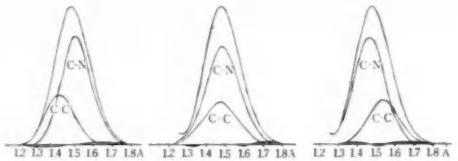

Fig. 4. Analysis of the second peak of the radial distribution curve.

TABLE III. ANALYSIS OF THE SECOND PEAK OF RADIAL DISTRIBUTION CURVE

Set	Atomic pair	Equilibrium distance, Å	Mean amplitude, Å
D	C-N	1.51	0.02
	C-C	1.42	0.02
E	C-N	1.49	0.05
	C-C	1.48	0.05
F	C-N	1.47	0.03
	C-C	1.54	0.03

equilibrium distances. So the reasonable ranges of equilibrium distances are C–H=1.05～1.11 Å and N–H=1.01～1.14 Å.

The second peak can also be resolved into two component peaks by three distinct sets of parameters (Fig. 4 and Table III).

Sets D and F are the extreme cases for the differences between C–N and C–C equilibrium distances. There is an intimate relation between the difference of atomic distances and their mean amplitudes, that is when the difference becomes larger, the assumed mean amplitudes must be smaller in order to explain the peak of radial distribution curve well. This relation shall be discussed once more later at the correlation method. Here the reasonable equilibrium distances are thought to be C–N=1.47～1.51 Å and C–C=1.42～1.54 Å.

The third peak is the lowest among the three and consists of three component peaks of non-bonded C···cH, N···cH and C···NH. Therefore there may be many reasonable sets of resolution into its components. Some probable examples are listed in Fig. 5 and Table IV. In set G the atomic distances are equivalent to $\angle CCH_2=160°$, $\angle HCH=117°$ and $\angle C_2NH=122°$, assuming C–C=1.48 Å, C–N=1.49 Å, C–H=1.08 Å and N–H=1.04 Å. In set H they are equivalent to $\angle CCH_2=130°$, $\angle HCH=117°$ and $\angle C_2NH=126°$ and in set I to $\angle CCH_2=170°$,

Fig. 5. Analysis of the third peak of the radial distribution curve.

TABLE IV. ANALYSIS OF THE THIRD PEAK OF RADIAL DISTRIBUTION CURVE

Set	Atomic pair	Equilibrium distance, Å	Mean amplitude, Å
G	C···cH	2.22	0.12
	C···NH	2.16	0.12
	N···cH	2.17	0.12
H	C···cH	2.11	0.11
	C···NH	2.21	0.11
	N···cH	2.25	0.11
I	C···cH	2.24	0.11
	C···NH	2.20	0.11
	N···cH	2.16	0.11

$\angle HCH=117°$ and $\angle C_2NH=125°$. Other sets of resolution show different atomic distances, so different bond angles. But by several attempts of resolution, the values $\angle HCH\approx117°$ and $\angle C_2NH=120～130°$ seem to be probable. When N···cH distances become longer, C···cH distances become shorter and vice versa, assuming the bonded distances are constant, and at that time a reasonable resolution of the peak is obtained, so $\angle CCH_2$ can not be determined more accurately than the range 130～170°.

Correlation Method.—The theoretical intensity curves were calculated using the following equation:

$$qM(q)=\sum_{i,j}Z_iZ_j/r_{ij}\exp(-b_{ij}q^2)\sin(\pi qr_{ij}/10) \qquad (3)$$

where r_{ij} is the equilibrium distance between atoms i and j and Z_i is the atomic number of atom i, apart from the value 1.25 for the hydrogen atom. The constant b_{ij} is equal to $(\langle\Delta r_{ij}^2\rangle/2)(\pi/10)^2$, where $\langle\Delta r_{ij}^2\rangle$ is the mean square amplitude of the atomic pair i and j.

Making reference to the results of radial distribution curve, various molecular models were selected for the theoretical intensity curves. At first in order to determine the acceptable C–C and C–N nuclear distances, theoretical intensity curves were drawn for the models in which both distances were varied in and out of the range found by the analysis of the second peak of radial distribution curve, assuming C–H=1.08 Å, N–H=1.04 Å, $\angle CCH_2=160°$ and $\angle C_2NH=120°$. In Table V the constants of the models which were examined and mean values and average deviations of q_{calcd}/q_{obs} were listed. In Fig. 1 some of the intensity curves were drawn. The features of the theoretical intensity curves of these models resembled each other, so the q_{calcd}/q_{obs} ratios were used to select reasonable models.

If the mean amplitudes of both C–C and C–N are assumed to be 0.05 Å, which is nearly equal to those of the normal single bonds in most cases, the most reasonable model is such

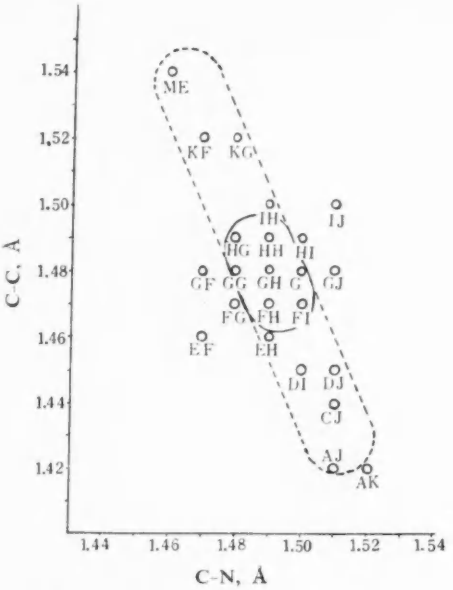

Fig. 6. The parameter chart. The area surrounded by a solid line is an acceptable region when the mean amplitudes are assumed to be 0.05 Å, and the area surrounded by a broken line includes an acceptable region when the smaller mean amplitudes than 0.05 Å are assumed.

that the C–C equilibrium distance is 1.48 Å and the C–N equilibrium distances are 1.49 Å. When C–N distances become longer than 1.49 Å, the acceptable model is such that the C–C distance becomes shorter than 1.48 Å and at that time the mean amplitudes of the atomic pairs should be smaller than 0.05 Å. If we fix the mean amplitudes as 0.05 Å, then in the case when the difference between C–N and C–C distances becomes larger, the amplitudes of the theoretical intensity curve become smaller at large q values compared to the experimental intensity curve, as the curve ME′ and AK′ in Fig. 1. So there is an intimate relation between the difference of the two distances and their mean amplitudes. From Fig. 6 and Table V reasonable C–C and C–N distances and acceptable regions of uncertainty are concluded as follows;

$$\text{C–C} = (1.48 \pm 2d) \pm 0.02 \text{ Å}$$

$$\text{C–N} = (1.49 \mp d) \pm 0.01 \text{ Å}$$

The parameter d is dependent upon the assumed mean amplitudes, M. A., of the atomic pairs. There is the following rough relation between them;

$$d = 0.05 - \text{M.A.}$$

TABLE V. LIST OF MEAN VALUES OF $q_{\text{calcd}}/q_{\text{obs}}$ AND THEIR AVERAGE DEVIATIONS WHEN C–C AND C–N DISTANCES WERE VARIED, ASSUMING THE OTHER PARAMETERS TO BE CONSTANT

Model	C–C Å	C–N Å	Mean amplitude	Mean value of $q_{\text{calcd}}/q_{\text{obs}}$	Average deviation of $q_{\text{calcd}}/q_{\text{obs}}$
GH	1.48	1.49	0.05	1.000	0.004
GG	1.48	1.48	0.05	1.004	0.006
GI	1.48	1.50	0.05	0.995	0.005
GF	1.48	1.47	0.05	1.008	0.004
GJ	1.48	1.51	0.05	0.990	0.006
FH	1.47	1.49	0.05	1.001	0.006
HH	1.49	1.49	0.05	0.997	0.007
EH	1.46	1.49	0.05	1.003	0.006
IH	1.50	1.49	0.05	0.993	0.006
FG	1.47	1.48	0.05	1.006	0.005
FI	1.47	1.50	0.05	0.997	0.006
HG	1.49	1.48	0.05	1.001	0.006
HI	1.49	1.50	0.05	0.993	0.007
EF	1.46	1.47	0.05	1.013	0.005
IF	1.50	1.47	0.05	1.004	0.005
IJ	1.50	1.51	0.05	0.986	0.006
EJ	1.46	1.51	0.04	0.994	0.007
DI	1.45	1.50	0.04	0.999	0.007
KF	1.52	1.47	0.04	1.001	0.004
KG	1.52	1.48	0.04	0.996	0.007
DJ	1.45	1.51	0.03	0.996	0.008
CJ	1.44	1.51	0.03	0.996	0.006
KE	1.52	1.46	0.03	1.006	0.004
ME	1.54	1.46	0.03	1.003	0.004
ME′	1.54	1.46	0.05	1.003	0.004
AJ	1.42	1.51	0.02	0.998	0.008
AK	1.42	1.52	0.02	0.993	0.007
AK′	1.42	1.52	0.05	0.993	0.009

Next C–H and N–H bond distances were investigated. There are similar relations among C–H and N–H bond distances and their mean amplitudes as in the case of C–C and C–N distances. But as the contributions of the former ones to the intensity curves are smaller than those of the latter ones, the above relation is somewhat obscure. The mean values of $q_{\text{calcd}}/q_{\text{obs}}$ and their average deviations for the models in which C–H and N–H distances have been varied, are represented in Table VI. Reasonable ranges of C–H and N–H distances are 1.05~1.11 Å and 1.00~1.11 Å, respectively.

Finally the angles HCH, CCH_2 and C_2NH were investigated. When ∠HCH is varied from 109.5° to 130°, the $q_{\text{calcd}}/q_{\text{obs}}$ values change but slightly (Table VII). The model of 117° seems to be the best, but the above range of angles will be within the experimental error. When the angles CCH_2 increase, C···cH distances increase and N···cH distances decrease, consequently the $q_{\text{calcd}}/q_{\text{obs}}$ values remain

Table VI. List of mean values of q_{calcd}/q_{obs} and their average deviations when C-H and N-H distances were varied, assuming the other parameters to be equal to model GH

Model	C-H Å	C-N Å	Mean amplitude	Mean value of q_{calcd}/q_{obs}	Average deviation of q_{calcd}/q_{obs}
MO	1.08	1.00	0.075	1.000	0.004
GH	1.08	1.04	0.075	1.000	0.004
MN	1.08	1.12	0.075	0.998	0.004
LP	1.05	1.04	0.075	1.000	0.005
LN	1.05	1.12	0.06	0.999	0.006
NP	1.12	1.04	0.06	0.997	0.004
ON	1.12	1.00	0.06	0.998	0.006

Table VII. List of mean values of q_{calcd}/q_{obs} and their average deviations when the angles HCH were varied, assuming the other parameters to be equal to model GH

Model	∠HCH	Mean value of q_{calcd}/q_{obs}	Average deviation of q_{calcd}/q_{obs}
Q	109.5°	0.999	0.005
GH	117°	1.000	0.004
R	130°	1.000	0.006

Table VIII. List of mean values of q_{calcd}/q_{obs} and their average deviations when the angles CCH_2 were varied, assuming the other parameters to be equal to model GH

Model	$\angle CCH_2$	Mean value of q_{calcd}/q_{obs}	Average deviation of q_{calcd}/q_{obs}
S	130°	0.999	0.005
T	140°	0.999	0.005
U	150°	0.999	0.005
GH	160°	1.000	0.004
V	170°	1.000	0.005

Table IX. List of mean values of q_{calcd}/q_{obs} and their average deviations when the angle C_2NH was varied, assuming the other parameters to be equal to model GH

Model	$\angle C_2NH$	Mean value of q_{calcd}/q_{obs}	Average deviation of q_{calcd}/q_{obs}
W	90°	0.999	0.006
GH	120°	1.000	0.004
Y	180°	0.998	0.005

almost unchanged (Table VIII). So the angles CCH_2 may be determined only in the range 130~170°, as having been mentioned in the radial distribution analysis. As the contribution of C···NH atomic pairs to the total molecular intensity curve is the smallest except that of H···H atomic pairs which is negligibly small in this case, and their distances are comparable to those of C···cH and N···cH, the angle C_2NH can not be determined unambiguously. But from the q_{calcd}/q_{obs} values (Table IX), the reasonable value seems to be about 120°.

Summary and Discussion

By the radial distribution and correlation methods, the molecular structure of ethylenimine was obtained as follows;

$$C\text{-}C = (1.48 \pm 2d) \pm 0.02\ \text{Å}$$

$$C\text{-}N = (1.49 \mp d) \pm 0.01\ \text{Å}$$

where

$$d = 0.05 - \text{M.A.}$$

$$C\text{-}H = 1.08 \pm 0.03\ \text{Å},\ N\text{-}H = 1.05 \pm 0.07\ \text{Å}$$

The angles CCH_2 could not be determined accurately. They seem to be in the range 130~170°. The angles HCH and C_2NH also could not be determined unambiguously, but $\angle HCH \approx 117°$ and $\angle C_2NH \approx 120°$ seem to be probable.

The above values of C-C and C-N nuclear distances are consistent with the values obtained by microwave spectroscopy (Table I). They are especially consistent when their mean amplitudes are assumed to be 0.05 Å.

As for the N-H bond distance and the angle C_2NH, the present values coincide with those of microwave spectroscopy within the extents of uncertainty, but the most probable values of the former are somewhat larger than the latter.

The C-C distance 1.48 Å is considerably shorter than the single bond distance 1.54 Å of normal chain compounds as the other three-membered ring compounds.

The author wishes to express his gratitude to Professor A. Kotera for his guidance and encouragement throughout the course of this research, to Professor Y. Morino, the University of Tokyo for the use of the diffraction apparatus, to Dr. K. Kuchitsu and Dr. E. Hirota, the University of Tokyo for their kind aid during the experiment and calculation by the Punched Card Machine, and to Dr. S. Shibata and Dr. H. Morimoto, Nagoya University, for the microphotometer tracing.

Department of Chemistry
Faculty of Science
Tokyo University of Education
Koishikawa, Tokyo

Intramolecular Hydrogen Bonding in α-Keto and α-Alkoxycarboxylic Acids. III. Comparison of the Spectra in the Carbonyl Region with Those in the O–H Stretching Region*

By Michinori ŌKI and Minoru HIROTA

(Received July 13, 1960)

It was previously reported[1] that the O–H stretching absorption of carboxylic acids with a proton accepting group at α-position, such as monoesters of oxalic acid, α-ketocarboxylic acid, α-alkoxycarboxylic acid and α-aryloxycarboxylic acid, had two maxima. The maximum at the higher frequency has been assigned to the free O–H stretching mode and the other at the lower frequency to the O–H of the hydrogen bonded form.

Since it is a well known fact that the C=O stretching absorption ($\nu_{C=O}$) shifts to the lower frequency on hydrogen bonding formation, the frequency shift of $\nu_{C=O}$ to the lower side is also expected in a carboxylic acid which forms hydrogen bonding. Alternately, a trans carboxyl group should show $\nu_{C=O}$ at the higher frequency, because the carbonyl group becomes free on hydrogen bonding formation between the carboxylic hydroxyl group and the hydrogen accepting group at α-position. In this respect, the authors measured $\nu_{C=O}$ together with the O–H stretching absorption (ν_{O-H}) and compared the spectra, thus establishing the assignment of the ν_{O-H} and $\nu_{C=O}$.

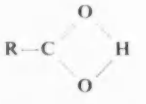

cis structure (I)

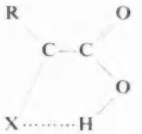

trans structure (II)

Experimental

Measurement and Calculation.—All spectral measurements were carried out with a Perkin Elmer 112G grating infrared spectrophotometer as a carbon tetrachloride solution. The absorption curves were regared as an overlap of the bands with Lorentzian type envelopes and separated graphically. The half-width ($\Delta\nu^a_{1/2}$) and extinction coefficients at the absorption maxima (ε_{max}) are obtained by the above calculation and the apparent integrated intensities are obtained. The concentration of the solution is about 0.002 mol./l. for the measurements in the ν_{O-H} region and 0.0005 mol./l. for the $\nu_{C=O}$ region. The measurements are carried out through the ranges of 3580~3350 cm^{-1} for the ν_{O-H} region and 1830~1690 cm^{-1} for the $\nu_{C=O}$ region.

Materials.—The compounds used for the measurement are known unless otherwise described and their physical constants were checked prior to the measurements.

β-Phenoxypropionic Acid.—A solution of 250 g. (1.6 mol.) of β-phenoxyethyl chloride and 120 g. (1.85 mol.) of potassium cyanide in 600 ml. of ethanol was refluxed for four hours with stirring and the insoluble material was removed by filtration after cooling. The solvent was evaporated and the residue hydrolyzed by refluxing with 1000 ml. of 20% aqueous sodium hydroxide. The acidification followed by recrystallization from aqueous ethanol gave colorless leaves, m. p. 97°C, in 55% overall yield.

Found: C, 65.21; H, 6.30. Calcd. for $C_9H_{10}O_3$: C, 65.05; H, 6.07%.

γ-Phenoxybutyric Acid.—To a sodium ethoxide solution prepared from 38.5 g. (1.67 mol.) of sodium and 700 ml. of ethanol, was added 520 g. (3.3 mol.) of diethyl malonate followed by 260 g. (1.67 mol.) of β-phenoxyethyl chloride and the reaction mixture was refluxed for six hours. The solvent was evaporated and the residue poured into water. The organic material was taken up in ether, dried over anhydrous sodium sulfate and then fractionated. A fraction boiling at 195~200°C/16 mmHg was collected, being crude diethyl α-(2-phenoxyethyl)-malonate (360 g.), which was refluxed with 1100 ml. of 60% acetic acid containing 85 g. of sulfuric acid. The product was treated according to the literature[2]. The acid was obtained as colorless needles, m. p. 64°C in 65% overall yield.

Found: C, 66.48; H, 6.75. Calcd. for $C_{10}H_{12}O_3$: 66.65; H, 6.71%.

Results and Discussion

Comparison in the Homologous Series.—The ν_{O-H} and the $\nu_{C=O}$ absorption spectra of some compounds are shown in Figs. 1 to 4 and the data obtained by assuming that the band envelopes are expressed by the Lorentz function are given in Table I.

Among the homologs of phenoxyacetic acid, the only compound which shows two ν_{O-H} maxima is phenoxyacetic acid. The band at

* Part II: This Bulletin, 33, 119 (1960).

1) M. Ōki and M. Hirota, *J. Chem. Soc. Japan, Pure Chem. Sec.* (*Nippon Kagaku Zasshi*), **81**, 855 (1960).

2) E. B. Vliet, C. S. Marvel and C. M. Husen, "Organic Syntheses" Col. Vol. 2, John Wiley & Sons, New York (1943), p. 416.

TABLE I. THE ν_{O-H} AND THE $\nu_{C=O}$ ABSORPTION SPECTRA OF VARIOUS CARBOXYLIC ACIDS WITH HYDROGEN-ACCEPTING GROUPS

Compound	ν_{O-H}, cm^{-1}		$\nu_{C=O}$, cm^{-1}		
Phenoxyacetic acid	3526.9	3487.5	1790.6	1762.9	1737.4
β-Phenoxypropionic acid	3531.7	—	—	1760.8	1719.0
γ-Phenoxybutyric acid	3534.2	—	—	1760.0	1715.8
Methoxyacetic acid	3526.7	3450.8	1791.3	1761.3	1730.9
Isopropyloxyacetic acid	3533.6	3437.4	1787.6	1760.8	1731.7
tert-Butoxyacetic acid	3528.0	3424.2	1788.5	1759.3	1733.3
α-Phenoxypropionic acid	3526.3	3475.1	1785.7	1758.7	1731.4
α-Phenoxyisobutyric acid	3526.3	3431.6	1786.1	1754.4	1716.4
Pyruvic acid	—	3430.7	1788.5	—	1725

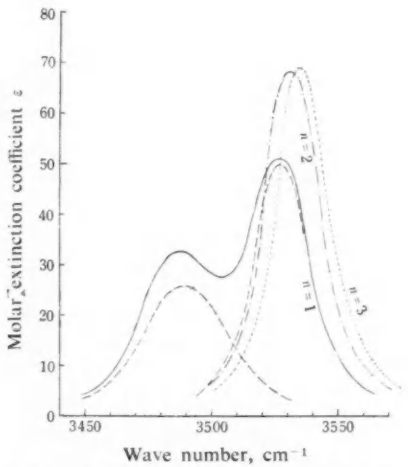

Fig. 1. The ν_{O-H} bands of $C_6H_5O\cdot(CH_2)_nCO_2H$
$n=1$ —— $n=2$ —·— $n=3$ ·····
The curve of phenoxyacetic acid is separated into the two symmetrical absorptions. (– – –)

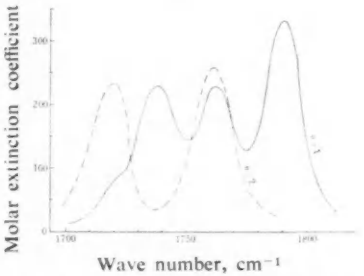

Fig. 2. The $\nu_{C=O}$ absorptions of $C_6H_5O(CH_2)_n\cdot CO_2H$. $n=1$ —— $n=2$ —·—

higher frequency has been assigned to the ν_{O-H} of the monomeric acid, whereas the band at lower frequency has been assigned to the monomeric acid with an intramolecular hydrogen bonding. The higher homologs exhibit one band at ca. 3530 cm^{-1} which can doubtless be assigned to the usual ν_{O-H} mode of monomeric acid. The results are indicative of the absence of hydrogen bonding between the carboxylic hydroxyl group and the oxygen atom of the phenoxyl group in β-phenoxypropionic and γ-phenoxybutyric acids.

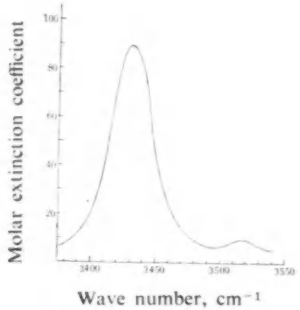

Fig. 3. The ν_{O-H} absorption of pyruvic acid.

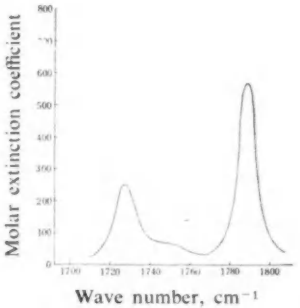

Fig. 4. The $\nu_{C=O}$ absorption of pyruvic acid.

In the carbonyl region, phenoxyacetic acid shows three maxima and a shoulder at ca. 1715 cm^{-1}, while β-phenoxypropionic and γ-phenoxybutyric acids exhibit only two bands. Acetic acid and benzoic acid also possess similar absorptions with the latter two compounds. Comparison of these data together with the study of the change in concentration as described later indicates that the band at about 1760 cm^{-1} is arising from the cis structure of

TABLE II. COMPARISON OF THE SPECTRA OF CARBOXYLIC ACIDS CARRYING α-HYDROGEN ACCEPTING GROUPS WITH THOSE OF THEIR ESTERS

Compound	R	$\nu_{C=O}$, cm^{-1}				
$CH_3COCOOR$	H	1788.5		—		1725
	Ethyl					1733.0
$C_6H_5OCH_2COOR$	H	1790.6		1762.9		1737.4
	Ethyl			1766.8		1739.4
COOR	H	1808.2	1788.9	1758.3		1739.9
COOCH$_3$	Methyl		1780.2		1752.3	
C_6H_5COOR	H	—		1744		1700
	Ethyl					1722.6
CH_3COOR	H	—		1769.3		1714.8
	Ethyl			1754		

a monomeric carboxylic acid illustrated by I, whereas the band at 1790 cm^{-1} must correspond to the trans structure.

The difference ($\Delta\nu_{max}$) of the wave number between the band maxima corresponding to the cis and the trans structures is about 30 cm^{-1} and may be explained in the following way. That is, the peak for the cis isomer shifts to the lower frequency because of the formation of the hydrogen bonding between the carboxylic hydroxyl and carbonyl groups, a non-planar[3] four-membered ring being formed. Although this may be taken as a peculiar phenomenon, a support is found in the accumulated data in this laboratory[4]. None of the phenylacetic, diphenylacetic and triphenylacetic acids show intramolecular interaction between the hydroxyl group and π-electrons, the existence of which is naturally expected from the analogy of *N*-methylphenylacetamide[5]. The absence of the interaction must be interpreted by considering that there is a favorable structure over the intramolecular O–H$\cdots\pi$ interaction, the energy of which is estimated as about 1 kcal./mol. The stabilization may be afforded by the presence of O–H$\cdots$O=C hydrogen bonding in the cis structure of the carboxylic acid.

The homologs of methoxyacetic acid which carries methyl groups show some variation in the $\nu_{C=O}$ absorptions according to the degree of substitution. Although the authors cannot comment precisely on the cause of the variation at the present time, it is probable that the electronic effect of the introduced methyl groups is playing an important role.

Pyruvic acid possesses two peaks at 1788.5 cm^{-1} and 1725 cm^{-1} and a shoulder at 1735 cm^{-1} but the band at 1760 cm^{-1} which is common for the other acids failed to appear. This is reasonable, since the band at 1760 cm^{-1} corresponds to the cis species, the absorption of which in the ν_{O-H} region is negligibly small. The band at the highest frequency is assigned to the free carbonyl group of the carboxyl group which is due to the hydrogen bonding formation between the carboxylic hydroxyl and the α-carbonyl groups. The origin of the two bands at the lower frequencies is determined through the study of concentration effects on the intensities. The band at 1735 cm^{-1} is assigned to the dimeric carboxyl group and the other at 1725 cm^{-1} to the α-carbonyl group.

It is well known that the α-ketocarboxylic acid has the monomer $\nu_{C=O}$ absorption at abnormally high frequency. The phenomenon has been attributed to the inductive and the field effects of the α-keto group. However, it is now evident that pyruvic acid exclusively exists as the trans monomer with the free carbonyl group of the carboxyl group which causes the absorption at the high frequency.

Comparison of the Spectra of the Acids with those of the Esters.—In Table II are listed the $\nu_{C=O}$ spectra of esters together with the corresponding acids. Since the esterification cancels all posibilities of hydrogen bonding, esters of the carboxylic acids which carry the hydrogen accepting group at α-position are expected to be normal when compared with the ordinary esters and this is proved to be the case. None of the esters show $\nu_{C=O}$ band as high as 1790 cm^{-1}.

Ethyl pyruvate shows one somewhat unsymmetrical $\nu_{C=O}$ band at 1733 cm^{-1}, which is believed to be an overlap of the ester and ketone bands. The band intensity is nearly twice that of the normal esters. Ethyl phenoxyacetate possesses two absorptions in the carbonyl region, the intensities being nearly equal. This phenomenon may be attributed to the

3) C. P. Smyth, "Dielectric Behavior and Structure", McGraw-Hill Book Co., Inc., New York (1955), p. 306,
4) H. Iwamura, unpublished work.
5) I. Suzuki, M. Tsuboi and T. Shimanouchi, *Spectrochim. Acta*, **16**, 467 (1960).

TABLE III. THE EFFECT OF THE CONCENTRATION ON THE INTENSITIES OF THE ABSORPTION BANDS OF PHENOXYACETIC ACID

Concentration mol./l.	Intensity of the absorption band: $\nu_{C=O}$ of the trans structure of the monomer (ε_t) at 1790.6 cm^{-1}	$\nu_{C=O}$ of the cis structure of the monomer (ε_t) at 1762.9 cm^{-1}	$\nu_{C=O}$ of the dimer at 1737.4 cm^{-1}	$\varepsilon_t/\varepsilon_c$
0.00092	204	153	281	1.33
0.00046	248	185	252	1.34
0.00023	300	226	221	1.33
0.000058	390	278	185	1.40

existence of the rotational isomers or to some other cause. The decisive comment cannot be made at the present stage.

The Effects of Concentration on the $\nu_{C=O}$ Bands of Phenoxyacetic Acid.—As was already pointed out, phenoxyacetic acid possesses three $\nu_{C=O}$ bands, the intensities of which are measured at various concentrations in carbon tetrachloride. The results are shown in Table III.

It is recognized that the intensities of the bands at 1762.9 cm^{-1} and 1790.6 cm^{-1} increase with the decreasing concentration, while the band at 1737 cm^{-1} decreases on lowering the concentration. These behaviors indicate that two bands at the higher frequencies must be attributed to the monomeric forms of the carboxylic acid and the other at 1737 cm^{-1} to the dimeric form. It is also found that the ratio of the intensities of the bands at 1762.9 cm^{-1} and 1790.6 cm^{-1} is almost constant at the various concentrations. This fact suggests that the equilibrium between the cis and the trans forms is not influenced by the concentration.

TABLE IV. ASSIGNMENT OF THE ν_{O-H} AND THE $\nu_{C=O}$ BANDS OF A CARBOXYLIC ACID WITH AN α-HYDROGEN-ACCEPTING GROUP

Structure	Monomer: Cis structure cm^{-1}	Monomer: Trans structure cm^{-1}	Dimer cm^{-1}
ν_{O-H}	3550～3500	3490～3390	3300～2500
$\nu_{C=O}$	ca. 1760	ca. 1790	1730～1710

Assignment of the Band. — From the above discussion, it is apparent that the bands can be assigned as shown in Table IV.

Summary

The $\nu_{C=O}$ and the ν_{O-H} absorption of carboxylic acids were measured and the following conclusion was obtained; 1) The carboxylic acids carrying a proton-accepting group at α-position give three absorption bands at ca. 1790 cm^{-1}, ca. 1760 cm^{-1} and 1740～1710 cm^{-1}, which can be assigned to the trans form of the monomeric acid, the cis form of the monomeric acid and the dimer, respectively. 2) The $\Delta\nu_{max}$ between the cis and the trans forms can be explained from an intramolecular hydrogen bonding between carboxylic hydroxyl and carbonyl groups.

The authors wish to express their hearty thanks to Professor Y. Urushibara for his encouragement and advice throughout this work. The authors are also indebted to Mr. H. Iwamura and Mr. K. Mutai for their technical assistance.

Department of Chemistry
Faculty of Science
The University of Tokyo
Hongo, Tokyo

Intramolecular Hydrogen Bonding in α-Keto and α-Alkoxycarboxylic Acids. IV[1]. *Electronic Effect in Aryloxyacetic Acids*

By Michinori Ōki and Minoru Hirota

(Received July 26, 1960)

The authors measured[1,2] the O–H stretching (ν_{O-H}) and the C=O stretching ($\nu_{C=O}$) bands of various carboxylic acids and concluded that there is a hydrogen bonding in the acids carrying a hydrogen-accepting group at α-position. The hydrogen bonding is doubtlessly formed between the carboxylic hydroxyl group and the hydrogen-accepting group. Phenoxyacetic acid satisfies the above conditions and is found to exist as "free" and "bonded"[3] species, from the data obtained in O–H stretching and carbonyl regions.

The strength of the hydrogen-accepting power of the oxygen atom in the phenoxyl group may be assumed to be proportional to the electron density on the oxygen atom. Since it is known that Hammett's σ constants and the pK_a values of phenols are in linear relation, it can be seen that the σ constant[4] is a measure of the electron density of the oxygen atom in the aryloxy group. Thus the electron-repelling group will enrich the electron-density on the oxygen atom to be favorable as a hydrogen acceptor and the contrary situation is expected for the electron-attracting group.

The present paper deals with the effect of the substituent in the phenyl group on the ν_{O-H} and the $\nu_{C=O}$ absorptions, thus giving another verification for the existence of a hydrogen bonding between the carboxylic hydroxyl group and the hydrogen-accepting group at α-position.

Experimental

Preparation of the Materials. — Aryloxyacetic acids[5] were prepared in the following way. Equivalent amounts of sodium aryloxide and sodium chloroacetate in water were heated on a water bath for one to two hours. The reaction mixture was acidified and extracted with ether. The ethereal extract was shaken with aqueous sodium bicarbonate and the aqueous layer was acidified. The aryloxyacetic acid was recrystallized from benzene. Those which are not listed in Table I are known compounds and their physical constants agreed with the literature.

Table I. Aryloxyacetic acid ($RC_6H_4OCH_2COOH$)

R	M. p. °C	Analyses C, % Found	C, % Calcd.	H, % Found	H, % Calcd.
m-NO_2	151	48.80	48.74	7.19	7.11
p-Cl*	158.5	51.62	51.47	3.96	3.75
m-CH_3O	119	59.35	59.33	5.41	5.33
p-CH_3O	112	59.48	59.33	5.60	5.33

* Since the melting point (152°C) reported in the literature disagreed with that measured in this work, the purity was checked by elemental analysis.

Measurement and Calculation.—The measurement of the spectra were carried out with a Perkin Elmer 112G grating spectrophotometer. The materials were dissolved in carbon tetrachloride to make up concentration of ca. 0.002 mol./l. for the ν_{O-H} and ca. 0.0005 mol./l. for the $\nu_{C=O}$ measurements[6]. The spectral slit width was 1.0 cm^{-1} for the ν_{O-H} region and 0.6 cm^{-1} for the $\nu_{C=O}$ region. The absorption curves were assumed to be an overlap of the bands which obey the Lorentz function and the half band-widths ($\Delta\nu^a_{1/2}$) and the extinction coefficients (ε^a_{max}) at the maxima were obtained by Ramsay's first method[7]. That is, the approximate absorption maxima, $\Delta\nu^a_{1/2}$'s and ε^a_{max} were obtained by dividing the curves graphically and the characteristic numericals were corrected by the trial and error method.

Results and Discussion

Locations of the absorption maxima and the integrated intensities of the bands of aryloxyacetic acids are summarized in Table II.

1) Part III: M. Ōki and M. Hirota, This Bulletin, **34**, 374 (1961).

2) M. Ōki and M. Hirota, *J. Chem. Soc. Japan, Pure Chem. Sec.* (*Nippon Kagaku Zasshi*), **81**, 855 (1960).

3) Although C. P. Smyth ("Dielectric Behavior and Structure", McGrawHill Book Co, Inc., New York (1955), p. 307) used the name cis and trans for the carboxyl group which has hydrogen atom between the two oxygen atoms and the other of which hydrogen atom is located outside the two oxygen atoms, respectively, "free" and "bonded" are used in this paper because of the nature of situation. However, as pointed out previously (Ref. 1), existence of a hydrogen bonding has been deduced in the cis form. Thus quotation marks are used to distinguish between the situation in this work and purely free form.

4) H. H. Jaffé, *Chem. Revs.*, **53**, 191 (1953).

5) A. Michael, *J. Am. Chem. Soc.*, **9**, 180 (1887).

6) *p*-Nitrophenoxyacetic, *m*-nitrophenoxyacetic and *h*-benzyloxyphenoxyacetic acids were exceptions, of which poor solubility in carbon tetrachloride did not allow to measure at this level of concentration. The measurements of the nitro compounds were run with the saturated solutions.

7) D. A. Ramsay, *J. Am. Chem. Soc.*, **74**, 72 (1952).

TABLE II. THE ν_{O-H} ABSORPTIONS OF SUBSTITUTED PHENOXYACETIC ACIDS

Substituent	σ	ν_f, cm^{-1}	A_f**	ν_b, cm^{-1}	A_b**	$\Delta\nu_{max}$	A_b/A_f	$\log(10 \cdot A_b/A_f)$	Concentration 10^{-3} mol./l.
p-NO_2	0.778	3521.8	—	not found	—	—	—	—	—*
m-NO_2	0.710	3522.3	—	3493.8	—	28.5	0.10	0.00	—*
m-Br	0.391	3522.5	7.59	3484.7	1.48	37.8	0.180	0.255	1.30
p-Br	0.232	3525.1	7.64	3494.0	2.95	31.1	0.386	0.587	0.828
p-Cl	0.227	3524.3	9.77	3492.8	2.58	31.5	0.264	0.422	1.09
m-CH_3O	0.115	3525.7	6.15	3484.0	2.60	41.7	0.426	0.629	1.71
H	0	3526.9	5.57	3487.5	2.69	39.4	0.484	0.685	1.18
m-CH_3	−0.069	3527.5	4.49	3486.7	3.15	40.8	0.698	0.844	1.47
p-CH_3	−0.170	3528.8	4.99	3484.5	3.48	44.3	0.699	0.845	1.60
p-CH_3O	−0.268	3527.7	4.72	3481.3	4.19	46.4	0.886	0.947	1.61
p-$C_6H_5CH_2O$	−0.41	3527.6	—	3482.4	—	45.2	0.993	0.997	—*

* Saturated solution.

** The integrated intensity can be calculated by the equation $A = 2.30 \times \frac{\pi}{2} \frac{1}{Cl} \log_{10}(T_0/T)_{max} \times \Delta\nu^{a}_{1/2}$, because the correction factors[2] are almost unity under the conditions for the measurement.

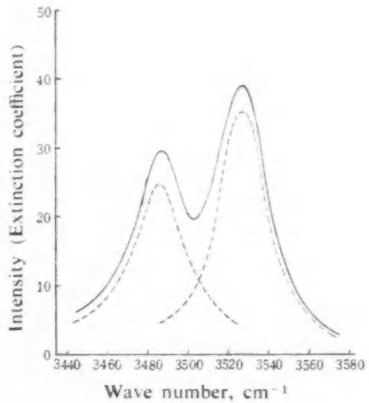

Fig. 1. The ν_{OH} absorption of *m*-methylphenoxyacetic acid.

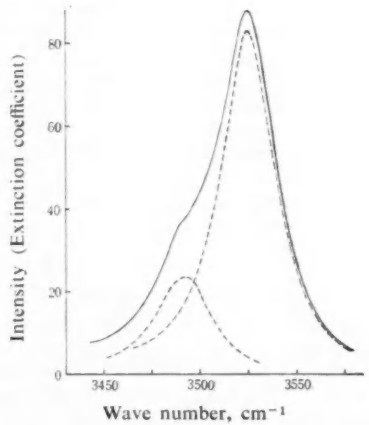

Fig. 2. The ν_{OH} absorption of *p*-chlorophenoxyacetic acid.

The aryloxyacetic acid with a substituent whose σ value is smaller than 0.115 (for meta-methoxyl) shows two apparent maxima, as exemplified by *m*-methylphenoxyacetic acid in Fig. 1. The separation of the two absorption maxima is fairly large. According to the previous paper, the band at ca. 3525 cm^{-1} is assigned to the cis structure (I) and the other at ca. 3490 cm^{-1} to the trans (II). Therefore, it can be said that the electron-repelling groups enhance the contribution of the trans, "bonded" form. If it can be assumed that the larger $\Delta\nu_{max}$ represents the more stabilization, then it is also clear that the aryloxyacetic acids carrying the electron-repelling group forms the more stable hydrogen bonding.

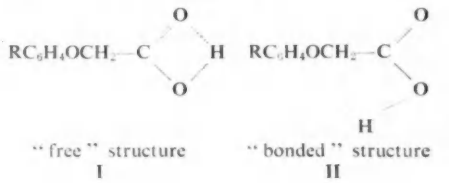

"free" structure I "bonded" structure II

As to the substitution of the electron-attracting group, the aryloxyacetic acids do not show two maxima. *p*-Chlorophenoxyacetic and *p*-bromophenoxyacetic acids possess absorption bands with a peak and a shoulder as shown in Fig. 2, *p*-chlorophenoxyacetic acid being taken as a representative. *m*-Nitrophenoxyacetic acid shows a somewhat unsymmetrical absorption, while *p*-nitrophenoxyacetic acid a nearly symmetrical band. The error caused by the poor solubility of *p*-nitrophenoxyacetic acid prevents the division of the band into two.

The bands at higher and at lower wave numbers are undoubtedly assigned to the "free" and to the "bonded" OH's, respectively, as

reported in the previous paper. Then it is evident that the electron repelling groups favor the "bonded" form and the electron-attracting groups the "free" form.

Since an equilibrium between the "free" and the "bonded" forms is considered to be operative, an equilibrium constant K_h may be expressed by Eq. 1.

$$K_h = \frac{[\text{bonded}]}{[\text{free}]} \tag{1}$$

On the other hand, the concentrations of each of the species are proportional to the intensities of the respective ν_{O-H}, as far as Beer's law is applicable. Therefore, Eq. 1 may be transformed to

$$K_h = a\frac{A_b}{A_f} \tag{2}$$

where A_b and A_f are the integrated intensities due to the "bonded" and the "free" molecules, respectively, and a is a constant pertaining to the magnifying power of the absorption intensity per molecule, when hydrogen bonding is formed. The value "a" is assumed to be equal for the series of compound.

Hammett's σ value is defined as

$$\sigma \equiv \log (K/K_0) \tag{3}$$

where K_0 and K are dissociation constants of benzoic acid and the substituted benzoic acid, respectively. Thus a linear relation is expected between σ value and $\log (A_b/A_f)$ from Eqs. 2 and 3, because σ value is also a measure of the basicity of the oxygen atom in the aryloxyl group. The $\log (A_b/A_f)$ versus σ diagram is shown in Fig. 3 and the relation is linear as expected.

The frequency shift ($\Delta\nu_{max}$) from the "free" molecule to the "bonded" is also plotted against the σ value. The result (Fig. 4) may be considered as linear relation. The larger the the A_b/A_f value, the more is the $\Delta\nu_{max}$. Since it is accepted that the energy of a hydrogen

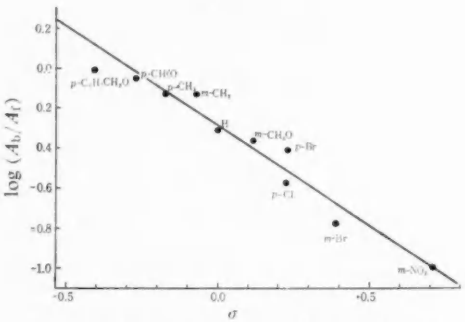

Fig. 3. The relation between the intensity ratio A_b/A_f and the Hammett's substituent constant.

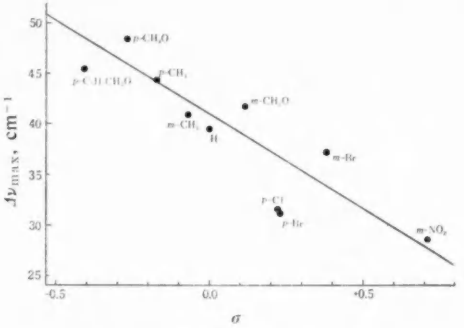

Fig. 4. The relation between the $\Delta\nu_{max}$ and the Hammett's substituent constant.

bonding is proportional to the shift of the the wave number as a rough approximation, this $\Delta\nu_{max}-\sigma$ relation seems to be reasonable.

The measurement was extended to the carbonyl region and the band at 1790 cm^{-1} which is assigned[1] to the "bonded" form and the band at 1790 cm^{-1} which is assigned[1] to the "bonded" form and the other at 1760 cm^{-1} due to the "free" form are also found in every case.

Although these bands are nearly symmetrical, the dimer band at ca. 1730 cm^{-1} always overlaps with these, making it hard to obtain the integrated intensities. $\varepsilon_b/\varepsilon_f$ is obtained in this regard, where ε_b and ε_f are the extinction coefficients of the "bonded" and the "free" molecules at the corresponding peaks. The results are summarized together with other data in Table III. The result indicates that, when the σ value is large with a plus sign, $\varepsilon_b/\varepsilon_f$ is small and agrees with the tendency obtained in the ν_{O-H} measurement.

TABLE III. THE $\nu_{C=O}$ ABSORPTION OF ARYLOXYACETIC ACIDS

Substituent	$\nu_{C=O}$ of the "free" structure	$\nu_{C=O}$ of the "bonded" structure	$\varepsilon_b/\varepsilon_f$
m-NO_2	1768.9	1788.9	1.20
m-Br	1764.2	1789.8	1.19
p-Cl	1763.6	1790.2	1.27
H	1762.9	1790.6	1.37
p-CH_3	1763.0	1791.0	1.55
p-CH_3O	1760.5	1790.4	1.63

The ν_{O-H} band of the dimeric carboxylic acid is known to be a very broad band and is often masked by the ν_{C-H} band. However, the $\nu_{C=O}$ band of the dimetric acid is easily observable and it is known in this measurement that the contribution of the dimer is fairly large even in a dilute solution. From this result, the direct comparison of the absolute

intensities of the bands corresponding to the "free" and the "bonded" forms becomes less significant. Thus, the ratio A_b/A_f or $\varepsilon_b/\varepsilon_f$ is exclusively used for the present discussion. The concentrations of the solutions are also included in Table III, because the contribution of the dimers may insert influence upon other data. The detailed discussion on the effect of concentration will be reported elsewhere in connection with the dissociation constant of the dimer.

Summary

The electronic effect on the hydrogen bonding formation in aryloxyacetic acid was examined. It is found that the electron-repelling groups enhance the band at the lower frequency in O–H stretching region and the band at ca. 1790 cm^{-1}. The result is completely agreeable with the expectation that the electron density on the oxygen atom in the aryloxyl group controls the hydrogen bonding formation.

The authors are grateful to Professor Y. Urushibara for his encouragement throughout this work.

Department of Chemistry
Faculty of Science
The University of Tokyo
Hongo, Tokyo

Stereoregular Polymers. VII.[1] *Infrared Spectra of Isotactic Polystyrene, Isotactic Poly-α, β, β-trideuterostyrene and Isotactic Poly-p-deuterostyrene*[*1]

By Hiroyuki TADOKORO, Yoshiyuki NISHIYAMA,[*2] Shun'ichi NOZAKURA and Shunsuke MURAHASHI

(Received September 12, 1960)

Isotactic polystyrene is a very interesting polymer from the point of view of fine structure and fine texture. Its crystallinity can be varied over wide range, from amorphous to highly crystalline state by heat-treatments, and also a highly oriented sample can be made by hot stretching. We are now studying this substance by use of the X-ray, infrared and density measurements. In this paper we wish to present a report on the results obtained from the changes of infrared spectra with crystallization and the infrared dichroism of isotactic polystyrene (IPS), isotactic poly-α, β, β-trideuterostyrene (IPTDS), $-(-CD_2-\underset{C_6H_5}{CD}-)_p-$ and isotactic poly-*p*-deuterostyrene (IPPDS), $-(CH_2-\underset{D}{\overset{|}{C}}H-)_p-$.

Natta[2] measured the infrared spectra of IPS both at solid and molten states. He showed that the spectrum of IPS at the molten state is similar to that of atactic polystyrene (APS), but did not discuss it further in detail. Liang and Krimm[3] reported the detailed analysis of the infrared spectrum of polystyrene. Their analysis was, however, based only on the commercial ASP, and they have not yet examined the dicroism and the deuteration of this polymer. Deuteropolystyrenes (probably atactic) were prepared by Beachell and Nemphos[4], but the infrared spectra of their products seem not to be published yet.

Samples. — The samples used in this work are IPS, IPTDS and IPPDS polymerized with Ziegler catalyst. The deuterated polymers were prepared according to the following schemes:

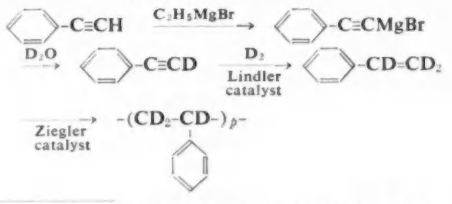

1) Part I of this series, S. Murahashi, S. Nozakura, M. Sumi and K. Hatada, This Bulletin, **32**, 1094 (1959).

*1 Presented at the Annual Meeting of the Society of High Polymer Science in Tokyo, June, 1958, and at the Symposium on High Polymers in Osaka, October, 1958.

*2 Present Address: Tôhô Rayon Co., Ltd., Research Institute, Tokushima.

2) G. Natta, *Makromol. Chem.*, **16**, 213 (1955).

3) C. Y. Liang and S. Krimm, *J. Polymer Sci.*, **27**, 241 (1958).

4) H. C. Beachell and S. P. Nemphos, ibid., **25**, 173 (1957).

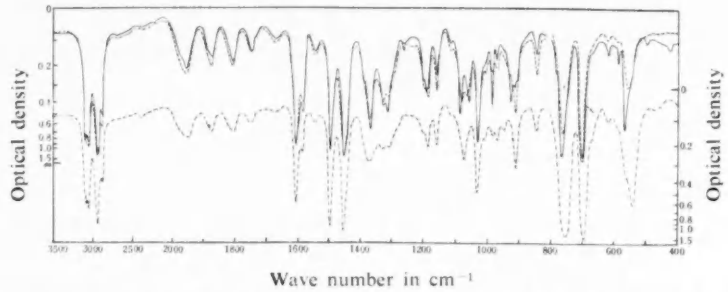

Fig. 1a. Infrared spectra of isotactic polystyrene (—— sample subjected to heat-treatment; - - - - quenched sample) and atactic polystyrene (-·-·-).

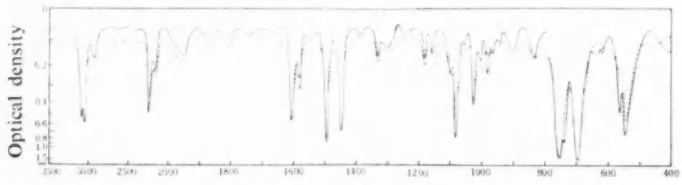

Fig. 1b. Infrared spectra of isotactic poly-α, β, β-trideuterostyrene (—— sample subjected to heat-treatment; - - - - quenched sample).

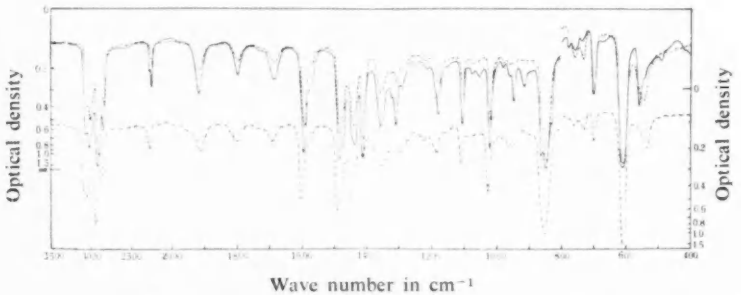

Fig. 1c. Infrared spectra of isotactic poly-*p*-deuterostyrene (—— sample subjected to heat-treatment; - - - - quenched sample) and atactic poly-*p*-deuterostyrene (-·-·-).

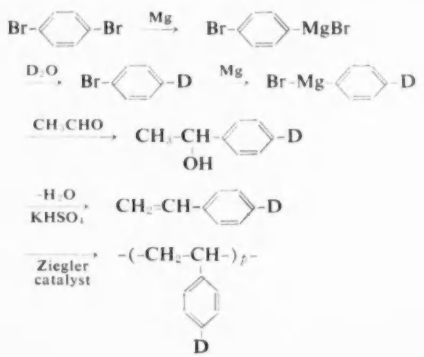

The films for the infrared measurements were cast on a metal plate*3 from toluene solution, and were subjected to one of the following treatments: 1) quenching, 2) heat-treatment after quenching, and 3) elongation and subsequent heat-treatment. The quenched sample was prepared by heating in Wood's alloy at about 240°C*4 for 15~30 sec., and subsequent quenching in cold water. The oriented sample was prepared by stretching very slowly in boiling water, until it could be stretched no more (about 5 times of the original length). Heat-treatment was taken in Wood's alloy at about 180°C for 30 min. The crystallization and the

*3 A glass plate and the surface of water were also used for casting the film.

*4 The melting point of IPS is reported to be 230°C[21].

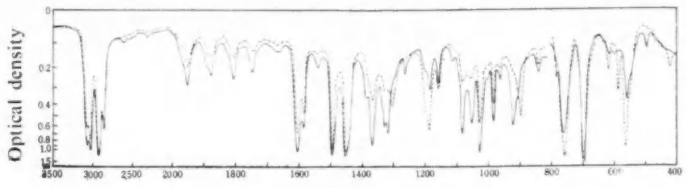

Fig. 2a. Infrared dichroism of isotactic polystyrene: —— electric vector perpendicular to elongation, - - - - electric vector parallel to elongation.

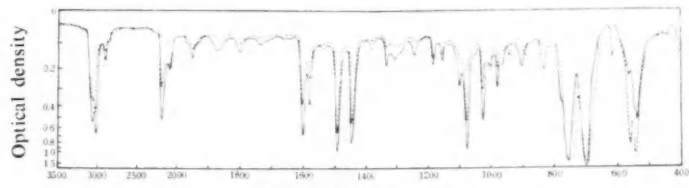

Fig. 2b. Infrared dichroism of isotactic poly-α, β, β-trideuterostyrene: —— electric vector perpendicular to elongation, - - - - electric vector parallel to elongation.

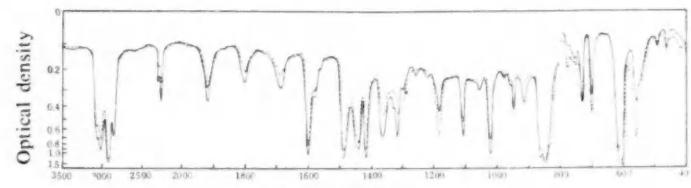

Fig. 2c. Infrared dichroism of isotactic poly-*p*-deuterostyrene: —— electric vector perpendicular to elongation, - - - - electric vector parallel to elongation.

orientation of the samples were confirmed by the X-ray photographs.

Infrared spectra were measured by using a Hitachi Model EPI-2 recording infrared spectrophotometer with sodium chloride and potassium bromide prisms and silver chloride polarizers.

Results and Discussion

Features of the Spectra. — Fig. 1 shows the spectra of IPS (a), IPTDS (b) and IPPDS (c), together with those of atactic samples (lower curve in Figs. 1a and 1c) for reference. In the figures the solid lines are for the samples subjected to heat-treatment and broken lines for the quenched samples. In Fig. 2, polarized infrared spectra of the oriented samples of IPS (a), IPTDS (b) and IPPDS (c) were shown. The solid lines represent transmission with the electric vector perpendicular to the stretching direction, and the broken lines that with the electric vector parallel to the stretching direction. In Figs. 1 and 2, the films used for the absorption measurements with sodium chloride prism are not all the same as those for the measurements with potassium bromide prism. The spectral data and the tentative assignments were also shown in Tables I—III.

As shown in Fig. 1, the spectra exhibit considerable changes with crystallization. The bands at 1364, 1314, 1297 and 1185 cm^{-1} in the spectrum of IPS are very sensitive to crystallization, and have strong dichroic nature. These four bands appear in weak intensity even in the spectrum of quenched samples of IPS, while do not appear in the spectrum of APS. On the other hand, the spectra of IPTDS do not show any bands at these four positions. The band at 1070 cm^{-1} of APS which splits slightly into two bands in the spectrum of the quenched IPS, undergoes large splitting with increase in intensity and sharpness in the spectrum of the crystallized IPS. The resulting two bands are at 1080 and 1048 cm^{-1}, showing strong perpendicular dichroism. The spectrum of the quenched IPS is similar

TABLE Ia. SPECTRAL DATA AND TENTATIVE ASSIGNMENT OF IPS (CRYSTALLIZED)

Frequency in cm^{-1}	Intensity[a]	Dichroism	Tentative assignment[b]
3103	w	⊥	
3082	m	⊥	
3060	s	⊥	$\nu(CH)_{ph}$
3026	s	⊥	
3002	w	⊥	
2924	vs	⊥	$\nu_a(CH_2)$
2849	m		$\nu_s(CH_2)$
1946	w	⊥	
1872	w	⊥	
1801	w	⊥	combination of $\gamma(CH)_{ph}$
1748	w	⊥	
1675	w	⊥	
1602	s	⊥	$\nu(CC)_{ph}$, k (A_1)
1583	m	⊥	$\nu(CC)_{ph}$, l (B_1)
1542	w		
1493	s	⊥	$\nu(CC)_{ph}$, m (A_1)
1452	vs	⊥	$\nu(CC)_{ph}$, n (B_1)
1444	sh		$\delta(CH_2)$
1387	sh	⊥	
1364	s	⊥	associated with helical configuration
1324	m	⊥	
1314	m	⊥	associated with helical configuration
1297	m	∥	associated with helical configuration
1260	w		
1197	sh		
1185	m	∥	associated with helical configuration
1181	w	∥	$\beta(CH)_{ph}$, a (A_1)
1154	w	∥	$\beta(CH)_{ph}$, c (B_1)
1111	w	⊥	
1080	m	⊥	$\beta(CH)_{ph}$, d (B_1)
1048	m	⊥	
1028	s	⊥	$\beta(CH)_{ph}$, b (A_1)
1004	vw	∥	
985	m	⊥	$\gamma(CH)_{ph}$, j (B_2)
965	w		$\gamma(CH)_{ph}$, h (A_2)
920	m	⊥	
906	w		$\gamma(CH)_{ph}$, i (B_2)
898	m	∥	
842	w		$\gamma(CH)_{ph}$, g (A_2)
775	sh	∥	
755	vs	∥	$\gamma(CH_{ph})$, f (B_2)
697	vs		
620	w	∥	
586	m	∥	
566	s	∥	
550	sh		
499	w	⊥	
429	w	∥	

a) vs: very strong, s: strong, m: medium, w: weak, vw: very weak.

b) Whiffen's notations for the vibrational modes of the monosubstituted benzenes were used in this table.
$\nu(CH)_{ph}$: phenyl CH stretching, $\nu(CC)_{ph}$: phenyl CC stretching, $\beta(CH)_{ph}$: phenyl CH in-plane deformation, $\gamma(CH)_{ph}$: phenyl CH out-of-plane deformation, $\nu_a(CH_2)$: CH_2 asymmetric stretching, $\nu_s(CH_2)$: CH_2 symmetric stretching, $\delta(CH_2)$: CH_2 bending.

Table Ib. Spectral changes of polystyrene with crystallization

APS	Quenched IPS	Crystallized IPS	Changes with crystallization
1583 (m)	1583 (m)	1583 (m)	increase intensity
—	—	1444 (sh)	appear
—	—	1387 (sh)	〃
1370 (m)	1367 (s)	1365 (s)	
1328 (m)	1324 (m)	1324 (m)	
1306 (m)	1312 (m)	1314 (m)	increase intensity
—	1297 (vw)	1297 (m)	
—	—	1260 (w)	appear
—	—	1185 (m)	
1070 (m)	1075 (m) 1056 (m)	1080 (m) 1048 (m)	
—	—	985 (s)	
980 (w)	980 (w)	—	
943 (w)	—	—	(APS only)
906 (m)	906 (m)	920 (m) 906 (m) 898 (m)	
—	—	775 (sh)	appear
755 (vs)	755 (s)	755 (vs)	increase intensity
620 (w)	620 (w)	620 (w)	〃
—	590 (w)	586 (m)	〃
557 (sh) 542 (s)	557 (m)	566 (s) 550 (sh)	
—	—	499 (w)	appear
—	—	429 (w)	〃

Table II. Spectral data of IPTDS

Frequency in cm^{-1} a)	Intensity	Dichroism	Changes with crystallzation
3102	w	⊥	
3083	m	⊥	
3058	s	⊥	
3021	s	⊥	
2997	w	⊥	
2910	w	⊥	
2195	s	⊥	
2095	m	(∥)	
1950	w	⊥	
1875	w	⊥	
1805	w	⊥	
1602	s	⊥	
1581	m	⊥	increase intensity
1537	vw	⊥	
1493	s	⊥	
1447	s	⊥	
1385	w	⊥	increase intensity
1328	w	⊥	
1303	w	⊥	
1292	vw(broad)		
1240	w	⊥	
1179	w	∥	
1154	w	⊥	
1100	m	⊥	increase intensity
1077	s	⊥	
1052	vw	⊥	increase intensity
1025	m	⊥	
1006	w	∥	increase intensity
1000	vw	⊥	

TABLE II (Continued)

980	m	⊥	increase intensity
965	w	⊥	
940	w	∥	appear
903	w	⊥	898 cm^{-1} (quenched IPTDS)
891	w	∥	
840	w	⊥	
834	w	⊥	
774	sh	⊥	appear
754	vs	∥	
740	s	∥	appear
697	vs	⊥	
620	w	∥	
562	m	∥	increase intensity
548	s	∥	545 cm^{-1} (quenched IPTDS)

a) Data on the crystallized IPTDS.

TABLE III. SPECTRAL DATA OF IPPDS

Frequency in cm^{-1} a)	Intensity a)	Dichroism	Changes with crystallization
3071	s	⊥	
3024	s	⊥	
2997	sh	⊥	
2925	vs	⊥	
2850	s		
2290	w	⊥	
2264	m	⊥	
1920	m	⊥	
1803	w	⊥	
1689	w	⊥	
1600	s	⊥	
1578	sh	⊥	
1487	s	⊥	
1441	s	⊥	1446 cm^{-1} (quenched IPPDS)
1417	s	⊥	
1363	m	⊥	increase intensity
1355	sh		
1325	vw	⊥	increase intensity
1314	m	⊥	〃
1297	w	∥	〃
1265	w	⊥	appear
1220	w	⊥	
1183	m	∥	increase intensity
1107	m	⊥	
1077			(toluene ?)
1055	w	⊥	appear
1021	s	⊥	
980	w		
960	w		
948	m	∥	increase intensity
915	w	⊥	appear
862	m	⊥	increase intensity
846	vs	⊥	
830	sh	∥	appear
776	w	⊥	
730			(toluene ?)
699	m	∥	
609	vs	⊥	605 cm^{-1} (quenched IPPDS)
560	m	∥	545 cm^{-1} (quenched IPPDS and APPDS)
493	vw	⊥	

a) Data on the crystallized IPPDS.

on the whole to that of APS, but is different on the points that 1) the 1070 cm^{-1} band splits in the quenched IPS and 2) the 542 cm^{-1} band in APS shifts to 557 cm^{-1} in the quenched IPS. These cases may be considered to be the examples that the infrared spectrum indicates the existence of localized regularity in some narrow region, which can be hardly observed from the X-ray photographs. The band at 985 cm^{-1} shows marked change of intensity with heat-treatment.*5 It is an interesting fact that a band which shows behavior similar to this band in the spectrum of IPS (crystallization-sensitive and perpendicular natures) appears also at the same wave number (980 cm^{-1}) in the case of IPTDS. This fact suggests that these bands appear from the similar origins and it would be considered that the bands can be used for the determination of the degree of crystallinity. In the spectra of IPPDS (Figs. 1c and 2c), the band at 948 cm^{-1} is also very sensitive to crystallization, but has parallel dichroism, differing from the 985 cm^{-1} band of IPS. The band which appears at about 906 cm^{-1} in the spectrum of APS as well as the quenched IPS splits with crystallization into two bands, i. e. the perpendicular band at 920 cm^{-1} and the parallel one at 898 cm^{-1} (Fig. 2a). The intensity of the 755 cm^{-1} band increases remarkably with crystallization.

Treatment with Factor Group. — The crystal structure of IPS analyzed by Natta et al.[5] and Bunn et al.[6] belongs to trigonal symmetry class. The molecular chain in the crystalline state has a structure of three-fold screw axis. An infinitely extended molecule of three-fold screw symmetry may be represented by a one-dimensional space group. When the interchain interaction is negligible, it is adequate to consider its factor group $C(2\pi/3)$ shown in Table IV[7]. The symmetry operation, C^1, bringing any structural unit into coincidence with an adjacent unit, consists of a rotation of $2\pi/3$ about the screw axis followed by a translation of 1/3 of the identity period of 6.65 Å along the axis. In the case of this group $C(2\pi/3)$, there appear the species A and E. In species A whole structural units vibrate in the same phase, and the direction of the transition moment is parallel with the screw axis. In species E, the phase of the vibration of a structural unit is different from that of the adjacent structural unit by $2\pi/3$, and consequently the direction of the transition moment is perpendicular to the screw axis. In the cases in which the interaction among the structural units is so strong that the frequencies of the A and the E modes clearly split, these bands should show strong dichroism. On the contrary, in the cases in which the interaction among the structural units is not so strong, and the frequencies of the A and the E modes are nearly equal, both bands, i. e. the parallel band of the species A and the perpendicular band of the species E, superpose in the same location of the spectrum. In this case the dichroism of the more intense component will appear. Which dichroism appears may be decided by the angle between the direction of the transition moment in each structural unit and the screw axis. It should be mentioned here that the vibrational modes, in which the interaction between the neighboring helical molecules is strong, can not be interpreted by the aforementioned method of factor group for a single molecular chain.

TABLE IV. SYMMETRY SPECIES, IRREDUCIBLE REPRESENTATIONS, NUMBER OF NORMAL MODES, AND SELECTION RULES FOR ISOTACTIC POLYSTYRENE UNDER THE GROUP $C(2\pi/3)$

	E	C^1	C^2	Null vib.		n	I. R.	Raman
A	1	1	1	$T_\parallel$	R	46	active ($\parallel$)	active
E	1	ε	ε^2	$T_\perp$		47	active ($\perp$)	active
	1	ε^{-1}	ε^{-2}	$T_\perp$		47		

$\varepsilon = \exp i(2\pi/3)$

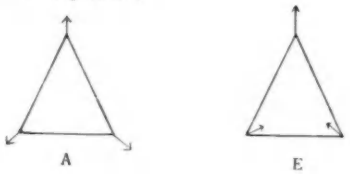

Methylene Group Vibrations.—The CH_2 antisymmetric stretching band at 2924 cm^{-1} shows a distinguished perpendicular nature, which is explainable by the fact that the direction of the transition moment of this vibrational mode of each structural unit is nearly perpendicular to the screw axis. On the other hand, the CH_2 symmetric stretching band at 2849 cm^{-1} shows only very weak dichroism. The direction of the transition moment of this vibrational mode is on the bisector of the angle H–C–H of the methylene group. The angle between this direction and the screw axis is considered to be about 58° from the angle 116° of the C–C–C of the main chain of this polymer estimated by Natta et al.[8]

*5 In the spectra of APS and quenched IPS, a weak band is observed at 980 cm^{-1}.

5) G. Natta and P. Corradini, *Makromol. Chem.*, **16**, 77 (1955).

6) C. W. Bunn and E. R. Howells, *J. Polymer Sci.*, **18**, 307 (1955).

7) A detailed description on the factor group analysis of a helical molecule will be found in C. Y. Liang and S. Krimm, *J. Chem. Phys.*, **25**, 563 (1956).

8) G. Natta and P. Corradini, *J. Polymer Sci.*, **20**, 251 (1956).

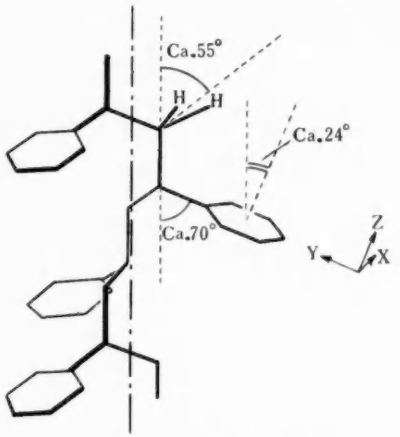

Fig. 3. The molecular structure of isotactic polystyrene in the crystalline state.

(Fig. 3). For perfect uniaxial orientation, the dichroic ratio, R, defined as the ratio of the optical densities with electric vector respectively parallel and perpendicular to the orientation direction, is given by $R=2\cot^2\varphi$, where φ is the angle between the transition moment and the orientation direction. If $\varphi=54°44'$, $R=1$, i. e., the band exhibits no dichroism. The critical angle for $R=1$ is considered to increase only a small amount, when the orientation deviates from the perfect one. For instance, if the transition moments are uniformly distributed in a 20° angular range, the critical angle is 54°54'.[9] Thus the absence of the dichroic nature of the CH_2 symmetric stretching band could be explained, since the aforementioned angle 58° is near this critical angle. These dichroic natures of CH_2 stretching bands are hence considered to be characteristic of the helical structure (alternate sequence of trans and gauche conformations) of isotactic polystyrene. The same feature was found in the case of CD_2 stretching bands of IPTDS (2195 and 2095 cm^{-1}).

In the region of 1400~1100 cm^{-1} the spectra of IPS and IPPDS change remarkably by heat-treatment (crystallization) and show distinguished dichroism as shown in Figs. 1 and 2. On the other hand, the absorption bands of IPTDS in this region which have comparatively weak dichroism, are not affected appreciably by heat-treatment, and are considerably different from those of IPS and IPPDS. The four bands (1364, 1314, 1297 and 1185 cm^{-1}), appearing in weak intensity in the spectra of quenched IPS and IPPDS, increase their intensity with crystallization, while they do not appear in the spectra of APS and APPDS (atactic poly-*p*-deuterostyrene). As these bands are absent in the spectra of IPTDS, these bands are considered to be not directly associated with the vibrations of the phenyl group, but mainly with that of the main chain. These four bands are also supposed to be closely associated with the helical structure of the IPS molecule in crystalline region, the detailed discussions of which we will report in the subsequent paper. On this problem we have briefly reported already.[10]

Phenyl Group In-plane Vibrations.—Now we wish to discuss the vibrational modes associated with the benzene ring. By calculating from the X-ray data of Natta et al.[5], it is estimated that the y and the z axes of the benzene ring shown in the figure in Table V are at an angle of about 70° and about 24° to the screw axis, respectively, and the x axis at an angle of about 14° from the plane normal to the screw axis as shown in Fig. 3.

The vibrations of monosubstituted benzene which has point symmetry of C_{2v} are useful for a step to the assignments of the bands due to phenyl group of polystyrene as studied by Liang et al.[3] in the case of APS previously. On the spectra and the vibrations of monosubstituted benzenes, a number of works have been done by many workers.[11-17] In Table V, we reproduce the symmetry species, the total number of normal vibrations associated with each species, n, and the infrared and the Raman activity to be expected, from the paper by Liang and Krimm[3]. As shown in this table, the transition moment for A_1 species is in the y direction, that for B_1 in the x direction and that for B_2 in the z direction, which is the out-of-plane vibration. We may presume the dichroism of the bands, placing these phenyl groups on the three-fold screw axis. In the cases of A_1 and B_1 species (of C_{2v}), the component E (of $C(2\pi/3)$) must be more intense than the component A and so the dichroism should be perpendicular. On the contrary in the case of species B_2, the component A must be more intense and thus the parallel nature should appear.

The fact that the bands mainly due to the

9) C. Y. Liang and S. Krimm, *J. Chem. Phys.*, **27**, 1437 (1957).

10) H. Tadokoro, S. Nozakura, T. Kitazawa, Y. Yasuhara and S. Murahashi, This Bulletin, **32**, 313 (1959).

11) C. R. Bailey et al., *J. Chem. Soc.*, **1946**, 299.

12) E. K. Plyler, *Discussions Faraday Soc.*, No. **9**, 100 (1950).

13) D. H. Whiffen, *J. Chem. Soc.*, **1956**, 1350.

14) R. R. Randle and D. H. Whiffen, "Molecular Spectroscopy", Institute of Petroleum, London (1955), p. 111.

15) Y. Kakiuchi, *J. Chem. Soc. Japan, Pure Chem. Sec.* (*Nippon Kagaku Zasshi*), **77**, 1591 (1956).

16) Y. Kakiuchi, ibid., **77**, 1839 (1956).

17) D. H. Whiffen, *Spectrochim. Acta*, **7**, 253 (1955).

TABLE V. SYMMETRY SPECIES AND NUMBER OF NORMAL MODES FOR MONOSUBSTITUTED BENZENE[3]

C_{2v}	E	$C_2(y)$	$\sigma(xy)$	$\sigma(yz)$	Null vib.	n	IR	R
A_1	1	1	1	1	T_y	12	a	a
A_2	1	1	−1	−1	R_y	4	f	a
B_1	1	−1	1	−1	T_x, R_z	12	a	a
B_2	1	−1	−1	1	T_z, R_x	8	a	a

f=forbidden a=active

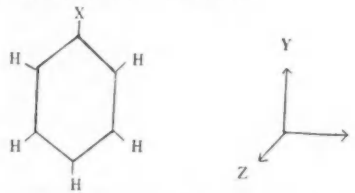

z-Axis is normal to the plane of the benzene ring.

CH stretching modes of phenyl group at about 3000 cm^{-1} show perpendicular dichroism, is in good agreement with the presumption described above, because these bands should belong to A_1 or B_1 symmetry species.

The bands at 1946, 1872, 1801, 1748 and 1675 cm^{-1} (IPS and IPTDS) all show perpendicular dichroism. The similar bands in the spectra of monosubstituted benzenes have been assigned to the binary combinations of the CH out-of-plane deformation vibrations of phenyl group as shown in Table VI by Whiffen[17] and Kakiuchi[16] independently. Liang and Krimm[3] have assigned these bands in the case of polystyrene as shown in the same table. The assignments of these bands to symmetry species A_1 or B_1 by all these authors are in accord with the perpendicular dichroism of the bands. But the assignments of the component fundamental frequencies 906 and 755 cm^{-1} by Liang and Krimm[3] are different from those by Whiffen[17] and Kakiuchi[16]. On this problem more detailed discussion will appear later.

TABLE VI. ASSIGNMENTS OF THE MAIN COMBINATION BANDS IN 2000~1700 cm^{-1} REGION BY LIANG ET AL., WHIFFEN AND KAKIUCHI

Wave number cm^{-1}	Assignments: Liang and Krimm[3]	Assignments: Whiffen[17] and Kakiuchi[16]
1946	$\nu_{17A}(A_2)+\nu_5(B_2)$, B_1	$j(B_2)+h(A_2)$, B_1
1872	$\nu_{17B}(B_2)+\nu_5(B_2)$, A_1	$i(B_2)+h(A_2)$, B_1
1801	$\nu_{10A}(A_2)+\nu_{17A}(A_2)$, A_1	$g(A_2)+h(A_2)$, A_1
1748	$\nu_{10A}(A_2)+\nu_{17B}(B_2)$, B_1	$i(B_2)+g(A_2)$, B_1

Notations of the vibrations in this table are those of Liang et al. and of Whiffen, respectively.

The four bands at 1602, 1583, 1493 and 1452 cm^{-1} (IPS and IPTDS) show perpendicular dichroism, and are not affected appreciably by deuteration. These facts are consistent with the assignments to the in-plane C–C stretching vibrations of phenyl group by Whiffen et al.[13,14] as follows*6.

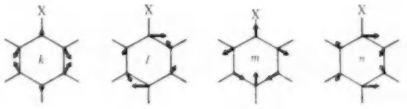

	(A_1)	(B_1)	(A_1)	(B_1)
IPS	1602	1583	1493	1452 cm^{-1}

Liang et al.[3] also have assigned these four bands to the C–C stretching model, except the assignments of 1602 and 1583 cm^{-1} bands (to the l and k modes, respectively).

In the region of 1400~1100 cm^{-1} the hydrogen deformation vibrations (CH_2 wagging and twisting, and CH wagging) of the main chain may couple to some extent with the in-plane vibrations of the benzene ring, showing the complex nature of the spectrum in the case of non-deuterated sample. In the spectrum of IPTDS the bands due to the vibrations of the deuterium of the main chain would shift to lower frequency region, and thus the aforementioned coupling may be removed. Accordingly the bands in this region may be considered to be mainly due to the vibrational modes of the benzene ring in the case of IPTDS. Thus the 1179 and 1154 cm^{-1} bands of IPTDS may be assigned to the a and c modes of monosubstituted benzene according to the Whiffen's notation.[9] It is difficult to settle the assignments of the 1328 and 1240 cm^{-1} bands from the present data.

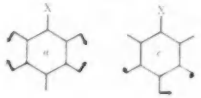

	(A_1)	(B_1)
IPS	1185	1158 cm^{-1}
IPTDS	1179	1154

The 1070 cm^{-1} band (APS) may be assigned to the d(ν_{18B})(B_1) mode. The splitting of this band in the case of IPS may be explained by the intramolecular interaction. The 1028 cm^{-1} band may be assigned to the b (ν_{18A})(A_1) mode, as Whiffen and Liang et al. assigned.

*6 In this paper the notation of the vibrational modes of the monosubstituted benzene by Whiffen (shown with h, j, ···) will be mainly used for convenience, but those by Liang and Krimm (ν_{10A}, ν_{17A}, ···) will also be added if necessary.

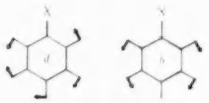

	(B_1)	(A_1)
IPS	1080, 1048	1028 cm^{-1}
APS	1070	1028

The 1183, 1107 and 1021 cm^{-1} bands of IPPDS are considered to be the following CH in-plane modes, as Whiffen[14] and Ingold[11] assigned in the cases of *p*-substituted benzenes.

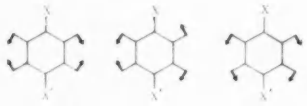

	(A_1)	(B_1)	(A_1)
IPPDS	1183	1107	1021 cm^{-1}
PPMS	1184	1110	1017

Here we have shown the data of poly-*p*-methylstyrene (PPMS) from our paper[10] for reference. The vibrational modes of the 1185 and 1028 cm^{-1} band of IPS are the same with those of the 1183 and 1021 cm^{-1} bands of IPPDS (and of the 1184 and 1017 cm^{-1} band of PPMS) respectively. In the cases of these two vibrational modes the hydrogen atom of the *p*-position does not move significantly. Thus, the experimental fact that the substitution of the *p*-hydrogen atom with deuterium or methyl group does not affect these two bands appreciably may be reasonably explained. The 1106 cm^{-1} band of IPPDS and the 1110 cm^{-1} of PPMS are supposed to be characteristic of the *p*-substituted benzenes. It is natural that the bands which correspond to the c and d modes of IPS do not appear in the spectra of IPPDS and PPMS, since these modes contain the displacement of *p*-hydrogen atom.

Phenyl Group Out-of-plane Vibrations. — As mentioned in the previous section, the assignments of the two bands at 906 and 755 cm^{-1} by Liang et al. are different from other authors (Whiffen[13] and Kakiuchi[16]), although the assignments of the other three bands (985, 965 and 842 cm^{-1}) in this region by all these authors are the same. They assigned these bands as shown in Table VII. The crystallization-sensitive 985 cm^{-1} band may be assigned to the j mode by considering the position. The 906 cm^{-1} band which splits into two bands of different polarizations with crystallization is assigned to the ν_{17B} vibration by Liang et al., while the band at 908±10 cm^{-1} of monosubstituted benzenes was assigned to the i mode by Whiffen. Kakiuchi has calculated the frequency of this i mode to be 897 cm^{-1} assuming the mass of the substituent atom to be infinite, and has made the similar assignment as Whiffen's. On the other hand, Liang and Krimm have assigned the 755 cm^{-1} band to this i mode. The 755 cm^{-1} band (the 751± 15 cm^{-1} band of monosubstituted benzene) was assigned to the f mode known as the "umbrella" vibrational mode by Whiffen. Kakiuchi has calculated the frequency of this mode to be 716 cm^{-1}, and has made similar assignment. To this f vibrational mode, Liang and Krimm have assigned the band at 700 cm^{-1}. Although it is difficult to decide which

TABLE VII. CH OUT-OF-PLANE VIBRATIONS OF IPS

IPS				Monosubstituted benzene			
Frequency in cm^{-1}	Intensity	Dichroism	Average frequency and intensity (Whiffen)		Vibrational mode (sym. species) (Whiffen)	Calculated frequency (Kakiuchi)	Polystyrene (Liang et al.)
985	m	⊥	982±6	vw	j(B_2)	1004	$\nu_5 \fallingdotseq$ j
965	w	⊥	962±6	w	h(A_2)	984	$\nu_{17A} \fallingdotseq$ h
906 { 920	m	⊥	908±10	mw	i(B_2)	897	ν_{17B}[a]
906 { 898	m	∥					
842	w	⊥	837±10	w	g(A_2)	837	$\nu_{10A} \fallingdotseq$ g
760	vs	∥	751±15	vvs	f(B_2)	716	$\nu_{10B} \fallingdotseq$ i
700	vs	—	697±11	vs	v(B_2)	—	$\nu_{11} \fallingdotseq$ f

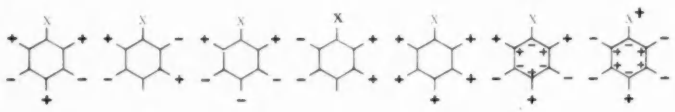

j h i g f v ν_{17B}

a) No vibrational mode which corresponds to the ν_{17B} of Liang and Krimm's notation is in Whiffen's assignment.

TABLE VIII. CH OUT-OF-PLANE VIBRATIONS OF IPPDS

IPPDS			*p*-Deuterotoluene(Kakiuchi[18])		
			Frequency in cm^{-1}		Vibrational mode
Frequency in cm^{-1}	Intensity	Dichroism	Calculated	Assigned	
960	w	—	984	951	e
948	m	∥	963	944	c
846	vs	⊥	837	840	d
			835	838	b
609	vs	⊥	630	607	a

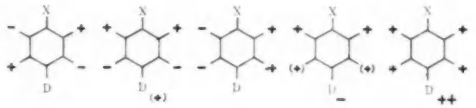

e c d b a

assignment we should accept for polystyrene, it seems to be more favorable to apply Kakiuchi's assignment for this case, because of the agreement of the calculated value with the observed. Here we should mention the unexplainable dichroism of the 985 and 906 cm^{-1} bands, which are expected to have parallel dichroism because of their symmetry species B_2. These complexities of the bands sensitive to crystallization, would have occurred from the interaction between the molecules in the crystalline lattice and could not be explained by the treatment on a single helical chain, which is a first approximation for the interpretation of the spectra of crystalline polystyrene.

The assignment of the CH out-of-plane vibrations of IPPDS can be made as shown in Table VIII on the basis of the work on *p*-deuterotoluene by Kakiuchi. Although the vibrational mode assigned to the 948 cm^{-1} band of IPPDS is similar to that of the 983 cm^{-1} band of IPS, the dichroisms of these two bands are different from each other, as described in the previous section. This difference may be explained by the change of the nature of the interaction between the molecular chains in the crystalline lattice owing to the deuteration of the *p*-position.

For detailed interpretation of the spectrum and the elucidation of the nature of intermolecular interaction in crystalline region, further accumulation of the experimental data is going on.

The authors express their sincere thanks to Professor T. Shimanouchi and Dr. M. Tsuboi of the University of Tokyo for helpful discussions and the measurements of parts of spectra by use of the Perkin-Elmer 112G spectrophotometer.

Department of Polymer Science
Faculty of Science
Osaka University
Nakanoshima, Osaka

18) Private communication.

An X-ray Study on the Phase Transition of Aniline Hydrobromide, $C_6H_5NH_3Br$

By Inao TAGUCHI*

(Received August 1, 1960)

Crystal structures of amine halides can be divided into two groups. To the first group belong methylammonium chloride[1] and *n*-propylammonium halides[2], in which the nitrogen atoms are surrounded by four halogen atoms. To the second group belong adenine hydrochloride[3], hexamethylenediamine dihalides[4], aniline hydrochloride[5] and cyclohexamine hydrochloride[6], in which the nitrogen atoms are surrounded by three halogen atoms. It is interesting to note that those crystals belonging to the first group always exhibit a phase transition at low temperature, whereas no report has ever been made of any phase transition in crystals belonging to the second group.

A preliminary report on the crystal structure of aniline hydrobromide, $C_6H_5NH_3Br$, has been published[7], in which it was shown that the nitrogen atom in this crystal is surrounded by four bromine atoms. During the course of refinement, it was found that the crystal exhibits a peculiar type of phase transition in the neighbourhood of room temperature. Detailed structure analyses of the crystal below and above the transition temperature will soon be reported[8]. In the present paper, an account of an X-ray study on the phase transition of aniline hydrobromide will be given.

Outline of the Phase Transition. — Large crystals of aniline hydrobromide in the form described by Groth[9] are easily obtained by evaporation from methanol, ethanol or acetic acid solutions. Preliminary X-ray examinations showed that most of these crystals contained stacking disorder as revealed by diffuse scattering. Crystals free from stacking disorder were found to be obtainable by slow evaporation from methanol solutions. The crystals obtained are long along the [010] axis, and the planes (001) and (100) are predominant. A sharp cleavage is found parallel with (001).

Using these 'single crystals', a series of oscillation and Weissenberg photographs were prepared, using Cu K radiations, about the three principal axes. It was found that not all but many reflections are split into two closely separated spots, appearing more or less blurred. If we ignore these splittings, all the reflections could be indexed based on an orthorhombic unit cell, in accord with the axial ratios given by Groth. It is suggested that these crystals are not really single crystals, but that they consist of repeated twins or polysynthetic twins[10], such as are found in orthorhombic pyroxene[11]. All the reflections appearing on oscillation photographs are split into two along the same ζ-lines, except those of $(hk0)$ and $(00l)$. These can be interpreted, if we assume that the twin components or domains are oriented to two different directions, and that each domain is in fact monoclinic with an axial angle β slightly deviated from 90°, and that all the domains have their b- and c-axes in common directions. All the reflections appearing on oscillation and Weissenberg photographs were satisfactorily indexed without any ambiguity by two axial systems, as schematically shown in Fig. 1.

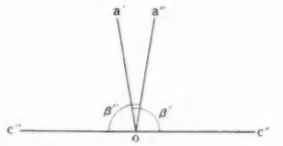

Fig. 1. Schematic representation of the orientations of the principal axes of the two components of the domains.

It was noticed that Weissenberg photographs prepared at different seasons of the year, using one and the same crystal, showed differences in detail. We were led to an assumption that these differences might be caused by a slight

* Deceased, May, 26 1959.

1) E. W. Hughes and W. N. Lipscomb, *J. Am. Chem. Soc.*, **63**, 1737 (1946).
2) M. V. King and W. N. Lipscomb, *Acta Cryst.*, **3**, 222, 227 (1950).
3) W. Cochran, ibid., **4**, 81 (1951).
4) W. P. Binne and J. M. Robertson, ibid., **2**, 180, 116 (1949).
5) C. J. Brown, ibid., **2**, 228 (1949).
6) A. Shimada, Y. Okaya and I. Nitta, ibid., **8**, 819 (1955).
7) I. Nitta, T. Watanabé and I. Taguchi, *X-rays*, **5**, 31 (1948).
8) I. Nitta, T. Watanabé and I. Taguchi, to be published in this Bulletin.
9) P. Groth, "Chemische Krystallographie" IV, (1917) p. 170.
10) I. Ito, "X-ray Studies on Polymorphism", (1950) p. 122.
11) T. Ito, *Z. Krist.*, **90**, 151 (1935).

variation of temperature. A series of Weissenberg photographs were taken at various temperatures, using a carefully designed temperature control camera[12], and confirmed the fact that they are really sensitive to temperature in the neighborhood of room temperature. Split reflections observed at 18°C became degenerated into a single one at 25°C, and blurred reflections at 18°C became more or less distinct. These changes were more marked at 50°C. From these observations, it was concluded that the crystal would undergo a phase transition in this temperature range, the splitting and blurring of reflections being associated with the formation of domains. The crystal does not shutter on passing the transition range.

Variation of the Axial Angle β with Temperature. — From the preliminary experiments stated in the preceding paragraphs, it became clear that the splitting distances of reflections depend upon temperature, implying that the axial angle β varies gradually with temperature. The variation of the axial angle β with temperature was determined from the splitting distances of the reflection (002), which is the largest and most intense. The results are shown in Fig. 2. It was also found that the

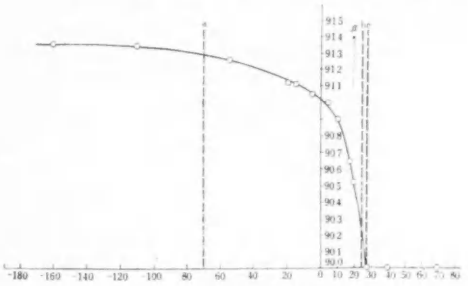

Fig. 2. Variation of the axial angle β with temperature.

relative intensities of reflections vary with temperature, parallel with the variation of β with temperature. The intensity variation ceases practically outside the range from +30°C to −70°C. The axial angle β also remains unchanged outside this region. There was found to be no other phase transition down to −160°C as far as X-ray methods were employed.

The temperature variations of the axial angle β, of the relative intensities and of the fine structure of reflections were found to be reversible. Photographs taken after cooling or heating are practically the same as those taken before heat treatment.

12) I. Taguchi, *Annual Report Inst. Fiber Research, Osaka Univ.*, **8**, 45 (1954).

Now, in order to investigate the variation of the axial angle β with temperature more precisely and to determine the transition temperature of the high temperature side, experiments at smaller temperature intervals were carried out at temperatures, ranging from 15°C to 30°C. Measurements for cooling were made after keeping the temperature of the crystal at 30°C for twenty hours. The results are shown in Fig. 3, where crosses and small circles are the values obtained for heating and cooling respectively. From all the observations and results obtained therefrom the following conclusions are made. (1) The transition temperature range is as wide as 100°C, i. e., from 27.5°C to ca. −70°C. (2) The phase change is perfectly reversible within the experimental error. (3) The phase transition is of a higher order. It was suggested that the specific heat curve would show the λ type anomaly. The temperature range between −40°C and 24.5°C, as is shown by dotted lines a and b, might correspond to the ascending part of the specific heat curve, and the range between 24.5°C and 27.5°C as is shown by curves b and c might correspond to the declining part of the same curve. This view was recently verified by a calorimetric measurement[13].

The Unit Cell Dimensions and Space Groups of the High and Low Temperature Modifications. —Above 27.5°C, the crystal is orthorhombic, and below this temperature it is monoclinic. The unit cell dimensions and space groups of the two modifications, determined at 70°C and at −110°C, respectively, are given in Table I. There are four formula units in each unit cell.

TABLE I. THE UNIT CELL DIMENSIONS AND SPACE GROUPS OF THE HIGH AND LOW TEMPERATURE MODIFICATIONS

	70°C	−110°C
a	16.77±0.06 Å	16.725±0.06 Å
b	6.05±0.03	5.95 ±0.03
c	6.86±0.03	6.81 ±0.03
β	90°	91°22′
Space group	D_{2h}^{10}-Pnaa	C_{2h}^{5}-$P2_1/a$

Nature of the Domain Structure.—It was found that the axis [010] and the plane (001) are in common with the two modifications and remain unaltered on passing the transition temperature. These features are illustrated schematically in Fig. 4. Since there are no appreciable changes in the axial parameters, the change of the axes can be taken as a kind of shear, which can be expressed by $\Delta\beta$ as is shown in Fig. 4.

13) H. Suga, This Bulletin, **34**, 426 (1961).

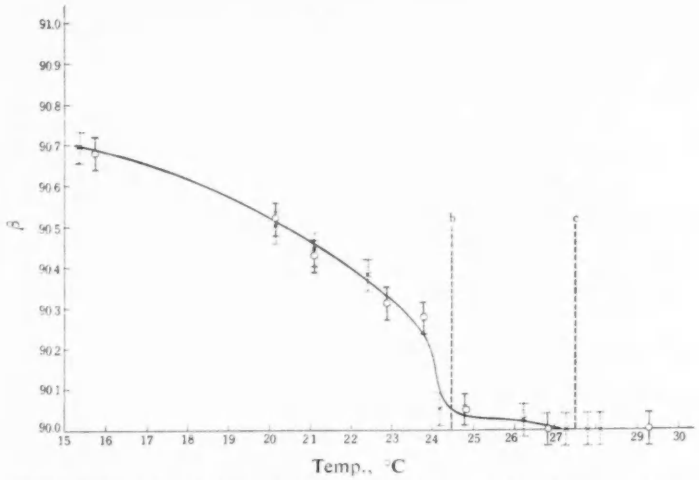

Fig. 3. Details of the variation of the axial angle β with temperature.
○: heating ×: cooling

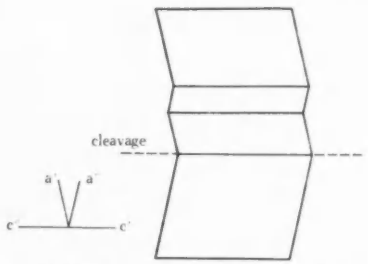

Fig. 4. Cleavage planes and the domain structure.

Below the transition temperature, the crystal is built up by domains which are oriented to the two directions, as shown in Fig. 4. These domains can be seen under a polarized microscope in certain specimens[14].

It was found that the ratios of the intensities within a pair of split reflections vary from specimen to specimen. For numerous specimens these ratios are found to be nearly at unity, as the formation of the two orientations of the domains is expected to occur with equal probability, though we have once found a specimen which is made of nearly a single domain.

Quite independent of these intensity ratios, or the abundance of the two orientations of the domains, each of a pair of split reflections shows a similar fine structure. There were found no complementary features in intensity in these split reflections, suggesting that these domains are interpenetrated.

On passing the transition temperature, no line broadening was ever found. This is in contrast to the observations reported for cobalt oxide[15], CoO, or potassium dihydrogen phosphate[16], KH_2PO_4. Thus the lower limit of the size of domains is of the order of 10^{-6} cm. No diffuse scattering associated with the splitted reflections was found, hence the domains are distributed in such a way that they are incoherent to X-ray. In this connection, it must be mentioned that in the cases of ferroelectric crystals there has never been reported any polysynthetic twinning associated with the domain formation.

As stated earlier, the (001) plane gives a perfect cleavage. The (100) plane also gives a cleavage at low temperature. It was observed that this latter cleavage becomes poorer as temperature increases, and finally vanishes at 30°C. This cleavage plane is the twinning plane between the two adjacent domains, as shown in Fig. 4. The vanishing of cleavage can be taken as a measure of the coalescence of the domain structure.

The Mechanism of the Phase Transition.—It will be interesting to discuss the structural change taking place during the transformation from symmetry considerations. There are four formula units in the unit cell, both of the high and low temperature modifications. The space group, D_{2h}^{16}–Pnaa, to which the high temperature modification belongs, requires that the anilinium ion, or more precisely the axis of anilinium ion passing through $N{-}C_1\cdots\cdots C_4$ atoms, should lie on a digonal axis. This

14) T. Iwai, to be published.

15) S. Greenwald, *Acta Cryst.*, **6**, 396 (1953).

16) A. R. Ubbelohde and I. Woodward, *Proc. Roy. Soc.*, **A188**, 358 (1947).

implies that the three hydrogen atoms bound to the nitrogen atom are arranged in a statistical way so that the anilinium ion assumes a digonal symmetry in a statistical sense. In the low temperature modification, the anilinium ion is no more restricted by the digonal symmetry by virtue of the low symmetry of the crystal, C_{2h}^5-$P2_1/a$. Above the transition temperature, the $-NH_3^+$ group assumes two (or a multiple of two) equally stable orientations with respect to the C–N bond, or it may be flipping among different orientations. When the crystal is cooled down and passes the transition temperature, all the atoms move onto new equilibrium positions and the flipping ceases. These will be the most essential features of this phase transition.

The author would like to express his sincere thanks to Professors I. Nitta and T. Watanabé for their continued interest, and to Dr. Suga for valuable discussions.

Department of Chemistry
Faculty of Science
Osaka University
Nakanoshima, Osaka

The Effect of Alcohols on the Solubilization of Oleic Acid in the Aqueous Solution of Sodium Dodecyl Sulfate

By Ryohei MATUURA, Kazuo FURUDATE, Hidetoshi TSUTSUMI and Seido MIIDA

(Received July 14, 1960)

It may well be established that the solubilizing power of the detergent towards hydrocarbons, such as *n*-heptane[1] and benzene[2], increases by adding alcohols in the detergent solution, the more markedly the longer the hydrocarbon chains of the added alcohols are. The solubilization of polar materials in the presence of alcohols in the detergent solution, however, has not been known well. Kolthoff and Graydon[3] studied the effect of *n*-amyl alcohol and *n*-octyl alcohol on the solubilization of some dyes in the potassium soap solutions and found no such regular and simple relations as for nonpolar substances. Some other studies also reported the complicated nature of the solubilization of polar materials in the presence of additives[4]. In order to make the situation clearer we have investigated the effect of various alcohols on the solubilization of oleic acid in the aqueous solution of sodium dodecyl sulfate.

Experimental

Materials.—Sodium dodecyl sulfate (SDS) used was synthesized from fractionally distilled *n*-dodecyl alcohol and purified by repeated ether extraction. Its purity was confirmed by elementary analysis and surface tension measurements. The alcohols used were purified by distillation and their boiling points were as follows: *n*-butyl alcohol (117°C), *n*-hexyl alcohol (157°C), *n*-amyl alcohol (137.5~138.5°C), *iso*-amyl alcohol (132°C), *n*-octyl alcohol (194°C), *n*-dodecyl alcohol (127°C/7 mmHg) and *n*-hexadecyl alcohol (190°C/15 mmHg). Oleic acid was obtained by distillation at 211°C/6 mmHg.

Method.—The solubilization end point was measured by the turbidity method using a Shimadzu AKA photoelectric nephelometer. The experiment was performed at a constant temperature of 25.0°C.

Results

In Fig. 1 the amount of oleic acid solubilized in the aqueous solution of SDS is plotted against the concentration of the latter. An almost linear relationship has been obtained. When an alcohol is added to the detergent solution beforehand, the solubilization of oleic acid decreases as shown in Figs. 2, 3 and 4 for the case of *n*-butyl, *n*-hexyl and *n*-hexadecyl alcohol, respectively. In Fig. 5 the amount of oleic acid solubilized is plotted against the amount of alcohols added to the detergent solution of 0.05 mol./l. It is seen that the solubilization of oleic acid decreases monotonously as the amount of alcohols added increases and this effect of decreasing the solubilization of oleic acid increases as the chain length of the alcohol increases.

1) H. B. Klevens, *J. Am. Chem. Soc.*, **72**, 3780 (1950).
2) K. Shinoda and H. Akamatsu, This Bulletin, **31**, 497 (1958).
3) I. M. Kolthoff and W. F. Graydon, *J. Phys. Chem.*, **55**, 699 (1951).
4) M. E. L. McBain and E. Hutchinson, "Solubilization", Academic Press Inc., New York (1955), p. 85.

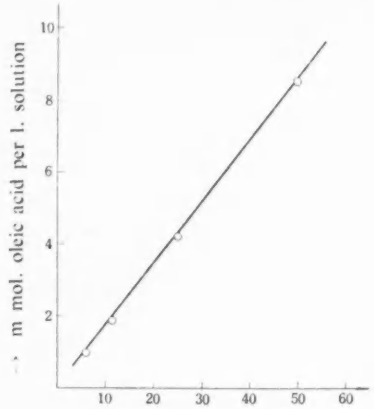

Fig. 1. The relation between the solubilized amount of oleic acid and the concentration of SDS.

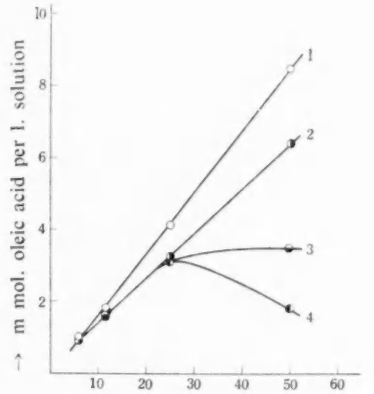

Fig. 2. The relation between the solubilized amount of oleic acid and the concentration of SDS containing *n*-butyl alcohol. Mol. SDS: mol. alcohol is 1, 1 : 0; 2, 1 : 1; 3, 1 : 2; 4, 1 : 3.

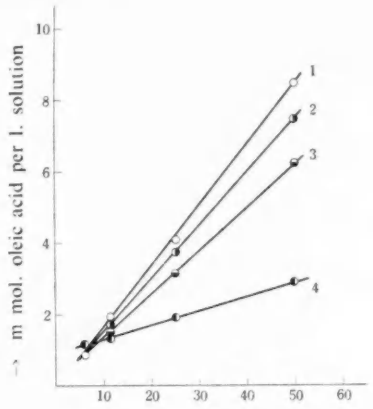

Fig. 3. The relation between the solubilized amount of oleic acid and the concentration of SDS containing *n*-hexyl alcohol. Mol. SDS: mol. alcohol is 1, 1 : 0; 2, 1 : 0.2; 3, 1 : 0.4; 4, 1 : 0.8.

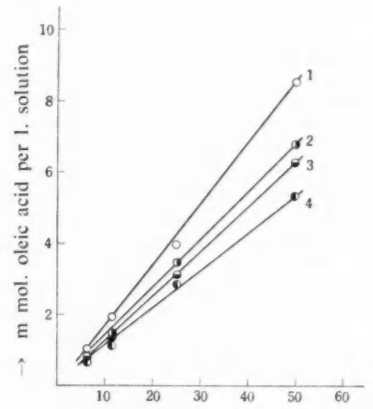

Fig. 4. The relation between the solubilized amount of oleic acid and the concentration of SDS containing *n*-hexadecyl alcohol. Mol. SDS: mol. alcohol is 1, 1 : 0; 2, 1 : 0.0081; 3, 1 : 0.0168; 4, 1 : 0.0276.

Discussion

It may be a general agreement that alcohols added can cause a decrease in cmc of the detergent solution and an increase in micelle volume by penetration into the micelle surface. In the case of SDS solutions, Hutchinson et al.[5] measured the cmc in the presence of *n*-hexyl, *n*-heptyl and *n*-octyl alcohols and found that the cmc decreases as the amount of alcohols added increases. When hydrocarbon is solubilized in the detergent solution in the presence of alcohols, therefore, it is evident that its solubilization increases as the amount of alcohols added increases, since hydrocarbon is considered to dissolve in the micelle interior which has been made larger by the presence of alcohols. A typical example of the solubilization of hydrocarbon in the detergent solution in the presence of alcohols may be given by the result obtained by Klevens[1], which is reproduced in Fig. 6. This shows

5) E. Hutchinson, A. Inaba and L. G. Bailey, *Z. phys. Chem., N. F.*, **5**, 344 (1955).

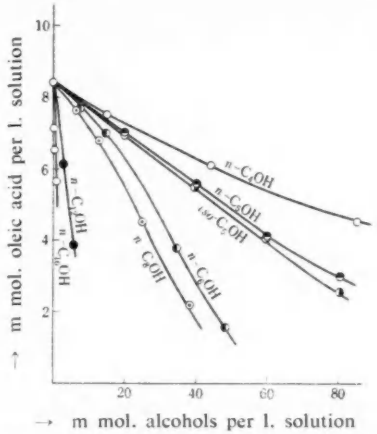

Fig. 5. The Effect of alcohols on the solubilization of oleic acid in 0.05 M SDS solution.

the effect of alcohols on the solubilization of *n*-heptane in the aqueous solution of potassium tetradecanoate. It is clearly seen that the solubilized amount of *n*-heptane increases as the amount of added alcohols increases and that the effect of alcohols to increase the solubilization of the hydrocarbon increases with the chain length of the alcohols. The result shown in Fig. 6 is quite contrary to the result obtained in the present experiment which is shown in Fig. 5. The solubilized amount of oleic acid decreases as the amount of alcohols added increases, the more markedly the longer the hydrocarbon chain of the alcohols is. It will be reasonable to ascribe this difference to the fact that hydrocarbon dissolves in the micelle interior, while polar materials, such as oleic acid in the present experiment, dissolve in the palisade layer of the micelle. Since alcohols also dissolve in the palisade layer, oleic acid will be hindered from dissolving in the same place by already existing alcohol molecules, the result being that the solubilization of oleic acid decreases as the amount of alcohols increases in the detergent solution, as shown in Fig. 5.

In connection with the above explanation it may be interesting to note the effect of electrolytes on the solubilization of nonpolar and polar materials in the detergent solution. Klevens[6] studied the solubilization of *n*-heptane and *n*-octyl alcohol in the aqueous solution of potassium myristate in the presence of potassium chloride, potassium sulfate and potassium ferrocyanate. He found that the solubility of *n*-octyl alcohol decreases, while that of *n*-heptane increases, with the increasing electrolyte concentration in the detergent solution. Klevens explained this difference as follows. The increased aggregation of the micelles in the presence of electrolytes results in an increase in micelle interior volume which is available to a nonpolar solute, butre sults in a decrease in the micellar area which is available for penetration by a polar solute. Richards and McBain[7] also report that the presence of sodium chloride and potassium chloride decreases the solubilizing power of cetyl pyridinium chloride towards polar materials such as *n*-octyl alcohol and benzaldehyde, but increases that towards nonpolar materials such as benzene and *n*-octane. These results

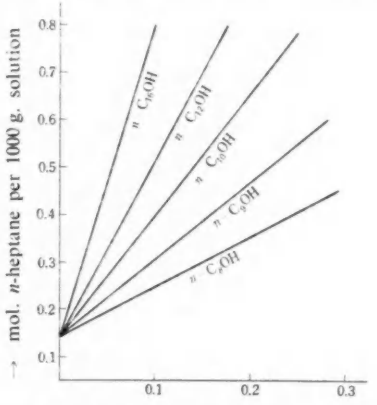

Fig. 6. The Effect of alcohols on the solubilization of *n*-heptane in 0.35 M K tetradecanoate solution (reproduced from Kleven's paper[1]).

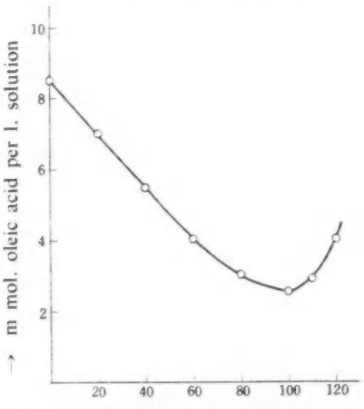

Fig. 7. The Effect of *n*-amyl alcohol on the solubilization of oleic acid in 0.05 M SDS solution.

6) H. B. Klevens, *J. Am. Chem. Soc.*, **72**, 3780 (1950).
7) R. H. Richards and J. W. McBain, ibid., **70**, 1338 (1948).

conform in their behaviors to the result obtained in the present experiment, the same explanation being applied, although the additives are electrolytes in the former and alcohols in the latter experiments.

It is to be noted that the concentration of alcohols in the detergent solution shown in Fig. 5 is not so great as that in Fig. 6. We found that, in the case of *n*-butyl and *n*-amyl alcohol, when the amount of alcohols in the detergent solution becomes greater than that shown in Fig. 5 the solubilization of oleic acid turns out to increase with the concentration of the alcohols in the detergent solution. The case of *n*-amyl alcohol is shown in Fig. 7. Since these alcohols are fairly soluble in water, the solvent property of water will alter as the amount of the alcohol in it becomes greater, the result being that the solubility of oleic acid in the solvent liquid will become appreciable. Also it may be probable that the micelle-forming property of the detergent is lessened by the presence of water soluble alcohols in fairly large concentrations, the result being that the solubilization of oleic acid in the detergent micelle will decrease. These two factors counteract each other in the determination of solubility of oleic acid in the detergent plus alcohol solutions. We see in Fig. 2 that the solubilization of oleic acid decreases when the concentration of the detergent containing *n*-butyl alcohol (mole ratio 1 : 3) exceeds a certain value. This may be attributed to the predomination of the factor of lessening the solubilization in the detergent micelle. On the contrary the result obtained in Fig. 7 may be attributed to the predomination of the factor of increasing the solubility of oleic acid in the water-alcohol mixture.

Summary

The solubilization of oleic acid in the aqueous solution of sodium dodecyl sulfate was studied in the presence of various kinds of alcohols in various concentrations. When the concentration of alcohols in the detergent solution is not so great, the solubility of oleic acid decreases as the amount of alcohols increases. This is explained by the solution of oleic acid and alcohols in the same place in the micelle, i. e., in the palisade layer. When the water soluble alcohols are used the solubilization of oleic acid turns out to increase at a certain concentration of the alcohols in the detergent solution. This is explained by the solution of oleic acid in the solvent liquid as well as in the detergent micelles.

Department of Chemistry
Faculty of Science
Kyushu University
Fukuoka

Synthesis and Physical Properties of Normal Higher Primary Alcohols. III. Synthesis of Normal Higher Primary Alcohols of Even Carbon Numbers from Dodecanol to Hexatriacontanol

By Akira WATANABE*

(Received July 23, 1960)

In the previous investigation of this series[1,2] the author confined his attention to the synthesis of normal higher alcohols of odd carbon numbers. In view of the interesting results on the physical properties, especially the transition phenomena of these alcohols in the solid state, it was felt desirable to extend the study to alcohols of even carbon numbers, and thirteen members with even carbon atoms ranging from C_{12} to C_{36} were synthesized and their transition points were observed.

The alcohols were all prepared by the lithium aluminum hydride reduction of the corresponding fatty acids or their ethyl esters, of which acids from C_{12} to C_{22} were obtained by careful purification of commercial specimens.

Tetracosanoic acid ($C_{23}H_{47}CO_2H$) was synthesized from docosyl bromide ($C_{22}H_{45}Br$) by the modified malonic ester synthesis[3]. The method employed for the synthesis of the fatty

* Some parts of this work were performed at the Department of Chemistry, Faculty of Science, Kyoto University, Sakyo-ku, Kyoto.

1) A. Watanabe, This Bulletin, **32**, 1295 (1959).
2) A. Watanabe, ibid., **33**, 531 (1960).
3) W. Bleyberg et al., *Ber.*, **64**, 2506 (1931).

acids with more than 24 carbon atoms is Bowman's synthesis:

$$C_2H_5O_2C(CH_2)_nBr \xrightarrow{\text{Ethyl malonate}}$$
(I)

$$C_2H_5O_2C(CH_2)_nCH(CO_2C_2H_5)_2 \xrightarrow{\text{Benzyl alcohol}}$$
(II)

$$C_6H_5CH_2O_2C(CH_2)_nCH(CO_2CH_2C_6H_5)_2 \xrightarrow{RCOCl}$$
(III)

$$C_6H_5CH_2O_2C(CH_2)_nC(CO_2CH_2C_6H_5)_2COR \xrightarrow{H_2(Pd)}$$
(IV)

$$HO_2C(CH_2)_nC(CO_2H)_2COR \xrightarrow{\text{Decarboxylation}}$$
(V)

$$RCO(CH_2)_{n+1}CO_2H \xrightarrow[\text{reduction}]{\text{Huang-Minlon}}$$
(VI)

$$R(CH_2)_{n+2}CO_2H \xrightarrow[LiAlH_4]{\text{Esterification}} R(CH_2)_{n+3}OH$$
(VII) (VIII)

Although this method was extensively applied in the preparation of odd members[1,2], the yields of the ketonic acids were low and fluctuated (maximum 37%) compared with those obtained by Bowman (70%). Nunn[4] and Hougen[5] reported similar low yields, and ascribed them to the ketonic hydrolysis of the ketoesters, although their studies appeared not to be extensive. Since it was felt necessary to increase the yield and convenience in order to develop the present study, several improvements in the synthetic technique were made and the results are reported in this paper.

It was found that partial hydrolysis of triester II occurred in spite of precautions during the reaction of alcoholysis as evidenced by the isolation of the carboxylic acid from the reaction mixture in an amount of 30% to the starting triester and by the recovery of a nearly corresponding amount of benzyl alcohol. It seemed quite probable that the presence of this acid and the alcohol was detrimental to the subsequent malonic ester condensation. The procedures were then improved as follows, giving the desired product with a fairly good and consistent yield.

After the alcoholysis the acid was removed with a sodium carbonate solution and benzyl alcohol was distilled off under reduced pressure. Tribenzyl ester III, freed from the acid and benzyl alcohol and obtained as an oil, was condensed with an acid chloride by means of sodium ethoxide to give compound IV. Hydrogenolysis of compound IV and subsequent decarboxylation yielded ketonic acid VI in a yield of 65% based on the acid chloride. Details of the procedures are given in the Experimental Part.

In order to avoid the hydrolysis of triester II, the use of sulfuric acid, hydrogen chloride, and zinc chloride as the catalysts for the alcoholysis were attempted with no success. Metallic sodium, instead of sodium ethoxide, was used in the malonic ester condensation without success, probably because the hydrogen from the reaction of sodium with the malonic ester cleaved the benzyl groups.

Another factor which affects the yield is the instability of compound IV as shown by the fact that this compound was decomposed even at room temperature by the hydrochloric acid liberated from the unchanged acid chloride on washing the reaction mixture with water. At temperature low enough to be harmless to the compound it was quite difficult to decompose the acid chloride with water when the carbon chain of the acid was long. Therefore, it is advisable to use slightly less than one equivalent of the acid chloride to obtain a good yield.

It has been known that Bowman's synthesis suffers from the catalyst poisoning which can not be avoided on account of the difficulty in purification of compound IV, and it was experienced in the previous study[2] that a long period was required for complete hydrogenolysis when the intermediate acid chloride could not be purified by distillation. However, in the present experiments, it was found advantageous to purify compound IV with activated aluminum oxide, permitting the complete hydrogenolysis with great saving in time and catalysts and with no lowering of the yield of ketonic acid V.

The ketonic acids thus obtained were all converted into the corresponding fatty acids by Huang-Minlon reduction[6] and the desired alcohols were obtained easily by the lithium aluminum hydride reduction of the fatty acids or their ethyl esters. The alcohols were purified with great care to obtain the final products with sharp melting points and excellent analytical values. For hexacosanol $C_{26}H_{53}OH$ and higher alcohols high vacuum (2×10^{-3} mmHg) distillation as well as recrystallization was employed.

An alternative chain-lengthening process for the synthesis of octacosanol $C_{28}H_{57}OH$ is Cason's method[7], which consists in the condensation of a dialkyl cadmium with a halfester-acid chloride. The accompanying flow chart indicates the reaction:

4) J. R. Nunn, *J. Chem. Soc.*, **1951**, 1742.
5) F. W. Hougen et al., ibid., **1953**, 98.
6) Huang-Minlon, *J. Am. Chem. Soc.*, **66**, 839 (1944).
7) J. Cason, ibid., **68**, 2078 (1946).

TABLE I

Alcohol	Formula	Calcd. C	Calcd. H	Found C	Found H	M. p., °C	F. p., °C	T. p., °C
Dodecyl	$C_{12}H_{26}O$	77.35	14.07	77.46	14.00	22.5(24.0[a])	22.3	
Tetradecyl	$C_{14}H_{30}O$	78.43	14.11	78.36	13.90	39.0(37.7[b])	37.5	33.5
Hexadecyl	$C_{16}H_{34}O$	79.26	14.14	79.02	14.22	48.5(49.0[c])	48.0	42.5
Octadecyl	$C_{18}H_{38}O$	79.92	14.16	80.11	14.25	58.5(58.5[d])	58.0	50.0
Eicosyl	$C_{20}H_{42}O$	80.46	14.18	80.41	14.02	65.3(66.5[e])	64.2	55.5
Docosyl	$C_{22}H_{46}O$	80.90	14.20	80.86	14.07	70.4(70.8[e])	69.3	61.0
Tetracosyl	$C_{24}H_{50}O$	81.28	14.21	81.43	14.29	76.0(75.3[e])	75.7	68.0
Hexacosyl	$C_{26}H_{54}O$	81.60	14.22	81.70	14.48	78.8(79.2[e])	78.2	73.0
Octacosyl	$C_{28}H_{58}O$	81.87	14.23	81.75	14.10	82.5(82.6[e])	82.0	
Triacontyl	$C_{30}H_{62}O$	82.11	14.24	82.22	14.19	86.3(86.5[e])	85.5	
Dotriacontyl	$C_{32}H_{66}O$	82.32	14.25	82.40	14.21	88.2(89.2[e])	87.0	
Tetratriacontyl	$C_{34}H_{70}O$	82.51	14.26	82.35	14.20	91.0(91.7[e])	89.5	
Hexatriacontyl	$C_{36}H_{74}O$	82.68	14.26	82.40	14.22	91.6(92.6[e])	89.5	

Melting points are uncorrected.

When a sample was cooled below its freezing point from the melt, a transition appeared with the change of the transparent waxy material into the opaque crystalline state. Transition points of the alcohols higher than hexacosanol could not be observed.

a) F. Krafft, *Ber.*, **16**, 1718 (1883).
b) W. E. Garner et al., *J. Chem. Soc.*, **1927**, 1357.
c) F. Krafft, *Ber.*, **16**, 1721 (1883).
d) P. A. Levene et al., *J. Biol. Chem.*, **59**, 914 (1924).
e) F. Francis et al., *Proc. Roy. Soc.*, **A 158**, 691 (1937).

TABLE II

Ethyl alkane-tricarboxylates	Acid chlorides (Cno.)	Ketonic acid (Cno.)	M. p., °C	Fatty acid	M. p., °C
n-Undecane	Myristoyl (C_{14})	$CH_3(CH_2)_{12}CO(CH_2)_{11}CO_2H(C_{26})$	95.5	Hexacosanoic	86.5(87.7)*
〃	Palmitoyl (C_{16})	$CH_3(CH_2)_{14}CO(CH_2)_{11}CO_2H(C_{28})$	99.5	Octacosanoic	90.2(90.9)
〃	Stearoyl (C_{18})	$CH_3(CH_2)_{16}CO(CH_2)_{11}CO_2H(C_{30})$	102.6	Triacontanoic	93.0(93.6)
n-Octane	Tricosanoyl (C_{23})	$CH_3(CH_2)_{23}CO(CH_2)_5CO_2H(C_{32})$	105.5	Dotriacontanoic	96.0(96.2)
n-Undecane	Docosanoyl (C_{22})	$CH_3(CH_2)_{20}CO(CH_2)_{11}CO_2H(C_{34})$	107.5	Tetratriacontanoic	97.8(98.2)
〃	Tetracosanoyl (C_{24})	$CH_3(CH_2)_{22}CO(CH_2)_{11}CO_2H(C_{36})$	110.0	Hexatriacontanoic	98.5(99.9)

* F. Francis et al., *Proc. Roy. Soc.*, **A 158**, 691 (1937).

$$C_{18}H_{37}OH \xrightarrow{HBr} C_{18}H_{37}Br \longrightarrow C_{18}H_{37}MgBr \xrightarrow{CdCl_2} (C_{18}H_{37})_2Cd \xrightarrow{ClOC(CH_2)_5CO_2C_2H_5}$$

$$C_{18}H_{37}CO(CH_2)_5CO_2C_2H_5 \xrightarrow[\text{reduction}]{\text{Huang-Minlon}}$$

$$C_{27}H_{55}CO_2H \xrightarrow[LiAlH_4]{\text{Ethyl ester}} C_{25}H_{51}OH$$

The alcohol obtained by this method was shown to be identical with that obtained by Bowman's method by the mixed melting point and the X-ray data[8].

Melting points, transition points and analytical data of the alcohols synthesized here are given in Table I. The transition points of the alcohols with more than 22 carbon atoms have been unknown. All the alcohols described in this paper and two previous papers, namely odd and even members from C_{11} to C_{37}, are being studied for their physical properties and part of the results has been published from the Department of Physics of Kyoto University[9-11]. Thermal data will be reported in this Bulletin in near future.

8) A. Watanabe, unpublished.

Experimental

Since the reactions used for the synthesis of the lower members are well known, descriptions of the experiments are omitted. Bowman's[4] method was applied with some improvements for the synthesis of the alcohols with more than 24 carbon atoms. As the conditions except those for isolation of the products, were essentially the same throughout the series, the synthesis of octacosanol is described as an illustration. Combinations of the starting materials and the intermediates are listed in Table II.

Ethyl n-Undecane-1, 1, 11-tricarboxylate. — It was

9) K. Tanaka, T. Seto and T. Hayashida, *Bull. Inst. Chem. Res. Kyoto Univ.*, **35**, 123 (1957).
10) K. Tanaka, T. Seto, A. Watanabe and T. Hayashida, ibid., **37**, 281 (1959).
11) K. Asai, *J. Phys. Soc. Japan*, **14**, 1084 (1959).

prepared by condensation of ethyl bromoundecanoate with ethyl malonate as already described[2]).

B. p. 187°C/1 mmHg, n_D^{28} 1.4435.

Benzyl n-Undecane-1, 1, 11-tricarboxylate.—In a 200 ml. three-necked flask, equipped with a mechanical stirrer, a dropping funnel and a reflux condenser fitted with a calcium chloride tube, were placed 0.65 g. of sodium sand (finely powdered in toluene) and 50 ml. of thiophene-free dry benzene. To the mixture was added from the dropping funnel 10 g. of ethyl *n*-undecane-1, 1, 11-tricarboxylate. The mixture was allowed to stand at room temperature for about 6 hr. with stirring and then moderately heated to the complete disappearance of the sodium. After 8.7 g. of freshly distilled benzyl alcohol was added, the condenser was replaced by a Fenske column and the mixture was heated to distill off ethanol as the benzene ethanol azeotrope. During the distillation reflux-ratio was controlled from 6 : 1 to 20 : 1 (2~3 drops per minute). When no more ethanol distilled over, the boiling point reaching 79°C and the absence of the ethanol in the final portion of the distillate being confirmed by the index of refraction, the mixture was cooled and acidified with dilute sulfuric acid. The benzene layer was separated, washed with water, with sodium carbonate solution, again with water to neutral reaction, and dried over sodium sulfate.

After evaporating the benzene, the residue was heated to 120°C in an oil bath under reduced pressure (3 mmHg), the flask being immersed into the bath as deeply as possible to remove the benzyl alcohol completely. Recovered benzyl alcohol weighed 2.5 g. The Tribenzyl ester III remained in the flask as an oil which weighed 11 g. On acidification of the above alkali washing with sulfuric acid, an oily substance separated out which gradually crystallized on standing several days. Recrystallization from ethyl acetate-petroleum ether gave the product in white crystals, m. p. 89°C. It was found not to depress the melting point when mixed with the acid obtained by hydrolysis of the triester.

13-Keto-octacosanoic Acid $C_{13}H_{27}CO(CH_2)_{11}CO_2H$. —In a 200 ml. three-necked flask, 0.41 g. of freshly cut sodium was placed. Absolute ethanol (5 ml.) was added to give a clear solution. All excess of the ethanol was distilled off until a crust of sodium ethoxide was formed on the surface of the residue. Then 15 ml. of dry thiophene-free benzene was added from the dropping funnel. To this suspension a solution of 11 g. of the tribenzyl ester in 10 ml. of benzene was added and the mixture was allowed to stand at room temperature with occasional shaking, while the solid gradually went into solution. The benzene was removed under reduced pressure at room temperature, leaving a brown syrup in the flask. Two portions of 10 ml. of fresh benzene were added and removed under reduced pressure to remove the last traces of ethanol. Thus the sodium salt of the tribenzyl ester was obtained as a brown viscous material, to which 30 ml. of fresh benzene was added, giving a colored solution. Then the flask was equipped with a stirrer and a reflux condenser fitted with a calcium chloride tube. A solution of 5.2 g. of palmitoyl chloride (prepared from pure acid and thionyl chloride, b. p. 148°C/1.5 mmHg) in 10 ml. of benzene was added from the dropping funnel with stirring and the mixture was refluxed for 30 min. with continued stirring.

After the reaction mixture attained room temperature the flask was immersed in an ice bath. Ice-cooled water containing 1 g. of sulfuric acid was added gradually with vigorous stirring, the temperature of the mixture being maintained at 3 to 5°C. The contents of the flask were then transfered to a separating funnel. The layers were separated with the aid of a small amount of ethanol and the benzene layer was washed with water to neutral reaction with occasional cooling to prevent the temperature from rising above 5°C. After the solution was dried over sodium sulfate the benzene was removed under reduced pressure at about 30°C of bath temperature. The condensation product remained as an oil (15 g.). A solution of 5 g. of the above product in a mixture of 15 ml. of ethyl acetate and 15 ml. of absolute ethanol was shaken with Pd-C (0.2 g.) and Pd-$SrCO_3$ (0.2 g.) in a hydrogen atmosphere at room temperature. Catalyst poisoning was so often encountered that it was necessary to add fresh catalysts frequently until a nearly theoretical amount of hydrogen was absorbed. The total amount of the catalyst used was 2.7 g. The time required for the complete hydrogenolysis was about 4 hr. The solution freed from the catalyst was refluxed for 30 min. to decarboxylate the product. Upon cooling the solution to room temperature white crystals appeared. These were collected and washed with ethyl acetate. The ketonic acid obtained showed the melting point of 91 to 94°C. Yield was 1.5 g. The filtrate and washing were combined and concentrated to a syrup. To this was added 10 ml. of acetic acid containing 1 ml. of sulfuric acid and the mixture was refluxed for 40 min. The solid residue obtained on removing acetic acid was taken up in benzene and the solution was washed and dried over sodium sulfate. Concentration and subsequent cooling of the benzene solution gave white crystals which melted at 93 to 97°C and weighed 0.6 g. The substance was combined with the acid obtained from the ethyl acetate solution and the combined crystals were recrystallized twice from benzene. The pure ketonic acid showed the melting point of 99.5°C. The yield was 1.8 g. or 65% based on palmitoyl chloride.

Found: C, 76.60; H, 12.45. Calcd. for $C_{28}H_{54}O_3$: C, 76.65; H, 12.41%.

Palmitic acid (0.15 g.) was recovered from the filtrate of the ketonic acid.

Purification of the Condensation Product (IV).— The product (5 g.) was dissolved in 20 ml. of pure benzene (dried over sodium wire) and the solution was shaken with active alumina for a short period. The alumina was filtered off and the filtrate was evaporated under reduced pressure at about 30°C of bath temperature to give a colorless liquid. This was hydrogenated in the same manner as described above. Absorption of the first 280 ml. of hydrogen proceeded rapidly (30 min.) with 0.4 g. of the catalyst. The second 140 ml. was absorbed in about 1 hr. with the addition of 0.3 g. of the catalyst. The product was treated in the same way as the

above. The yield of the pure ketonic acid was 1.8 g. (65%).

Octacosanol $C_{28}H_{57}OH$. — Octacosanoic acid ($C_{27}H_{55}CO_2H$) was obtained from 3 g. of the ketonic acid by the Huang-Minlon reduction[6] in a yield of 77% (2.2 g.). Details were given in the previous paper[2] for the reaction of other higher alcohols. The melting point was 90.2°C (recrystallized from toluene).

Found: C, 79.10; H, 13.34. Calcd for $C_{28}H_{56}O_2$: C, 79.18; H, 13.29%.

The acid was converted into its ethyl ester by a usual method. The lithium aluminum hydride reduction[2] of 2 g. of the pure ester (recrystallized from benzene, m. p. 64°C) afforded 1.4 g. of the desired alcohol after recrystallization from benzene. The melting point was 82.5°C. Further purification of the alcohol was tried by high vacuum distillation (2×10^{-3} mmHg) followed by recrystallizations. Although the melting point and analytical data were not changed, the physical data[7] indicated that these procedures seemed to be necessary to obtain a pure sample.

The author expresses his sincere thanks to Professor Ryozo Goto, Kyoto University, for his kind guidance throughout this study. Thanks are also due to Mr. T. Araki and Mr. H. Horino for their assistance in some of the experiments. The cost of this work was partly defrayed from a grant (Shigenkagaku Kenkyuhi) from the Ministry of Education.

Department of Applied Chemistry
Himeji Technical College
Idei, Himeji

Distribution of Neptunium between Di-(2-ethyl hexyl)-phosphoric Acid and Mineral Acids

By Eiko NAKAMURA

(Received June 28, 1960)

Solvent extraction studies on neptunium have been carried out using tri-*n*-butyl phosphate[1-4], tertiary amines[5], thenoyl tri-fluoro acetone[6], diethyl ether[7] or methyl isobutyl ketone[7], as an extractant.

However, the extraction behavior of neptunium using di-(2-ethyl hexyl)-phosphoric acid, HDEHP, has not been reported. The experimental results in the works referred to above have usually been complicated unless careful precautions were taken, because the neptunium tracer solution often contains neptunium in two or three oxidation states. Giving special attention to the oxidation states of neptunium, the extraction behavior of quadri-, quinqui- and sexi-valent neptunium in the system of diluted HDEHP vs. hydrochloric or perchloric acid was studied in this work.

Di-(2-ethyl hexyl)-phosphoric acid has been proved to be useful as a solvent extracting agent for uranium(VI) and other metals. Some works about this extracting agent have been published by a number of investigators[8-10]. Recently a comprehensive study on the extraction of metal ions from hydrochloric acid solution has been reported by Kimura[11]. According to these previous works, it seems that HDEHP behaves as a cation extracting reagent in the low acidity region. In other words, HDEHP-metal ion complex is formed with the inorganic cation in the aqueous phase, and extracted into the organic phase which is composed of the organic diluent and HDEHP. The neptunium(IV), (V) and (VI) cations also seemed to be extracted as the HDEHP-neptunium(IV), (V) or (VI) cation complex.

Experimental

Reagents.—The HDEHP received from Virginia Chemicals, Co. Ltd. was purified by the method of Peppard et al.[12] It was diluted with toluene. C. P.

1) T. Ishimori and E. Nakamura, This Bulletin, **32**, 713 (1959).
2) H. A. C. McKay, J. S. Nairn and M. B. Waldron, *Second United Nations International Conference on the Peaceful Uses of Atomic Energy*, p/304 (1958).
3) J. S. Nairn, D. A. Collins, H. A. C. McKay and A. G. Maddock, ibid, p/1458 (1958).
4) W. H. Lewis, ibid, p/537 (1958).
5) J. C. Sheppard, HW-51958 (1957).
6) L. B. Magnusson, J. C. Hindman and T. J. LaChapeli, ANL-4066 (1947).
7) J. Kooi, *First United Nations International Conference on the Peaceful Uses of Atomic Energy*, Vol. VII, p/929, United Nations Publication, New York (1956).
8) C. F. Baes, Jr., R. A. Zingaro and C. C. Coleman, *J. Phys. Chem.*, **62**, 129 (1958).
9) D. F. Peppard, G. W. Mason, W. J. Driscoll and R. J. Sironen, *J. Inorg. & Nucl. Chem.*, **7**, 276 (1958).
10) D. F. Peppard and J. R. Ferraro, ibid., **10**, 275 (1959).
11) K. Kimura, This Bulletin, **33**, 1038 (1960).
12) D. F. Peppard, G. W. Mason, J. L. Maier and W. J. Driscoll, *J. Inor. & Nucl. Chem.*, **4**, 334 (1957).

grade, in this work. Hydrochloric and perchloric acids, analytical grade, were used as received.

Carrier-free 2.3d-neptunium-239, 27.5d-protactinium-233 and 24.1d-thorium-234 were prepared as described in the previous paper[1-13]. The activities of these nuclides were measured by a gamma-scintillation counter. Zirconium-niobium-95 imported from the Oak Ridge National Laboratory, Tenn. USA, was used as received and measured the hard beta-rays of zirconium-95 cutting off the soft beta-rays of niobium-95.

The radiochemical purity of the tracers was checked by gamma-spectrometry, beta-ray absorption and decay.

According to the method written in the previous work[1], the quadri-, quinqui- and sexi-valent neptunium tracers were prepared. In the case of quadrivalent neptunium, hydrochloric acid was used as the aqueous medium, because neptunium(IV) is unstable in a perchloric medium[1].

Distribution Measurement.—All experiments were carried out with radioactive tracers. The distribution ratio, K_d, of a given nuclide was determined in the usual way[1,11]. The scrubbing techniques were used in every case in order to obtain the K_d values exactly. In all cases both acid and solvent dependence of the K_d values were determined.

Results and Discussion

Distribution of Sexivalent Neptunium in the System of HDEHP vs. Perchloric Acid.— The distribution ratios of sexivalent neptunium were determined in the system of about 0.6% (v/v) HDEHP-toluene vs. perchloric acid varying the acidity from 0.1 to 0.5 N. Experimental results are shown in Fig. 1 where the curve for uranium(VI), taken from the work of Baes et al.[5], is also given for comparison. Baes et al. determined the distribution ratio of uranium in the system of 0.1 M (3.33% v/v) HDEHP-hexane vs. perchloric acid changing the acidity from 0.01 to 2.0 N.

From these results it is found that both sexivalent neptunium and uranium are extracted very well with HDEHP from perchloric acid solution. As Fig. 1 shows, both lines for neptunium and uranium have the slope of −2, suggesting a close similarity between uranium (VI) and neptunium(VI) ions.

The solvent dependence of K_d values for sexivalent neptunium was determined at 0.52 N perchloric acid concentration using toluene as the diluent. Experimental results for neptunium(VI) are shown in Fig. 2 together with the solvent dependence curve for uranium at 1 N perchloric acid, which is quoted from the work of Baes et al.[5] The distribution ratios of neptunium(VI) and uranium(VI) show the second power dependence on the HDEHP concentration, again suggesting the similarity

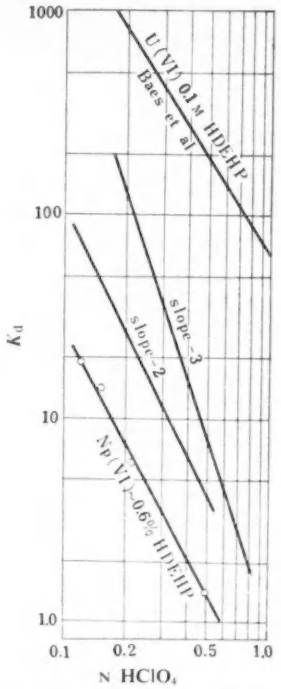

Fig. 1. The acid dependence of K_d values for neptunium(VI) and uranium(VI).

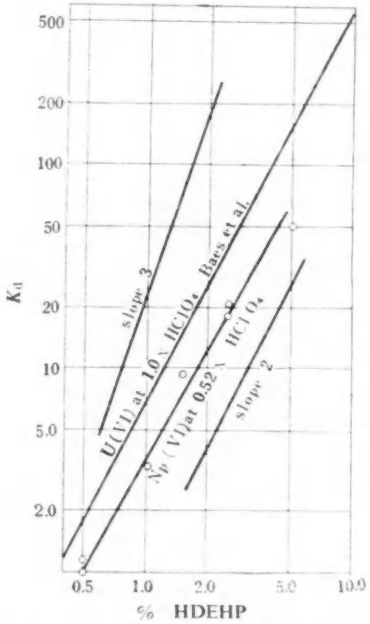

Fig. 2. The solvent dependence of K_d values for neptunium(VI) and uranium(VI).

13) T. Ishimori, K. Watanabe and E. Nakamura, This Bulletin, 33, 636 (1960).

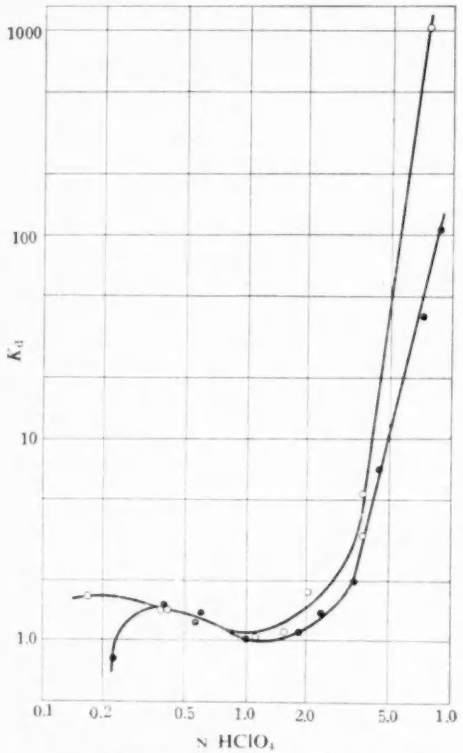

Fig. 3. The variation of the K_d values for sexivalent neptunium[5] and uranium[14] in the system of 100% TBP vs. perchloric acid.
—○— U(VI) by Naitō —●— Np(VI)

between the chemistry of sexivalent neptunium and uranium in an acid solution.

The similarity between sexivalent neptunium and uranium is also found in other systems:

The acid dependence curves for neptunium(VI)[1] and uranium(VI) in the system of 100% TBP vs. perchloric acid are given in Fig. 3 which shows that the behavior of sexivalent neptunium resembles that of uranium quite well, where the uranium curve is taken from the work of Naito[14]. Besides that found in the perchloric acid system similar behavior is also found in the nitric acid system. The acid dependence curve for neptunium(VI) also resembles that for uranium(VI)[1,2] in 100% TBP* vs. nitric acid system or in the trioctylamine vs. nitric acid system[5]. Thus it is likely that sexivalent ions of neptunium and uranium show almost the same behavior in the distribution experiments discussed above. In

* Tri-*n*-butyl phosphate.
14) K. Naito, This Bulletin, 33, 363 (1960).

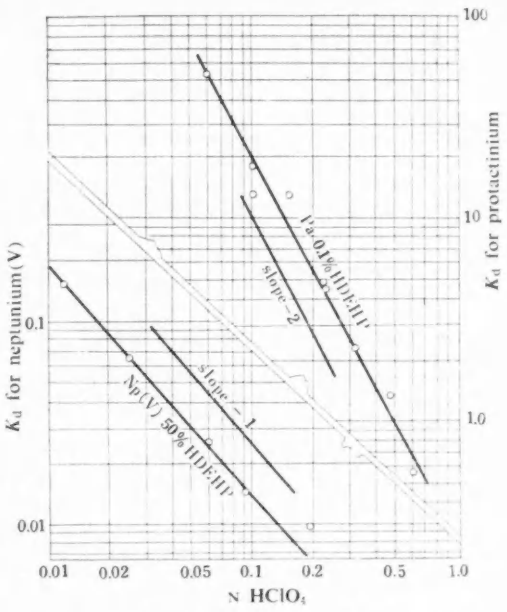

Fig. 4. The acid dependence of K_d values for neptunium(V) and protactinium.

other words, the extraction mechanism of neptunium(VI) seems to be analogous to that of uranium(VI).

According to Baes et al.[5], who discussed the composition of uranium-HDEHP complex based on the acid and the solvent dependence of the K_d values for uranium in the system of HDEHP vs. perchloric acid, the uranium-HDEHP complex is $UO_2A_1H_2$, where HA represents HDEHP molecule. As mentioned above, both acid and solvent dependence of K_d values for neptunium(VI) in the HDEHP vs. perchloric acid system coincide with those of uranium(VI), so that it is presumed that the neptunium(VI) ion is extracted forming the neptunium(VI)-HDEHP complex, $NpO_2A_1H_2$.

Distribution of Quinquivalent Neptunium in the System of HDEHP vs. Perchloric Acid.— The distribution ratios of quinquivalent neptunium were determined in the system of 50% HDEHP-toluene vs. perchloric acid varying the acidity from 0.01 to 0.2 N. The results obtained are given in Fig. 4, where the K_d values for protactinium are also shown. The K_d values for protactinium were so high that the relationship between the acidity and the K_d values for protactinium could not be found clearly using 50% HDEHP with which the extraction of neptunium(V) was studied. Therefore, 0.1% HDEHP-toluene was chosen as the extractant in the determination of the K_d values for

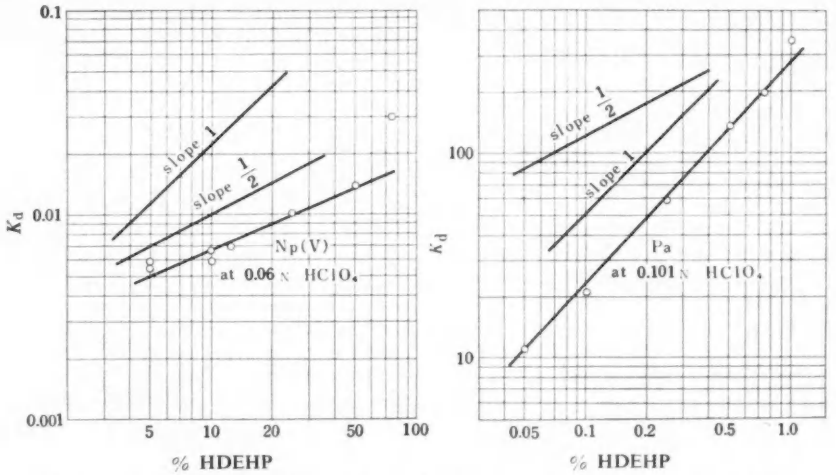

Fig. 5. The solvent dependence of K_d values for neptunium(V) and protactinium.

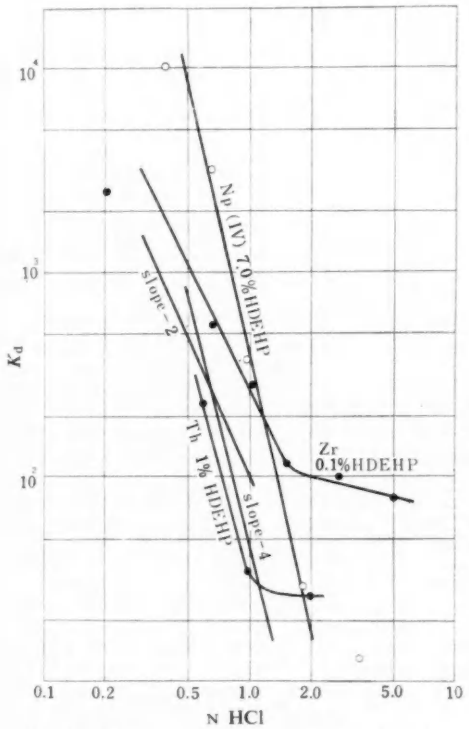

Fig. 6. The acid dependence of K_d values for neptunium(IV), thorium and zirconium.

protactinium varying the acidity of perchloric acid from 0.05 to 1.0 N. As Fig. 4 shows, the slope of the line for neptunium(V) is −1, whereas that for protactinium is −2. Thus it is likely that the neptunium(V) ion behaves differently from the protactinium ion in a dilute perchloric acid medium.

The variation of the K_d values of neptunium-(V) and protactinium with the concentration of HDEHP in the organic phase, keeping the concentration of perchloric acid in the aqueous phase constant, is shown in Fig. 5. As Fig. 5 shows, the line for neptunium(V) has the slope of 1/2, whereas that for protactinium has the slope of 1. Assuming that the solvent dependence of K_d values for protactinium is kept at the first power up to 50% HDEHP at 0.1 N perchloric acid solution, it is calculated that the K_d value for protactinium is about 10^4, 500 times that of the K_d value shown in Fig. 4. On the other hand, in the 0.1 N perchloric acid-50% HDEHP system quinquivalent neptunium shows the K_d value of about 10^{-2} (Fig. 4). The difference of the K_d values between neptunium(V) and protactinium, 10^4 and 10^{-2}, shows that quinquivalent neptunium is less extractable than protactinium with the organic extractant from the aqueous phase. Similar relationships are seen in other cases like the system of 100% TBP vs. some mineral acids[1].

As mentioned above, the both acid and solvent dependence of K_d values for neptunium-(V) show different values from those of protactinium. These facts suggest the difference between the chemistry of quinquivalent neptunium and protactinium.

Distribution of Quadrivalent Neptunium in the System of HDEHP vs. Hydrochloric Acid. —The distribution ratio of quadrivalent neptunium was determined in the system of 7.0%

HDEHP vs. hydrochloric acid varying the acidity from 0.5 to 3.0 N. The results are shown in Fig. 6, where the K_d values for thorium and zirconium are also given. The behavior of thorium was studied in the acidity range from 0.6 to 2.0 N using 1% HDEHP-toluene solution. Although zirconium is not a member of the actinide elements, the behavior of zirconium was studied as a quadrivalent species in the system of 0.1% HDEHP vs. hydrochloric acid varying the acidity from 0.2 to 4.0 N, where the K_d values for zirconium are so high that HDEHP-toluene solution had to be diluted to 0.1%.

From these results, it is found that thorium and zirconium are more extractable than quadrivalent neptunium. As is shown in Fig. 6, the lines for neptunium(IV) and thorium both have the slope of −4. The behavior of thorium had been studied by Peppard and Ferraro who had also found negative fourth power dependence of the K_d values on the acidity of hydrochloric acid[10]. On the other hand, zirconium shows a negative second power dependence on the acidity. The difference between the neptunium(IV) and zirconium ion seems to be greater than that between the neptunium(IV) and thorium ion.

The K_d values for quadrivalent neptunium in the system of 0.5 N hydrochloric acid vs. HDEHP-toluene are studied, the HDEHP concentration being varied. In Fig. 7, the neptunium(IV) curve is compared with those for thorium and zirconium. The behavior of thorium is taken from the work of Ishimori[15] in the system of 0.5 N perchloric acid vs. HDEHP-toluene. Peppard and Ferraro had also given a third power dependence of the K_d values for thorium on the hydrochloric or perchloric acid concentration. On the other hand, the results for zirconium obtained presently fall on a line of slope 2 in Fig. 7. Thus it is shown again that the quadrivalent neptunium ion behaves in a manner more nearly similar to thorium ion than to zirconium ion in the hydrochloric acid solution.

It is likely that the HDEHP extraction mechanism of neptunium(IV) from hydrochloric acid is similar to that of thorium ion, because both acid and solvent dependence of K_d values for neptunium(IV) coincide with those of thorium. That is to say, neptunium-(IV)-HDEHP complex is supposed to have an

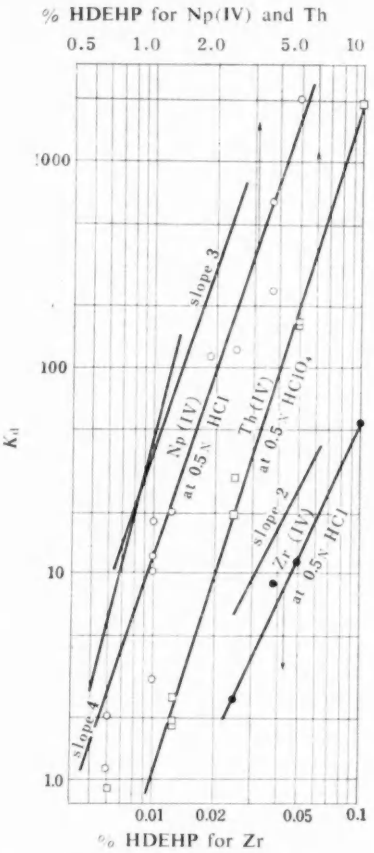

Fig. 7. The solvent dependence of K_d values for neptunium(IV), thorium and zirconium.

iso-morphous structure with that of thorium-(IV)-HDEHP complex. As the formula for the thorium complex, Peppard and Ferraro gave $ThA_2(HA_2)_2$ which was proposed from the results of the infrared spectra and the elementary analysis, where HA denotes the HDEHP molecule. Therefore it might be reasonable to give $NpA_2(HA_2)_2$ for the neptunium(IV)-HDEHP complex.

The author wishes to thank Dr. Tomitaro Ishimori for criticism and suggestions which made a major contribution to this work.

Chemistry Division, Tokai Laboratory
Japan Atomic Energy
Research Institute
Tokai, Ibaraki-Ken

15) Unpublished work performed during the writer's stay in the Argonne National Laboratory, Lemont, Illinois, USA.

The Competitive Reduction of Nitrobenzene and para-Substituted Nitrobenzenes with Nickel Catalysts

By Akira SUGIMORI*

(Received July 26, 1960)

Several approaches to the elucidation of the mechanism of catalytic reduction may be possible. The present paper describes the competitive reduction of nitrobenzene and substituted nitrobenzenes with nickel catalysts. In all the cases examined, the nitro compounds with an electron attracting group in para position were reduced preferentially to those with an electron repelling group in the same position.

Experimental

Materials. — Nitro compounds were purified by recrystallization or redistillation. The melting points and boiling points are listed in Table I.

TABLE I

Compound	M. p.	B. p.
Nitrobenzene		95.5～97°C/ 17～18 mmHg
p-Nitrophenol	113°C	
p-Nitroanisole	52 ～ 53°C	
p-Nitroaniline	145.5～146.5°C	
Ethyl *p*-nitrobenzoate	55 ～ 56°C	
p-Nitrobenzaldehyde	105 ～105.5°C	

Preparation of Catalysts. — a) Raney nickel catalyst. The method of Adkins and Billica[1] was modified in order to obtain stable catalytic activity. One gram of nickel-aluminum alloy (Ni 40%) was treated with 7 ml. cf. 20% aqueous sodium hydroxide at 50°C for 50 min. Then the catalyst was washed ten times by decantation with 20 ml. of cold water. The pH of the last washing wad 8.5～9.0. The catalyst was then washed twice with 20 ml. of 95% ethanol.

b) Urushibara nickel A (U-Ni-A) was prepared according to Urushibara, Nishimura and Uehara[2].

Catalytic Reduction.—A suspension of the Raney nickel (0.4 g.) from 1 g. of the alloy in 30 ml. of 95% ethanol was shaken with hydrogen under ordinary pressure in a shaking type catalytic reduction apparatus until the catalyst absorbed no more hydrogen. Then 5 mM of a nitro compounds in 30 ml. of ethanol was added to the catalyst suspension, hydrogen was charged, and the reaction was started by shaking the reaction vessel. The temperature was maintained at 25°C, and the rate of hydrogen absorption was measured. In the reduction with U-Ni-A catalyst, 1.67 mM of a nitro compound, 1.0 g. of the catalyst and 20 ml. of 95% ethanol were used.

Competitive Reduction.—An equimolar mixture of two nitro compounds (each 5 mM) was reduced under the condition described above until 8～13 mM of hydrogen was absorbed, whereas complete reduction to amines requires 30 mM of hydrogen. The catalyst was removed by filtration and was washed several times with ether. The products in the filtrate and washings were analysed. In the reduction with U-Ni-A, 6.67 mM each of two nitro compounds, 1.0 g. of the catalyst and 80 ml. of 95% ethanol were used.

Analysis of Products.—*Competitive Reduction of Nitrobenzene and p-Nitrophenol.* — Amines were removed from the ethereal solution of the products by shaking with dilute hydrochloric acid. Then the ethereal solution was extracted with dilute aqueous sodium hydroxide, the alkaline solution was acidified with hydrochloric acid and extracted with ether, and *p*-nitrophenol, m. p. 113°C, was obtained after removal of ether from the extract. The quantity of unchanged nitrobenzene was estimated from the volume of absorbed hydrogen in the catalytic reduction of the ethereal mother liquor of the alkaline extraction.

Competitive Reduction of Nitrobenzene and p-Nitroaniline. — *p*-Nitroaniline, *p*-phenylenediamine and aniline were separated from unchanged nitrobenzene by extracting ten times the ethereal solution of the reaction products with hydrochloric acid. Then the ethereal solution containing the unchanged nitrobenzene was evaporated in vacuum and the residue was catalytically reduced in alcoholic solution. The quantity of absorbed hydrogen was the same as that of unchanged nitrobenzene. The acidic extract was basified with aqueous sodium hydroxide and shaken with ether. The residue from the ethereal extract was catalytically reduced in alcoholic solution to know the quantity of unchanged *p*-nitroaniline.

Competitive Reduction of Ethyl p-Nitrobenzoate and Nitrobenzene.—After the solvent was distilled off from the reaction products, the residue was dissolved in a mixture of 30 ml. of dioxan and 40 ml. of concentrated hydrochloric acid. The solution was heated under reflux for 5 hr. The solution was made alkaline with aqueous sodium carbonate. Then nitrobenzene was steam-distilled, and the distillate was extracted with ether. After removal of ether from the extract, the residue was dissolved in alcohol and catalytically reduced to estimate the

* Present address: Division of Radiation Applications, Japan Atomic Energy Research Institute, Tokai, Ibaraki-Ken, Japan.

1) H. Adkins and H. R. Billica, "Organic Syntheses" Vol., 29, John Wiley & Sons, Inc., New York (1949), p. 24.

2) Y. Urushibara, S. Nishimura and H. Uehara. This Bulletin, **28**, 446 (1955).

quantity of nitrobenzene. The quantity of reduced ethyl *p*-nitrobenzoate was estimated by weighing *p*, *p'*-diethoxycarbonylazoxy-benzene which precipitated on exposure of the reaction mixture to air.

Competitive Reduction of p-Nitrobenzaldehyde and Nitrobenzene.—The unchanged nitrobenzene and *p*-nitrobenzaldehyde were steam-distilled from the mixture produced, and the nitro compounds were extracted from the distillate with ether. The ethereal solution was divided into two portions of known volume. The total molar quantity of the nitro compounds was calculated from the quantity of absorbed hydrogen in catalytic reduction of one portion. An acidic solution of 2,4-dinitrophenylhydrazine was added to another portion. The quantity of *p*-nitrobenzaldehyde in the unchanged nitro compounds was obtained from that of the 2,4-dinitrophenylhydrazone. The quantity of nitrobenzene was given by the difference of the quantities of the total nitro compounds and *p*-nitrobenzaldehyde.

Competitive Reduction of Ethyl p-Nitrobenzoate and p-Nitroanisole.—The solution resulting from the competitive reduction was left under exposure to air for two days, and ethyl *p*-hydroxylaminobenzoate was changed to the corresponding azoxy compound[3]. After the precipitated *p*, *p'*-diethoxycarbonylazoxybenzene was collected by filtration, the solution was analysed chromatographically, and *p*-nitroanisole was obtained in white crystals. The quantity of *p*, *p'*-diethoxycarbonylaxoxybenzene gave the quantity of reduced ethyl *p*-nitrobenzoate, and the unchanged *p*-nitroanisole was directly weighed.

Results and Discussion

Separate Reduction Rates of Nitro Compounds. — The hydrogenation curves of several nitro compounds were given in the preceding paper[3]. The increasing rates towards the end of the hydrogenation of nitrobenzene and of ethyl *p*-nitrobenzoate with Raney nickel catalyst are due to stepwise hydrogenation. Namely, the nitro compounds are reduced first to the hydroxylamines with $2H_2$, and then the hydroxylamines to amines with H_2, the latter process being faster than the former. In the hydrogenation of *p*-nitrobenzaldehyde and of ethyl *p*-nitrobenzoate with U–Ni–A the hydrogenation rates go down, making a break after 2 mol. of hydrogen has been consumed. This is also due to stepwise hydrogenation and here hydroxylamines are reduced more slowly than the parent compounds.

Competitive Reduction. — In the competitive catalytic reduction, a more reactive substance is not necessarily reduced in a greater quantity than a less reactive competitor. For example, in separate reduction nitrobenzene is reduced three times as quickly as ethyl *p*-nitrobenzoate with Raney nickel. But, when a mixture of nitrobenzene and ethyl *p*-nitrobenzoate was catalytically reduced, more ethyl *p*-nitrobenzoate was reduced than nitrobenzene. While nitrobenzene and *p*-nitrophenol are almost equally reactive in separate reduction with U–Ni–A catalyst, nitrobenzene was reduced exclusively at first in the competition with *p*-nitrophenol.

These phenomena can be explained by the difference in the affinities of substrates to nickel catalysts. In the above example, ethyl *p*-nitrobenzoate must be adsorbed, and thus reduced, preferentially to nitrobenzene. The same interpretation applies to the competitive reduction of nitrobenzene and *p*-nitrophenol with U–Ni–A catalyst.

In order to find out the sequence, if any exists, in the strengths of affinities of nitrobenzene and substituted nitrobenzenes, the following considerations will be made:

To make the matter simple, any difference in the adsorption areas of the molecules of a pair of nitro compounds is neglected until later discussion.

If it is assumed that there was no selectivity in the adsorption of the nitro compounds, each component being adsorbed with equal ease, the rates of separate hydrogenation of the two compounds will give the quantities of both compounds to be reduced in a partial hydrogenation of their mixture, and comparison of the false values calculated in this way with observed ones will give a suggestion regarding the different affinities of the two nitro compounds to the nickel catalyst.

One or two examples will be illustrated below:

A mixture of 5 mM each of ethyl *p*-nitrobenzoate and nitrobenzene was hydrogenated with Raney nickel until 251 ml. of hydrogen was absorbed, and 2.60 mM of the former was reduced and 3.15 mM of the latter remained unchanged. Both ethyl *p*-nitrobenzoate and nitrobenzene are hydrogenated stepwise and, therefore, the competing reactions are:

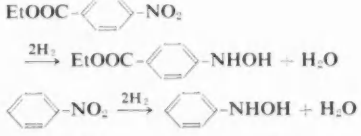

As the initial rates of separate hydrogenation of ethyl *p*-nitrobenzoate and nitrobenzene are 73 ml./5 min. and 216 ml./5 min., respectively, the quantity of hydrogen to be consumed for the hydrogenation of ethyl *p*-nitrobenzoate would be from the above assumption:

$$H_1 = \frac{73}{73+216} \times 251 = 63 \text{ ml.}$$

that for nitrobenzene:

$$H_2 = \frac{216}{73+216} \times 251 = 188 \text{ ml.}$$

3) A. Sugimori, submitted to this Bulletin.

The quantities of the nitro compounds to be hydrogenated would respectively be:

$$R_1 = \frac{63}{2\times 22.4} = 1.41 \text{ mM}$$

$$R_2 = \frac{188}{2\times 22.4} = 4.19 \text{ mM}$$

Accordingly, the quantities of the nitro compounds left unchanged would be:

$$L_1 = 5.00 - 1.41 = 3.59 \text{ mM}$$

$$L_2 = 5.00 - 4.19 = 0.81 \text{ mM}$$

The calculated values are compared with the observed values in Table II, which is interpreted as showing that ethyl *p*-nitrobenzoate has a stronger affinity with the nickel catalyst than nitrobenzene has.

TABLE II

Compound		Calcd. mM	Obs. mM
Ethyl *p*-nitrobenzoate	reduced	1.41	2.60
	unchanged	3.59	—
Nitrobenzene	reduced	4.19	—
	unchanged	0.81	3.15

The competitive hydrogenation of nitrobenzene and *p*-nitroaniline with Raney nickel catalyst is more complicated, because the former gives phenylhydroxylamine while the latter is reduced to *p*-phenylenediamine:

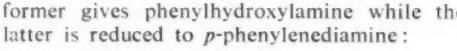

The separate hydrogenation rates of nitrobenzene and *p*-nitroaniline are 216 ml./5 min. and 134 ml./5 min., respectively. The hydrogenation of a mixture of 5 mM each of nitrobenzene and *p*-nitroaniline was stopped when 291 ml. of hydrogen was absorbed, and 4.10 mM of *p*-nitroaniline remained unchanged. From the above assumption, the quantities of hydrogen to be consumed by nitrobenzene and *p*-nitroaniline would respectively be:

$$H_1 = \frac{216}{216+134}\times 291 = 180 \text{ ml.}$$

$$H_2 = \frac{134}{216+134}\times 291 = 111 \text{ ml.}$$

The quantity of nitrobenzene to be hydrogenated to phenylhydroxylamine with 180 ml. of hydrogen is:

$$R_1 = \frac{180}{2\times 22.4} = 4.24 \text{ mM}$$

and the quantity of *p*-nitroaniline to be hydrogenated to *p*-phenylenediamine with 111 ml. of hydrogen is:

$$R_2 = \frac{111}{3\times 22.4} = 1.65 \text{ mM}$$

Table III gives the comparison, which shows that nitrobenzene has a stronger affinity to the nickel catalyst than *p*-nitroaniline.

TABLE III

Compound		Calcd. mM	Obs. mM
Nitrobenzene	reduced	4.24	
	unchanged	0.76	
p-Nitroaniline	reduced	1.65	
	unchanged	3.35	4.10

Similar treatments of the other competitions are shown in Table IV.

TABLE IV

i) Nitrobenzene and *p*-nitrobenzaldehyde with Raney nickel.

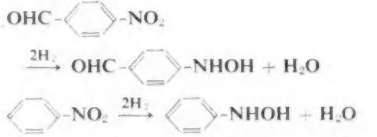

Compound		Calcd. mM	Obs. mM
p-Nitrobenzaldehyde	reduced	1.18	
	unchanged	3.82	0.52
Nitrobenzene	reduced	4.78	
	unchanged	0.22	3.10

Affinity to the catalyst: *p*-Nitrobenzaldehyde >Nitrobenzene

ii) Ethyl *p*-nitrobenzoate and *p*-nitroanisole with Raney nickel.

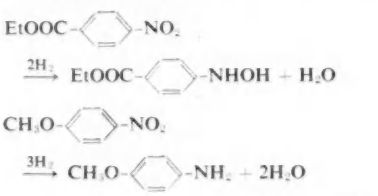

Compound		Calcd. mM	Obs. mM
Ethyl *p*-nitrobenzoate	reduced	1.83	3.15
	unchanged	3.17	
p-Nitroanisole	reduced	2.54	
	unchanged	2.46	2.85

Affinity to the catalyst: Ethyl *p*-nitrobenzoate >*p*-Nitroanisole

Separate and competitive hydrogenation of the nitro compounds were also studied with U-Ni-A catalyst. Results are shown in Table V.

TABLE V

(A) Initial hydrogenation rates of separate hydrogenations.

Nitro compound	1.67 mM
U-Ni-A	1.0 g.

Compound	Rate of hydrogen absorption
Nitrobenzene	126 ml./5 min.
p-Nitrobenzaldehyde	126 ml./2.5 min.
Ethyl *p*-nitrobenzoate	141 ml./5 min.
p-Nitrophenol	138 ml./5 min.
p-Nitroaniline	68 ml./5 min.

(B) Competitive reduction

Nitro compounds	6.67 mM each
U-Ni-A	1.0 g.

i) *p*-Nitrobenzaldehyde and nitrobenzene.

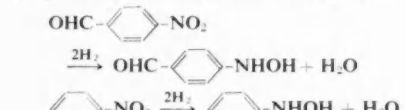

Compound		Calcd. mM	Obs. mM
p-Nitrobenzaldehyde	reduced	4.74	
	unchanged	1.93	
Nitrobenzene	reduced	2.37	
	unchanged	4.30	5.60

Affinity to the catalyst: *p*-Nitrobenzaldehyde >Nitrobenzene

ii) Nitrobenzene and ethyl *p*-nitrobenzoate.

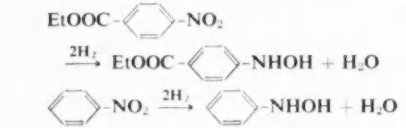

Compound		Calcd. mM	Obs. mM
Ethyl *p*-nitrobenzoate	reduced	3.82	
	unchanged	2.85	
Nitrobenzene	reduced	3.37	
	unchanged	3.30	5.13

Affinity to the catalyst: Ethyl *p*-nitrobenzoate >Nitrobenzene

iii) Nitrobenzene and *p*-Nitrophenol

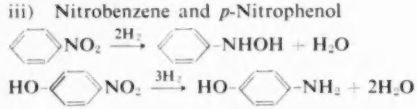

Compound		Calcd. mM	Obs. mM
Nitrobenzene	reduced	4.80	
	unchanged	1.87	0.34
p-Nitrophenol	reduced	3.47	
	unchanged	3.20	5.10

Affinity to the catalyst: Nitrobenzene >*p*-Nitrophenol

iv) Nitrobenzene and *p*-nitroaniline.

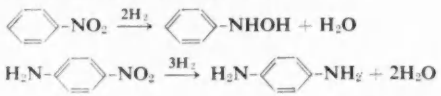

Compound		Calcd. mM	Obs. mM
Nitrobenzene	reduced	5.47	
	unchanged	1.20	0.47
p-Nitroaniline	reduced	1.92	
	unchanged	4.70	6.10

Affinity to the catalyst: Nitrobenzene >*p*-Nitroaniline

To examine further the selectivity in adsorption, the initial rates of hydrogenation of mixtures were measured and compared with the initial rates of separate reduction in Table VI.

TABLE VI

Compound	Initial rate of separate reduction (ml. of H_2/5 min.)	Initial rate of the reduction of mixture (ml. of H_2/5 min.)
Nitrobenzene	216	54
Ethyl *p*-nitrobenzoate	73	
Nitrobenzene	216	63
p-Nitrobenzaldehyde	52	
Nitrobenzene	216	208
p-Nitroaniline	134	

Table VI shows that the reduction rate of a mixture is almost the same as that of the component which is considered to have a stronger affinity to the catalyst. These data also indicate that the difference in affinities of the two components of each combination is great enough to cause completely selective adsorption.

The comparisons of the affinities of the nitro compounds to the nickel catalysts are summarized in Table VII.

TABLE VII

Raney nickel	U-Ni-A
Ethyl *p*-nitrobenzoate >Nitrobenzene	Ethyl *p*-nitrobenzoate >Nitrobenzene
p-Nitrobenzaldehyde >Nitrobenzene	*p*-Nitrobenzaldehyde >Nitrobenzene
Nitrobenzene >*p*-Nitroaniline	Nitrobenzene >*p*-Nitrophenol
Ethyl *p*-Nitrobenzoate >*p*-Nitroanisole	Nitrobenzene >*p*-Nitroaniline

In all the systems studied, an aromatic nitro compound with an electron attracting group in para position has a stronger affinity to the nickel catalysts than the compound with an electron repelling group in the same position.

Other factors that might have effects on the affinities of nitro compounds to the nickel catalysts must also be examined.

Cross Section in Adsorption.—The cross section in adsorption has been neglected in the above discussion but it might affect the apparent affinity of the nitro compound to the nickel catalysts. The molecule with a larger cross section in adsorption may be adsorbed in a smaller number than the molecule with a smaller cross section. Therefore, the same observed rate of separate hydrogenation with U-Ni-A catalyst may suggest that the hydrogenation of one molecule of *p*-nitrophenol is more rapid than that of nitrobenzene. Thus, if there were no selectivity in adsorption, *p*-nitrophenol might be reduced to a greater extent than nitrobenzene in the competitive reduction, but this was not true, and so the selectivity in adsorption rather than the molecular cross section governs the results.

Carbonyl group in ethyl *p*-nitrobenzoate and *p*-nitrobenzaldehyde can attack the active centers of the nickel catalysts, and the strong affinity of *p*-nitrobenzaldehyde and ethyl *p*-nitrobenzoate to the catalyst might be attributed to the adsorption of the carbonyl group. But this is denied, because the partial reduction of *p*-nitrobenzaldehyde gave *p*-hydroxylaminobenzaldehyde, and nitro group is preferentially adsorbed to carbonyl group by the catalysts.

The author wishes to express his hearty thanks to Professor Y. Urushibara for his kind guidance and encouragement throughout this work. He is also very grateful to Dr. M. Kobayashi and Dr. S. Nishimura for their helpful discussion.

Department of Chemistry
Faculty of Science
The University of Tokyo
Hongo, Tokyo

Studies on Extraction of Polonium(IV) by Hexone from Acid Solution

By Niro MATSUURA, Akira OUCHI* and Masuo KOJIMA**

(Received June 10, 1960)

Solution chemistry of polonium(IV) with a weighable quantity of polonium was developed by Bagnall et al.[1] for several years past. However, one of the present authors found that polonium(VI), having a higher oxidation potential with regard to polonium(IV), was not stable, owing to its own α radiation[2]. Accordingly, it is necessary to employ a minute quantity of this element (which does not cause any radiolysis) in order to distinguish the results from self radiolysis. The extraction study of polonium(IV) was undertaken, therefore, with quantities of less than one microcurie of polonium per millilitre. In the course of the present studies on polonium extraction with hexone (methyl isobutyl ketone,) some peculiarities in the extraction characteristics were observed in a certain range of acidity, suggesting that there will be one or more unestablished complex species of polonium other than PoX_6^{2-}[3,4]. These phenomena appeared to be closely related with the history of employed polonium sources as well as with the acid nature of the aqueous phase from which polonium was extracted[3,5-7]. In order to find out new species of polonium(IV) responsible for this peculiarity in aqueous medium, the experiments were carried out under well defined conditions concerning the history of polonium source and the acidity of the extraction system.

Experimental

1) Materials.—Polonium received from Amersham, England, dated June 1959, was in the form of nitrate in 1 N nitric acid. It was used after purification in our laboratory as described below:

A portion of polonium solution was converted into 0.3 N hydrochloric acid solution from which

* A. Ouchi (formerly A. Iguchi).

** Present address: Government Chemical Industrial Research Institute of Tokyo, Yoyogi P. O., Tokyo.

1) K. W. Bagnall, "Chemistry of the Rare Radioelements", Butterworths Scientific Publications, London, (1957), pp. 3–94.

2) N. Matsuura and M. Haissinsky, *J. chim. phys.*, **55**, 475 (1958).

3) M. Guillot, ibid., **28**, 107 (1931).

4) K. W. Bagnall, R. W. M. D'Eye and J. H. Freeman, *J. Chem. Soc.*, **1955**, 3959.

5) G. Hevesy, *Phys. Z.*, **14**, 49, 1202 (1913).

6) K. W. Bagnall and D. S. Robertson, *J. Chem. Soc.*, **1957**, 509.

7) T. Ishimori, This Bulletin, **27**, 529 (1954).

polonium was deposited on a silver foil by electrochemical displacement. The deposited polonium was redissolved in 1 N nitric acid together with metallic silver and was freed from silver by precipitating silver as chloride. The supernatant liquid thus obtained was evaporated to dryness, while the residue was extracted with hot dilute hydrochloric acid. After this purification procedure was repeated several times, the extracted polonium solution was stored in 6 N hydrochloric acid. The resulting solution was the usual starting source of our experiments, though other solutions of different kinds of acid and acidities were sometimes used as well.

2) Activity Measurement.—Twenty microlitres of the solution, containing polonium, was pipetted by a glass micro-syringe furnished with a micrometer. In order to obtain the homogeneity of the samples for the α counting of polonium, two different methods were applied, one by evaporating the pipetted sample directly on a glass plate and the other depositing the polonium on a silver foil by the electrochemical displacement. The simple evaporation method was not suitable for obtaining consistent α activity of polonium, especially when some non-volatile material was present. In the electrochemical method it was desirable to make preliminary extraction with hexone from acid solution in the presence of an excess amount of potassium iodide. By this method all polonium activities could be transferred to an organic phase as hexa-iodo polonium complex, PoI_6^{2-}. The hexone solution thus obtained was placed on a silver foil, while polonium was deposited electrochemically for activity measurement. The discharge rate of electroscope, 5.575 div./min. was standardized against the counting rate of 4π flow counter for the same sample under the same condition of measurement. This yielded 977 counts/min. against 5.575 div./min., i. e., 1 div./min. corresponds to 4.7×10^{-3} microcurie of ^{210}Po.

3) Partition of Polonium between Two Liquid Phases.—For determining the distribution of polonium between hexone and aqueous acid solution the sample solution was shaken at room temperature in a stoppered glass test tube with the same volume of solvent, preliminarily saturated with the acid of the same concentration. The correction of volume change after extraction was needed when the extraction was made from concentrated acid solution. Although in our measurements only several ten micro microlitres of the sample was taken, the errors fell within the limit of 10%. The equilibrium of partition was established in less than 5 min. at the temperature of 20 ± 5°C.

4) Aging of Polonium Solution.—About 80 microlitres of the stock solution which contained a known amount of polonium was taken in 4 ml. of hydrochloric, sulfuric or nitric acid. Just after mixing a portion of polonium was extracted with hexone from the mixture. This provided the data at time 0. The rest of the polonium solution was boiled in a glass flask with reflux condenser for several hours on a steam bath, before it was cooled to room temperature. This aged solution was used as a sample for extraction of polonium.

Results and Discussion

1) Adsorption of Polonium on Glass Wall.—Polonium is generally adsorbed strongly on a number of substances. For example, the adsorption on ion-exchange resins, either cationic or anionic, is so strong that polonium is hardly eluted even by an eluant of high ionic concentration. In this respect, ion-exchange technique did not give any reliable data for studying the complex chemistry of polonium. It seemed to us that the partition method was rather preferable. In the extraction method, however, the adsorption on a glass wall caused another difficulty in the accurate determination of polonium activity. In order to obtain a correct partition coefficient, it is necessary to know the loss of polonium by adsorption from the extraction system. In Fig. 1 the actual adsorption loss was shown in

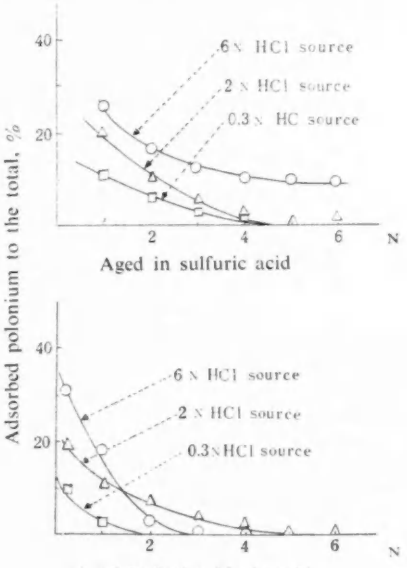

Fig. 1. Adsorption of polonium(IV) on the wall of 1 ml. glass stoppered vessel for hexone extraction.

(Po lost/Total Po used) $\times$ 100% as the function of acidity of the medium from which polonium was extracted. In the hydrochloric acid vs. hexone system the adsorption on a glass wall was very small, if the acid was stronger than 2 N. On the other hand in sulfuric acid-hexone system several hundredths of polonium was left on the surface of the glass wall regardless of the acidity so far as we examined it. Therefore, the adsorption loss cannot be neglected for the correct extraction data.

2) Aging Effect on Nitric Acid.—The amount of polonium extracted from nitric acid solution was nearly constant, 80% being found in the organic phase. This constant value of extraction coefficient can be obtained if the polonium source stored in 6 N nitric acid is employed for extraction after immediate dilution to a given concentration of the acid. Much lower extraction coefficients were observed, on the other hand, if polonium in 0.4 N nitric acid was extracted. In Fig, 2, the extraction

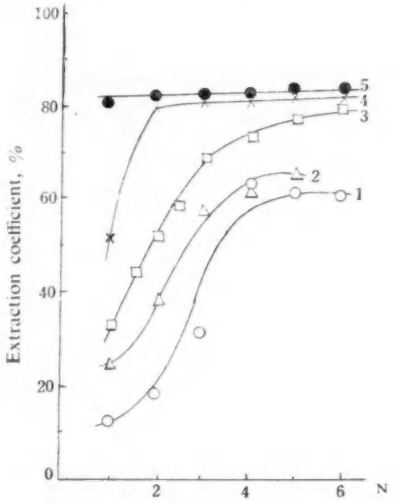

Fig. 2. Aging effect on polonium(IV) extraction with hexone from nitric acid medium for the source stored in 0.4 N (1~4) and in 6 N (5).
-○- 1. Extraction immediately after dilution.
-△- 2. Extraction after 1 hr.'s heating.
-□- 3. Extraction after 2 hr.'s heating.
-×- 4. Extraction after 12 hr.'s heating.
-●- 5. Extraction without aging.

coefficient curve 1 for polonium source in 0.4 N nitric acid fell with decreasing acidity. The aging before extraction by heating under reflux for 1, 2 and 12 hr. at 80°C increased the extraction coefficients up to 80% as shown in corresponding curves 2, 3 and 4 in Fig. 2. This fact suggests that polonium(IV) nitrate complex $Po(NO_3)_5^{2-}$ or $Po(NO_3)_5^-$ [8,9], which is stable in 6 N nitric acid, can be readily extracted by hexone, whereas the hydrolysed complex produced in weak nitric acid below

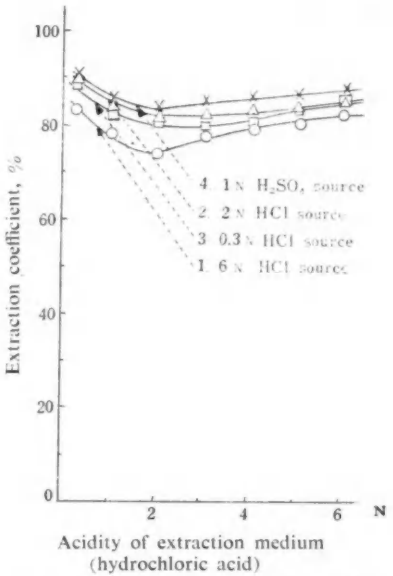

Fig. 3A. Aging effect on extraction coefficients. (Immediately after dilution.) 1. 6 N HCl source 2. 2 N HCl source 3. 0.3 N HCl source 4. 1 N H_2SO_4 source

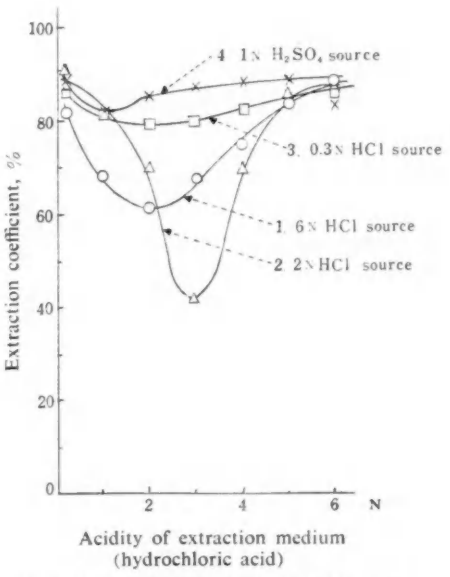

Fig. 3B. Aging effect on extraction coefficients. (Aged for 6 hr. at boiling point.)
1. 6 N HCl source 2. 2 N HCl source 3. 0.3 N HCl source 4. 1 N H_2SO_4 source

8) J. Danon and A. A. L. Zamith, *J. Phys. Chem.*, **61**, 431 (1957).
9) K. W. Bagnall, D. S. Robertson and M. A. A. Stewart. *J. Chem. Soc.*, **1958**, 3633.

1 N is hardly extracted at all. The form of the latter hydrolysed ionic species cannot be detected in our experiments, though some authors suggest that the ionic formula is PoO^{2+} or $Po(OH)_2(NO_3)_4^{2-}$[7].

3) Aging Effect in Hydrochloric Acid.— Aging effect on the extraction characteristics of polonium was also observed in hydrochloric acid as well as in nitric acid. The results were represented in Fig. 3 for the several different polonium sources aged and stored in 0.3, 2 or 6 N hydrochloric acid. In this case polonium was extracted from hydrochloric acid of 0.3~6 N for the samples aged 6 hr. under reflux (A) and non-aged (B). The minimum extraction coefficient was observed at about 2 N hydrochloric acid. This minimum appeared only in the extraction from hydrochloric acid medium. Hence, it was assumed that in hydrochloric acid there would be two different ionic species of polonium complex easily soluble in hexone. A well-established form of polonium(IV) complex in hydrochloric acid is $PoCl_6^{2-}$ which is believed to be formed easily in hydrochloric acid of higher than 6 N and stable even in more dilute acid after it was formed[10,11]. But by aging in more dilute acid solution for prolonged time, the solubility of polonium in hexone decreased as it formed some kinds of hydrolytic products which were hardly soluble in hexone.

4) Ionic Species of Hydrolytic Product.— It is very interesting to estimate the ratio of insoluble species to soluble species from the data of Fig. 3B. This ratio depends not only on the acidity of the extraction system but also on the history of the polonium source. Then, for example, the curve 2 in Fig. 3B, having a sharp minimum at nearly 2 N, can be analysed into two separated curves, as shown in Fig. 4 with dotted lines. These separated curves indicate two different hexone soluble complex species contributed to the extraction at the same time, though in different ways, in the acidity region, one in the range over 3 N and the other in the acidities less than 2 N. The dependence of each curve on the acidity of the extraction system can be shown in Fig. 5 by the logarithmic plots of Polonium soluble/Polonium insoluble or $E'/(1+E')$ as a function of acidity in linear scale. Here, E' denotes the extraction coefficient for separated species. These plots have linear character with the tangential increment 4. Applying mass action law to this system for the hydrolytic reaction given by (1), an equilibrium relation (2) is obtained between two polonium species, soluble and insoluble, which shows dependence on the fourth power of acidity.

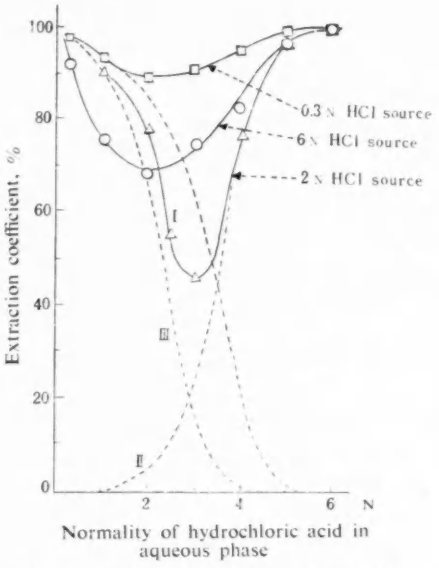

Fig. 4. Analysis of the extraction coefficient curve.

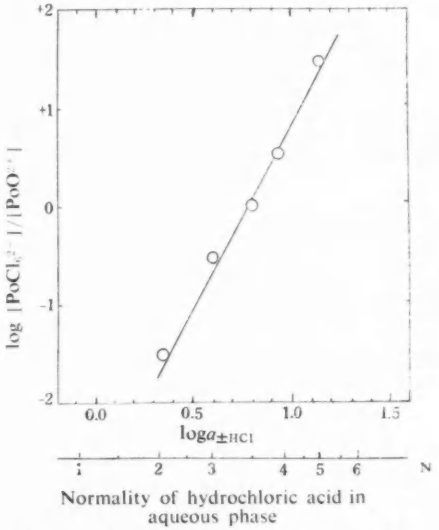

Fig. 5. Logarithmic plots of curve II in Fig. 4.

$$PoCl_6^{2-} + 2H_2O = Po(OH)_2Cl_4^{2-} + 2H^+ + 2Cl^- \quad (1)$$

$$\frac{PoCl_6^{2-}\ \text{soluble in hexone}}{Po(OH)_2Cl_4^{2-}\ \text{insoluble}} = K\cdot[H^+]^2\cdot[Cl^-]^2$$

10) D. J. Hunt, *Amer. Rep.*, MLM, 979 (1954).
11) K. W. Bagnall and J. H. Freeman, *J. Chem. Soc.*, 1956, 2770.

$$\text{or} \quad \frac{\text{Po(IV) soluble}}{\text{Po(IV) insoluble}} = \frac{E'}{1-E'} = K \cdot a^2_{\pm HCl}$$

Where, $a_{\pm HCl}$ is the mean activity of hydrochloric acid. It seemed from the above consideration that the species of $Po(OH)_2Cl_4^{2-}$ or $PoO^{2+}(H_2O+4Cl^-)$ is responsible for the appearance of minimum extraction from hydrochloric acid medium at the concentration about 2 N.

However, the idea is not entirely excluded that polonium nitrate complex formed in the purification process is partly extracted even from hydrochloric acid. Accordingly, it is possible to assume that the minimum value of extraction appears in the acidity most favorable to hydrolytic reaction succeeded by the following schema:

$$Po(NO_3)_6^{2-} + 2H_2O = PoO^{2+} + 2H^+ + 6NO_3^- + H_2O$$

$$PoO^{2+} + 2H^+ + 6Cl^- + H_2O = PoCl_6^{2-} + 2H_2O$$

$$Po(NO_3)_6^{2-} + 6Cl^- = PoCl_6^{2-} + 6NO_3^-$$

Here, unconverted nitrate complex contributes to the extraction in the concentration range of hydrochloric acid lower than 2 N. In this hypothesis, an assumption of an uncertain soluble complex of polonium is not necessary.

However, there is no reason to believe that the nitrate complex is more stable than chloro-complex nor that the conversion of nitrate complex into chloro-complex is incomplete.

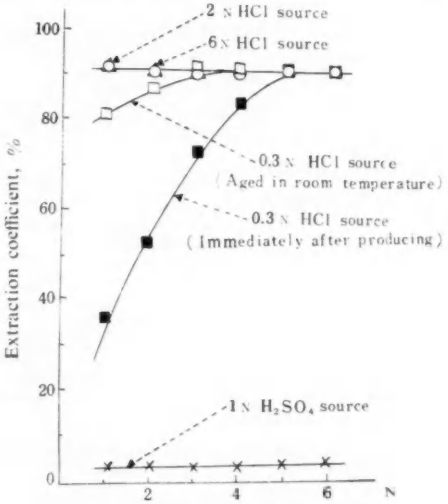

Fig. 6A. Aging effect on extraction coefficient. (Immediately after dilution.)

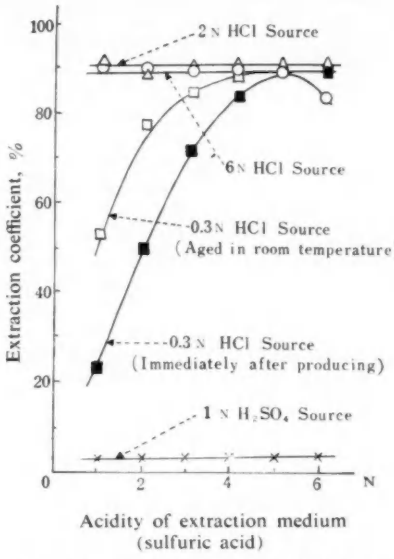

Fig. 6B. Aging effect on extraction coefficient. (Aged for 6 hr. at boiling point.)

5) Aging Effect on the Extraction from Sulfuric Acid Medium.—Partition equilibrium of polonium(IV) between hexone and aqueous solution of sulfuric acid was also studied with the different sources of polonium, stored in 6, 2 and 0.3 N hydrochloric acid and 1 N sulfuric acid, respectively. The results were shown in Fig. 6. Among them only the polonium source prepared and stored in sulfuric acid

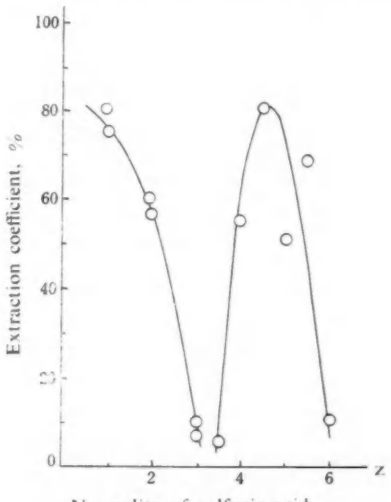

Fig. 7. Extraction of polonium(IV) in sulfuric acid.

gives extraction coefficient nearly nul in the entire range of acidity examined. This indicates that a trace quantity of chloride, if present in sulfuric acid, causes a remarkable increase of extraction yield and that the yield attains the maximum value corresponding to that of hexachloro-polonium(IV) complex, $PoCl_6^{2-}$. It can be said that one of the complex species, $PoCl_5^{2-}$ is readily formed in the presence of a minimum quantity of chloride in sulfuric acid. In our latest publication on polonium the extraction of polonium(IV) from sulfuric acid medium passed through maximum and minimum phases as shown in Fig. 7. This was observed by using the polonium source of 6 N hydrochloric acid after diluting 100 times with sulfuric acid before extraction. In this case the aging was made at 80°C for one hour by heating on a steam bath. A minimum value of extraction that appeared in the proximity of 2 N sulfuric acid is consistent with the results obtained for the extraction from hydrochloric acid by using an aged polonium source as already mentioned in 3). From this consideration the present authors prefer the ionic form PoO^{2+} as the stable species of polonium(IV) in sulfuric acid to that of PoO_3^{2-} which is regarded as stable in less acidic solution according to the analogy of $Te(IV)O_3^{2-}$.

Summary

The ionic state of polonium(IV) in hydrochloric and sulfuric acid solution was studied by the solvent extraction with hexone (methyl isobutyl ketone).

1) The polonium solution stored in 0.4 N nitric acid is strongly hydrolysed by aging. The low extraction coefficient caused by hydrolysis became higher by heating the polonium solution in stronger nitric acid. On the other hand, the polonium stored in 6 N nitric acid can be extracted with constant extraction coefficient, about 80%, through the entire acidity range from 1 to 6 N., if the extraction was carried out without any aging.

2) The aging effect of polonium(IV) in hydrochloric acid is rather complicated. A minimum extraction appeared in the acidity range near 2 N hydrochloric acid. By applying mass action law the probable form of polonium(IV) in that range was $Po(OH)_2Cl_4^{2-}$ or PoO^{2+}, assuming that $PoCl_5^{2-}$ was the stable form of polonium(IV) in 6 N hydrochloric acid which is readily soluble in hexone.

3) Almost no polonium(IV) was extracted by hexone from sulfuric acid solution. Here, the polonium(IV) in sulfuric acid exists probably as PoO^{2+} rather than as PoO_3^{2-}.

The authors wish to express their thanks to Professor T. Shirai and to their colleagues in the laboratory for their helpful discussions. A part of the expenses of these studies was defrayed by a grant from the Ministry of Education.

College of General Education
The University of Tokyo
Meguro-ku, Tokyo

On the Differences in Monolayer Properties of Poly-γ-benzyl-L-glutamate and Poly-β-benzyl-L-aspartate

By Shoichi IKEDA and Toshizo ISEMURA

(Received July 28, 1960)

Recently great progress has been made in the studies on synthetic polypeptides, especially concerninig their solutions. Among them, the solutions of poly-γ-benzyl-L-glutamate in various solvents have been investigated extensively and it is found that this polymer has a right-handed α-helical configuration in some solvents[1]. More recently it has been reported, however, that poly-β-benzyl-L-aspartate, the side chain of which has a length by one methylene group less than that of poly-γ-benzyl-L-glutamate, is quite different from poly-γ-benzyl-L-glutamate in its behavior and that the α-helix of the former polymer may be left-handed rather than right-handed[2].

1) P. Doty, J. H. Bradbury and A. M. Holtzer, *J. Am. Chem. Soc.*, **78**, 947 (1956); J. T. Yang and P. Doty, ibid., **79**, 761 (1957); E. R. Blout, P. Doty and J. T. Yang, ibid., **79**, 749 (1957).

2) E. R. Blout and R. H. Karlson, ibid., **80**, 1259, 6701 (1958); E. M. Bradbury, L. Brown, A. R. Downie, A. Elliott, W. E. Hanby and T. R. R. McDonald, *Nature*, **183**, 1736 (1959); R. H. Karlson, K. S. Norland, G. D. Fasman and E. R. Blout, *J. Am. Chem. Soc.*, **82**, 2268 (1960).

According to the surface chemical studies, synthetic polypeptides with non-polar or unionized side chains are known to give monolayers of condensed type on aqueous surfaces, the surface viscosity of which is manifest at a very low surface pressure region, but only those which contain prolyl residues in some high amounts give monolayers of expanded type, the surface viscosity of which is manifest first at a very high surface pressure region[3,4]. In general, therefore, the monolayers of ordinary unionized polypeptides are of condensed type and exhibit high surface viscosities, and the only difference among those which are composed of different amino acid residues are reflected explicitly in the behavior of the surface potential, according to the difference in polarities or electric moments of their side chains. Considering the striking difference in properties of poly-γ-benzyl-L-glutamate and poly-β-benzyl-L-aspartate in crystals or in solutions, as cited above, however, it is expected that the two polymers behave in a different way in their spread monolayers, since the difference of the two polymers in solutions and in crystals will be based on the different kinds of interactions of side chain with main chain or with other side chains and such an effect of side chain of polymers will be most distinctly revealed in monolayer states.

We have thus studied the monolayers of poly-γ-benzyl-L-glutamate (PBLG) and poly-β-benzyl-L-aspartate (PBLA) by the measurements of surface pressure, potential and viscosity. We will report any marked differences in their behavior and propose possible chain configurations of these polymers in monolayers and then discuss the differences on the basis of these configurations. Further we have examined the monolayer of a copolymer of γ-benzyl-L-glutamate and β-benzyl-L-aspartate, copoly-1 : 1-(γ-benzyl-L-glutamate, β-benzyl-L-aspartate) (CP(BLG, BLA)), and the equimolar mixture of PBLG and PBLA.

Experimental

PBLG (Code No. J11A) and PBLA (J826) were prepared by polymerizing *N*-carboxy-anhydrides of the corresponding L-amino acids in dioxane with triethylamine and CP(BLG, BLA) (A227B) by copolymerizing the equimolar mixture of *N*-carboxy-anhydrides of these amino acids in (1 : 1 v/v) chloroform-dioxane with triethylamine. Their intrinsic viscosities in dichloroacetic acid solution at 25°C were 0.13, 0.11 and 0.34, respectively. Their solutions in (1 : 4 v/v) dichloroacetic acid-benzene were spread on aqueous surfaces. The equimolar mixed monolayer of PBLG and PBLA was spread from their mixed solution in the same solvent.

The surface pressure was measured by a surface balance of the hanging plate type, the surface potential by a vibrating electrode and the surface viscosity by a rotatory oscillating disk[3,4]. The temperature was regulated by heating the inside of the shielding box with a voltage controlled lamp, if necessary.

Results

The surface pressure, Π, surface potential, ΔV, and surface viscosity, η, of PBLG, PBLA and CP(BLG, BLA) are plotted against the area, expressed in the unit of Å² per (average)

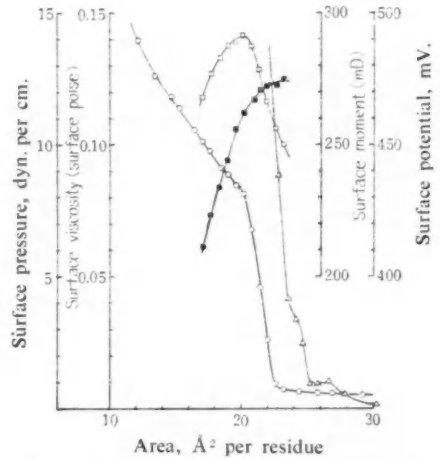

Fig. 1. Monolayer of PBLG at 9.0°C. ○, surface pressure; □, surface potential; ■, surface moment; △, surface viscosity.

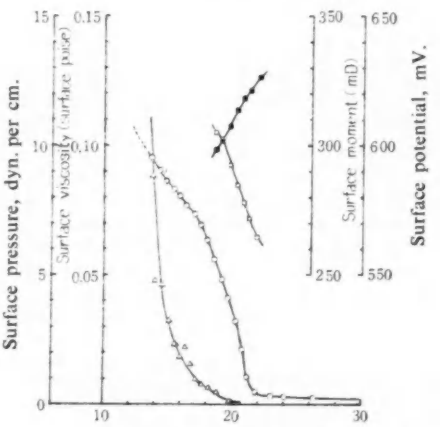

Fig. 2. Monolayer of PBLA at 10.8°C. ○, surface pressure; □, surface potential; ■, surface moment; △, surface viscosity.

3) T. Isemura and S. Ikeda, This Bulletin, 32, 178 (1959).
4) S. Ikeda and T. Isemura, ibid., 32, 659 (1959).

TABLE I. MONOLAYER CHARACTERISTICS OF POLYPEPTIDES

	$A_{II\to 0}$, Å^2	$A_{\Delta V}$, Å^2	$\mu_{21\text{Å}^2}$, mD	$A_{\eta=0.10}$, Å^2
PBLG	22.8	23.2	270	22.7 (9.0°C)
PBLA	21.5	22.0	322	13.5 (10.8°C)
CP(BLG, BLA)	23.0	22.6	305	23.4 (12.3°C)
1 : 1 PBLG+PBLA	22.4	22.5	240	13.4 (19.3°C)

TABLE II. SURFACE COMPRESSIBILITIES

	δ_1, cm./dyn.	δ_2, cm./dyn.	δ_3, cm./dyn.
PBLG	0.0126 (22.8~20.3Å^2)	0.0855 (20.3~ca. 11.4Å^2)	—
PBLA	0.0222 (21.5~20.3Å^2)	0.0329 (20.3~ca. 17Å^2)	0.129 (ca. 17~14.0Å^2)
CP(BLG, BLA)	0.0195 (23.0~18.3Å^2)	1.21 (18.3~ca. 12Å^2)	—
1 : 1 PBLG+PBLA	0.0191 (22.4~19.5Å^2)	0.114 (19.5~ca. 14Å^2)	—

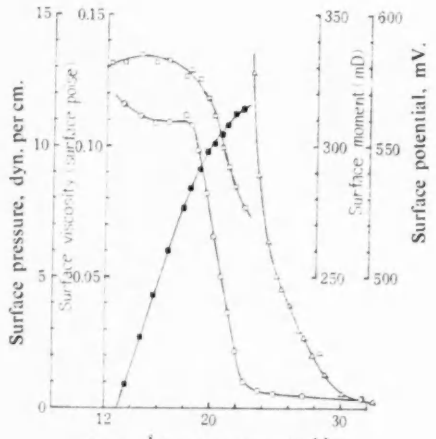
Surface pressure, dyn. per cm.
Surface viscosity (surface poise)
Surface moment (mD)
Surface potential, mV.
Area, Å^2 per average residue

Fig. 3. Monolayer of CP(BLG, BLA) at 12.3°C. ○, surface pressure; □, surface potential; ■, surface moment; △, surface viscosity.

amino acid residue, as shown in Figs. 1, 2 and 3. All the monolayers are of condensed type. The surface potential was not definite but fluctuated from time to time at the region of large areas. However, reproducible values were observed as the surface pressure began to rise. Values of the area, $A_{II\to 0}$, at which the surface pressure steeply increases on compression, and of the area, $A_{\Delta V}$, at which the surface potential becomes reproducible on compression, are tabulated in Table I. The surface pressure and potential were scarcely at all influenced by temperature. The $A_{II\to 0}$ is nearly equal to $A_{\Delta V}$ for each polymer and they will represent the actual area occupied by an (average) amino acid residue.

The values of surface compressibility calculated by

$$\delta = -\frac{1}{A}\frac{\partial A}{\partial II}$$

are given in Table II, which shows clearly the difference in surface pressure-area curves of the three polymers. In the region of low surface pressure the surface compressibility is in the order: PBLA>CP(BLG, BLA)>PBLG. The surface pressure-area curve of CP(BLG, BLA) is characterized by the region of very high surface compressibility such as that observed for poly-γ-benzyl-DL-glutamate[5].

The surface moments per amino acid residue calculated by the Helmholtz equation

$$\mu = \frac{A \cdot \Delta V}{4\pi}$$

are plotted against the area, as is also shown in Figs. 1, 2 and 3, and the values at 21 Å^2 are also listed in Table I. It is noticed that the surface moment of PBLA is about 50 mD higher than that of PBLG and CP(BLG, BLA) has an intermediate value of these two.

Although some differences are observed in surface pressure and potential between PBLG and PBLA, as described above, they are most distinctly reflected in surface viscosity behavior. The surface viscosity of PBLG is very high at very low surface pressure region, but that of PBLA is manifest first at high surface pressure region; the surface viscosity of the former is much lower than that of the latter. It is remarkable that, in spite of the condensed nature of monolayer reflected in surface pressure, PBLA has a very low surface viscosity. A monolayer of polymer with such composite properties, i. e., a monolayer of condensed type with a low surface viscosity, has never been reported. The surface viscosity-area curve of CP(BLG, BLA) is similar to that of PBLG rather than being an intermediate between PBLG and PBLA.

The surface viscosities of PBLG and PBLA were markedly influenced by temperature and they were higher as the temperature was high.

5) T. Isemura and K. Hamaguchi, ibid., 27, 125 (1954).

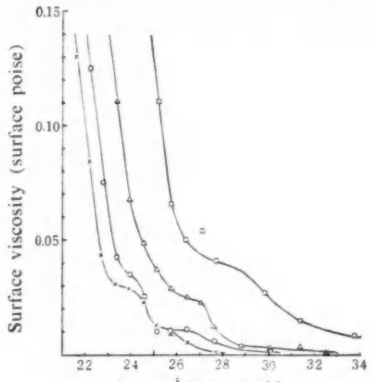

Fig. 4. Variation of surface viscosity of PBLG with temperature. □, 24.0°C; △, 16.2°C; ○, 9.0°C; ×, 5.6°C.

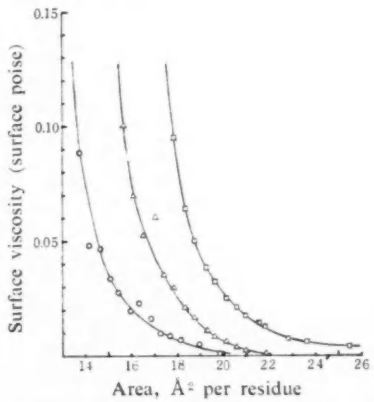

Fig. 5. Variation of surface viscosity of PBLA with temperature. □, 24.5°C; △, 17.9°C; ○, 10.8°C.

The variations of surface viscosity with temperature are shown in Figs. 4 and 5. Contrary to the common nature of the expanded monolayer[4], PBLA has a positive temperature coefficient of surface viscosity rather than a negative one.

Values of the area, $A_{\eta=0.10}$, at which the surface viscosity reaches 0.10 surface poise, are also given in Table I.

Discussion

Chain Configurations of PBLG and PBLA in Monolayer.—The values of the limiting area, $A_{//\to 0}$, derived from the surface pressure-area curves imply that these three polymers assume a configuration such as the β-form in monolayers. Although the limiting area, 22 Å², of these polymers is somewhat larger than that of some other polypeptides such as poly-DL-alanine, 15 Å²[3,6], this suggests that the area occupied by a residue is not defined by the main chain only but by the large side chain for these polymers. As the polymers are composed of L-amino acid residues exclusively, the side chains are oriented up and down alternatively when spread on an aqueous surface, assuming a β-configuration[6,7] but the hydrophilic or hydrophobic nature and the orientation of side chain should be different from that of non-polar polypeptides owing to the presence of two oxygen atoms.

Since the three polymers have polar groups on a side chain as well as on the main chain and then the side chain has both hydrophilic and hydrophobic nature, the side chain can change its orientation with greater ease sometimes rising into the air, sometimes lying on the surface and sometimes submerging into the water. The fluctuation of surface potential at large areas might be ascribed to such a thermal motion of the side chain. On high compression, however, the orientation of the side chain is forced to be fixed into a definite position, as given below. Thus the area, $A_{\perp V}$, at which the surface potential gives a definite value, is nearly equal to the limiting area, $A_{//\to 0}$.

As shown in Table I, the surface moments of these three polymers are much higher than those of polypeptides with non-polar side chains such as poly-DL-alanine, 160 mD[3]. This can be attributed to the contributions of the polar groups on side chain, i.e., the electric moments of the carbonyl group and the H–C–O bond, to the surface moment besides that of the main chain. If the carbonyl group on the side chain is directed towards the aqueous surface with an angle $90° - \theta$, then the 'surface moment' of the side chain of PBLG and PBLA is given by

$$\text{(A)} \qquad \mu_{C=O}\cos\theta - \mu_{C-O}\cos(\theta + 30°)$$

if all the bonds on the side chain are assumed to be in trans form, or by

$$\text{(B)} \qquad \mu_{C=O}\cos\theta + \mu_{C-O}\cos(\theta + 30°)$$

if the O–C–O bond alone takes cis form. About half of the side chains are submerged into the aqueous subphase and surrounded by water molecules; this does not contribute to the surface moment[5]. Thus the total surface moment observed experimentally consists of

6) C. W. N. Cumper and A. E. Alexander, *Trans. Faraday Soc.*, **46**, 235 (1950).
7) J. T. Davies, *Biochim. Biophys. Acta*, **11**, 165 (1953).
8) J. T. Davies, *Trans. Faraday Soc.*, **49**, 949 (1953).

TABLE III. CALCULATED VALUES OF SURFACE MOMENTS

$\mu = 160\,\text{mD} + 1/2\,\mu(\text{side chain})$

θ (°)		0	30	35	40	45	50	55	60	90
μ(mD)	(A)	242	274	272	269	266	261	252	250	203
	(B)	439	359	344	327	309	291	271	250	117

the contributions of the main chain, 160 mD[9], and of half the 'surface moment' of the side chain. If it is assumed that $\mu_{C=O} = 360$ mD and $\mu_{C-O} = 170$ mD[9], the total surface moment can be calculated for various values of θ in either case, (A) or (B). The results are given in Table III. Comparing these calculated values with the observed values in Table I, it is found that the side chain of PBLA has a configuration with $\theta = 40°$ in which all the bonds are trans except that the O–C(=O) bond is cis. On the other hand, the configuration of the side chain of PBLG has two possible configurations from the data on surface moment alone, but it is confined to the one with all the bonds being trans other than the O–C(=O) bond and with $\theta = 55°$, if the limiting area derived from the surface pressure is taken into account. The configurations deduced thus are illustrated as follows:

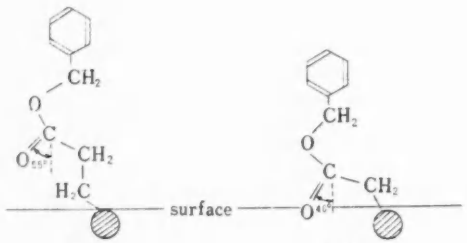

PBLG PBLA

It can be seen that the orientations of side chains of PBLG and PBLA are quite different from each other, although the difference in their structure is only by one methylene group in side chain length. In other words, the carbonyl group on the side chain of PBLG seems to play the role of a hydrophobic part and does not serve for the hydrophility of the side chain very well, but that of PBLA is submerged into the aqueous subphase and is indistinguishable from the carbonyl group on the main chain, thus greatly increasing the hydrophilic nature of the side chain.

The value of surface moment of CP(BLG, BLA) intermediate between PBLG and PBLA supports the configuration similar to the β-form for these three polymers in monolayer and the value, 305 mD, slightly higher than the mean value, 296 mD, suggests that the side chains of γ-benzyl-L-glutamate residue are influenced by β-benzyl-L-aspartate residue in this copolymer.

The observed value of surface moment of γ-benzyl-L-glutamate residue in PBLG, $\mu_{21A^2} = 270$ mD, may be compared with that of γ-methyl-L-glutamate residue in copoly-1 : 1-(γ-methyl-L-glutamate, DL-phenylalanine). The latter copolymer has a surface moment per amino acid residue, $\mu_{19A^2} = 197$ mD[9]. Since the surface moment of poly-DL-phenylalanine is 110 mD[9], the contribution of γ-methyl-L-glutamate residue to the surface moment of the copolymer should be 284 mD, which is in accord with the surface moment of γ-benzyl-L-glutamate residue in PBLG.

Relation of Surface Viscosity with Surface Pressure.—As was noted before, whereas PBLG gives a high surface viscosity at areas larger than the area at which the surface pressure begins to rise steeply or the limiting area, i. e., at a very low surface pressure region, PBLA shows a high surface viscosity only at areas far smaller than the limiting area, i. e., at a high surface pressure region. In other words, the surface viscosity is much higher for PBLG than for PBLA. The behavior as was observed for PBLG has the general characteristics of monolayers of condensed type. However, that for PBLA has not been noticed for monolayers of any polymers so far examined, but only for monolayers of long chain fatty acids[10] and their mixtures with each other or with long chain alcohols[11]. This striking difference between PBLG and PBLA may be interpreted on the basis of the configurations of side chains presented above.

The monolayer of PBLG would correspond to the glassy state polymers in three dimensional state in which the interaction between segments are very strong, and consequently the monolayer is condensed and the surface viscosity is very high[4]. In this case the interaction between segments would mainly be the hydrogen bonding between peptide bonds in the main chain. The monolayer of PBLA would also correspond to the glassy state. In the case of PBLA, however, the carbonyl group on the side chain is submerged into water like

9) A. E. Alexander and J. H. Schulman, *Proc. Roy. Soc.*, **A161**, 115 (1937).

10) G. E. Boyd and W. D. Harkins, *J. Am. Chem. Soc.*, **61**, 1188 (1939).

11) G. E. Boyd and F. Vaslow, *J. Colloid Sci.*, **13**, 275 (1958).

the one on the main chain, as referred to before, and, therefore, the interactions between segments are not necessary ascribed to the hydrogen bonding between peptide bonds but also possibly to the hydrogen bonding of the carbonyl group on the side chain with the imino group on the main chain. The monolayer configuration of PBLA would be less stable than that of other polypeptides and a part of the molecular chain can easily be submerged into the aqueous subphase under compression or under shear flow. Further, the hydrophilic nature of the side chain is greatly enhanced owing to the carbonyl group in contact with water and would be responsible for reducing the resistance against compression or shear. Thus the high surface compressibility and the low surface viscosity of PBLA will be exhibited after the surface pressure begins to rise or the monolayer is compressed to the limiting area.

The specific nature of the side chain of PBLA seems to be related to its reactivity when it is reduced to remove the benzyl group on the side chain. By this treatment, PBLA does not produce poly-α-L-aspartic acid but gives poly-anhydro-L-aspartic acid[12], while PBLG gives poly-α-L-glutamic acid. This also suggests that the carbonyl group on the side chain is scarcely distinguishable from that on the main chain.

The variations of surface viscosity with temperature for PBLG and PBLA are given in Figs. 4 and 5. If the logarithms of surface viscosity of PBLA at different temperatures are plotted against surface pressure, a part of each curve gives a straight line expressed by

$$\log \eta = \log \eta_0 + c\Pi$$

as shown in Fig. 6. The same type of equation has been found for some other monolayers[4,10,11,13]. The constants of this equation for PBLA are tabulated in Table IV. No further implication of these constants is clear.

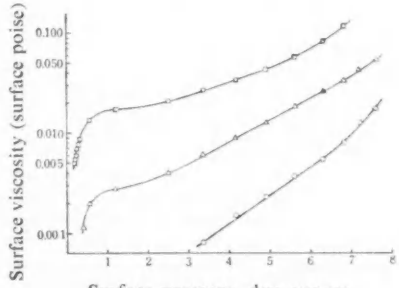

Fig. 6. The $\log \eta$-Π plots for PBLA at different temperatures. □, 24.5°C; △, 17.9°C; ○, 10.8°C.

TABLE IV. CONSTANTS OF THE $\log \eta$-Π RELATION FOR PBLA

Temperature, °C	$\log \eta_0$	c	Π, dyn./cm.
24.5	−1.99	0.124	2.0~5.0
17.9	−2.92	0.207	2.2~6.5
10.8	−3.77	0.249	2.2~7.0

The Equimolar Mixed Monolayes of PBLG and PBLA. — The monolayer characteristics of the equimolar mixture of PBLG and PBLA are shown in Fig. 7. The limiting areas

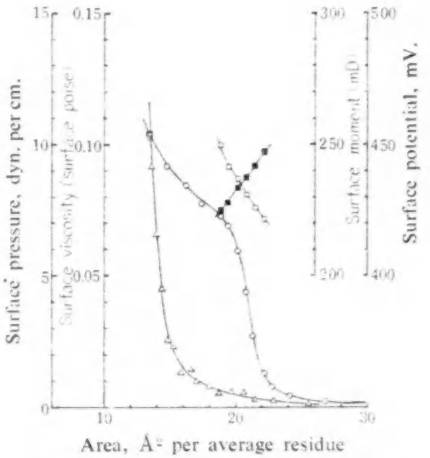

Fig. 7. Equimolar mixed monolayer of PBLG and PBLA at 19.3°C. ○, surface pressure; □, surface potential; ■, surface moment; △, surface viscosity.

derived from the surface pressure and from the surface potential are equal to each other and are about 22 Å², and the surface compressibility at the region of rise of surface pressure is intermediate between those for PBLG and PBLA and almost equal to that of CP(BLG, BLA). However, the surface moment and viscosity are much lower than those of CP(BLG, BLA). These characteristics are also given in Tables I and II. The reason for the low surface moment and the low surface viscosity of the mixed monolayer is not clear, since the dipole-dipole interaction would not be strong enough to influence monolayer properties very appreciably[14].

12) J. Noguchi, T. Saito and M. Asai, *J. Chem. Soc. Japan, Pure Chem. Sec.* (*Nippon Kagaku Zasshi*), **81**, 620 (1960).

13) T. Isemura and K. Fukuzuka, *Mem. Inst. Sci. Ind. Res., Osaka Univ.*, **13**, 137 (1956).

14) J. Marsden and J. H. Schulman, *Trans. Faraday Soc.*, **34**, 748 (1938); W. D. Harkins and R. T. Florence, *J. Chem. Phys.*, **6**, 847 (1938).

Summary

In view of the marked differences of PBLG and PBLA in crystals and in solutions, we have investigated their differences in monolayer states and further examined the monolayers of CP(BLG, BLA) and of the equimolar mixture of PBLG and PBLA.

All these polymers were found to be of condensed type and their limiting areas to be about 22 Å^2. The surface compressibility at the region of rise of surface pressure was in the order: PBLA>CP(BLG, BLA)>PBLG. The surface moments of all these polymers were considerably higher than those of non-polar polypeptides. The surface moment of PBLA was 50 mD higher than that of PBLG, and that of CP(BLG, BLA) gave a value intermediate between them. PBLG and CP(BLG, BLA) exhibited high surface viscosities at a very low surface pressure region, but, in spite of the condensed nature of the monolayer, PBLA showed appreciable surface viscosity first at a high surface pressure region. The surface viscosities of PBLG and PBLA were higher at higher temperatures.

From the data on surface pressure and surface moment, all these polymers were considered to have a configuration similar to the β-form in the spread state and possible configurations of side chains of PBLG and PBLA were deduced. It was found that the carbonyl group on the side chain of PBLG is far from the aqueous surface but that of PBLA is in contact with the surface and scarcely distinguishable from the carbonyl group on the main chain. Accordingly, PBLG can take a stable configuration like the β-form in monolayer, but the correspounding configuration of PBLA will be less stable owing to possible hydrogen bonding of the carbonyl group on the side chain with the imino group on the main chain and the resulting enhanced hydrophility of the side chain. This might be ascribed to the differences in surface compressibility and surface viscosity of PBLG and PBLA.

The surface pressure behavior of the mixed monolayer of PBLG and PBLA was such as was expected, but its behavior in surface potential and viscosity was very anomalous.

We wish to acknowledge to Professor J. Noguchi of Kanazawa University our indebtedness for his kind guidance in preparing the polypeptides.

Faculty of Science (S. I. & T. I.) and
Institute for Protein Research (T. I.)
Osaka University
Osaka

Monolayer Studies on Polyanhydro-L-glutamic and Polyanhydro-L-aspartic Acids

By Shoichi IKEDA and Toshizo ISEMURA

(Received August 15, 1960)

When poly-γ-benzyl-L-glutamate is reduced to remove the benzyl group in an anhydrous state, poly-α-L-glutamic acid is obtained[1]. However, even if poly-β-benzyl-L-aspartate is treated in the same way, no poly-α-L-aspartic acid but only polyanhydro-L-aspartic acid can be obtained[2]. Berger et al.[3] has reported that poly-α-L-aspartic acid is prepared by this method, but Noguchi et al.[2] has suggested that the polymer obtained by Berger et al. would be a copolymer of L-aspartic acid with its andydride. Furthermore, Asai et al.[4] has shown that polyanhydro-L-glutamic acid can be produced by dehydrating poly-α-L-glutamic acid with acetic anhydride. Polyanhydro-L-glutamic acid may be identified with either poly-L-glutarimide (I) or poly-L-pyrrolidone-2-carboxylic acid (II), and polyanhydro-L-aspartic acid with either poly-L-succinimide (III) or poly-L-propiolactam-2-carboxylic acid (IV). Noguchi et al.[2,4] has demonstrated from the

1) W. E. Hanby, S. G. Waley and J. Watson, *J. Chem. Soc.*, **1950**, 3239; E. R. Blout and M. Idelson, *J. Am. Chem. Soc.*, **78**, 497 (1956); M. Idelson and E. R. Blout, ibid., **80**, 4631 (1958).

2) J. Noguchi, T. Saito and M. Asai, *J. Chem. Soc. Japan, Pure Chem. Sec. (Nippon Kagaku Zasshi)*, **81**, 622 (1960).

3) M. Frankel and A. Berger, *J. Org. Chem.*, **16**, 1513 (1951); A. Berger and E. Katchalski, *J. Am. Chem. Soc.*, **73**, 4084 (1951).

4) M. Asai, K. Imai and J. Noguchi, *J. Chem. Soc. Japan, Pure Chem. Sec. (Nippon Kagaku Zasshi)*, **81**, 624 (1960).

syntheses of appropriate polymers and the comparison of their infrared spectra that polyanhydro-L-glutamic acid is poly-L-glutarimide itself and polyanhydro-L-aspartic acid is poly-L-succinimide.

We have examined the monolayers of polyanhydro-L-glutamic acid, poly-DL-pyrrolidone-2-carboxylic acid, polyanhydro-L-aspartic acid and poly-L-succinimide at air-water interfaces and attempted to obtain further information concerning the structure of the polyanhydro acids. Some of these polymers are interesting in themselves for monolayer studies, since they are composed of chains of rings directly connected with each other and expected to have highly rigid structures.

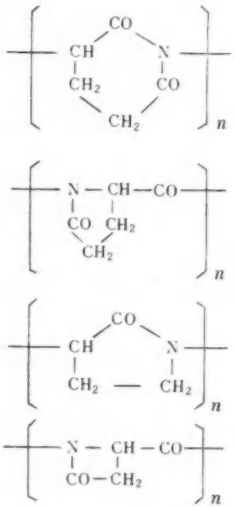

Experimental

Polyanhydro-L-glutamic acid and poly-DL-pyrrolidone-2-carboxylic acid were prepared by Professor Noguchi and his collaborators[4]. Polyanhyro-L-aspartic acid was prepared by reducing poly-β-benzyl-L-aspartate[5] in glacial acetic acid with anhydrous hydrobromic acid. Poly-L-succinimide was also prepared by Professor Noguchi et al.[2]

Surface pressure, potential and viscosity were measured by the methods as described previously[5]. Surface moment was calculated by the usual Helmholtz equation. Area was expressed in the unit of $Å^2$ per residue, a residue being assumed to consist of an anhydro acid residue plus a water molecule. The spreading solvent was a mixture of dichloroacetic acid-benzene (1 : 1 v/v) throughout the present investigation.

Results and Discussion

Polyanhydro-L-glutamic Acid.—Two kinds of polymers, i. e., poly-L-glutarimide and poly-L-pyrrolidone-2-carboxylic acid, are possibly assumed as polyanhydro-L-glutamic acid. The former has a structure composed of rings exclusively, each connected directly by a C–N linkage, and is expected to be rigidly folded. The latter has a structure similar to poly-L-proline but is different from poly-L-proline by the presence of a carbonyl group in the pyrrolidone ring and expected to be highly hydrophilic. Poly-DL-pyrrolidone-2-carboxylic acid did not spread on distilled water but gave stable films on aqueous salt solutions, as illustrated in Fig. 1. The films of poly-DL-

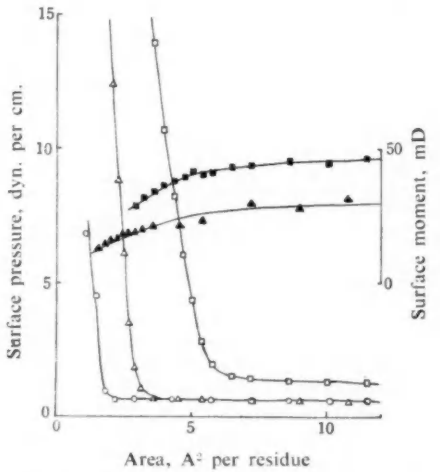

Fig. 1. Plots of surface pressure and surface moment of poly-DL-pyrrolidone-2-carboxylic acid against area (10°C). Aqueous subphases: potassium chloride solutions; ○, 0.01 M; △, ▲, 0.1 M; □, ■, 1 M.

pyrrolidone-2-carboxylic acid are of condensed type, in contrast to the expanded nature of poly-L-proline film. The reason why the film is condensed is not clear, since an expanded nature of polypeptide monolayer is ascribed to the structure devoid of hydrogen bonding[6] and polypyrrolidone carboxylic acid can include no hydrogen bond as polyproline.

On the other hand, polyanhydro-L-glutamic acid gave a stable monolayer of condensed type on distilled water, as shown in Fig. 2. This already indicates that polyanhydro-L-glutamic acid is not identical with poly-L-pyrrolidone-2-carboxylic acid but is poly-L-glutarimide itself. The limiting areas from surface pressure and surface viscosity were equally 13 A^2, which was smaller than those assigned to a

5) S. Ikeda and T. Isemura, This Bulletin, 34, 416 (1961).
6) T. Isemura and S. Ikeda, ibid., 32, 178 (1959).

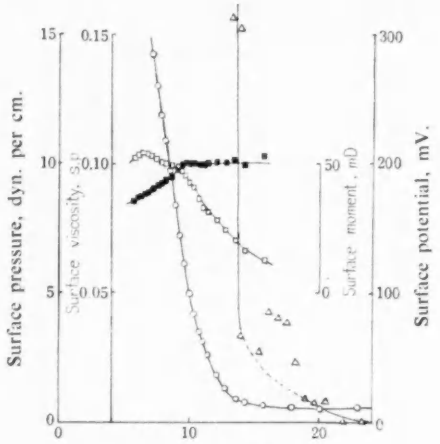

Fig. 2. Monolayer of polyanhydro-L-glutamic acid on distilled water (10°C).
○, surface pressure; □, surface potential; ■, surface moment; △, surface viscosity.

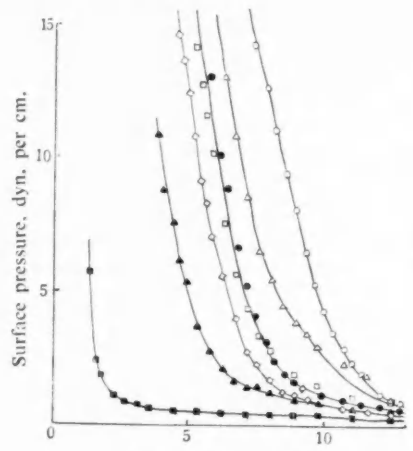

Fig. 3 Variation of surface pressure-area curves of polyanhydro-L-glutamic acid with alkalinity of aqueous subphase (10°C).
○, H_2O; △, 0.01 M, □, 0.1 M; ◇, 0.2 M K_2CO_3; ●, 0.01 M; ▲, 0.02 M; ■, 0.05 M KOH.

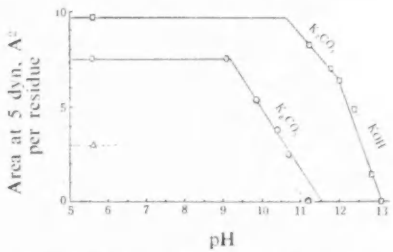

Fig. 4. Plots of area at 5 dyn. per cm. against pH.
□, polyanhydro-L-glutamic acid; ○, poly-L-succinimide; △, polyanhydro-L-aspartic acid.

β-configuration[6,7]. The surface potential was also low and the surface moment was about 50 mD. The low values of limiting area and surface moment also suggest that polyanhydro-L-glutamic acid might be poly-L-glutarimide, which can not be spread on aqueous surface as a monomolecular layer but has a folded configuration in film, as expected from its structure consideration.

The condensed nature of the monolayer of poly-L-glutarimide may be attributed to the rigid structure of this polymer, i. e., to its low configurational entropy. On the contrary, poly-L-proline has a relatively loose configuration in film, since its film is of an expanded type. Thus the pyrrolidine rings would not influence the flexibility of polymer chain in film very profoundly.

As referred to later, the monolayer of polyanhydro-L-glutamic acid behaves very similarly to that of poly-L-succinimide; this also supports the identity of polyanhydro-L-glutamic acid with poly-L-glutarimide. All these are consistent with the results of Asai et al.[4] and Bruckner et al.[8]

Since the ring of poly-L-glutarimide can be cleaved by dilute alkali[8,9], we have examined the monolayers of polyanhydro-L-glutamic acid on alkaline solutions of different pH's. The results on surface pressure-area relations are shown in Fig. 3 and the areas at 5 dyn. per cm. are plotted against the pH in Fig. 4. It can be seen that the film occupies smaller area as the rise of pH at the region of pH higher than 10.5 and no film can be formed at pH 13. This indicates that poly-L-glutamic acid produced by the cleavage of ring of polyanhydro-L-glutamic acid does not cause any expansion of film. When polyanhydro-L-glutamic acid was spread from its alkaline solution, no film was obtained on distilled water and even on 0.01 N hydrochloric acid or on potassium chloride solution. This suggests that the poly-L-glutamic acid thus formed should be composed of both α- and γ-linkages of peptide bonds, because poly-α-L-glutamic acid

7) C. W. N. Cumper and A. E. Alexander, *Trans. Faraday Soc.*, **46**, 235 (1950).
8) V. Bruckner, J. Kovács and K. Medzihradszky, *Naturwiss.*, **42**, 96 (1955).
9) V. Bruckner, M. Szekerke and J. Kovács, ibid., **42**, 179 (1955).

can make films on the acid side[10], but poly-γ-L-glutamic acid forms no film on aqueous subphases of various compositions[11]. Although the cupric salt of the poly-L-glutamic acid is insoluble[8], the poly-L-glutamic acid spread from an alkaline solution gave no film on cupric sulfate solution.

Polyanhydro-L-aspartic Acid.—We will proceed to examine the relation of polyanhydro-L-aspartic acid with poly-L-succinimide. The behavior of the monolayer of poly-L-succinimide on distilled water is shown in Fig. 5. The

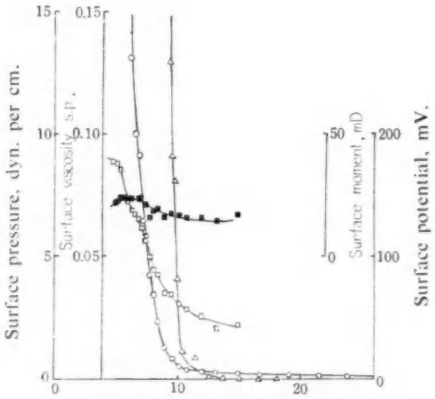

Fig. 5. Monolayer of poly-L-succinimide on distilled water (17°C).
○, surface pressure; □, surface potential; ■, surface moment; △, surface viscosity.

monolayer was of a condensed type and the limiting area determined from both surface pressure and viscosity was about 11 Å², and the surface potential was low and the surface moment was 20 to 25 mD. These low values may be attributed to the rigidly folded configuration of this polymer, which is maintained even in the spread state. Since poly-L-succinimide can be converted into poly-L-aspartic acid by dilute alkaline solutions[12-14], as poly-L-glutarimide to poly-L-glutamic acid[8,9], we have examined the monolayer properties on alkaline solutions of different pH's. The results are shown in Figs. 6 and 4. The cleavage of ring occurred at less alkaline pH for poly-L-succinimide than for poly-L-glutarimide; the

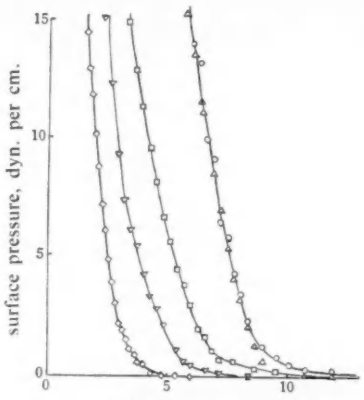

Fig. 6. Variation of surface pressure-area curves of poly-L-succinimide with alkalinity of aqueous subphase (17°C).
○, H_2O; △, 0.0002 M; □, 0.001 M; ▽, 0.003 M; ◇, 0.005 K_2CO_3.

film spreads less completely as the rise of pH at the region of pH higher than 9.0 and no film can be formed at pH 11. By the same procedures as for poly-L-glutarimide, it was found that the poly-L-aspartic acid thus formed might include both α- and β-linkages. This is in accord with the result of Kovács et al.[14]

Polyanhydro-L-aspartic acid gave a stable monolayer on distilled water, as shown in Fig. 7. The spreading of this polymer was far less than that of poly-L-succinimide, and it could not be increased by the addition of salt into the aqueous subphase. Except for the

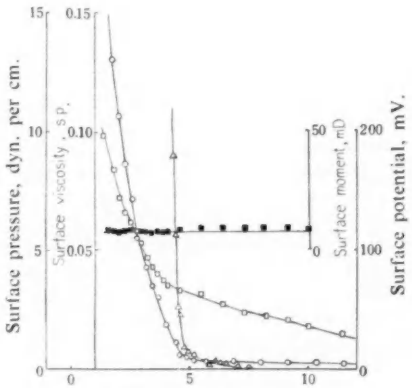

Fig. 7. Monolayer of polyanhydro-L-aspartic acid on distilled water (12°C). ○, surface pressure; □, surface potential; ■, surface moment; △, surface viscosity.

10) T. Isemura and K. Hamaguchi, This Bulletin, **27**, 339 (1954).
11) T. Yamashita, personal communication.
12) J. Kovács, J. Könyves and J. Császár, *Naturwiss.*, **41**, 575 (1954).
13) A. Vegotsky, K. Harada and S. W. Fox, *J. Am. Chem. Soc.*, **80**, 3361 (1958).
14) J. Kovács, I. Könyves and A. Pusztai, *Experientia*, **9**, 459 (1953); J. Kovács and I. Könyves, *Naturwiss.*, **41**, 333 (1954).

poorer spreading, however, polyanhydro-L-aspartic acid behaved very similarly to poly-L-succinimide in the monolayer state; e.g., no film was formed on an alkaline solution of pH 11, as shown in Fig. 4. Noguchi et al.[2] has confirmed that polyanhydro-L-aspartic acid is just poly-L-succinimide itself but never poly-L-propiolactam-2-carboxylic acid. Further they have referred to the Berger's polyaspartic acid[3] and concluded that it might be a copolymer of L-succinimide and L-aspartic acid. Our polyanhydro-L-aspartic acid might also be the same kind of copolymer since it occupies smaller area than poly-L-succinimide.

Summary

To examine the structures of polyanhydro-L-glutamic acid and polyanhydro-L-aspartic acid, we have studied their monolayer properties and compared them with those of poly-DL-pyrrolidone-2-carboxylic acid and poly-L-succinimide. It was found that polyanhydro-L-glutamic acid is not identical with polypyrrolidone carboxylic acid but with poly-L-glutarimide, which has a rigidly folded configuration even in monolayer. This conclusion is in agreement with the results obtained by other methods. It was shown, however, that polyanhydro-L-aspartic acid can not be identified with poly-L-succinimide but it might be a copolymer of L-succinimide and L-aspartic acid.

We are grateful to Professor J. Noguchi of Kanazawa University for the gift of the polymers as well as for his guidance in preparing polyanhydro-L-aspartic acid.

Faculty of Science and
Institute for Protein Research
Osaka University
Kita-ku, Osaka

On the Orientational Order-Disorder Transition in Crystalline Aniline Hydrobromide

By Hiroshi SUGA*

(Received August 1, 1960)

In the course of X-ray structural analyses[1] of aniline hydrobromide, Taguchi[2] has recently observed a phase transition from the orthorhombic to the monoclinic system, which occurs on cooling at about 27°C. He also found that the monoclinic angle β, between the a and c axes, is not constant below the critical temperature but varies continuously over a wide range of temperature as the temperature is lowered. The detailed analyses of crystal structures above and below the transition temperature range were carried out by the same author. He found further anomalous spectra in oscillation and Weissenberg photographs below the critical temperature associated with the appearance of a hybrid structure. The detailed knowledge concerning the crystal structures above and below the transition temperature range, the unusual variation of the monoclinic angle, and the appearance of a hybrid structure stimulated us to study the thermal properties of this compound to look into the mechanism of this peculiar phase transition.

Experimental

Material. — Aniline (extra pure grade manufactured by Wakō Chem. Ind., Ltd.) was added to an excess of an aqueous solution of hydrobromic acid (1st grade, the same company). The precipitated salt was washed with cold distilled water and then recrystallized from warm ethanol. The crude product thus obtained was slightly colored and found to have some lattice imperfection as revealed by X-ray photographs[1]. In order to purify the product further, it was finally subjected to fractional sublimation under high vacuum (10^{-5} mmHg). The final product obtained by this procedure is colorless powder. Single crystals were also obtained by sublimation. They are transparent and colorless

* Present address: Department of Physics, Osaka University, Osaka.

1) I. Nitta, T. Watanabé and I. Taguchi, *X-rays*, 5, 31 (1948); to be published in this Bulletin.

2) I. Taguchi, This Bulletin 34, 392 ((1961).

and are found to be free from lattice imperfection; m. p. 283°C.

Apparatus and Procedure.—For the preliminary study to ascertain the occurrence of the phase transition, a differential thermal analysis was carried out in the temperature range from −150 to +300°C. The apparatus was the same in its main feature as the one used hitherto in this laboratory[3] except for attachment of an automatic recording of the temperature difference between the sample and the reference substance (in this case, KCl). The detailed description of the recorder was recently given[4]. To determine the accurate transition temperature and to study the thermal behavior more in detail, measurements of heat capacity were also carried out in the temperature range from −80 to +60°C by the use of the conduction calorimeter[5]. For the heat capacity measurements 4.4 g. of the material was used, the heating rate being 0.25~0.30°C/min. over the full temperature range. Further, the relative thermal expansion below and above the transition temperature as well as the hysteresis phenomenon associated with the phase transition were studied by employing a simple double-walled glass-made dilatometer filled with mercury as the confining liquid. About 29 g. of the material was used, and the heating and cooling rates were about 0.2°C/min.

Results

One of the typical curves of the differential thermal analysis is reproduced in Fig. 1. From this curve it was found that there is a comparatively broad thermal anomaly over the temperature range from −50 to +25°C, with sufficient reproducibility in the repeated measurements and also there is no detectable hysteresis either in the heating or in the cooling direction. The data of heat capacity

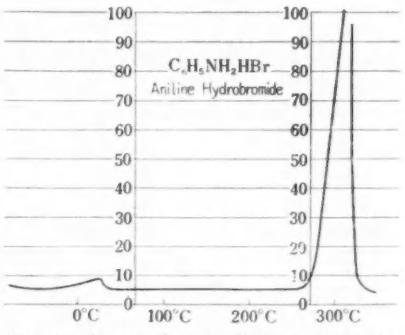

Fig. 1. Automatic recording curve of the differential thermal analysis for aniline hydrobromide.

3) H. Chihara and S. Seki, ibid. **26**, 88 (1953); I. Nitta, S. Seki and H. Chihara, *J. Chem. Soc. Japan, Pure Chem. Sec.* (*Nippon Kagaku Zasshi*), **70**, 387 (1949).
4) H. Suga, H. Chihara and S. Seki; ibid., **82**, 24 (1961).
5) I. Nitta, S. Seki and M. Momotani, *Proc. Japan Acad.*, **26-9**, 25 (1950); S. Seki, M. Momotani, K. Nakatsu and T. Ōshima, This Bulletin, **28**, 411 (1955).

TABLE I. HEAT CAPACITY DATA OF ANILINE HYDROBROMIDE

t°C	C_p(cal./mol. deg.)	t°C	C_p(cal./mol. deg.)
−73.93	28.62	2.63	40.64
−71.27	28.84	5.27	41.10
−68.08	29.24	7.88	41.80
−66.78	29.51	10.46	42.52
−63.28	29.93	13.01	43.16
−58.60	30.31	15.57	43.98
−53.91	30.98	18.10	44.69
−50.90	31.42	20.62	45.72
−47.83	31.81	23.18	42.60
−44.85	32.04	24.43	38.54
−41.85	32.41	25.60	38.13
−38.92	32.91	28.22	38.13
−36.01	33.34	31.98	38.26
−33.10	33.92	34.43	38.39
−30.23	34.39	38.12	38.60
−27.35	35.00	41.80	39.18
−24.58	35.56	44.21	39.31
−18.98	36.62	47.80	39.74
−16.21	36.99	50.22	40.22
−13.43	37.34	52.63	40.29
−10.73	38.11	55.03	40.64
− 8.04	38.54	61.00	41.63
− 5.35	39.11	64.53	42.00
− 2.67	39.71	66.88	41.81

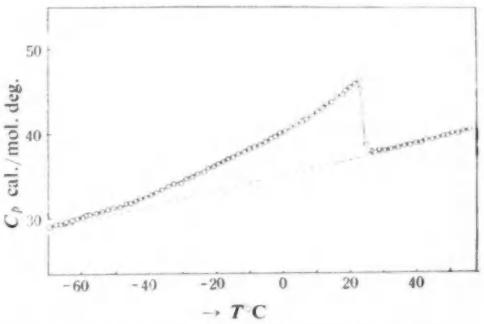

Fig. 2. Heat capacity versus temperature curve of aniline hydrobromide.

in this temperature range are given in Table I and they are plotted in Fig. 2. As this figure shows, the excess heat capacity starts to rise gradually at about −70°C, reaches a maximum value at 22°C (critical temperature), and then drops down abruptly by as much as 9 cal./mol. deg. The general trend of the heat capacity versus temperature curve reminds us of the similarity to that of the order-disorder phase transition of binary alloy systems[6]. Table II gives enthalpy and entropy of the

6) H. Moser, *Physik. Z.*, **37**, 737 (1936); F. W. Jones and C. Sykes, *Proc. Roy. Soc.*, **A167**, 440 (1937).

TABLE II. HEAT AND ENTROPY OF TRANSITION AND DIFFERENCE OF HEAT CAPACITIES AT T_c

ΔH (transition)	297 ± 10 cal./mol.
ΔS (transition)	1.10 ± 0.05 e. u.
ΔC_p (at T_c)	~9 cal./mol. deg.

transition and the difference of heat capacities at the critical temperature. To evaluate the enthalpy of transition, the excess heat capacities over the dotted line given in the figure are integrated graphically. Here the dotted line is drawn as the normal contribution of the lattice vibration to the heat capacity. By dividing the abnormal part into many sections of temperature intervals, the entropy of transition was evaluated by summing up the quotients obtained by dividing each area of these sections with the corresponding mean absolute temperature. The entropy of transition thus obtained, 1.10 e. u. is comparable in magnitude with those of NH_4Cl and ND_4Cl[7] at their lambda point, 1.30~1.40 e. u. As is evident from Fig. 2, the heat capacity curve is of typical lambda type and there is no indication of the latent heat at the critical temperature, showing that this transition is of higher order nature.

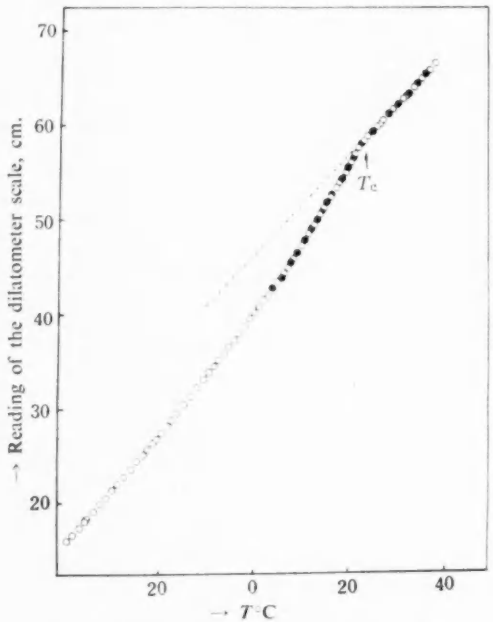

Fig 3. Volume versus temperature curve of aniline hydrobromide.

○ heating direction ● cooling direction

7) C. C. Stephenson, R. W. Blue and J. W. Stout, *J. Chem. Phys.*, **20**, 1046 (1952).

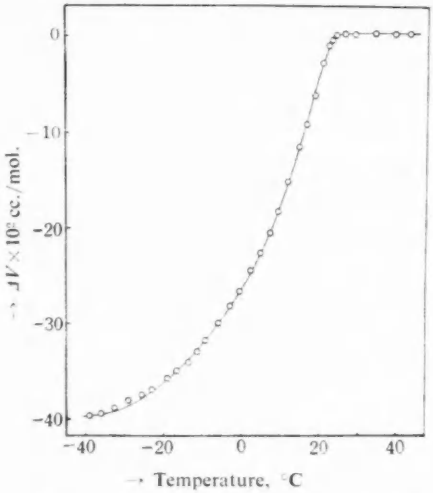

Fig. 3a. Anomalous thermal contraction of aniline hydrobromide.

Dilatometric studies revealed also the existence of abnormal expansion over the same transition range, as shown in Fig. 3. In this figure one can see that all the observed points in the heating and cooling directions can be represented by one and the same curve, showing again no hysteresis phenomenon. The dotted line in this figure means the thermal contraction extrapolated from the curve above the critical temperature by the use of the method of least squares. Fig. 3a gives the excess contraction ΔV below the dotted line and Fig. 4 the "abnormal" expansion coefficient calculated by $(1/V_0)\mathrm{d}(\Delta V)/\mathrm{d}T$, where V_0 is the molar volume of the crystal at the critical temperature. Although the expansion coefficient changes discontinuously at the critical point, the volume itself changes continuously over the whole range of measurements. These facts

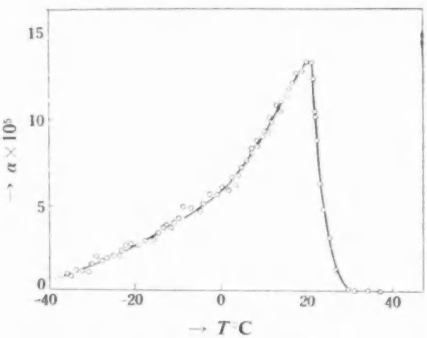

Fig. 4. Abnormal expansion coefficient of aniline hydrobromide.

also reasonably support the proposition that the transition is of higher order nature. The fact of non-existence of hysteresis phenomenon in the higher order phase transition was interpreted by Staveley et al.[8] from the point of view of lattice strain energy accompanying the phase transition.

Discussion

Prior to the discussion of the plausible mechanism of this phase transition, it is necessary to give a brief account of the crystal structure[1,2] above and below the critical temperature. The high temperature phase belongs to the orthorhombic system ($D_{2h}^{10}-Pnaa$). In this structure, it is required from the crystal symmetry that both the principal axis of anilinium ion ($N-C_1\cdots C_4$ axis) and the Br^- ion are found to lie on two different two-fold symmetry axes along the a axis. Although the positions of hydrogen atoms attached to the nitrogen atom are not yet determined, $-NH_3^+$ ionic group is surrounded by four Br^- ions, of which two are slightly more distant than the other two. On cooling the crystal through the critical temperature, it is transformed into the monoclinic system ($C_{2h}^5-P2_1/a$); the monoclinic angle deviates gradually from 90° and reaches 91°22′ asymptotically in a manner shown in Fig. 8, where the unit of the ordinate is twice the quantity $\Delta\beta(=\beta-90^\circ)$, for convenience. In the structure of the low temperature modification, the requirement of two-fold symmetry imposed to the C–N axis is lost. In this phase, in response to the variation of β, the positions of Br^- ions and $-NH_3^+$ ionic groups are displaced with respect to each other, with the following sequence that the interionic distances between Br^- ions and an $-NH_3^+$ ionic group become different from each other, and also that the pseudo electric dipole moments due to the displacements of the two kinds of ions in the neighboring ionic array along the a axis may be found to be antiparallel with each other in a similar manner as in the anti-ferroelectric crystal which was proposed originally by Kittel[9].

Considering the crystal structures as well as the thermal behaviors above and below the critical temperature described above it is suggested that a mechanism of orientational order-disorder of the $-NH_3^+$ group as an interpretation of this phase transition be given, based on the reason given below. In the first place, it will be natural to assume the pyramidal configuration (C_{3v}) of the $-NH_3^+$ ionic group. In the high temperature phase, since the C–N axis should lie on the two-fold symmetry axis, the potential energy of $-NH_3^+$ group associated with the rotational motion of this group will also have the same two-fold axial symmetry around this axis. Therefore, one has to consider necessarily some statistical randomness for the azimuthal orientation of $-NH_3^+$ group with respect to the C–N bond so far as one puts an $-NH_3^+$ group having three-fold symmetry on the axis of two-fold symmetry. On the other hand, in the low temperature phase such a requirement of two-fold symmetry is lost owing to the different crystal symmetry. Taking into account the possible formation of the N–H···Br weak hydrogen bond, possible orientations of the $-NH_3^+$ group with respect to the hydrogen atoms may be expected to be such as are represented in Fig. 5.

Fig. 5. Possible orientations of $-NH_3^+$ group (a- and b-types).

It is obvious from the symmetry consideration that these a- and b-type orientations are equally probable in the orthorhombic phase, whereas in the monoclinic phase one of these two types would be stabilized. We shall call this the a-type for convenience. Then, the requirement of two-fold axial symmetry in the high temperature phase will be satisfied if we distribute the $-NH_3^+$ groups between these two equilibrium orientations (a- and b-types), statistically in space and time. Thus, we may call tentatively this transition the "orientational order-disorder" type in the sense that an equal number of the a- and b-type orientations of $-NH_3^+$ groups can exist above the critical temperature whereas the number of the a-type orientation is predominant below the critical temperature. A simplified hindering potential energy curve for such a rotational motion of the $-NH_3^+$ group in the lattice may be represented schematically as in Fig. 6. This potential energy curve has 60° periodicity in the high temperature phase, while that corresponding to the low temperature phase will have 120° periodicity. As is shown in the figure, the degree of increase or decrease in depth of potential minima is assumed to be a linear function of $\Delta\beta$. Since the extent of displacement of the atomic position is assumed to be proportional to the variation of macroscopic quantity β in a first approximation, some of the physical properties of the present crystal

8) D. G. Thomas and L. A. K. Staveley, *J. Chem. Soc.*, **1951**, 2572.
9) C. Kittel, *Phys. Rev.*, **82**, 729 (1951).

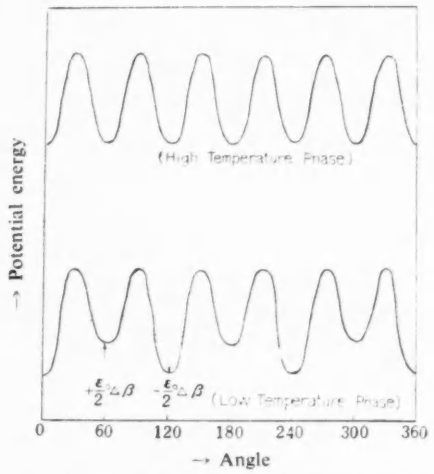
(High Temperature Phase)
$+\frac{\varepsilon}{2}\angle\beta$ $-\frac{\varepsilon}{2}\angle\beta$ (Low Temperature Phase)
→ Potential energy
0 60 120 180 240 300 360
→ Angle

Fig. 6. Schematic representation of hindering potential for the rotational motion of $-NH_3^+$ group.

associated with the variation of β may be considered to change proportionally with the variation of β. As a matter of fact, Horie et al.[10] have recently given an example of the temperature dependence of the angle between optic elasticity axes, γ, in adjacent domains in the hybrid structure of aniline hydrobromide in the vicinity of the critical temperature (Fig. 7); one can see here a fairly linear relationship between the temperature variation of $\Delta\beta$ and γ.

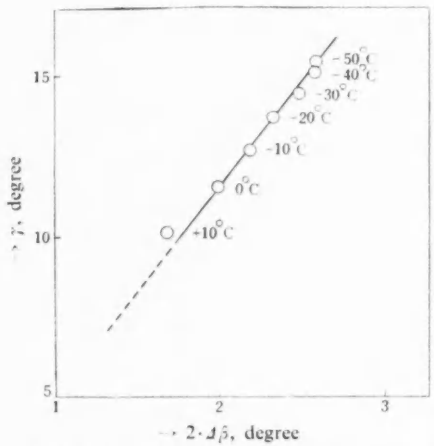

Fig. 7. Linear relationship between the temperature variation of $\Delta\beta$ and of the angle γ between the two optic elasticity axes in adjacent domains (after Horie et al.[10]).

Now, let us calculate the temperature dependence of $\Delta\beta$ on the basis of the proposed model in order to compare the result with the experimental value reported by the X-ray method[2]. We define the degree of order s as follows; let it be assumed that in a state specified by a set of values (T, s), $N(1+s)/2$ $-NH_3^+$ groups in the a-type orientation and $N(1-s)/2$ in the b-type are distributed over the whole N lattice points. The order parameter s thus defined has the same character as the one proposed for the theory of order-disorder phase transition of binary alloy[11]. That is, when $s=1$ all the $-NH_3^+$ groups are in the a-type orientation; this corresponds to the state of perfect order. When $s=0$ there are as many a-type groups as b-type groups; the state of complete disorder. It is somewhat difficult to calculate the hindering potential energy for rotational motion of the $-NH_3^+$ group in the crystalline field owing to an ambiguity in the estimation of effective charge distribution of the $-NH_3^+$ group, the unknown N–H distance and also the complexity of the crystal structure, so that we shall confine our calculation at the present stage only to the differences in the energy and entropy between the two phases. The notation Δ used in the following calculation stands for the excess of any thermodynamic quantities of the ordered state over that of the completely disordered state extrapolated above the transition point. The difference in the internal energy ΔU will consist of two parts in its origins; one is the contribution from the variation of the arrangements of ions and ionic groups and the other is that from the change of orientations of $-NH_3^+$ ionic groups when the ordered state changes to the disordered state. The first part of energy difference, ΔU_1, may be expressed formally by a power series in $\Delta\beta$ of which all the odd terms are omitted by the requirement that ΔU should be an even function of $\Delta\beta$, because the gradual change of either direction from the orthorhombic to the monoclinic crystal system should produce the same energy change. For example, the electro-static part of ΔU_1, which is the mutual interaction energy between the pseudo electric dipole moments produced by the displacements of ions and ionic groups, is expressed by

$$-1/2\sum_{i>j}\frac{\mu_i\mu_j}{r_{ij}^3}\{3\cos(\theta_i+\theta_j)+\cos(\theta_i-\theta_j)\}$$

10) T. Horie, T. Iwai and I. Taguchi, Annual Meeting of Phys. Soc. Japan, 1956,: To be published in near future. The author would like to express his appreciation for their permission to refer to their result before its publication.

11) W. L. Bragg and E. L. Williams, *Proc. Roy. Soc.*, **A145**, 699 (1934); **A151**, 540 (1935); F. C. Nix and W. Shockley, *Rev. Mod. Phys.*, **10**, 1 (1938).

where μ_i, μ_j, θ_i, θ_j and r_{ij} have the usual meanings. Since μ_i and μ_j may be reasonably considered to be proportional to $\Delta\beta$, the term may be rewritten by $J(\Delta\beta)^2$, where J is a constant. If the higher terms in $\Delta\beta$ can be neglected, then $\Delta U_1 = A(\Delta\beta)^2$, where A is another constant. The second part of energy difference ΔU_2, which is due to the change of potential energy at an $-NH_3^+$ group caused by the variation of the degree of order s, may be expressed by $\frac{1+s}{2}N\left(-\frac{\varepsilon_0}{2}\Delta\beta\right)+\frac{1-s}{2}N\left(\frac{\varepsilon_0}{2}\Delta\beta\right)$

In this case it has been assumed that the change in the depth of potential minima is proportional to the change in $\Delta\beta$ with a constant of proportionality $\varepsilon_0/2$ (see Fig. 6). Thus,

$$\Delta U = \Delta U_1 + \Delta U_2 = A(\Delta\beta)^2 - sE\Delta\beta/2 \qquad (1)$$

where $E = N\varepsilon_0$.

On the other hand, the entropy difference ΔS is given approximately by the possible number of $N(1+s)/2$ a-type and $N(1-s)/2$ b-type arrangements of $-NH_3^+$ groups over the N whole lattice points.

$$\Delta S = k \ln \frac{N!}{\left(\frac{1+s}{2}N\right)!\left(\frac{1-s}{2}N\right)!} - R\ln 2$$

$$= -R\left\{\frac{1+s}{2}\ln\frac{1+s}{2} + \frac{1-s}{2}\ln\frac{1-s}{2} + \ln 2\right\} \qquad (2)$$

Here, the additional term $R\ln 2$ appears since the completely disordered state was taken as the reference. Accordingly, the difference of Helmholtz free energy ΔF between the two phases is given by

$$\Delta F = \Delta U - T\Delta S = A(\Delta\beta)^2 - sE\Delta\beta/2 + RT\left\{\frac{1+s}{2}\ln\frac{1+s}{2} + \frac{1-s}{2}\ln\frac{1-s}{2} + \ln 2\right\} \qquad (3)$$

By the equilibrium conditions, we can obtain the following set of equations. From $\partial(\Delta F)/\partial(\Delta\beta)=0$ (since there is no external shear stress), it follows

$$\Delta\beta = Es/(4A) \qquad (4)$$

$$\Delta U = -E^2s^2/(16A) \qquad (4')$$

Eq. 4′ shows that the present treatment corresponds formally to the Bragg-Williams approximation. From $\partial(\Delta F)/\partial s = 0$, we have

$$s = \tanh E^2 s/(8RAT) \qquad (5)$$

$$T_c = E^2/(8RA) \qquad (6)$$

where T_c is the critical temperature, above which s becomes zero. Inserting the value of s derived from 5 into 2, we get a calculated total entropy change 0.83 e. u. ($-70\sim+35$°C) in comparison with the observed value 1.10 e. u. In this case, the additional entropy increment due to the increase of the available volume of ion, which may be reasonably given by $R\ln(V+\Delta V)/V$, is quite negligible in magnitude, less than 0.01 e. u., in the same temperature interval. Combination of Eqs. 5 and 6 with Eq. 4 gives the temperature dependence of $\Delta\beta$ including the numerical factor $E/(4A)$, which can be determined, for example, by fitting the calculated value with the observed value of $\Delta\beta$ at a single temperature, say -40°C. The temperature dependence of $\Delta\beta$ obtained in this way is given by the dotted line in Fig. 8. Although qualitative agreement is obtained, the details are

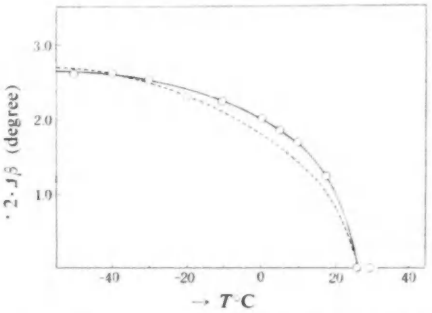

Fig. 8. Comparison of observed temperature variation of $\Delta\beta$ with the theoretical one.
○ Observed by Taguchi[2]
---- Theoretical curve ignoring volume effect.
—— Theoretical curve including volume effect.

not fully explained especially in the following points; one is that the degree of covergence of this curve to the critical point is not so steep as that of the experimental curve, and another point is that the calculated $\Delta\beta$ should increase to 1.37 times as large a value as that at -40°C if the curve is extrapolated to 0°K, while the corresponding value obtained by experiment[2] is only 1.12.

As already mentioned, an anomalous thermal expansion in the vicinity of the critical point appears (see Fig. 3). According to the results by Eisenschitz[12], Sato[13] and Nagamiya[14], the temperature dependence of the order parameter is appreciably affected by taking into account the anomalous thermal expansion accompanied

12) R. Eisenschitz, *Proc. Roy. Soc.*, **A168**, 546 (1938).
13) Y. Sato, *J. Phys. Soc. Japan*, **2-1**, 17 (1947).
14) T. Nagamiya, "Kotai-ron (Solid State Physics)", 1, Kyōritsu, Tokyo (1951), p. 20.

with the order-disorder phase transition in the case of binary alloy systems. We have then attempted to examine the effect of volume change in the present case as the next stage of refinement. After Sato's treatment, we can get the following expression for the abnormal expansion coefficient

$$\Delta\alpha=\alpha(s)-\alpha(0)=\kappa_0 ds^2/dT\cdot E_0 d(E/E_0)/dV$$
$$=\kappa_0 RT_c/2\cdot ds^2/dT\cdot d(E/E_0)/dV \quad (7)$$

Here, κ_0 is isothermal compressibility of the disordered phase; V the molar volume; E and E_0 the ordering energy at T°K and 0°K, respectively. Then, the abnormal expansion over V^0, the molar volume at 0°K, is given by

$$v=\int_0^T V^0\Delta\alpha dT=\int_1^s V^0 C ds^2=-CV^0(1-s^2) \quad (8)$$

where the following abbreviations were used

$$d(E/E_0)/dV=B, \qquad BRT_c=C$$

By using the observed v_{max} value 0.41 cc./mol. and $V_0=110$ cc.*, C becomes -3.76×10^{-3}.

Based on these expressions the following thermodynamic functions are derived as functions of s, v and T.

$$U(s, v, T)=E_0-Es^2=E_0\{1-(1+Bv)s^2\} \quad (9)$$

$$G(s, v, T)=E_0\{1-(1+Bv)s^2\}$$
$$+RT/2\{(1+s)\ln(1+s)+(1-s)\ln(1-s)$$
$$-2\ln 2\} \quad (10)$$

Here, G is the Gibbs free energy**. From $\partial G/\partial s=0$ and $\partial^2 G/\partial s^2=0$, we have

$$s=\tanh 2E_0 s\{(1+Bv)+BCV_0 s^2\}/RT \quad (11)$$

$$RT_c/E_0=2(1+Bv_{max}) \quad (12)$$

The differentiation of $U(s, v, T)$ with T gives an expression for excess heat capacity over that arising from lattice vibration. The maximum value is obtained from the limitation of $s\to0$.

$$C_{max}=\lim_{s\to0}(\partial U/\partial s)/(\partial T/\partial s)$$
$$=3R/2\{1-(6BCV_0)/(1+Bv_{max})\}^{-1} \quad (13)$$

On the assumption that the C_{max} value thus defined is identical with the experimentally observed ΔC_p, the following set of values can be obtained: $B=-2.44\times10^{-1}$ cc^{-1}, $\kappa_0=1.25\times10^{-6}$ atm^{-1}. By using these numerical values and the observed volume change, the refined $\Delta\beta-T$ curve is calculated and drawn by the full line in Fig. 8, where a fairly satisfactory agreement between this curve and the observed points is seen. It is to be noted that the calculated total entropy change 1.06 e. u. (from -70 to $+35$°C) is in good agreement with the observed one 1.10 e. u., if the same numerical values for parameters are used. The value of κ_0 obtained above seems to be somewhat smaller for this kind of crystal including organic complex ion, since the compressibility is in the range of $(2\sim7)\times10^{-6}$ atm^{-1} for usual ionic crystals. Although the model proposed here is merely a possible one, it may be said that rather satisfactory results were obtained.

A preliminary study of proton magnetic resonance absorption of the powdered specimen of this crystal was recently made by Yamagata* over the temperature range between -190 and $+40$°C and there was no detectable change in the line width at the critical point. The observed second moment 8.35 Gauss^2 almost coincides with 7.82 Gauss^2 of the calculated value obtained by assuming the isolated $-NH_3^+$ group (the value 1.032 Å for N–H distance and tetrahedral angle were assumed) with rotational flipping motion about the C–N axis. The situations are very similar in the cases of ammonium halides[15].

Summary

Measurements of the heat capacity ($-80\sim+60$°C) and the thermal expansion ($-40\sim+60$°C) of aniline hydrobromide were carried out covering the transition temperature which has been observed recently by X-ray methods. The observed heat capacity versus temperature curve was of the λ-shape, similar to that of the order-disorder phase transition of binary alloy systems. The following results were obtained; T_c (the temperature corresponding to the heat capacity peak) 22°C, ΔH (heat of transition, $-70\sim+35$°C) 297 ± 10 cal./mol., ΔS (entropy of transition, the same temperature interval) 1.10 ± 0.05 e. u., ΔC_p (drop of heat capacity at T_c) ~9 cal./mol. deg. Also the anomalous behavior of thermal expansion was observed in the vicinity of the critical temperature. These observations showed that the transition was of higher order nature.

Based on the lits of knowledge of the crystal structures above and below the critical temperature, the author has discussed the main feature of the phase transition from the sandpoint of the orientational order-disorder of the $-NH_3^+$ ionic group and obtained fairly satisfactory results.

* This value was taken from $d_{25}=1.58$, by the picnometric measurement of Taguchi et al.[1]

** The G function expressed here does not correspond exactly to the Gibbs free energy, since the PV term was neglected.

* Private communication.

15) H. S. Gutowsky, G. E. Pake and R. Bersohn, *J. Chem. Phys.*, **22**, 643 (1954); R. Bersohn and H. S. Gutowsky, ibid., **22**, 651 (1954).

The author wishes to express his sincere thanks to Professor I. Nitta, Professor T. Watanabe and Dr. I. Taguchi for their valuable advice and continued interest in the present study, to Professor T. Nagamiya for his valuable suggestion, and to Professor S. Seki for his kind guidance and illuminating discussion. He is also grateful to Dr. H. Chihara for his kind support, and to Mr. K. Nakatsuka for his technical assistance.

Department of Chemistry
Faculty of Science
Osaka University
Nakanoshima, Osaka

Optical Properties of Colored Colloidal Systems. II. Apparent Refractive Index and Extinction Coefficient of the System of Small Spherical Particles

By Masayuki NAKAGAKI* and Tomiko FUJII

(Received September 26, 1960)

In the preceding paper of this series[1], the extinction of light by the system of colored small spheres were theoretically calculated. As a result, it was concluded that the scattering of light by colored spheres is affected by the absorption of light, the latter being expressed by the imaginary part of the refractive index of the dispersed phase. In the present paper, the calculation will be extended to the apparent refractive index of the system. The result thus obtained will be applied to the system of infinitesimally small particles, and will be used to discuss the optical properties of a dyestuff solution as an example.

Theoretical Calculations

Principle of the Calculation. — The relation between the refractive index of a colloidal system or a solution, μ_{12}, and the refractive indices and compositions of the components is usually given by the following equation called a mixture rule,

$$\mu_{12}=\mu_1\varphi_1+\mu_2\varphi_2 \tag{1}$$

where μ_1 and μ_2 are the refractive indices of the solvent and dispersed phases, respectively, and φ_1 and φ_2 are the volume fractions of the respective phases. If the concentration of the dispersed phase, c, is given in mol./l. unit, Eq. 1 may be rewritten as,

$$\mu_{12}=\mu_1+(M/1000\rho_2)(\mu_2-\mu_1)c \tag{2}$$

where M is the molecular weight of the material of the dispersed phase and ρ_2 is the specific gravity of the same phase. The linear relationship between μ_{12} and c as predicted by Eq. 2 has been verified experimentally by many investigators, but the value of μ_2 is not equal[2] to the refractive index in bulk of the dispersed phase, μ_2 (bulk). Therefore the value of μ_2 obtained experimentally on the basis of Eq. 2 is an apparent refractive index of the dispersed phase. If the apparent relative refractive index m' defined by

$$m'=\mu_2/\mu_1 \tag{3}$$

is used, the inclination of the straight line to give the variation of μ_{12} with the concentration c is expressed as

$$\partial\mu_{12}/\partial c=(M\mu_1/1000\rho_2)(m'-1) \tag{4}$$

This equation is to be used to determine the value of m' experimentally.

On the other hand, $(m'-1)$ is given theoretically by the equation[2],

$$m'-1=(3/2)\mathrm{R}[j_\perp(180)]/\alpha^3 \tag{5}$$

where α is a parameter defined by

$$\alpha=2\pi a/\lambda \tag{6}$$

Here, a is the radius of the sphere and λ is the wave length of light in the medium. The sign R in Eq. 5 means the real part of a complex function $j_\perp(180)$, the latter being

$$j_\perp(180)=\frac{m^2-1}{m^2+2}\alpha^3+\left(\frac{m^2-1}{m^2+2}\right)^2\times\frac{(m^4+27m^2+38)}{15(2m^2+3)}\alpha^5-i\frac{2}{3}\left(\frac{m^2-1}{m^2+2}\right)^2\alpha^6 \tag{7}$$

* Present address: Faculty of Pharmacy, Kyoto University, Sakyo-ku, Kyoto.

1) M. Nakagaki, This Bulletin, **31**, 980 (1958).

2) M. Nakagaki and W. Heller, *J. Appl. Phys.*, **27**, 975 (1956).

as already given in the previous paper[1], where m is a complex quantity in the case of colored particles:

$$m = \mu_2^*(\text{bulk})/\mu_1 = m_0 - ik_0 \tag{8}$$

where μ^* means the complex refractive index.

Apparent Refractive Index as a Function of Particle Size.—If $k_0 \ll m_0$, the theoretical equation may be expanded in a power series,

$$m' - 1 = M_1 - M_2 k_0 + M_3 k_0^2 + \cdots\cdots \tag{9}$$

where

$$\left.\begin{aligned} M_1 &= (3/2)(X_1 + Y_1\alpha^2) \\ M_2 &= (3/2)Z_2\alpha^3 \\ M_3 &= (3/2)(X_3 - Y_3\alpha^5) \end{aligned}\right\} \tag{10}$$

Here,

$$\left.\begin{aligned} X_1 &= \frac{m_0^2-1}{m_0^2+2} \\ Y_1 &= \frac{1}{15}\left(\frac{m_0^2-1}{m_0^2+2}\right)^2 \frac{(m_0^4+27m_0^2+38)}{(2m_0^2+3)} \\ Z_2 &= 8m_0 \frac{m_0^2-1}{(m_0^2+2)^3} \\ X_3 &= \frac{3(3m_0^2-2)}{(m_0^2+2)^2} \\ Y_3 &= \frac{\left.\begin{matrix}(4m_0^{18}+66m_0^{16}-1104m_0^{14}-5033m_0^{12} \\ +12966m_0^{10}+105525m_0^8+218152m_0^6 \\ +182376m_0^4+37824m_0^2-16176\end{matrix}\right)}{15(m_0^2+2)^6(2m_0^2+3)^3} \end{aligned}\right\} \tag{11}$$

The results of the numerical computation are shown in Fig. 1. Crosses in the figure are the values for colorless particles calculated on the basis of the Mie theory without any approximation[2]. The agreements between these Mie values and the values obtained from Eqs. 9, 10 and 11 and shown with open circles for colorless particles are very good, although a small discrepancy can be seen in the case where both α and m_0 are large ($\alpha = 0.8$, $m_0 = 1.3$). When k_0(which shows the absorption of light) is small, the apparent relative refractive index m' increases with α (or particle size), but when k_0 is large, the value of m' decreases (after passing a flat maximum when m_0 is large) with the increase of α.

Optical Properties of Infinitesimally Small Particles.—The equation used in the preceding paper as well as in the preceding paragraphs of this paper are for small values of k_0. In the present paragraph, equations for infinitesimally small particles ($\alpha \to 0$) are examined without any restriction on k_0. The equations are

$$m' - 1 = \frac{3}{2} - \frac{9}{2} \times \frac{(m_0^2 + 2 - k_0^2)}{(m_0^2 + k_0^2 + 2)^2 - 8k_0^2} \tag{12}$$

and

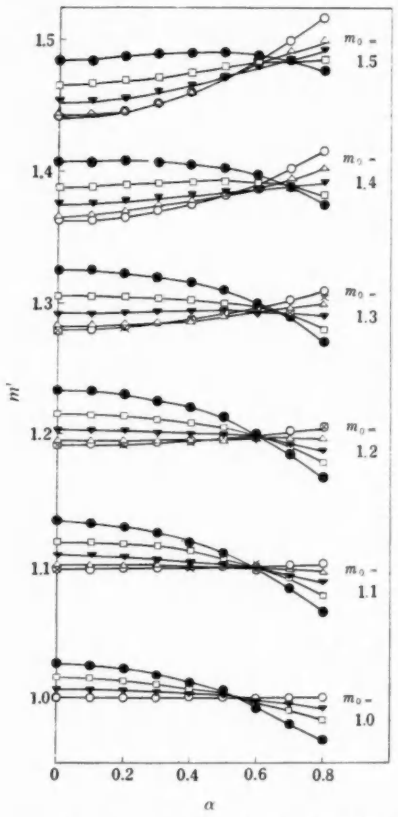

Fig. 1. $m'-\alpha$ relation for $k_0=0$ (○); 0.1 (△); 0.2 (▼); 0.3 (□); 0.4 (●). Mie's values are shown with (×).

$$\left.\begin{aligned} x \equiv (\lambda\rho_2/3\pi)\varepsilon &= \frac{12m_0k_0}{(m_0^2+k_0^2+2)^2-8k_0^2} \\ x(\text{bulk}) &= (4/3)k_0 \end{aligned}\right\} \tag{13}$$

where x is a quantity proportional to the extinction coefficient ε as already introduced in the preceding paper[1].

The numerical values of m' as a function of k_0 were calculated for various values of m_0 from 0.88 to 1.24 with the interval of 0.02. A part of the results is shown in Fig. 2. Although the apparent relative refractive index m' and the relative refractive index in bulk m_0 are parallel when k_0 is small, the sequence is inverted when k_0 is larger than about 1.4. The smaller m' the larger is the m_0. Moreover, the value of m' approaches 2.5 when k_0 becomes infinitely large. These results shown in Fig. 2 have not been expected by any previous investigator.

The numerical values of x as a function of

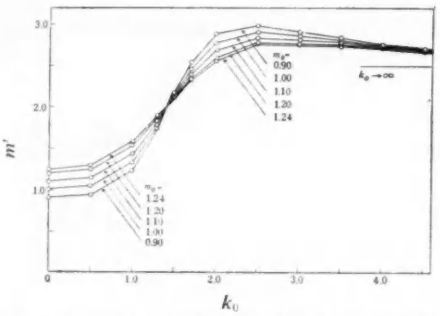

Fig. 2. $m'-k_0$ relation calculated theoretically.

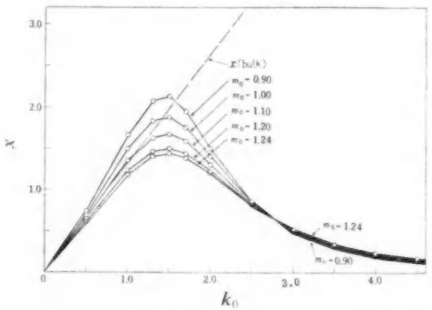

Fig. 3. $x-k_0$ relation calculated theoretically.

k_0 were calculated for various values of m_0 from 0.88 to 1.24 with the interval of 0.02. A part of the results is shown in Fig. 3. The curves have the maximum at the k_0 value of about 1.5. The apparent extinction coefficient or x decreases for the larger value of k_0 and approaches zero when k_0 becomes infinitely large.

These results, too, have not been expected by any previous investigator[3].

An Example for the Treatment of Experimental Data

Materials.—It is generally believed that acid dyes dissolve in water monomolecularly, showing a small tendency to form micelles in contradistinction to direct cotton dyes which form micelles when the temperature is not high. Therefore, an acid dye solution is used as a model of the system of colored infinitesimally small particles.

The acid dye used in this experiment was Acid Orange R (C. I. 15575, Acid Orange 8) purified by the sodium acetate-alcohol method. The purity determined by titanium trichloride titration was 96.32%.

3) In Figs. 2 and 3, theoretically calculated points were connected with straight lines for the convenience of the drawings. The actual theoretical curves should, of course, be curved smoothly.

Determination of Refractive Index.—The difference of the refractive index between the solution and the solvent was measured by using a differential refractometer of modified Brice type as shown in Fig. 4. Light from a

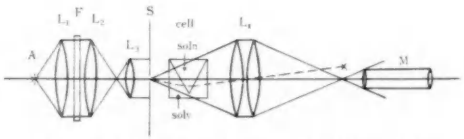

Fig. 4. Schematic diagram of differential refractometer of modified Brice type.

tungsten lamp A was collimated with lenses L_1 and L_2 ($f_1=6$ cm., $f_2=6$ cm.), filtered with a gelatine filter F, made parallel with a lens L_3 ($f_3=3$ cm.) and projected to a slit S. The image of the slit focused by a lens L_4 ($f_4=15$ cm. lens for a slide projector was used) was observed with a microscope M of the magnification of 40 times (4×10). The location of the image of the slit was shifted when a solution was put in the prism cell containing solvent outside the prism in the cell. The shift of the image of the slit was measured by a micrometer in the eyepiece of the microscope M. The reading θ is proportional to the difference of the refractive index,

$$\mu_{12}-\mu_1=K\theta \qquad (14)$$

The proportionality constant K was determined to be $K=4.15\times10^{-5}$ by using potassium chloride solution as a standard, the refractive index of the latter being cited in the literature[4]. The value of μ_1 is also given in the literature[5].

In order to convert the experimental values of $(\partial\mu_{12}/\partial c)$ to m' according to Eq. 4, the value of the density of dye, ρ_2, should be known. The density was assumed to be 1.5 by Robinson[6] and to be 1.0 by Atherton et al.[7] Since the accurate value of the density for the dispersed state can not be known, calculations were made here for both these density values. The results are shown in Fig. 6 with broken lines. A typical anomalous dispersion was observed as already reported for some other dye solutions[7]. In Fig. 6 and also Fig. 7, λ_0 is wavelength in vacuum.

Determination of Extinction Coefficient.—The extinction coefficient was determined by Shimazu spectrophotometer QR-50. The results were recalculated to x by Eq. 13 for $\rho_2=1.0$ and $\rho_2=1.5$. The results are shown in Fig. 7 with broken lines.

4) "International Critical Tables", VII, 13, 75 (1930).
5) "International Critical Tables", VII, 13 (1930).
6) C. Robinson, *Trans. Faraday Soc.*, **31**, 245 (1935).
7) E. Atherton and E. Cowill, *J. Soc. Dyers Colorists*, **70**, 116 (1954).

Calculation of m_0 and k_0. — The quantities obtainable by experiments are m' and x, but the fundamental quantities of theoretical interest are m_0 and k_0. To determine m_0 and k_0 from m' and x, a graphical method is shown in Fig. 5. The $m'-x$ relation calculated theoretically for systematically varied values of parameters m_0 and k_0 make a network. A pair of experimental values of m' and x give one plot on this chart. Then, the values of m_0 and k_0 corresponding to this plot can be read off by interpolation. The values of m_0 thus obtained are shown in Fig. 6 with solid lines, and the values of x(bulk) calculated by Eq. 13 from the values of k_0 thus obtained are shown in Fig. 7 with solid lines.

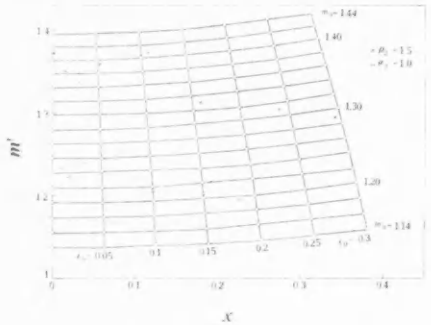

Fig. 5. $m'-x$ relation. Network shown with (○) is theoretical. Experimental data for $\rho_2=1.0$ (△) and for $\rho_2=1.5$ (×) are also ploted.

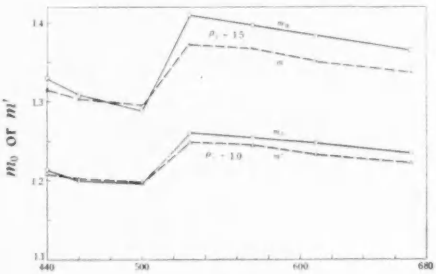

Fig. 6. Dependencies of m_0 and m' on λ_0.

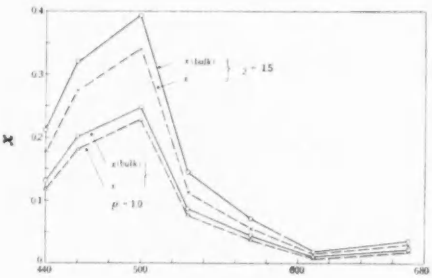

Fig. 7. Dependencies of x(bulk) and x on λ_0.

The discrepancies between solid curves and broken curves in Fig. 6 and Fig. 7 show the error committed if one assume that the experimental m' and x values are equal to m_0 and x(bulk)—the latter is equal to $(4/3)k_0$—of the dispersed phase in bulk. The errors in this sense are given in Table I for the present solutions. The table shows that the error in m' is less than 2.6% at the greatest, but the error in x reaches as far as 21% at the greatest.

TABLE I. ERRORS COMMITTED BY IGNORING THE PRESENT THEORY

λ_0	$\rho_2=1.5$		$\rho_2=1.0$	
	Δm	Δx	Δm	Δx
mμ	%	%	%	%
440	−1.27	−15.7	−0.43	− 9.6
460	−0.37	−14.4	−0.24	− 9.0
500	0.55	−13.1	0.08	− 8.0
530	−2.56	−20.6	−0.96	−11.5
570	−2.51	−19.6	−1.10	−10.4
610	−2.41	−19.5	−1.05	− 8.1
670	−2.10	−17.7	−0.91	− 8.7

Summary

The theoretical values of apparent relative refractive index m' of colored particles was calculated as a function of particle size for various values of m_0 and k_0.

The theoretical values of m' as well as x were calculated for infinitesimally small particles. It was shown that m' increases and, after passing a maximum point, approaches a limiting value of 2.5 with the increase of k_0, and that x approaches zero, after passing a maximum, with the increase of k_0.

The values of m' and x of Acid Orange R solutions were measured by a modified Brice type differential refractometer and by a spectrophotometer. A method to convert m' and x values into m_0 and k_0 values was illustrated. The errors committed by assuming experimental m' and x values as m_0 and $(4/3)k_0$ values of bulk phase are estimated for the dye solution. The error of x reached 21%, while the error of m' was not larger than 2.6%.

Faculty of the Science of Living
Osaka City University
Nishi-ku, Osaka

A Diffusion Mechanism for Liesegang Rings. I. Spacing Law*

By Prem Behari MATHUR**

(Received August 18, 1960)

Jablczynski's equation for spacings between Liesegang rings

$$x_n = ak^n \tag{1}$$

where x_n is the distance of nth ring from the diffusion level, and a and k are constants, may be written as

$$\frac{x_{n-1}}{x_n} = \frac{1}{R} \tag{2}$$

or $$1-\frac{x_{n-1}}{x_n} = \left(1-\frac{1}{R}\right)$$

or $$(x_n - x_{n-1}) = kx_n \tag{3}$$

From statistical consideration, Eq. 3 is more sensitive form of Jablczynski's relation 1. According to the Eq. 3 the plot of $(x_n - x_{n-1})$ against x_n should be straight line curves passing through the origin. In practice the curves are not found to pass through the origin when the distances of the rings are measured from diffusion level for which Eq. 1 stands. The author has advanced a theory and deduced from Fick's diffusion law a few general expressions for the Liesegang phenomenon. The theory reflects light on the mechanism of ring formation, fine structure, influence of various environmental conditions, etc.

Fick's diffusion equation

$$\frac{\partial c}{\partial t} = D\frac{\partial^2 c}{\partial x^2} \tag{4}$$

may have a solution

$$c = a\,e^{-\alpha x}\cos(\omega t + \beta x + y) \tag{5}$$

given by Riemann[2] for similar type of differential equations. Such a solution would be possible under conditions analogous to those operating in the propagation of sound in air, discharge of a current through a condenser and a resistance, where the motion of the matter is met by an opposing force.

In the phenomenon of Liesegang rings the two electrolytes meet and get precipitated and thus forms a new phase at the boundary of the diffusing salt and the medium. By virtue of the electrical forces at its surface and the fine nature of the particles distributed there, the boundary phase or say 'membrane' will have the tendency in certain cases to oppose the diffusion of salt and so to develop a situation where diffusion may be governed by Eq. 6.

The concentration distribution at a particular instant t_i may be given by

$$c = a\,e^{-\alpha x}\cos(\beta x + \phi) \tag{6}$$

where ϕ is another constant equal to $(\omega t_i + y)$.

During the process of Liesegang ring formation of say silver chromate rings, the diffusion wave front of silver ions moves forward and gives rings one after another. The latter changes in concentration at the preceeding levels when one of the precipitating ions is completely removed cannot influence a ring position. By determining the values of arbitrary constants a and ϕ in Eq. 6 from the known boundary conditions of reacting ions the equations for their concentration distribution can be obtained.

For silver ions, when $x=0$, $C \to$ maximum. In Eq. 6 C will be maximum, when $\cos(\beta x+\phi)$ is unity or $(\beta x+\phi)=0$. Since $x=0$, ϕ must be zero to satisfy the above condition. Hence

$$c = a\,e^{-\alpha x}\cos(\beta x) \tag{7}$$

Now, the limiting maximum value of C at $x=0$ is the same as the initial bulk concentration C_0 of silver ions; substituting this value into above equation we have $a=C_0$. Eq. 7 reduces to

$$c = C_0\,e^{-\alpha x}\cos(\beta x) \tag{8}$$

Relation 8 geometrically represents a simple harmonic curve whose amplitude $C_0\,e^{-\alpha x}$ diminishes exponentially to zero with increasing distance. As the chromate ions diffuse in the upward direction their distribution may be represented by the equation

$$C' = C_1\,e^{\alpha' x}\sin(\beta' x) + C_2\,e^{\alpha' x}\cos(\beta' x) \tag{9}$$

where damping coefficient α' has a positive sign. The constants C_1 and C_2 in the above equation can be determined from boundary conditions of chromate ions.

In a thin region of the precipitate the concentration of chromate ions may be taken to be equal to zero because the traces of ions

* This work is the part of author's Ph.D thesis submitted to the University of Allahabad (1956).

** Present address: Senior Scientific Officer, Central Electrochemical Research Institute, Karaikudi-3, India.

1) K. Jablczynski, *Bull. soc. chim., France* (4), 33, 1592 (1923).

2) Riemann, "Particlle Differentialgleichungen", Edit Hattendorff (1938), p. 110.; P. B. Mathur, *Bull. Acad. Polona. Sci.*, 8, 8, 429 (1960).

left there after precipitation get absorbed by the precipitates rendering practically a complete disappearance of the ions. Hence at $x=0$, $C'=0$. Substituting this condition into Eq. 9, we have $C_2=0$, so we have,

$$C'=C_1 e^{\alpha' x}\sin(\beta' x) \tag{10}$$

Let us suppose, when $x=x_0$, $C'\to$ maximum. So, in Eq. 10, C' is maximum when $\sin(\beta' x_0)$ is unity or $\beta' x_0=\pi/2$ or $x_0=\pi/2\beta'$ and so

$$C'=C_1 e^{(\alpha'\pi/2\beta')}$$

Now the limiting maximum value of C' at a distance of x_0 is the same as the initial bulk concentration C_0' of chromate ions. Substituting this value into the above equation we have

$$C_1=C_0' e^{-(\alpha'\pi/2\beta')}$$

Eq. 10 thus reduces to the form,

$$C'=(C_0' e^{-(\alpha'\pi/2\beta')}) e^{\alpha' x}\sin(\beta' x) \tag{11}$$

Eq. 11 represents the distribution of chromate ions where x is measured from zero concentration level.

Let us now suppose that $(n-1)$ rings have already formed and nth ring is in the process of formation. So the concentration of chromate ions at $(n-1)$th level has fallen to zero. Let C_n and C_n' be the concentrations of silver and chromate ions respectively at nth rings, and x_n and x_{n-1}, the distances of nth and $(n-1)$th levels respectively from the initial diffusion level. The reference line for chromate ions corresponding to the nth ring is $(n-1)$th ring level, while for silver ions it is the initial diffusion level. In order that the two equations could be combined, the line of reference for the two ions must be the same. Substituting $x=(x_n-x_{n-1})$ into Eq. 11 for chromate ions and $x=x_n$ in Eq. 8 for silver ions and corresponding concentrations in the two equations, we get the following equations for silver and chromate ions respectively,

$$C_n=C_0 e^{-\alpha x_n}\cos(\beta x_n) \tag{12}$$

$$C_n'=C_0' e^{-(\alpha'\pi/2\beta')} e^{\alpha'(x_n-x_{n-1})} \times\sin[\beta'(x_n-x_{n-1})] \tag{13}$$

The distribution of the concentration product of silver and chromate ions can be obtained by combining Eqs. 12 and 13

$$C_nC_n'=C_0C_0' e^{-(\alpha'\pi/2\beta')} e^{-\alpha x_n} e^{\alpha'(x_n-x_{n-1})} \times\sin[\beta'(x_n-x_{n-1})]\cos(\beta x_n) \tag{14}$$

The above equation represents the curve shown in Fig. 1. The periodic terms cos. and sin. alternate between the limits ± 1, and the concentration curve shows two types of periodicities one by broad wave PQRS and the other by narrow waves. By putting $\cos(\beta x_n)=1$, we get the curve PQRS which is the locus

Fig. 1

of the points of maxima of narrow curves, and by putting $\sin(\beta'(x_n-x_{n-1}))=1$, the remaining equation represents only the finer structures of a half wave PQ.

The condition for the precipitation at the place is that the ionic product should exceed or be equal to the solubility product of the sparingly soluble salt at the level

$$C_nC_n'\geq S$$

In critical case $C_nC_n'=S$; so substituting the condition into Eq. 14, we have

$$S=[C_0C_0' e^{-(\alpha'\pi/2\beta')} e^{-\alpha x_n} e^{\alpha'(x_n-x_{n-1})} \times\sin[\beta'(x_n-x_{n-1})]\cos(\beta x_n) \tag{15}$$

The above equation represents the phenomenon of Liesegang Rings in general form. The graphical representation of the equation is made in Fig. 2. The dotted liness in Fig.

Fig. 2

Fig. 3

2 indicates the solubility product of sparingly soluble salt. The spaces where the ionic product curve falls below SS' level indicates void regions while those places where the curve crosses the line SS' indicates the precipitate regions. Void spaces and precipitate regions have been represented in the figure by clear and dark areas respectively. The broader band structure of Liesegang systems will be given by

$$S=[C_0C_0'\,e^{-(\alpha'\pi/2\beta')}\,e^{-\alpha x_n}\,e^{\alpha'(x_n-x_{n-1})}] \times\sin\{\beta'(x_n-x_{n-1})\} \quad (16)$$

In case where the modulus of decay α and frequency factor β' of the wave profile of chromate ions are sufficiently small, Eq. 16 can be simplified further by putting $e^{\alpha'(x_n-x_{n-1})}$ =unity, and

$$\sin[\beta'(x_n-x_{n-1})]=\beta'(x_n-x_{n-1})$$

So, we get

$$S=(C_0C_0'\,e^{-(\alpha'\pi/2\beta')})e^{-\alpha x_n}\beta'(x_n-x_{n-1}) \quad (17)$$

or $$(x_n-x_{n-1})=\left(\frac{S\,e^{(\alpha'\pi/2\beta')}}{C_0C_0'}\right)e^{\alpha x_n} \quad (18)$$

or $$(x_n-x_{n-1})=\left[P\left(\frac{S}{C_0C_0'}\right)\right]e^{\alpha x_n} \quad (19)$$

P is a constant.

Since $\beta'=2\pi/\lambda'$, λ' being the wave length of chromate ions wave, Eq. 18 can be written as

$$(x_n-x_{n-1})=\left(\frac{S\lambda'\,e^{\alpha'\lambda'/4}}{2\pi C_0C_0'}\right)e^{\alpha x_n} \quad (20)$$

or $$(x_n-x_{n-1})=\psi\,e^{\alpha x_n} \quad (21)$$

Taking the logarithm, we have

$$\log(x_n-x_{n-1})=A+\alpha x_n \quad (22)$$

where A is another constant.

It may be noted here that the nature of Eq. 22 is not affected by changing the line of reference in the measurement of the rings. If d is the distance of n' order ring from a new reference level, then

$$x_n=(x_{n'}-d)$$

or $$\log(x_{n'}-x_{n'-1})=A+\alpha(x_n-d)$$

or $$\log(x_{n'}-x_{n'-1})=A'+\alpha' x_{n'} \quad (23)$$

Two Eqs. 22 and 23 differ only in constants.

In a Liesegang ring system αx_n may be considered as a small quantity for first few rings and so $e^{\alpha x_n}$ can be expanded and higher terms may be neglected. Eq. 21 thus reduces to

$$(x_{n'}-x_{n'-1})=\beta'+\alpha' x_{n'} \quad (24)$$

Eq. 24 differs from Eq. 3 in the constant β. The derivations here thus lead to an equation which is a corrected form of Jablczynski's empirical relation 1 or 3 which has already been studied by several workers. It may be noted that even Eq. 24 is a special case of more general expressions (15, 19, 20 and 23) for the phenomenon of Liesegang rings.

Discussion

Eq. 15 has graphically been represented in Fig. 1. The figure predicts the presence of fine structure between precipitate bands. Such structures have already been reported by Riegel and Reinhands[4], Hedges[5] and Friend[6] for the silver chromate system in gelatin gel. The author also made studies on the growth of rings. Liesegang rings of silver chromate were obtained by diffusing 2.5, 5, 7.5 and 10% silver nitrate solutions through test tubes containing 2, 4, 6 and 8% gelatin gels impregnated with 0.01 M chromate. The temperature was maintained befow 16°CF during the experiment. Distinct fringes of bright yellow color closely packed rings were seen when gelatin was dilute. The rings obtained were watched continuously for 12 hr. and it was found that even precipitate rings developed not as one single ring but as an aggregate of two or more closely packed fine rings which grew thicker and thicker with time and finally small gaps in between them gradually disappeared and thick layers of precipitates were formed. The observation proves the validity of Eqs. 14 and 15. For close study of the phenomenon, it is always useful to carry out experiments at low temperature and with low concentrations of gel.

Eq. 19 indicates that the rings would get more and more packed as the initial concentrations of ions increase and solubility product decreases. The effect of solubility on silver chromate rings has been studied by Varma and Ghosh[7] and influence of ionic concentration by several other workers[8]. Their results are in conformity with the conclusions drawn above.

The theory indicates that the nature of diffusion is mainly responsible for rhythmic phenomenon; a proper type of membrane[9] however becomes a necessary condition for the occurance of the process. Several factors such as colloidal formation super-saturation, etc., may help or hinder the formation of a proper type of membrane, but they themselves cannot be considered as the cause for Liesegang rings. The phenomenon may occur even in the absence of any of these conditions.

The experimental support of various expressions obtained above for Liesegang rings justifies the use of Raimann solution for Fick's diffusion equation. The theory thus indirectly throws light on the mechanism of diffusion.

In subsequent communications other aspects

3) R. Matalon and A. Packter, *J. Colloid Sci.*, **10**, 1, 46 (1955).
4) E. R. Riegel and M. C. Reinhard, *J. Phys. Chem.*, **31**, 713 (1927).
5) E. S. Hedges and R. V. Henley, *J. Chem. Soc.*, **1928**, 2715.
6) J. A. N. Friend, ibid., **121**, 472 (1922).
7) K. K. Varma and S. Ghosh, *Kolloid-Z.*, **133**, 1, 32 (1953).
8) R. Metalon and A. Packter, *Loc. Cit.* A. Packter, *Kolloid-Z.*, **142**, 109 (1955).
9) P. B. Mathur, *J. Sci. Ind. Research, (India)*, **14B**, 12, 668 (1955).

of Liesegang ring phenomenon will be treated quantitatively.

The author takes this opportunity to thank Professor S. Ghosh for discussions and for his interest and encouragement during the course of this research work and also to the Scientific Research Committee uttar Pradesh Government for granting a research scholarship during the period of the work.

Department of Chemistry
Allahabad University
Allahabad India

---

*Structural Analysis of Liesegang Ring Systems**

By Prem Behari MATHUR**

(Received May 17, 1960)

Since the discovery of the phenomenon of Liesegang ring several types of ring systems have been produced which on the structural basis may be broadly classified into the following categories:

a) Direct and revert systems
b) Macro and micro ring systems
c) Void spaced and continuous banded systems.

In the present paper these classifications have been analyzed in the light of the quantitative theory advanced by the author[1] in an earlier communication to this journal for the phenomenon of Liesegang rings.

Direct and Revert Systems

In the previous communication, the author obtained the following equations for Liesegang ring phenomenon,

$$(x_n - x_{n-1}) = a\left(\frac{S}{C_0 C'_0}\right)e^{\alpha x_n} \qquad (1)$$

or

$$(x_n - x_{n-1}) = K \qquad (2)$$

where x_n and x_{n-1} represent the distances of nth and $(n-1)$th rings respectively from the initial level of diffusion, S the solubility product, C_0 and C_0' the initial concentrations of the two ions and a, α and K the characteristic constants.

It can be seen that the two different types of ring systems are possible as α in Eq. 1 is negative or positive. When α is positive the distances between the successive rings $(x_n - x_{n-1})$ would increase with the increase of x_n as is commonly observed for this phenomenon. When α is negative the rings separation would decrease in the direction of diffusion of flocculating solution. Thus two different types of ring systems, which may be called a "Direct" and Revert" systems respectively could be produced.

Mathur and Ghosh[2] noted that if a diffusing electrolyte renders high peptizing influence or dissolves out the precipitate formed as a result of the interaction of the two ions, the decrease in the concentration of the peptizing ion along the diffusion path would lead to the "Revert" system of rings. The authors have noted that the ferricyanides of copper, iron, nickel and silver are peptized by the excess of the same metal ions, and this effect is more marked in the case of copper, iron, nickel and uranium ferricyanides and at the same time the revert systems have also been observed to be more prominent in these precipitate systems. Pactor[3] obtained a revert type of rings system by diffusing a solution of ammonia through a silver chromate solution peptized by acitic acid in gelatin gel. Hook[4] has obtained revert type of Liesegang ring systems of zinc, nickel, cobalt, ferrocyanides, nickel, zinc and iron cyanides, barium and mercury vandates and cerrous oxalate in gelatin medium and of chromium hydroxide and uranyl carbonate in agar-agar gel.

Periodic precipitations of "Direct" nature are of common occurrence. Silver chromate system in gelatin gel is a well known example of this type of banded structure.

* This work is the part of the Ph. D. Thesis submitted by the author to the University of Allahabad in September, 1956.

** Present Address: Senior Scientific Officer, Central Electrochemical Research Institute, Karaikudi-3, S. India.

1) P. B. Mathur, This Bulletin, **34**, 437 (1961); Ph. D. Thesis, Allahabad University, p. 25—51, (1956); *J. Colloid Sci.*, June (1960).

2) P. B. Mathur and S. Ghosh, *Kolloid-Z*, **159**, 2, 143 (1958).

3) A. Packter, *Nature*, **175**, 556 (1955).

4) A. van Hook, *J. Phys. Chem.*, **41**, 593 (1937).

Macro and Micro Ring Systems

Gel or other peptizing agents influence the precipitation of an sparingly soluble salt by keeping the coarser matter in colloidal state. The nature of the distributed matter in a system of periodic precipitation under the influence of environmental conditions can be ascertain from Fig. 1 which is a graphical representation of the ionic product relation obtained in the previous communication[5].

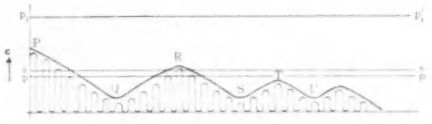

Fig. 1

$$C_nC_n' = [C_0C_0'e^{-(\alpha'\pi/2\beta')}]\,e^{\alpha'(x_n-x_{n-1})} \times \sin\{\beta'(x_n-x_{n-1})\} \times \cos(\beta' x_n)e^{-\alpha x_n} \quad (3)$$

or

$$C_nC_n' = a\,e^{[\alpha'(x_n-x_{n-1})]}e^{-(\alpha x_n)} \times \sin[\beta'(x_n-x_{n-1})]\cos(\beta x_n) \quad (4)$$

where $C_nC'_n$ is the ionic product and α, α', β' β and a are characteristic constants. In Fig. 1, SS′ represents the solubility product level and PP′ the peptizing level. The insoluble substance formed by interaction of diffusing ions would exist in precipitate or in peptized form according as PP′ is very close to or high above the SS′ level.

When the peptizing level PP′ is little above SS′ and cuts the ionic product curve at several places, the sparingly soluble matter will precipitate out in the regions where the ionic product curve rises above PP′. Thus, at P, R, T regions the precipitate bands would appear. At intermediate spaces Q, S, U etc., where the ionic curve falls below PP′ the residual matter will exist in colloidal state. The distribution of this colloidal matter along the diffusion column would also be of periodic nature following the curve 1. Thus, translucent micro-sealed ring systems of tracer colloidal material would be produced in between the precipitate bands. Such a type of structure has been observed by several workers notedly Hedges and Henley[6], Dounin and Shamyakin[7] and Mathur and Ghosh with silver chromate in gelatin medium.

5) P. B. Mathur, *Loc. cit.*
6) E. S. Hedges and R. V. Henley, *J. Chem. Soc.*, **1928**, 2715.
7) M. S. Dounin and F. M. Shemyakin, *Kolloid-Z*, **48**, 167 (1928).

The possibility of another type of such fine system is also apparent from Eq. 4. If in Eq. 4 the damping coefficients α and α' are almost negligible the factor

$$\exp[\alpha'(x_n-x_{n-1})-\alpha x_n]$$

tends to unity and Eq. 4 reduces to the form

$$C_nC_n' = a\sin[\beta'(x_n-x_{n-1})]\cos(\beta x_n)$$

which is an equation of the Simple Harmonic Curve (Fig. 2). In such systems whatsoever be the position of PP′ closely packed fine rings without any large size void spaces in between them, would be discerned. The fine ring systems will be of precipitated material when PP′ would cut the ionic produt curve, and of colloidal matter when PP′ would be situated above it. Mathur and Ghosh have been able to obtain the micro-sized Liesegang ring systems of cobalt and silver ferricyanide under suitable experimental conditions.

Void Spaced and Continuous Banded Systems

Let us now consider the case where damping factor $\exp(\alpha x_n)$, in Eq. 4 is large enough and at the same time the peptizing influence of the medium or of the ions present therein is moderately high on the insoluble substances. Such a system will graphically be represented by the curve P, Q, R, S and P_1P_1' shown in Fig. 1. If, due to high peptizibility of the

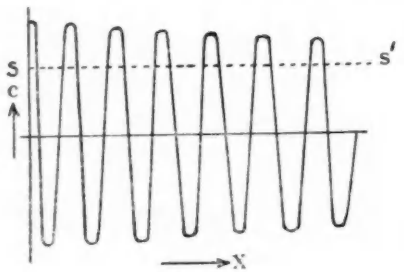

Fig. 2

insoluble salt the position of PP′ is just above the ionic product curve or if PP′ cuts the curve at some of its maxima points, the insoluble substance will exist both in colloidal as well as in precipitate form showing a continuous deposition of matter throughout the diffusion column. Due to the fact that the concentrations of ions in the regions of maxima and minima points very markedly, the colloidal particles in the neighbourhood of maxima points P, R, T will be much coarser due to the high concentration of the peptizing matter in this region in comparison to that in the minima regions. Such a system will therefore form bands of different size particles within a

continuous deposition, which will appear as alternate bands of different colors.

In cases where peptizing level is very high so much so that high concentration of a stable colloid may be produced, a very fine ring structure of colloidal matter, may appear but if it is too packed it may be left undetected.

Dhar and Chatterji[8] obtained a continuous banded system for mercuric iodide in agar gel, where a thick red color precipitate bands are followed by yellow ones and vice versa. Hatschek[9] noted a similar structure for cadmium sulphide in gelatin gel; Rastogi and Chatterji[10] reported for certain insoluble rare earth salts; Mathur and Ghosh for silver ferrocyanide and uranium ferricyanide.

Void spaced systems have already been discussed in the earlier communication. From Fig. 1, it can be seen that when peptizing level PP′ is close to the ionic product curve P, Q, R, S, the precipitate regions will be followed by void spaces and not by thick colloid bands, and so a void spaced ring system will be obtained.

It may, therefore, be concluded that the factors which control the Shape of Liesegang ring systems in gel media are (a) the damping coefficients α and α' of Eq. 3, and (b) the peptizability of the precipitate in particular environment, or say, the stability of the colloid formed under the conditions of the system. However, it may clearly be understood that colloidal formation like other factors simply influence the shape of rings in gel media, but it itself is not the cause of rhythemic phenomenon. The nature of diffusion is mainly responsible for the phenomenon, as explained in the earlier communication.

My thanks are due to Professor S. Ghosh, Head of the Department of Chemistry, Allahabad University for his keen interest in the work and valuable suggestions and also to the Scientific Research Committee of Uttar Pradesh for granting a research scholarship during the period of the work.

Department of Chemistry
Allahabad University
Allahabad India

8) N. R. Dhar and A. C. Chatterji, *J. Phys. Chem.*, **28**, 41 (1924); *Kolloid-Z.*, **37**, 2 (1925).
9) E. Hatschek, *Kolloid-Z*, **37**, 297 (1925).
10) M. C. Rastogi and A. C. Chatterji, *J. Indian Chem. Soc.*, **28**, 283 (1951).

"Frontier Electron Density" in Saturated Hydrocarbons

By Kenichi FUKUI, Hiroshi KATO and Teijiro YONEZAWA

(Received August 8, 1960)

Several simple quantum-mechanical methods have been proposed to discuss the physical properties of aliphatic compounds[1-3], but they were not always successful in interpreting quantum-chemically the chemical reactivity of these compounds.

In our previous papers treating aliphatic compounds, we calculated the ionization potential, the bond energy[4] and the reactivity in nucleophilic substitution[5] by using Yoshizumi's C-C skeleton method[6].

In the present paper, we have investigated the chemical reactivity of several aliphatic hydrocarbons in a metathetical reaction by using the simple LCAO MO method including all of the atomic orbitals which participate in forming C–C and C–H σ bonds in these compounds. The molecular orbital of aliphatic hydrocarbons, ψ_j, may be represented by a linear combination of 1s orbitals of hydrogen atoms, ϕ_{Hl}, and sp^3 orbitals of carbon atoms, ϕ_{Cr}.

$$\psi_j=\sum_r C_{rj}\phi_{Cr}+\sum_l C_{lj}\phi_{Hl}$$

where C_{rj}, C_{lj} are the coefficients of the rth sp^3 orbital of carbon atom and the lth 1s orbital of hydrogen atom in the jth molecular orbital, respectively.

The resonance integrals between neighboring atomic orbitals are assumed

$$\int \phi_{C,n} H \phi_{H,n+1} d\tau = b\beta$$

1) R. D. Brown, *J. Chem. Soc.*, **1953**, 2615.
2) M. J. S. Dewar and R. Pettit, ibid., **1954**, 1625.
3) J. Lennard-Jones and G. G. Hall, *Disc. Faraday Soc.*, **53**, 127 (1957).
4) K. Fukui, H. Kato and T. Yonezawa, This Bulletin, **33**, 1197 (1960).
5) K. Fukui, H. Kato and T. Yonezawa, ibid., **33**, 1202 (1960).
6) H. Yoshizumi, *Trans. Faraday Soc.*, **53**, 125 (1957).

the sp^3 orbital of carbon and the 1s orbital of hydrogen in a C–H σ bond:

$$\int \phi_{C,r} H \phi_{C,r+1} d\tau = \beta$$

between two sp^3 orbitals of two adjacent carbon atoms each:

$$\int \phi_{C,r} H \phi_{C,r+1} d\tau = m\beta$$

between two sp^3 orbitals belonging to one and the same carbon atom:

The Coulomb integrals are taken as

$$\int \phi_{H_l} H \phi_{H_l} d\tau = \alpha + a_l\beta$$

$$\int \phi_{C,r} H \phi_{C,r} d\tau = \alpha$$

All overlap integrals are neglected.

The values of m is taken as 0.34 determined by Yoshizumi, a is put equal to -0.2 referring the value of C–H bond moment ($C^{-\delta}$–$H^{+\delta}$, 0.4 D),* and b is put 1.1 which is the ratio of the overlap integral S_{C-H} to S_{C-C}[7].

The calculated values of ionization potential and heat of formation of several compounds are listed in Table I, where the values of α and β are taken as -5.05 eV. and -8.8 eV., tentatively.

Since a good agreement between the calculated and experimental values is observed in this table, the numerical estimation of these parameters is considered to be reasonable.

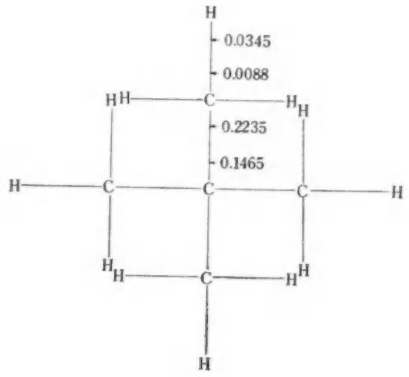

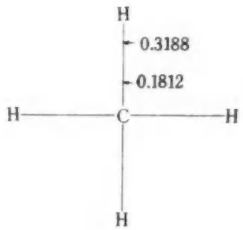

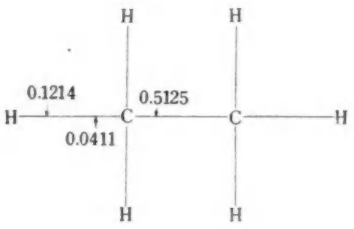

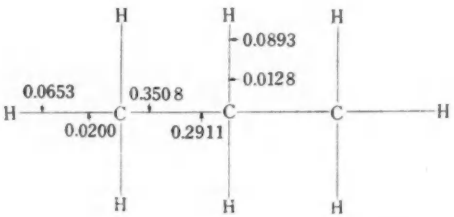

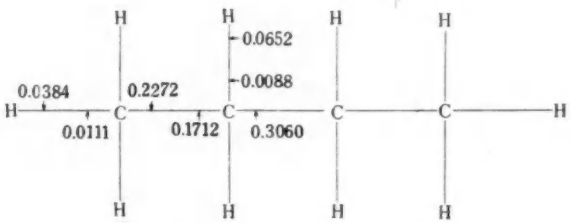

7) R. S. Mulliken, C. A. Rieke, D. Orloff and H. Orloff, *J. Chem. Phys.*, **17**, 1248 (1949).

* The value of a varies according as the hydrogen atom is primary, secondary or tertiary. In the present treatment a is taken as the same for simplicity's sake. Future improvement is expected with regard to this point.

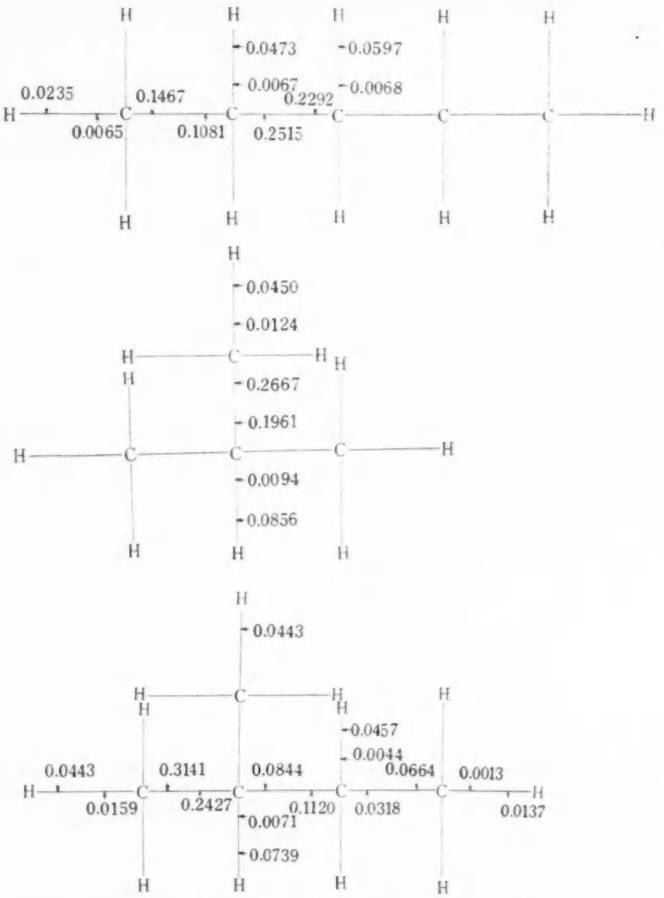

Fig. 1. The values of $f^{(R)}$ in several saturated hydrocarbons.

TABLE Ia. IONIZATION POTENTIAL

	Calcd. I. P.		Obs. I. P.[a]
	λ_{ho}	ε_{ho} eV.	eV.
CH_4 (1st)	0.8322	12.37	13.16
CH_4 (2nd)	1.6546	19.61	19.80
C_2H_6	0.7254	11.43	11.76
C_3H_8	0.7009	11.22	11.21
C_4H_{10}	0.6871	11.10	10.80

where λ_{ho} is the coefficient $\varepsilon_{ho}=\alpha+\lambda_{ho}\beta$, ε_{ho} is the highest occupied orbital energy.

The metathetical reaction of paraffins is expressed by the equation

$$R\text{-}H + \cdot X \rightarrow R\cdot + H\text{-}X$$

where R is an alkyl group and $\cdot X$ is an attacking radical.

We previously proposed the frontier electron

TABLE Ib. TOTAL ENERGY AND HEAT OF FORMATION

	Calcd.	Obs. heat of formation[b] kcal./mol.	Difference: Calcd. $-\beta$	Difference: Obs. kcal.
CH_4	$8\alpha+8.329\beta$	−17.9		
			6.334	−2.3
C_2H_6	$14\alpha+14.663\beta$	−20.2		
			6.337	−4.6
C_3H_8	$20\alpha+21.000\beta$	−24.8		
			6.368	−5.4
C_4H_{10}	$26\alpha+27.368\beta$	−30.2		

a) R. E. Hornig, *J. Chem. Phys.*, **16**, 105 (1948).

b) F. D. Rossini, K. S. Pitzer et al., "Selected Values of Physical and Thermodynamic Properties of Hydrocarbons and Related Compounds", Carnegie Press (1953).

density[8], $f^{(R)}$, as an excellent reactivity index for a radical reaction of conjugated systems. Now we can show that $f^{(R)}$ is found to be also available as the reactivity index of saturated compounds.* The calculated values of $f^{(R)}$ in several compounds are listed in Fig. 1. It is observed that the values of $f^{(R)}$ on hydrogen atoms in these compounds is parallel with the experimental results. That is to say, the activity of hydrogen-extraction in saturated hydrocarbons increases in the order *prim.* H $<$*sec.* H $<$*tert.* H[9].

Thus, the frontier electron density has been found to relate with the experimental chemical reactivity of aliphatic saturated molecules.

An application of this fact to explaining the reaction mechanism of oxidation or pyrolysis in aliphatic hydrocarbons seems to be possible.

Faculty of Engineering
Kyoto University
Sakyo-ku, Kyoto

8) K. Fukui, T. Yonezawa, C. Nagata and H. Shingu, ibid., **22**, 1432 (1954).

* According to the electronegativity of the attacking radical, $f^{(E)}$ or $f^{(N)}$ (frontier electron densities for electrophilic or nucleophilic attack) may be used in lieu of $f^{(R)}$. In the present case we are imagining e. g.·CH_3 for the attacking radical, whose energy level seems to lie between the highest occupied and the lowest vacant orbitals of R-H.

9) A. F. Trotman-Dickenson, *Quart. Revs.*, **7**, 198 (1953).

Studies on the Catalytic Double Wave of Cystine by Oscillographic Polarography

By Mutsuaki SHINAGAWA, Hideo IMAI and Hiroyuki NEZU

(Received July 16, 1960)

Brdicka[1] has reported that in a conventional polarography cystine and cysteine develop a pronounced single catalytic wave in an ammonia buffer containing divalent cobalt. In the previous paper[2] it was reported that this catalytic wave gives a rounded maximum of good reproducibility by the addition of gelatin and that the maximum wave is split off into two waves by the addition of methyl cellulose (cf. Fig. 1). The form of these double waves resembles that of the catalytic double wave of protein, and the evolution of hydrogen as the electrolytic reductant is facilitated by the catalytic action of the cobalt(II)-cysteine complex* adsorbed on the surface of the dropping mercury electrode (DME). Accordingly, one can expect to clarify the nature of the protein wave from the analogy to the cystine wave.

The present experiment was carried out as a tentative model of the protein wave, and a possible mechanism of the cystine wave is proposed from the consideration of the adsorption equilibria among three surface active substances, i. e., the cobalt(II)-cysteine complex anion, methyl cellulose and gelatin.

1) R. Brdicka, *Collection Czechoslov. Chem. Communs.*, **4**, 148 (1933).

2) M. Shinagawa and H. Nezu, This Bulletin, **33**, 272 (1960).

* This catalytic wave occurs at a more negative potential than the potential of the reduction of cystine to cysteine, and therefore, must be caused by the reduced form, cystein.

Experimental

A Sevcik type oscillographic polarograph[3] constructed in our laboratory[4] was used. Effects of the mercury head and the frequency of the applied triangular sweep on the oscillographic current voltage pattern were observed. The mercury head was changed from 25 to 65 cm., when the life-time of the DME changed from 5.4. to 2.0 sec. under the applied span voltage from -0.28 to -2.16 V. vs. S. C. E. (20 cycles/sec.). The rate of the mercury flow was 0.755 mg./sec. at the mercury head of 25 cm. The frequency applied was 20~60 cycles/sec., when the rate of potential change was 75~225 V./sec.

All the reagents were of analytical grade. The test solutions used are tabulated as follows:

Test solution No.	Constituent
0	0.1 F NH_3-NH_4Cl buffer
1	1×10^{-4} F $CoCl_2$ + 2×10^{-5} F cystine in solution 0
2	0.02% methyl cellulose in solution 1
3	0.01% gelatin in solution 1
4	0.02% methyl cellulose + 0.01% gelatin in solution 1
5	0.005~0.08% methyl cellulose in solution 0

3) A. Sevcik, *Collection. Czechoslov. Chem. Communs.*, **13**, 349 (1948).

4) M. Shinagawa, H. Imai and S. Chaki, *J. Electrochem. Soc. Japan*, **23**, 132 (1955); H. Imai, This Bulletin, **29**, 276 (1956).

An H-cell with low impedance was used, and the dissolved oxygen in the test solution was not removed. The temperature was 29±0.5°C.

Results and Discussion

Under the experimental conditions described in the preceding section, the cobalt(II)-ammine complex behaves irreversibly at the DME, and the charging current, which flows when the adsorption or desorption of surface active substances occurs, becomes markedly great. The effect of the mercury head on the peak current gives information concerning the difference between the electrolytic current and the charging current and also concerning the irreversibility of an electrode process. One can obtain similar information from the effect of the sweep frequency on the peak current and the peak potential**.

The Oscillographic Current-Voltage Pattern. — The oscillographic current-voltage pattern of solutions 1, 2, 3 and 4 are illustrated in Figs. 2-A, B, C and D, respectively. In Fig. 2-A, two reduction steps represented by i_p1 and i_p2 are noticeable***. i_p1, the peak potential of which is −1.27 V. vs. S. C. E., corresponds to the reduction of the cobalt(II)-ammine complex ion. The peak height of i_p1 is decreased and rounded off by the addition of methyl cellulose and gelatin as is illustrated in Figs. 2-B, C and D, simultaneously the peak potential being shifted toward more negative potentials (E_p = −1.27, −1.31 and −1.36 V. vs. S. C. E. in solutions 2, 3 and 4, respectively.).

The second step (E_p=ca. −1.7 V. vs. S. C. E.)

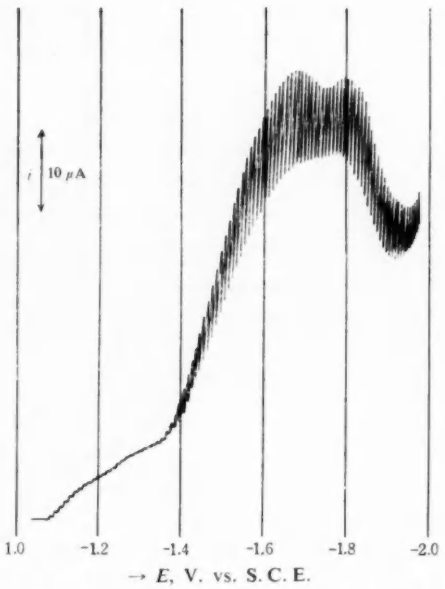

Fig. 1. The catalytic double wave of cystine by a conventional polarograph. Solution: 1×10^{-3} F $CoCl_2$, 2×10^{-5} F cystine, 0.002% methyl cellulose in 0.1 F NH_3-NH_4Cl buffer. m=2.46 mg./sec., t=3.5 sec.

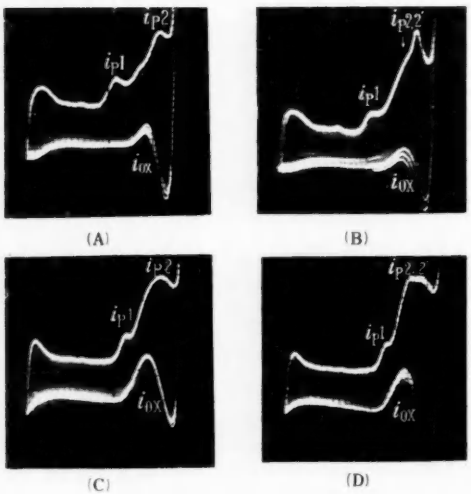

Fig. 2. The oscillographic current-voltage pattern of 1×10^{-3} F $CoCl_2$ and 2×10^{-5} F cystine in 0.1 F ammonia buffer (A). (B): +0.02% methyl cellulose, (C): +0.01% gelatine, (D): +0.02% methyl cellulose and 0.01% gelatin, Sweep frequency=20 cycles/sec., v=75 V./sec., h=25 cm., t=4.9 sec.

** These points of view are summarized in detail as follows in order to help the subsequent considerations.

(1) The peak of the oscillographic pattern is rounded off and the peak potential (E_p) is shifted toward more negative potentials in the cathodic branch as the electrode process becomes irreversible[5].

(2) No reoxidation peak can be observed in the anodic branch unless the DME forms the amalgam with the reductant.

(3) The maximal peak current (i. e. the peak current just before the electrode mercury droplet falls) of a reversible electrode process ($i_{p,r}$) is independent of the mercury head, while that of an irreversible one ($i_{p,ir}$) varies with the mercury head[6].

(4) $i_{p,r}$ is proportional to the square root of the rate of the potential change (v)[6], while $i_{p,ir}$ deviates from this proportionality[7].

(5) The maximal charging current is independent of the mercury head, and it is linearly proportional to v.

(6) The peak potential of the charging current, which flows at the adsorption or the desorption potential of surface active substances, will be shifted by the change in the concentration of the adsorbed substance.

5) P. Delahay, *J. Am. Chem. Soc.*, **75**, 1190 (1953); H. Matsuda and Y. Ayabe, *Z. Elektrochem.*, **59**, 494 (1955).

6) P. Delahay, *J. Phys. Colloid Chem.*, **54**, 630 (1950); H. Imai, *J. Electrochem. Soc. Japan*, **23**, 530 (1955).

7) P. Delahay and G. Perkins, *J. Phys. Colloid Chem.*, **55**, 586, 1146 (1951).

*** i_p2 is accompanied by a barely perceptible peak at −1.5 V. vs. S. C. E. This peak corresponds to an irregular wave observed at the same potential by a conventional polarograph. The nature of this wave is unknown at this stage.

represented by i_p2 in Fig. 2 is the catalytic current. This catalytic current is accompanied by a sharp peak at -1.72 V. vs. S. C. E. in the presence of methyl cellulose. Since a similar sharp peak is developed at -1.7 V. vs. S. C. E. by the desorption of methyl cellulose in solution 5 (cf. Fig. 3), the above-mentioned sharp

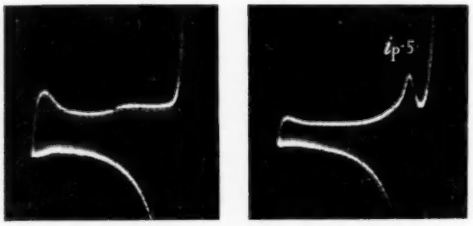

(A) (B)

Fig. 3. The oscillographic current-voltage pattern of 0.1 F ammonia buffer (A) and 0.06% methyl cellulose in 0.1 F ammonia buffer (B). Sweep frequency = 20 cycles/sec., v = 75V./sec., h = 45 cm., t = 2.4$_3$ sec.

peak of solution 2 can be assigned to the charging current change caused by the desorption of methyl cellulose. By the addition of gelatin, the catalytic current is rounded off (E_p = 1.72 V. vs. S. C. E.) as is illustrated in Fig. 2-C, and this wave is split off into two waves by the addition of methyl cellulose (Fig. 2-D), the potential of the first and the second peak being -1.62 and -1.73 V. vs. S. C. E., respectively. Undoubtedly, these double peaks are different in nature from the catalytic double waves developed by a conventional polarograph (Fig. 1), because the charging current becomes predominant in an oscillographic method. It may safely be assumed, however, from the coincidence of the peak potential of i_p2' with the desorption potential of methyl cellulose that the desorption of methyl cellulose is closely connected with the occurrence of i_p2' and presumably with that of the second maximum wave in the conventional polarography.

In the anodic branch, the current change represented by i_{ox} is noteworthy. The pattern of i_{ox} is pronounced by the addition of gelatin, and in this case it can be seen from Figs. 2-C and 2-D that this current is obviously cathodic (the reduction current). A cathodic current of a similar character has been observed in the solution containing indium(III) and chloride[8], corresponding to the well-known minimum wave in the conventional polarography. It is supposed that this minimum wave is caused by the electrostatic repulsion of $InCl_6^{3-}$ from the negatively charged electrode. By analogy, it can be assumed that the cobalt-(II)-cysteine complex anion behaves likewise. When the electrode potential is shifted toward less negative values in the anodic branch after the repulsion of the complex anion in the cathodic branch, the complex anion will be readsorbed on the electrode surface and contributes to the catalytic reduction of the hydrogen ion. Thus, the mechanism of i_{ox} leads to the idea of the repulsion of the cobalt(II)-cysteine complex anion at the potential more negative than -1.63 V. vs. S. C. E.

The Variation of the Peak Current with the Mercury Head.—The peak current is plotted against the mercury head in Fig. 4, where the

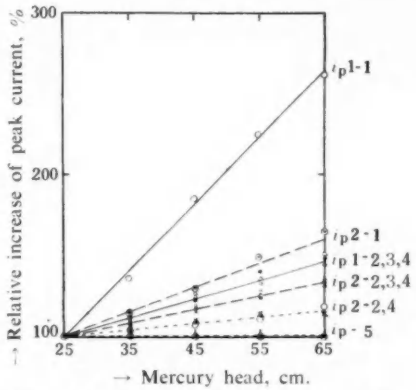

Fig. 4. The relative variation of the peak current with the mercury head. The symbols of the peak current are given in Fig. 2, and the second figure of the symbol represents the solution number given in the section of the experimental. Sweep frequency = 20 cycles/sec., v = 75 V./sec.

peak current is represented by the same symbols as those used in Fig. 2, and the second figure in the symbols represents the solution number given in the section of Experimental. In Fig. 4 three groups are classified according to their inclination. The first group involves i_p1-1 and i_p2-1 which have the steepest inclination among i_p1's and i_p2's, respectively. When the recovery of the diffusion layer in each cycle of the voltage sweep imperfect owing to the imcomplete reoxidation of the reductant (Note that i_p1 and i_p2 give no reoxidation peak in Fig. 2.), the repetition of the reduction process during the life-time of the DME results in the depletion of the oxidant at the vicinity of the electrode surface except for the supply due to the duffusion from the bulk of solution. Under

8) M. Shinagawa, H. Imai and H. Sunahara, *J. Chem. Soc. Japan, Pure Chem. Sec.* (*Nippon Kagaku Zasshi*), **77**, 1482 (1956).

this condition, the thickness of the diffusion layer will be markedly decreased by the rapid rate of the DME growth. Moreover, the fresh surface of the DME is increased by the rapid rate of the DME growth. Since the rate of the DME growth increases as the mercury head is increased, it is easy to see why these currents increase as the mercury head is increased.

The second groups involves i_p1-2, 3, 4 and i_p2-2, 3, 4, which show a moderate change with the mercury head. In this group, the effect of the drop growth seems to be retarded by the presence of the surface active substances.

The third group involves i_p-5. This desorption peak current of methyl cellulose is practically independent of the mercury head.

The peak heights of i_p2'-2 and i_p2'-4 were measured from the height of the charging current without paying any attention to the superposition of the preceding peak current, i_p2, which is markedly affected by the mercury head. Keeping this fact in mind, one can assign the slight inclination of i_p2' to the superposition of the intrinsic current of i_p2' on the decreasing current of i_p2. Accordingly, it is assumed that i_p2' is practically independent of the mercury head and will be tacitly controlled by the desorption of methyl cellulose. This assumption is best realized from Fig. 5 which illustrates the relative change of i_p2-4 and i_p2'-4 with the mercury head.

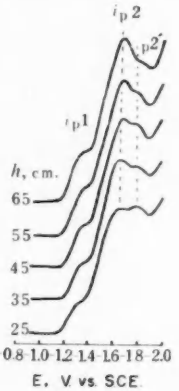

Fig. 5. The variation of the oscillographic current-voltage pattern of 1×10^{-3} F $CoCl_2$ and 1×10^{-5} F cystine in 0.1 F ammonia buffer containing 0.02% methyl cellulose and 0.01% gelatin with the mercury head (h, cm.). Sweep frequency = 20 cycles/sec., v = 75 V./sec.

The Effect of the Sweep Frequency. — The effect of the sweep frequency on the cathodic peak current is illustrated in Fig. 6. Any peak, except for the desorption peak of methyl cellulose, becomes more rounded and the peak

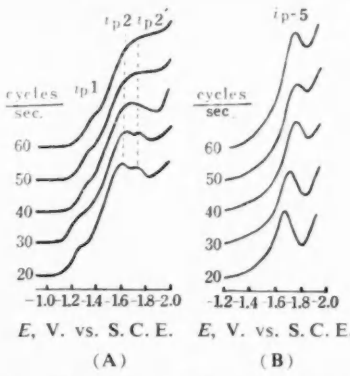

Fig. 6. The variation of the oscillographic current-voltage pattern of 1×10^{-3} F $CoCl_2$ and 1×10^{-5} F cystine in 0.1 F ammonia buffer containing 0.02% methyl cellulose and 0.01% gelatin (A) and the desorption charging current of 0.06% methyl cellulose (B) with the sweep frequency. h = 45 cm.

potentional is shifted toward more negative potentials as the sweep frequency is increased. This result indicates that all of these electrode processes are irreversible. It must be pointed out here that the electrode process of i_p2'-4 is irreversible in nature, though it relates to the desorption of methyl cellulose as is described in the preceding section.

Conclusion

By a conventional polarograph, cystine develops the pronounced double maximum in an ammonia buffer containing divalent cobalt, gelatin and methyl cellulose. This double wave is of interest because of the resemblance to the protein wave in the wave form and in the catalytic behavior. In the following description, it is explained why the cystine wave is developed in the form of the double maximum.

In this experiment, it was confirmed that cobalt(II)-cysteine complex, which acts as a catalyser for the depolarization of the hydrogen

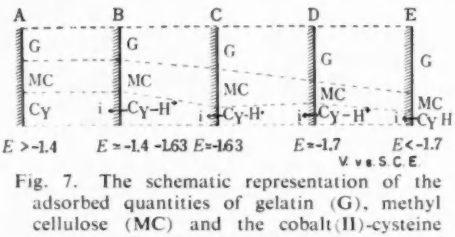

Fig. 7. The schematic representation of the adsorbed quantities of gelatin (G), methyl cellulose (MC) and the cobalt(II)-cysteine complex (Cy) on the unit surface area of the DME at each electrode potential. In this figure, i←Cy-H$^+$ means that Cy behaves as a catalysis of the hyrogen ion depolarization.

ion, desorbs from the electrode surface at about −1.63 V. vs. S. C. E. When the electrode potential becomes more negative than −1.7 V. vs. S. C. E., methyl cellulose also desorbs from the electrode surface. Accordingly, the quantity of the surface active substances adsorbed on the unit surface area of the DME at each electrode potential can be schematically expressed as is illustrated in Fig. 7.

In Fig. 7, G, MC and Cy represent the adsorbed quantity of gelatin, methyl cellulose and cobalt(II)-cysteine complex anion, respectively, on the unit surface area of the DME. The quantity of G, MC and Cy depends on each adsorbed concentration, which is in equilibrium with each concentration of the bluk of the solution and on the mutual equilibria among G, MC and Cy on the electrode surface. When the electrode potential is less negative than −1.6 V. vs. S. C. E., all of the surface active substances are adsorbed on the electrode surface as is illustrated in Fig. 7-A. As the electrode potential becomes more negative than −1.5 V. vs. S. C. E., the catalytic current gradually increases (Fig. 7-B). The cobalt(II)-cysteine complex anion, however, begins to desorb at −1.63 V. vs. S. C. E. and results in the decrease of the catalytic current (Fig. 7-C). Thus, the first maximum wave will be developed by the conventional polarograph. It is noteworthy, here, that the quantity of G and MC will be increased, corresponding to the desorption of Cy-complex. This is because the surface area to be occupied by G and MC will increase when Cy-complex desorbs.

At the potential of −1.7 V. vs. S. C. E. methyl cellulose begins to desorb from the electrode surface (Fig. 7-D). In this case, the quantity of G and Cy-complex will be increased, though the increase of Cy-complex is limited in the potential region where the desorption of methyl cellulose appreciably proceeds. Accordingly, the catalytic current will temporarily increase near the potential of −1.7 V. vs. S. C. E. (Fig. 7-E). Thus, the second maximum wave will be developed.

In the above-mentioned conclusion, the present authors proposed a possible mechanism of the cystine double wave from the consideration of the adsorption equilibria among gelatin, methyl cellulose and cobalt(II)-cystein complex anion. The criticism of this idea and its application to the protein wave is left for future.

Part of the expenses has been covered by the Grant in Aid for Fundamental Scientific Research, Ministry of Education.

Laboratory of Analytical Chemistry
Faculty of Science and Minami College
Hiroshima University
Higashisendamachi, Hiroshima

SHORT COMMUNICATIONS

Radiolysis of Crystalline Oxalato Complexes

By Akira Sugimori and Gen-ichi Tsuchihashi

(Received December 2, 1960)

The effects of metal ions on the radiolysis of organic compounds have mainly been studied in aqueous solutions[1]. The present authors previously studied the radiation chemistry of aqueous metal salicylate complexes, and found that chelated Fe^{3+} and Cu^{2+} effectively increase the decarboxylation of salicylic acid[2]. The study on the radiolysis of crystalline metal complexes was also considered to be very helpful for the elucidation of the mechanism of the reaction affected by metal ions. In this paper, the radiolysis of various crystalline metal oxalato complexes is repoted.

Oxalic acid ($H_2C_2O_4 \cdot 2H_2O$), anhydrous oxalic acid ($H_2C_2O_4$), ferrous oxalate ($Fe(C_2O_4) \cdot 2H_2O$), sodium oxalate ($Na_2C_2O_4$), potassium trisoxalatoaluminate ($K_3Al(C_2O_4)_3 \cdot 3H_2O$), potassium trisoxalatochromate ($K_3Cr(C_2O_4)_3 \cdot 3H_2O$), potassium trisoxalatocobaltate ($K_3Co(C_2O_4)_3 \cdot 3H_2O$) and potassium trisoxalatoferrate ($K_3Fe(C_2O_4)_3 \cdot 3H_2O$) were irradiated with Co-60 gamma rays at room temperature, mainly

1) J. H. Baxendale and D. Smithies, *J. Chem. Phys.*, **23**, 604 (1955); *J. Chem. Soc.*, **1959**, 779.

2) A. Sugimori and G. Tsuchihashi, This Bulletin, **33**, 713 (1960).

TABLE I. THE ANALYSIS OF THE GASEOUS PRODUCTS

Compound	Dose rate r./hr.	Dose, r.	G(gas)	CO/CO_2
$H_2C_2O_4 \cdot 2H_2O$	4.4×10^5	1.45×10^5	1.1	0.0
$Na_2C_2O_4$	4.4×10^5	1.45×10^5	0.03	0.1
$K_3Al(C_2O_4)_3 \cdot 3H_2O$	4.4×10^5	1.31×10^5	2.0	0.1
$K_3Cr(C_2O_4)_3 \cdot 3H_2O$	4.4×10^5	1.45×10^5	1.5	0.6
$K_3Fe(C_2O_4)_3 \cdot 3H_2O$	4.4×10^5	1.45×10^5	7.5	0.0
$K_3Co(C_2O_4)_3 \cdot 3H_2O$	4.4×10^5	1.45×10^5	9.8	0.0

TABLE II. THE DECOMPOSITION OF THE COMPLEXES

Compound	Condition	Dose rate r./hr.	Dose, r.	G(-complex)
$K_3Cr(C_2O_4)_3 \cdot 3H_2O$	vacuum	4.4×10^5	1.45×10^5	0.7
	air	4.6×10^5	1.46×10^5	0.7
$K_3Co(C_2O_4)_3 \cdot 3H_2O$	vacuum	4.4×10^5	1.31×10^5	8.9
	air	4.6×10^5	1.46×10^5	9.1

TABLE III. THE DECOMPOSITION OF $C_2O_4^{2-}$

Compound	Condition	Dose rate r./hr.	Dose, r.	$G(-C_2O_4^{2-})$
$H_2C_2O_4 \cdot 2H_2O$	vacuum	4.6×10^5	1.46×10^5	2.3
	air	2.6×10^5	5.15×10^7	5.1
$H_2C_2O_4$	vacuum	4.6×10^5	1.46×10^5	3.6
	air	4.6×10^5	1.46×10^5	4.3
$Na_2C_2O_4$	vacuum	4.6×10^5	1.46×10^5	<0.03
	air	2.6×10^5	5.15×10^7	<0.3
$K_3Al(C_2O_4)_3 \cdot 3H_2O$	vacuum	4.4×10^5	1.31×10^5	4.6
	air	4.4×10^5	1.46×10^5	5.5
$Fe(C_2O_4) \cdot 2H_2O$	vacuum	1.6×10^5	1.46×10^5	0.1

at a does rate of 4.4×10^5 r./hr. and at a total dose of 1.5×10^5 r. both in the presence and in the absence of air.

After the quantity of evolved gas was measured, the gas was analyzed mass-spectrometrically. The quantity of decomposed complex was measured by visible light absorption spectrometry of aqueous solutions of irradiated complexes. The quantity of decomposed oxalate was measured by titrating the solutions of irradiated samples with acid permanganate solution. G(gas) (the number of the molecules of evolved gas), the ratio of CO to CO_2 in the evovled gas, G(−complex) (the number of the decomposed molecules of the complex) and G ($-C_2O_4^{2-}$) are shown in Tables I, II and III. From the experimental results, the followings are concluded.

(1) Oxalate ions such as in sodium oxalate and ferrous oxalate are very stable to gamma ray irradiation, compared with those in metal oxalato complexes. The fairly large reactivity of oxalic acid and potassium trisoxalatoaluminate toward gamma irradiation might be attributed to the covalent character of oxalate-M (M=metal ion or hydrogen) bond. Oxalate ions with larger covalent character decompose more easily by gamma irradiation.

(2) The much larger G values of Fe^{3+} and Co^{3+} complex than those of Al^{3+} complex can not be explained only by the covalent character of oxalato-metal bond. They seem to be related with the reduction of metal ions. On gamma irradiation of Fe^{3+} and Co^{3+} complex, the reduction of the metal ions also occurs, and ferrous and cobaltous oxalate precipitates when the irradiated complexes are dissolved in water. Therefore, the electron transfer from oxalate to metal ions might increase the radiation-induced decomposition of oxalate.

(3) Chromium is stable in the state Cr^{3+} and Cr(VI) whereas very unstable in the state Cr^{2+}; therefore on gamma irradiation of $K_3Cr(C_2O_4)_3 \cdot 3H_2O$ the electron transfer from oxalato to metal ion might be difficult and this might cause the lower G values of Cr^{3+} complex than those of Fe^{3+} and Co^{3+} complex. But on the reaction of Cr^{3+} complex, the oxidation of Cr^{3+} to Cr(VI) might occur, and a fairly large amount of CO is formed in place of CO_2 which is the main product in the gamma irradiation of oxalic acid and the oxalate complexes other than those with Cr^{3+}.

Details of this study will be published later.

Radiation Applications Division
Japan Atomic Energy Research Institute
Tokai, Ibaraki-ken

Steric Effects of ortho-Groups on Hydrogen Bond Formation in Phenol Derivatives as Studied by Nuclear Magnetic Resonance

By Ichiro YAMAGUCHI

(Received December 20, 1960)

In the previous report[1], the author pointed out that the chemical shift of the OH proton depends greatly on the relative position of the methyl groups to the OH group in dimethyl phenol isomers, and this was attributed to the steric effects of the methyl group on the formation of intermolecular hydrogen bond. The present report shows a dependence of the OH proton chemical shift on the size of the ortho-group.

The compounds investigated are 2, 6-dichlorophenol, 2, 6-dimethyl phenol and 2, 6-di-*t*-butyl-*p*-cresol. The chemical shifts of the OH proton in various solutions were determined by the side band technique refering to water as an external standard. The correction for the bulk diamagnetic susceptibility was not applicable except to the values extrapolated to infinite dilution because reliable data of the susceptibility for these compounds were not available.

In Figs. 1a and 1b, the OH resonance shifts (in p.p.m.) are plotted against the concentration of the solutions (in mole fraction). The curves for various solutions are comparatively separated in a wide range of the magnetic field from one another for 2, 6-dichlorophenol and 2, 6-dimethyl phenol, but not for 2, 6-di-*t*-butyl-*p*-cresol. This suggests that the size of the ortho-group would be a factor which affects the ability of the formation of an intermolecular hydrogen bond of a phenol. This effect was qualitatively pointed out by Batdorf with his NMR measurements[2].

As a measure of the extent of the ability of the hydrogen bond formation, the difference between the chemical shift at infinite dilution (extrapolated and then corrected for bulk diamagnetic susceptibility of the solvents) for carbon tetrachloride solution and that for acetone solution is taken. In Fig. 2, the values of the difference, Δ, are plotted against the size of the ortho-groups, for instance the Van der Waals radii. The data for phenol[2,3] are also plotted.

In Fig. 2, the followings are observed: First, the Δ value is larger as the radius is smaller. Secondly, the Δ value for 2, 6-dichlorophenol is found above the line connecting the points for phenol and dimethyl phenol. This discrepancy may be due to weak intramolecular hydrogen bond between OH and Cl groups. Linear extrapolation of the

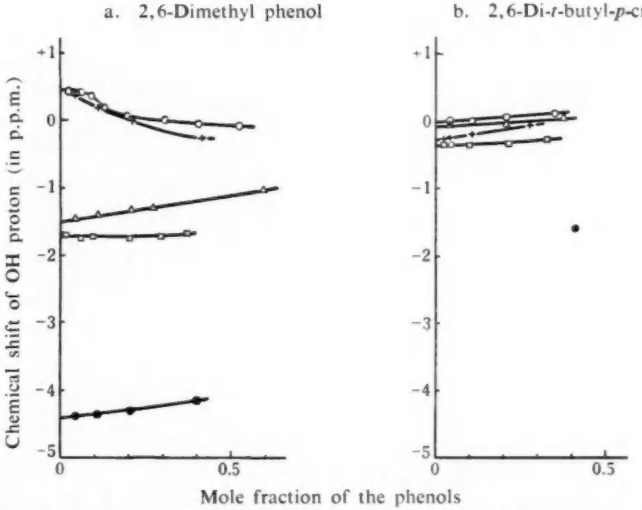

Fig. 1. OH proton resonance shift refer to H_2O proton (susceptibility correction is not applied.).
Solvent: -○- CCl_4 -+- $CHCl_3$ -△- Ether -□- Acetone -●- Pyridine

1) I. Yamaguchi, This Bulletin, **34**, 353 (1961).
2) R. L. Batdorf, Ph. D. thesis, Univ. of Minnesota, 1955.
3) C. M. Huggins, G. C. Pimentel and J. N. Shoolery, *J. Phys. Chem.*, **60**, 1311 (1956).

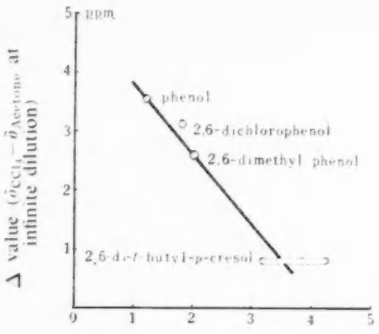

Fig. 2. Dependence of the ability of hydrogen bond formation of phenols on the size of ortho-group.

line connecting two points for 2, 6-di-alkyl phenols (alkyl = H and CH_3) to the Δ value of 0.8 gives a value approximately 3.5 Å as the Van der Waals radius corresponding to the size of the *t*-butyl group. This value seems to be reasonable for this group. Therefore it may be concluded that the ability of the formation of an intermolecular hydrogen bond in phenol derivatives is a linear function of the size of the ortho-group.

Radiation Applications Division
Japan Atomic Energy Research Institute
Tokai, Ibaraki-ken

New Stable Olefin Complexes of Cobalt(I)

By Akira NAKAMURA and Nobue HAGIHARA

(Received December 8, 1960)

In a previous communication the authors described the synthesis of cyclopentadienyl cobalt cyclooctatetraene (I)[1]. In that report the authors reported that I took up 2 mol. of hydrogen on catalytic hydrogenation to give orange crystals (II), m. p. 102°C. The authors supposed this compound II to be cyclopentadienyl cobalt 1, 5-cyclooctadiene considering from the proposed structure of I (cf. Fig. 1). In order to determine the correct structure of II, an attempt was made to obtain the same compound from 1, 5-cyclooctadiene. Thus 1, 5-cyclooctadiene was refluxed with cyclopentadienyl cobalt dicarbonyl in xylene under nitrogen for 15 hr. After removal of the unreacted starting materials, orange crystals were obtained by sublimation at 80°C under reduced pressure in 30% yield. These crystals were recrystallized from petroleum ether, m. p. 102.5°C. Found: C, 67.05; H, 6.76. Calcd. for $C_{13}H_{17}Co$: C, 67.24; H, 7.38%. The infrared spectrum of this compound was identical with that of II and showed the presence of π-cyclopentadienyl group. No absorption was observed at usual C=C stretching region. These facts indicate the structure of II to be $(C_8H_{12})Co(C_5H_5)$ which is shown in Fig. 2.

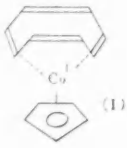

Fig. 1

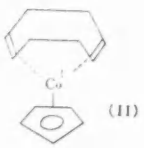

Fig. 2

1, 3, 5-Cyclooctatriene yielded brown crystals (III), m. p. 90°C, by the similar reaction with cyclopentadienyl cobalt dicarbonyl. The infrared spectrum of III showed C=C stretching absorption at 1625 cm.$^{-1}$ III also gave II on catalytic hydrogenation.

II was stable in air, soluble in organic solvents and readily decomposed by bromine or by iodine in carbon tetrachloride. It also reacted with carbon monoxide (50 atm.) to give cyclopentadienyl cobalt dicarbonyl. The ultraviolet spectrum of II showed maximum at 361 mμ (log ε: 2.87, in alcohol) and had shoulders at 235, 267 and 420 mμ, as well as increasing absorption in the shorter wavelengths. I and II reacted with diphenyl acetylene in refluxing xylene to give yellowish brown crystals (IV), m. p. 256°C, in 40 and 47% yield respectively. These crystals were purified by recrystallization from benzene or by chromatography on alumina. Found: C, 81.82; H, 5.2. Calcd. for $C_{33}H_{25}Co$: C, 82.48; H, 5.24%. The analysis conformed to the composition, $(C_5H_5C{\equiv}CC_6H_5)_2Co(C_5H_5)$. IV was soluble in organic solvents and was quite stable in air. IV was thermally stable up to ca. 360°C under nitrogen and surprisingly oxidation resistant as a univalent cobalt compound. For example the solution of IV in benzene was oxidized neither by air on heating nor by iodine on warming. The ultraviolet spectrum of IV showed maxima at 241, 257 and 278 mμ (log ε: 4.51, 4.50, 4.46, in alcohol) and had shoulders at 287, 295 and 400 mμ.

The infrared spectrum of IV showed the

1) A. Nakamura and N. Hagihara, This Bulletin, 33, 425 (1960).

presence of π-cyclopentadienyl group and mono-substituted phenyl group.

IV was reduced by sodium in liquid ammonia to give 1, 2, 3, 4-tetraphenylbutane, m. p. 181°C. IV did not react with concentrated hydrochloric acid, alcoholic potassium hydroxide and lithium aluminum hydride. It was attacked neither by carbon monoxide (100 atm.) at 290°C, by triphenyl phosphine at 150°C nor by acetylene dicarboxylic acid ester at 200°C. This remarkable stability of the compound IV together with its chemical and spectroscopic properties seems to indicate its structure involving a cyclobutadiene ring as shown in Fig. 3. Alternative structures such as those involving Co–C sigma bonds or involving tetraphenylbutadiene are less probable.

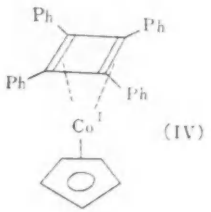

(IV)

Fig. 3

The Institute of Scientific and Industrial Research
Osaka Unversity
Sakai-shi, Osaka

The Absolute Configuration of Rotenone

By Masao Nakazaki and Hisao Arakawa

(Received December 22, 1960)

A recent short communication by Büchi et al.[1] on the absolute configuration of rotenone (I) prompts us to report our current work in this field. They submitted (−)dihydrotubaic acid (II) to exhaustive ozonolysis and obtained (+)3-hydroxy-4-methylpentanoic acid. In order to secure enough starting material, they synthesized (±)3-hydroxy-4-methylpentanoic acid and resolved it through the quinine salt to obtain the (−)acid (enantiomer of III, or IVa in Fischer projection), which they converted, via three steps into (−)2-methylpenta-3-ol with a known absolute configuration[2]. They thus established the (R) configuration[3] at position 5′ of rotenone. We also exhaustively ozonolysed (−)dihydrotubaic acid[4], m. p. 166°C, $[\alpha]_D^{25}$ −103.7° (methanol), then oxidized it with peracetic acid following our previous method[5]. The resulting hydroxy acid III was treated with diazomethane to afford the methyl ester IVb, b. p. 77~86°C/18 mmHg $[\alpha]_D^{20}$ +19° (ethanol), which was converted into (−)3-hydroxy-4-methylpentanohydrazide IVc.

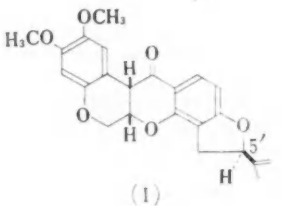

(I)

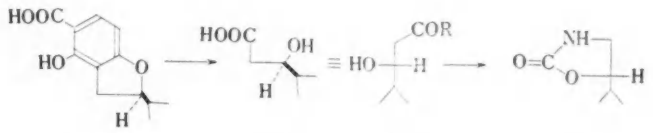

(II) (III) (IV) (V)

(a) R=OH
(b) R=OCH_3
(c) R=$NHNH_2$

1) G. Büchi, J. S. Kaltenbronn, L. Crombie, P. L. Godin and D. A. Whiting, *Proc. Chem. Soc.*, **1960**, 274.
2) See the footnote 4 and 5 of Büchi and Crombie's paper 1).
3) R. S. Cahn, C. K. Ingold and V. Prelog, *Experientia*, **12**, 18 (1956).
4) S. Takei and M. Koide, *Ber.*, **62**, 3030 (1929).
5) H. Arakawa and M. Nakazaki, *Ann.*, **636**, 111 (1960).

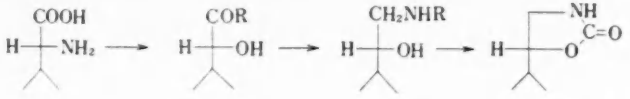

(VI) (VII) (VIII) (IX)

(a) R=OH
(b) R=OCH_3
(c) R=NH_2

(a) R=H
(b) R=$COOC_2H_5$

m. p. 152~153°C, $[\alpha]_D^{19}+43°$ (ethanol) with hydrazine. To relate this hydrazide IVc with D-valine, IVc was treated with nitrous acid[5] to afford (−)5-isopropyloxazolidone (V), m. p. 113~114°C, $[\alpha]_D^{18}-44.5°$ (ethanol). Found: C, 55.93; H, 8.55; N, 10.98. Calcd. for $C_6H_{11}O_2N$: C, 55.79; H, 8.58; N, 10.84%.

Racemic hydrazide IVc, m. p. 149~150°C, was prepared from ethyl 3-hydroxy-4-methylpentanoate which was prepared by the reduction of ethyl 3-oxo-4-methylpentanoate with sodium borohydride. Reaction with nitrous acid converted the racemic hydrazide IVc into the oxazolidone V, m. p. 87~88°C, the I. R. spectrum of which was found sound superimposable on that of the (−)oxazolidone V from rotenone.

(−)Methyl 2-hydroxy-3-methylbutanoate[7], b. p. 62~63°/15 mmHg, $[\alpha]_D^{12}-1.4°$ (etahnol) prepared from D-valine[8], $[\alpha]_D^{19}-27.6°$ (6 N hydrochloric acid), was treated with liquid ammonia to give the amide VIIc, m. p. 99~100°C, $[\alpha]_D^{15}+65.1°$ (methanol) (racemic compound, m. p. 104~105°C), which in turn was reduced with lithium aluminumhydride to the aminoalcohol VIIIa.

Reaction of sodium methoxide with the ethyl carbamate drivative VIIIb, which was obtained from the aminoalcohol VIIIa by the action of ethyl chlorocarbonate in pyridine, gave (+)5-isopropyloxazolidone (IX), m. p. 113~114°C, $[\alpha]_D^{18}+44.2°$ (ethanol). Found: C, 56.18; H, 8.68; N, 11.13%.

(−)5-Isopropyloxazolidone (V) derived from rotenone and (+)5-isopropyloxazolidone (IX) prepared from D-valine exhibited I. R. spectra which could be superimposed in every detail.

In order to make sure that they are enantiomorphic, an equal amount of (+) and (−) oxazolidone were mixed and recrystallized to give the racemic 5-isopropyloxazolidone which melted at 87~88°C, alone and admixed with the synthetic racemic oxazolidone from the racemic hydrazide.

6) Cf. C. Schöpf, G. Dummer and W. Wüst, ibid., **626**, 134 (1959); C. Schöpf and W. Wüst, ibid., **626**, 150 (1959).
7) E. Fischer and H. Scheibler, *Ber.*, **41**, 2891 (1908); P. D. Bartlett, M. Kuna and P. A. Leven, *J. Biol. Chem.*, **118**, 303 (1937); W. Klyne, "Progress in Stereochemistry", Vol. I, Butterworth, London (1950), p. 195.
8) We are indebted to Dr. Setsuji Sakurai, Ajinomoto Co., for his generous gift of D-valine.

Thus we could confirm Büchi and Crombie's result that rotenone has the (R) configuration at position 5'.

Department of Chemistry
Institute of Polytechnics
Osaka City University
Kita-ku, Osaka

On Some Dark-colored Chlorocuprates(I, II) and Related Compounds. II. Magnetic Susceptibility and Color at Liquid Helium Temperatures

By Masayasu Mori

(Received December 19, 1960)

A series of dark-colored chloroplumbates(II, IV) and chlorocuprates(I, II) of hexamminechromium(III) and hexamminecobalt(III) were reported in previous papers[1]. In the present paper a study on the magnetic susceptibility and the color of some of these compounds at liquid helium temperatures will be reported.

The samples studied in this research were "mixed valence compounds", $[Co(NH_3)_6]\cdot[PbCl_6]$ (I), $[Co(NH_3)_6][CuCl_5]_x[CuCl_4]_{1-x}$ ($x\sim0.75$) (II) and a single valence compound, $[Co(NH_3)_6][CuCl_5]$ (III). Measurements of magnetic susceptibility were carried out by the a.c. method[2] using a Hartshorn bridge in the temperature range, 1.3~4.2°K. The frequency used was 90 cycles/sec. The reciprocal values of the molar susceptibility (χ_M) of II and III obtained in this way are plotted against absolute temperature T in Fig. 1.

It is seen that the susceptibility obeys the Curie-Weiss law, $\chi_M=C/(T-\Theta)$, down to the temperature of about 2°K. The Weiss constant, ca. −2.3°K, for both II and III as seen from

1) M. Mori, This Bulletin, **24**, 285 (1951); **33**, 985 (1960).
2) C. J. Gorter, "Paramagnetic Relaxation", Elsevier, Amsterdam (1947).

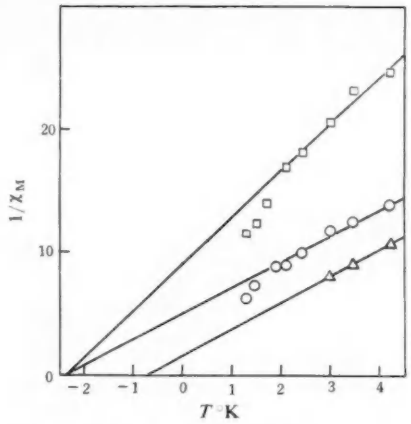

Fig. 1. Plots of $1/\chi_M$ vs. T°K.
—△— $CuSO_4 \cdot 5H_2O$
—○— $[Co(NH_3)_6][CuCl_5]_x[CuCl_4]_{1-x}$
—□— $[Co(NH_3)_6][CuCl_5]$

Fig. 1 is considerably different from that of $CuSO_4 \cdot 5H_2O$ (ca. −0.7°K). The magnetic moments per each bivalent copper atom calculated from the slopes are 1.57 B. M. for II and 1.47 B. M. for III*. These values are also abnormal as compared with the value of $CuSO_4 \cdot 5H_2O$, 1.92 B. M. These anomalies seem to be due to the trigonal-bipyramidal structure[3] of chlorocuprate ion, $[CuCl_5]^{3-}$, and not to the Cu^{I}–Cu^{II} interaction, since II and III exhibit similar magnetic behaviors.

No marked change of color was observed when II (brownish black) and III (yellowish orange) were dipped in liquid helium except that the color of III appeared a little lighter. On the other hand the color of I (brownish black) changed into brown in liquid air and brick red in liquid helium. The cause and reason of such different behaviors of chloroplumbate(II, IV) and chlorocuprate(I, II) are not yet clear.

The author is very grateful to Professor Taiichiro Haseda of Tohoku University for his kind guidance and valuable suggestions in the magnetic measurement. The experiment has never been possible without the offer of the laboratory facilities for liquid helium experiments at the Research Institute for Iron, Steel and Other Metals in the Tohoku University.

Institute of Polytechnics
Osaka City University
Kita-ku, Osaka

* In the calculation of this value the ratio of Cu^{II} content to the total copper was assumed to be x 0.75.

3) M. Mori, Y. Saito and T. Watanabe, This Bulletin, to be published.

The Nuclear Magnetic Resonance Spectra of Some Aconite Bases: Lucaconine and Lucidusculine

By Akira Suzuki, Takashi Amiya and Takeshi Matsumoto

(Received December 26, 1960)

An alkaloid lucaconine has beeen isolated from *Aconitum luciduscululm*, Nakai[1]. Recently, the alkaloid was identified[2] as delcosine[3] obtained from *Delphinium conolida* L. Based on several reactions of delcosine, Marion and others[4] assumed that the alkaloid possesses the same carbon-nitrogen framework and oxygen pattern as lycoctonine II[5] and suggested a tentative structure I. However, there has been no direct evidence for this substance bearing the CH_2OCH_3 group for R.

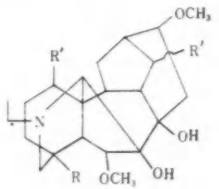

I R = CH_2OCH_3, R' = OH
II R = CH_2OH, R' = OCH_3

In *Aconitum* and *Delphinium* alkaloids, R is generally the methyl, hydroxymethyl or methoxymethyl group[6]. However, the possibility of the presence of the hydroxymethyl group in lucaconine can be excluded, since corresponding aldehydic or acidic products have not been obtained by the oxidation conditions which are expected to lead to these products[1,4,7]. The observation of NMR spectrum of lucaconine has been made to determine whether R is methyl or methoxymethyl. The NMR spectrum at 40 Mc. of lucaconine in pyridine solution is shown in Fig. 1. In this figure, although the other *Aconitum* alkaloids in which R is methyl have a strong singlet absorption characteristic of

1) H. Suginome, S. Kakimoto, J. Sonoda and S. Noguchi, *Proc. Japan Acad.*, **22**, 122 (1946); H. Suginome and S. Furusawa, This Bulletin, **32**, 352 (1959); S. Furusawa, ibid., **32**, 399 (1959); T. Amiya and T. Shima, ibid., **31**, 1083 (1958).
2) T. Amiya and T. Shima, in preparation.
3) L. N. Markwood, *J. Am. Pharm. Assoc.*, **13**, 696 (1924).
4) R. Anet, D. W. Clayton and L. Marion, *Can. J. Chem.*, **35**, 397 (1957); R. Anet and L. Marion, ibid., **36**, 766 (1958); V. Skaric and L. Marion, *J. Am. Chem. Soc.*, **80**, 4434 (1958).
5) M. Przybylska and L. Marion, *Can. J. Chem.*, **34**, 185 (1956).
6) O. E. Edwards, L. Marion and K. H. Palmer, *Can. J. Chem.*, **36**, 1097 (1958); K. Wiesner, D. L. Simmons and L. R. Fowler, *Tetrahedron Letters*, No. **18**, 1 (1959).
7) E. Ochiai, T. Okamoto and M. Kaneko, *Chem. Pharm. Bull.*, **6**, 730 (1958).

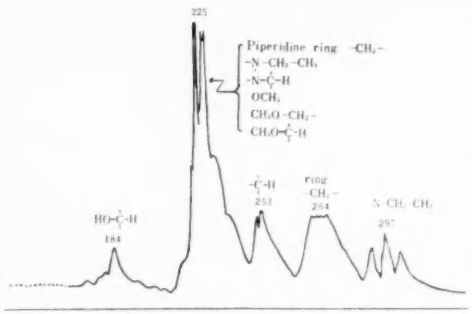

Relative area	Found	1.6	19	4.8	7.6	3
	(Calcd. on formula I)	(2)	(18)	(4)	(8)	(3)

Fig. 1. The proton spectrum of lucaconine (taken on Varian 40 Mc. instrument).

$-\overset{|}{C}-CH_3$ group at about 318 c. p. s. from the signal of α-proton of pyridine[8], such absorption can not be recognized for lucaconine. Accordingly, R is concluded to be CH_2OCH_3 in lucaconine. The anticipated singlet peak due to the methylene group of $-\overset{|}{C}-CH_2-OCH_3$ is, however, obscure[9] in Fig. 1, probably because of the overlapping with strong peaks of methoxyl groups, and of possible broadening due to the unequivalence of two methylene protons caused by the neighbouring asymmetric carbon atom[10]. A tentative interpretation based on the suggested structure I is also given in Fig. 1[11].

We next examined NMR spectrum of an aconite base lucidusculine[12]. Recently, one of us (T. A.) proposed formula III for the partial structure of lucidusculine on the basis of some chemical transformations[13].

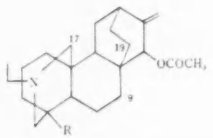

III R=CH_2OH, one secondary OH group on the ring. Possible linkage between C_{17}-C_{19} or C_{17}-C_9.

IV R=CH_3, two secondary OH groups on the ring. Possible linkage between C_{17}-C_{19} or C_{17}-C_9.

8) A. Suzuki, T. Amiya, K. Takahashi and T. Matsumoto, unpublished work.

9) In the NMR spectrum of lycoctonine[8], the absorption due to methylene group of $-\overset{|}{C}-CH_2OH$ is also obscure.

10) L. M. Jackman, "Applications of Nuclear Magnetic Resonance Spectroscopy in Organic Chemistry", Pergamon Press, London (1959), p. 102.

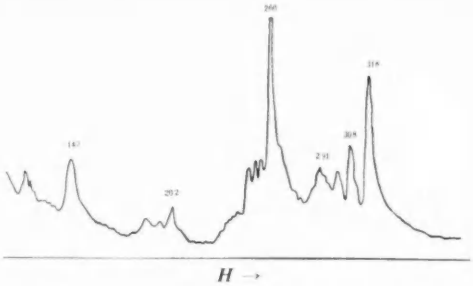

Fig. 2. The proton spectrum of lucidusculine.

The NMR trace at 40 Mc. of lucidusculine in pyridine is shown in Fig. 2. Clearly, the singlet band at 318 c. p. s. is to be ascribed to the methyl group on a quaternary carbon atom. This observation forces one to the conclusion that in lucidusculine R is actually the methyl group. The two hydroxyl groups in lucidusculine may both be secondary, since they are easily acetylated[12]. From above described results, a modified formula IV is now suggested as the partial structure of lucidusculine.

The authors express thier sincere thanks to Professor Genjiro Hazato and Dr. Kensuke Takahashi of Tohoku University for the measurement of NMR spectra. They are also grateful to Professor Harusada Suginome for his encouragement in this work.

Department of Chemistry
Faculty of Science
Hokkaido University
Sapporo

11) The signal of the methine proton of methoxycyclohexanes (H-C-OCH_3) has been shown to appear at a position very close to the methoxyl group. R. U. Lemieux, R. K. Kullning, H. J. Bernstein and W. G. Schneider, *J. Am. Chem. Soc.*, **80**, 6098 (1958).

12) R. Majima and S. Morio, *Ber.*, **65**, 599 (1932); H. Suginome, S. Kakimoto and J. Sonoda, *J. Fac. Sci. Hokkaido Univ.*, Ser. III, Chem., **4**, 25 (1950); H. Suginome and S. Kakimoto, This Bulletin, **32**, 352 (1959); T. Amiya, ibid., **32**, 1133 (1959).

13) T. Amiya, This Bulletin, **33**, 1175 (1960).

The Interaction of a Surfactant with a Monolayer Studied by Radiotracer Method

By Ryosuke SHIMOZAWA and Ryohei MATUURA

(Received February 6, 1961)

The adsorption of sodium alkyl sulfates at the solution-air interface was studied by radiotracer method and the result was already reported[1-3]. In this case if an insoluble monolayer is present on the surface of the solution, the surface count of the radioactive detergent may be different from that of the free surface, and it is expected that we may be able to know the interaction of the detergent with the monolayer substance from this difference in the surface count. We measured the interaction of sodium dodecyl sulfate (SDS) with the monolayer of octadecyl amine, octadecyl alcohol and nylon 6 spread on the surface of the solution by tracing sulfate sulfur tagged with ^{35}S. The apparatus was almost the same as that used for measuring the adsorption of the detergent at the free surface[3]. The radioactivity of the surface of the SDS solution in the lucite tray was measured first. Then the monolayer was spread on this solution and the surface area was kept constant with the surface pressure of about 10 dyn. cm. The radioactivity of the surface in this state was measured with the same geometry as above. The spreading solvents used were a mixture of one volume ethanol and two volume benzene for octadecyl amine and octadecyl alcohol and a mixture of one volume phenol and three volume benzene for nylon 6. The result is shown in Fig. 1, in which the abscissa represents the time after spreading the monolayer on the surface and the ordinate is the surface count.

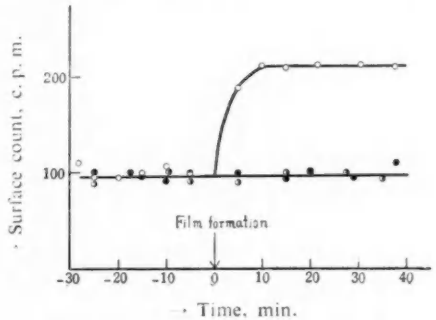

Fig. 1. Change in surface counting rate before and after film formation. Substrate is 8×10^{-5} mol./l. SDS solution.
○ Octadecyl amine-SDS series
◑ Octadecyl alcohol-SDS series
● Nylon 6-SDS series

From this figure it is evident that in the presence of octadecyl amine monolayer the surface count increases to more than twice the value of the free surface, while in the case of octadecyl alcohol and nylon 6 no change is observed after spreading the monolayer of these substances. These results may show that the monolayer of octadecyl amine interacts with the molecule of SDS in the substrate solution remarkably but that of octadecyl alcohol and nylon 6 affects no such interaction as the amine monolayer. Goddard and Schulman[4] measured the surface pressure of an eicosyl amine monolayer at constant area on the surface of water and found that a remarkable increase in pressure took place by injecting sodium hexadecyl sulfate (SHS) into the substrate solution beneath the monolayer. They explained the result in terms of penetration of SHS into the monolayer and formation of a 1 to 1 stoichiometric complex. The present experiment confirms directly the strong interaction of the long chain amine monolayer with sodium alkyl sulfate in the solution. However, we found that the surface pressure of the monolayer of octadecyl alcohol and nylon 6 increases appreciably by the presence of SDS in the solution just as is the case with the amine monolayer, but the surface count with the monolayer of the former substances does not differ from the value without the monolayer contrary to the case of the latter substance, as shown in Fig. 1. These results suggest that the mechanism of the interaction of the long chain amine monolayer with SDS is different from that of the monolayer of long chain alcohol or nylon 6 with it. The quantitative treatment of the data and the detailed discussion will be reported in future.

Department of Chemistry
Faculty of Science
Kyushu University
Hakozaki, Fukuoka

1) R. Matuura, H. Kimizuka, S. Miyamoto and R. Shimozawa, This Bulletin, **31**, 532 (1958).
2) R. Matuura, H. Kimizuka, S. Miyamoto, R. Shimozawa and K. Yatsunami, ibid., **32**, 404 (1959).
3) R. Matuura, H. Kimizuka and K. Yatsunami, ibid., **32**, 645 (1959).
4) E. D. Goddard and J. H. Schulman, *J. Colloid Sci.*, **8**, 309 (1953).

Electron Spin Resonance Study on Photolysis of Acetone and Benzophenone

By Keiji KUWATA and Kōzō HIROTA

(Received December 24, 1960)

Recently several trapped radicals formed in photolysis have been identified with organic compounds of low molecular weight by the ESR method[1]. By the use of a X-band spectrometer of high sensitivity it became possible to study the radical intermediates formed in photolysis of some ketones. Preliminary investigation on acetone and benzophenone will be reported here.

According to the kinetic studies on the photolysis of gaseous acetone, formation of several types of free radicals was proposed[2]:

$$CH_3COCH_3 + h\nu \longrightarrow \dot{C}H_3 + \dot{C}H_3CO$$

$$(\dot{C}H_3CO \longrightarrow \dot{C}H_3 + CO)$$

$$\dot{C}H_3 + CH_3COCH_3 \longrightarrow CH_4 + \dot{C}H_2COCH_3$$

$$\dot{C}H_2COCH_3 \longrightarrow \dot{C}H_3 + CH_2CO$$

$$\dot{C}H_3 + \dot{C}H_2COCH_3 \longrightarrow CH_3COCH_2CH_3$$

In the liquid phase photolysis of the both ketones, formation of the active intermediates was proposed[3], but their natures were not well known. Observation of ESR for these free radical intermediates will give a confirmative evidence for such mechanisms.

The spectrometer used was a type of high frequency field modulation, being similar to that of Fujimoto and Ingram, but the frequency of the field modulation was 455 kilocycles/sec. Design of a low temperature resonant cavity is shown in Fig. 1.

After an irradiation of ultraviolet light for several hours, any signal could not be observed in pure acetone, while a broad singlet was observed in pure benzophenone and in 0.1～1% solutions of the both ketones. However, the intensity of the signal decreased rapidly in the case of acetone, a half life being 50 min. at about 77°K. The characteristics of the signals observed are shown in Table I.

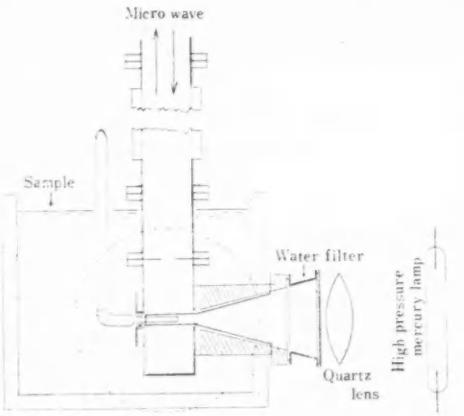

Fig. 1

TABLE I. ESR OF TRAPPED RADICALS AT ABOUT 77°K

	Line width (H_{msl})	Line shape	g-Factor
Acetone in ethanol and EPA (Ether, iso-Pentane and Alcohol)	30 gauss	(gaussian)	2.003
Benzophenone	23 gauss	〃	2.003
Benzophenone in ethanol and EPA	24 gauss	〃	2.003

An unstable free radical in the solution of acetone would be the methyl radical, but confirmative evidence for this assignment was not yet given since no hyperfine structure was observed. In the case of benzophenone a hyperfine structure neither of a quartet for the phenyl radical nor of a quartet with the small separations for the benzoyl radical was observed. The result indicates that two types of free radicals were present together or broadning of the line width occurred by some reasons, so that the hyperfine structure was smeared out. Detailed research will be published elsewhere.

The authors wish to express their thanks to Dr. M. Fujimoto and also to Dr. K. Morigaki of Osaka University for their suggestions on design of the low temperature cavity.

Department of Chemistry
Faculty of Science
Osaka University
Nakanoshima, Osaka

1) Cf. A. M. Bass and H. P. Broida, "Formation and Trapping of Free Radicals", Academic Press, New York (1960), p. 239.
2) Cf. J. A. Leermakers, *J. Am. Chem. Soc.*, **16**, 1899 (1934).
3) H. H. Glazebrock and T. G. Pearson, *J. Chem. Soc.*, **1937**, 537.
4) S. W. Benson and G. S. Fordes, *J. Am. Chem. Soc.*, **65**, 1399 (1943).
5) E. J. Bowen and E. de la Prandiere, *J. Chem. Soc.*, **1934**, 1503.

Reaction of Tetraphenyl Titanate with Amines

By Takeshi Yoshino, Ichiro Kijima and Miyoko Ochi

(Received on December 26, 1960)

In the previous paper, the reaction of tetraphenyl titanate with ammonia, phenols, acetophenone and esters have been reported[1]. In the course of the synthetical studies on the organo titanium compounds, it has been found that the addition compounds of tetraphenyl titanate were more stable than that of tetraalkyl titanates. In the present communication, the reaction of tetraphenyl titanate (TPhT) with aliphatic or aromatic amines are described.

When TPhT was made to react with aliphatic amines (*n*-butylamine, tri-ethylamine, tri-*n*-butylamine) in toluene solution, addition compounds of TPhT could not be isolated. However, when aromatic amines (aniline, α-naphthylamine, pyridine) were used, they gave addition compounds with TPhT (molar ratio of 1:1). When the addition compound of TPhT with phenol I reacted with aromatic amines, the addition compound I was converted into the addition compounds of the corresponding amines used. They also were converted into the addition compound of TPhT with ammonia. The reaction of TPhT with hexamethylenediamine gave yellow crystals, which were considered as the addition compound of TPhT with hexamethylenediamine (molar ratio of 2:1).

Experimental

1) Addition Compounds of TPhT with Aromatic Amines.—Into a solution of TPhT (8.0 g.) in toluene (50 ml.), freshly distilled aniline (2.1 g.) was added and refluxed for 15 min. After the reaction mixture was allowed to stand at room temperature, the crystals separated out were collected by filtration and dried under reduced pressure, 8.0 g. of yellowish orange crystals were obtained. They were recrystallized from toluene. M. p. 181~183°C. (Found: Ti, 9.64; N, 2.80. Calcd. for $C_{30}H_{27}O_4NTi$: Ti, 9.33; N, 2.73%). In a similar way the following addition compounds were obtained: $Ti(OC_6H_5)_4 \cdot C_{10}H_7NH_2$, orange crystals, m. p. 168~169°C. (Found: Ti, 8.49; N, 2.60. Calcd. for $C_{34}H_{29}O_4NTi$: Ti, 8.50; N, 2.49%); $Ti(OC_6H_5)_4 \cdot C_5H_5N$, reddish orange crystals, m. p. 191~192°C. (Found: Ti, 9.53; N, 2.83. Calcd. for $C_{29}H_{23}O_4NTi$: Ti, 9.59; N, 2.80%).

When aliphatic amines (*n*-butylamine, tri-ethylamine, tri-*n*-butylamine) were used, addition compound of TPhT could not be isolated.

2) Reaction of the Addition Compound $Ti(OC_6H_5)_4 \cdot C_6H_5OH$ (I) and Aromatic Amines.—To a solution of the addition compound I (4.0 g.), in toluene (15 ml.), aniline (2.0 g.) was added and the solution was refluxed for 15 min. After allowed to stand at room temperature, it deposited yellowish orange crystals. They were purified as described under (1), m. p. 183°C. (Found: Ti, 9.08; N, 2.86. Calcd. for $C_{30}H_{27}O_4NTi$; Ti, 9.33; N, 2.73%). $Ti(OC_6H_5)_4 \cdot C_6H_5OH + C_6H_5NH_2 \rightarrow Ti(OC_6H_5)_4 \cdot C_6H_5NH_2 + C_6H_5OH$. In a similar way, by the use of α-naphthylamine or pyridine, the addition compound I was converted into the corresponding addition compounds of TPhT with the above amines respectively: $Ti(OC_6H_5)_4 \cdot C_{10}H_7NH_2$, m. p. 167~168°C. (Found: Ti, 8.91; N, 2.63, Calcd. for $C_{34}H_{29}O_4NTi$: Ti, 8.50; N, 2.49%); $Ti(OC_6H_5)_4 \cdot C_5H_5N$, m. p. 191~192°C. (Found: Ti, 9.67; N, 2.88. Calcd. for $C_{29}H_{23}O_4NTi$: Ti, 9.59; N, 2.80%).

3) Reaction of the Addition Compound $Ti(OC_6H_5)_4 \cdot C_6H_5NH_2$ (II) and Ammonia.—When excess of dry ammonia gas was passed at room temperature to a solution of the addition compound II (2.5 g.), in toluene (10 ml.), the addition compound II was converted into the addition compound of TPhT with ammonia III, (molar ratio of 1:1). M. p. 201~202°C. (Found: Ti, 10.89; N, 3.17. Calcd. for $C_{24}H_{23}O_4NTi$: Ti, 10.95; N, 3.20%).

$$Ti(OC_6H_5)_4 \cdot C_6H_5NH_2 + NH_3 \rightarrow Ti(OC_6H_5)_4 \cdot NH_3 + C_6H_5NH_2$$

In a similar way, the addition compounds $Ti(OC_6H_5)_4 \cdot C_{10}H_7NH_2$ and $Ti(OC_6H_5)_4 \cdot C_5H_5N$ were converted into III.

4) Reaction of TPhT with Hexamethylenediamine.—Into a solution of TPhT (8.7 g.) in toluene (60ml.), hexamethylenediamine (0.6 g.) was added and refluxed for 30 min. After the reaction mixture was allowed to stand at room temperature, the crystals were collected by filtration, washed with toluene and dried under reduced pressure, 4.7 g. of powdery yellow crystals were obtained. M. p. 237~239°C. The analytical data showed this compound to be an addition compound of TPhT with hexamethylenediamine (molar ratio of 2:1), (Found: Ti, 10.13; N, 3.45. Calcd. for $C_{54}H_{56}O_8N_2Ti_2$: Ti, 10.01; N, 2.92%).

Department of Applied Chemistry
Tokyo College of Science
Shinjuku-ku, Tokyo

1) T. Yoshino et al., *J. Chem. Soc. Japan, Ind. Chem. Sec.* (*Kogyo Kagaku Zasshi*), **63**, 1758 (1960).